

The Constitution and Structure of the Lunar Interior

Mark A. Wieczorek¹, Bradley L. Jolliff², Amir Khan³,
Matthew E. Pritchard⁴, Benjamin P. Weiss⁵, James G. Williams⁶,
Lon L. Hood⁷, Kevin Righter⁸, Clive R. Neal⁹, Charles K. Shearer¹⁰,
I. Stewart McCallum¹¹, Stephanie Tompkins¹², B. Ray Hawke¹³,
Chris Peterson¹³, Jeffrey J. Gillis¹³, Ben Bussey¹⁴

¹*Institut de Physique du Globe de Paris, Saint Maur, France*

²*Washington University, St. Louis, Missouri, U.S.A.*

³*Niels Bohr Institute, University of Copenhagen, Denmark*

⁴*Cornell University, Ithaca, New York, U.S.A.*

⁵*Massachusetts Institute of Technology, Cambridge, Massachusetts, U.S.A.*

⁶*Jet Propulsion Laboratory, California Institute of Technology, Pasadena, CA, U.S.A.*

⁷*University of Arizona, Tucson, Arizona, U.S.A.*

⁸*Astromaterials Branch, Johnson Space Center, Houston, Texas, U.S.A.*

⁹*University of Notre Dame, Notre Dame, Indiana, U.S.A.*

¹⁰*University of New Mexico, Albuquerque, New Mexico, U.S.A.*

¹¹*University of Washington, Seattle, Washington, U.S.A.*

¹²*Science Applications International Corporation, Chantilly, Virginia, U.S.A.*

¹³*University of Hawaii, Honolulu, Hawaii, U.S.A.*

¹⁴*Applied Physics Laboratory, Laurel, Maryland, U.S.A.*

e-mail: wieczor@ipgp.jussieu.fr

"This picture, though internally consistent, is subject to revision or rejection on the basis of better data." Don Wilhelms (1987) *The Geologic History of the Moon*, USGS Prof. Paper 1348.

1. INTRODUCTION

The current state of understanding of the lunar interior is the sum of nearly four decades of work and a range of exploration programs spanning that same time period. Missions of the 1960s including the Rangers, Surveyors, and Lunar Orbiters, as well as Earth-based telescopic studies, laid the groundwork for the Apollo program and provided a basic understanding of the surface, its stratigraphy, and chronology. Through a combination of remote sensing, surface exploration, and sample return, the Apollo missions provided a general picture of the lunar interior and spawned the concept of the lunar magma ocean. In particular, the discovery of anorthite clasts in the returned samples led to the view that a large portion of the Moon was initially molten, and that crystallization of this magma ocean gave rise to mafic cumulates that make up the mantle, and plagioclase flotation cumulates that make up the crust (Smith et al. 1970; Wood et al. 1970). This model is now generally accepted and is the framework that unifies our knowledge of the structure and composition of the Moon. The intention of this chapter is to review the major advances that have been made over the past decade regarding the constitution of the Moon's interior. Much of this new knowledge is a direct result of data acquired from the successful Clementine and Lunar Prospector missions, as well as the analysis of new lunar meteorites. As will be seen, results from these studies have led to many fundamental amendments to the magma ocean model.

Much of what we know from sample analyses has been previously summarized elsewhere, and only their most important aspects will be discussed in this chapter. The reader is referred to the relevant chapters in the books *Basaltic Volcanism on the Terrestrial Planets* (Basaltic Volcanism Study Project 1981), *The Lunar Sourcebook* (Heiken *et al.* 1991), and *Planetary Materials* (Papike *et al.* 1998) for more in-depth assessments. Fortunately, the lunar samples were curated carefully and with forethought as to the possibility that there might be no sample-return missions for a long time after Apollo. Thus, as new analytical methods are developed and old ones are improved, analyses of the samples continue to yield important results.

Much of our geophysical knowledge of the Moon comes from instruments that were deployed during the manned Apollo landings. As part of the Apollo Lunar Surface Experiments Package (ALSEP), Surface magnetometers, heat-flow probes, and seismometers operated until 1977 when the transmission of data was terminated. While re-analyses of these data occasionally yield surprises (such as the Apollo seismic data), many aspects of the pre-1990s geophysical reviews are just as relevant today as when they were written. The electromagnetic sounding data of the Apollo era is thoroughly reviewed by Sonnett (1982), much of the geophysics as reviewed by Hood (1986) is still highly relevant, and the paleomagnetism of the lunar samples has been comprehensively reviewed by Fuller and Cisowski (1987) and Collinson (1993). One suite of passive surface instruments deployed during the Apollo and Russian Luna missions that is still operational are the corner-cube retroreflectors. Laser ranging to these stations continues to the present day, and with the gradual accumulation of data, our knowledge of the deep lunar interior is slowly being revealed. The results of this experiment up to 1994 have been reviewed by Dickey *et al.* (1994).

The remote sensing missions of the 1990s—Galileo, Clementine, and Lunar Prospector—for the first time obtained near-global compositional data sets that enable us to assess the nature of materials at the surface of the Moon. One of the major results of global remote sensing has been to locate regions of the lunar surface that differ from the Apollo landing sites and that are difficult to explain given the known compositions of the present lunar sample collection. In particular, the floor of the South Pole-Aitken basin, which is the largest recognized impact structure in the solar system, may contain rocks that formed deep in the crust and as yet, not sampled elsewhere. The mineralogy and petrology of known rock types, nevertheless, provide constraints on lunar petrogenetic processes, which then allow informed extrapolation to those areas that were not directly sampled. Near-global topography, magnetic data, and improved models of the lunar gravity field from these missions have further offered vastly improved datasets in comparison to the spatially limited Apollo observations. By combining general characteristics of the lunar samples and surface-derived geophysical constraints with these near-global orbital data, our understanding of the Moon's interior structure has been much improved over the general sketch provided during the Apollo era.

The Apollo and Luna samples were found to contain many different rock components brought together by impact processes. Any given sample of soil or breccia thus might contain a much wider diversity of rock types than whatever the local bedrock material might be. In fact, because of the potentially widespread effects of mixing together of widely separated materials by large impact events, a general (although incorrect) argument could be made that the Moon was adequately sampled by the Apollo and Luna missions. The discovery of lunar meteorites (Warren 1994), coupled with telescopic and global remote sensing, prove this argument wrong. Furthermore, recent studies of basin-ejecta deposits and deposition processes suggest that most of the Apollo sites were strongly influenced by material derived from one or a few late basin-forming events, especially Imbrium (e.g., Haskin 1998; Haskin *et al.* 1998). Thus, the feldspathic lunar meteorites provide our best samples of the lunar highland crust far removed from the effects of contamination by Imbrium ejecta. Several of the lunar meteorites also provide samples of basalt that differ from any of the basalt types known from the Apollo and Luna suites.

The information presented and discussed in this chapter is set within the context of the new datasets. Key constraints based upon the samples, Apollo-era geophysical experiments, and pre-1990s remote sensing are reviewed and then coupled with recent results to reassess the makeup and structure of the lunar interior. One of the recurring themes of this chapter will be to demonstrate that the traditional “pie-wedge” cross-sectional view of the lunar interior can no longer be considered as being globally representative. Instead, the lunar crust and underlying mantle appear to be best characterized as being composed of discreet geologic terranes, with each possessing a unique composition, origin, and geologic evolution. This concept is best illustrated by the gamma-ray spectrometer data obtained from the Lunar Prospector mission, which shows that incompatible and heat-producing elements are highly concentrated in a single region of the Moon that was once volcanically very active. This recognition has led many workers to reassess the significance of the data derived from the Apollo era, particularly in light of the fact that all six Apollo landing sites straddle the border between two of the most distinctive terranes—the Procellarum KREEP Terrane and the Feldspathic Highlands Terrane (e.g., Jolliff et al. 2000a). The fact that a body as small as our Moon possesses vastly different geologic crustal provinces should be borne in mind when one attempts to assess the geologic history of a less understood and larger planetary body, such as Mercury and Mars.

Because the concept of a magma ocean is so thoroughly ingrained in modern notions of how lunar rocks types are distributed as a function of depth in the crust and upper mantle (and for good reasons), we use it as a general framework for discussion. We do not maintain that we understand how it originated or solidified in detail, nor how deep it might have been and how it might have evolved. Indeed, fundamental questions remain that relate to these topics, and some of these are addressed in more detail later in this chapter and in Chapter 4 of this book. Nevertheless, we begin this chapter with a very brief summary of some of the key implications that a magma ocean has for the makeup and structure of the Moon, and what types of question we might address within the context of this model. From this point, we sequentially review our current knowledge of the crust, mantle, and core of the Moon (Sections 2, 3, and 4). In Section 5, we emphasize the concept that the lunar crust and mantle are best understood in terms of unique geologic terranes. Following this, we address some of the fundamental unanswered questions in lunar science dealing with the lunar interior, and end with a discussion of how these may be addressed in future studies and exploration.

1.1. The magma ocean model and its many questions

Since the time of the first Apollo sample studies, the oldest lunar crust was correctly inferred to be rich in plagioclase (Smith et al. 1970; Wood et al. 1970). Assuming an average crustal thickness of ~60 km and a bulk Moon aluminum concentration similar to the Earth’s mantle, a significant differentiation event must have occurred in the Moon’s early evolution to have formed this crust (e.g., Warren 1985). On the basis of petrologic experiments, the mare basalts were shown to have been derived from an ultramafic pyroxene and olivine source. Trace-element geochemistry, especially rare earth element (REE) patterns, has further shown that the ultramafic sources of the mare basalts are complementary to the feldspathic crust.

To explain these observations, the global magma ocean (or magmasphere) hypothesis was developed (e.g., Smith et al. 1970; Wood et al. 1970; Warren and Wasson 1977, 1979b; Warren 1985). In its simplest form, this hypothesis postulated that the magma ocean differentiated during crystallization to form a dense, ultramafic mantle rich in olivine and pyroxene that was overlain by a buoyant, globe-encircling, plagioclase-rich crust. This hypothesis has served well because it accommodates many remotely sensed observations as well as much of the data collected on the samples returned by the Apollo and Luna missions. In addition, the magma-ocean hypothesis is consistent with a hot accretion of the Moon as would be expected if it formed as a result of a giant impact between the early Earth and a Mars-sized object (e.g., Pritchard and Stevenson 2000) (see Chapter 4).

Estimated depths of the primordial magmasphere range from whole Moon melting to thin melt layers above partially molten zones. Deep magma oceans are currently favored in the literature, and a popular hypothesis is that a seismic discontinuity located about 500 km below the surface might represent this maximum depth of melting. Whether the middle and lower mantle escaped melting and differentiation remains one of the key unknowns regarding the Moon's evolution. Regardless of its initial depth, isotopic evidence and thermal considerations suggest that the materials that make up the lunar mantle crystallized within a period of about 30 m.y. (Lee *et al.* 2002; Shearer and Righter 2003) to 200 m.y. (Solomon and Longhi 1977; Nyquist and Shih 1992).

Several thermal and petrologic models have been developed that track the compositional evolution of a crystallizing magma ocean (see Shearer and Papike 1999 and references therein). In general, the first mineral to crystallize and sink would have been a magnesium-rich olivine, and as crystallization proceeded the cumulus phases would have become more iron rich. After about 75% of the magma ocean had crystallized, plagioclase would have become a liquidus phase, and because of its low density, it would have been buoyant with a tendency to rise. After the magma ocean was about 90% crystallized, dense Ti-bearing phases (ilmenite, armalcolite) would have crystallized. In all models, efficient fractional crystallization would produce a chemically evolved, late-stage residual melt referred to as urKREEP (Warren and Wasson 1979b) that was initially sandwiched between the crust and mantle. This residual magma would have been extremely enriched in iron and the incompatible and heat-producing elements that are represented by the acronym KREEP (Potassium, Rare Earth Elements, and Phosphorous). Because of the high concentration of heat-producing elements, concentrations of this material at depth could remain in a molten phase for many hundreds of millions of years (Solomon and Longhi 1977). Somewhat paradoxically, though, samples directly related to urKREEP have not yet been identified, though KREEP-rich samples that are rich in magnesium have. Although the high concentrations of incompatible elements in these rocks are consistent with a late-stage magma ocean origin, their high magnesium concentrations remain enigmatic. The origin of these magnesian KREEP-rich samples remains one of the major unresolved problems in understanding the Moon's magmatic evolution.

In simple models of magma-ocean crystallization, depending upon the density of the cumulate phases, they are either sequentially laid down at the base of the magma ocean, or at the base of the crust. Because the mantle cumulates become increasingly rich in iron with the progress of crystallization (culminating in dense ferropyroxene and ilmenite-rich cumulates), this mantle cumulate pile would have been gravitationally unstable. Several studies have shown that the late-stage ilmenite cumulates should have sunk through the mantle. Others have predicted that the deep, olivine-rich mantle cumulates should have participated in the overturn as well, bringing early-crystallized magnesium-rich olivine to the upper mantle (see Chapter 4). A key question regarding these overturn models is their timing, extent, and efficiency. In particular, did this event act to homogenize the composition of the mantle? Or was mixing inefficient such that any original stratification within the magma-ocean cumulates might still be present, though in an inverted sequence? Did such overturn occur globally, or was it localized in one or several regions of the mantle? Chapter 4 considers the internal evolution of the Moon in great detail; in this chapter, we mainly focus on sample, remote sensing, and geophysical evidence for the present-day lithology and structure of the interior.

The compositional stratigraphy that results from a crystallizing magma ocean has commonly been illustrated by the use of simple circular cross sections, or 1-dimensional pie-wedge diagrams (for a recent example, see Fig. 3.1). Implicit in such drawings is the assumption that early lunar differentiation was spherically symmetrical and that any asymmetry was imparted by later basin-forming impact processes. This view of an initially laterally uniform internal composition (and hence laterally uniform internal processes) was widely accepted

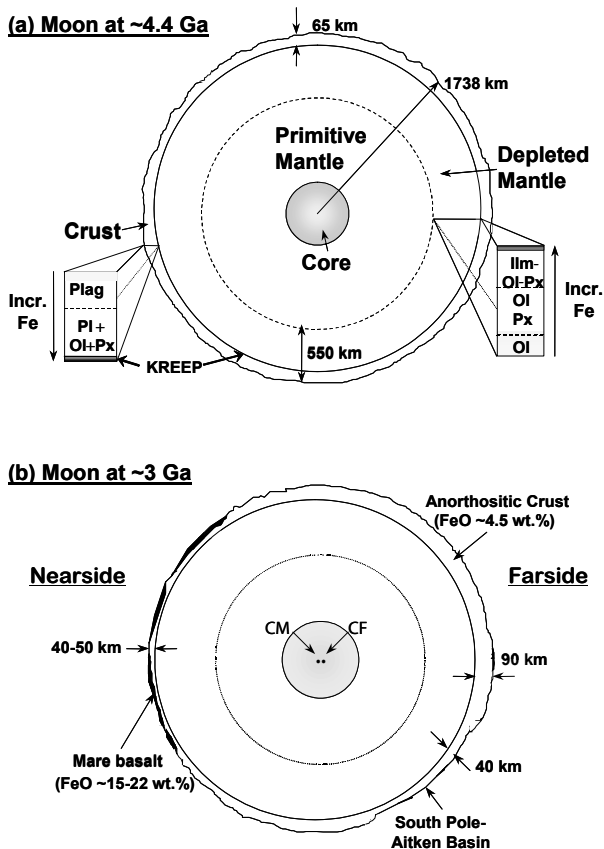


Figure 3.1. One possible interpretation of the Moon's internal structure (a) just after magma-ocean crystallization and (b) near the end of mare basaltic volcanism. With the exception of a hemispheric dichotomy in crustal thickness and mare basaltic volcanism, this model, like many pre-Lunar Prospector models, represents the crust and mantle as being laterally uniform in composition. (a) The lunar magma ocean is assumed to have a depth of 550 km, the lower mantle is composed of “primitive” unmelted materials, and a small core is assumed. The sequences of major mineralogy as a function of radius in the mantle (olivine \rightarrow olivine + pyroxene \rightarrow ilmenite + olivine + pyroxene) and crust (plagioclase-rich in the upper crust and plagioclase + pyroxene + olivine in the lower crust), as well as the existence of a global KREEP-rich layer at the crust-mantle boundary, are a result of a fractionally crystallizing magma ocean. Complex processes, such as mantle overturn and asymmetric solidification of the magma ocean, are not considered in this model. (b) The lunar interior at ~ 3 Ga, emphasizing the nearside-farside dichotomy in both the distribution of mare basalts and the thickness of the lunar crust. (CM and CF represent the center of mass and center of figure, respectively, which are offset from each other by about 2 km). Compare with the more recent interpretations presented in Figure 3.27. [Used by permission of Springer, from McCallum (2001), *Earth Moon Planets*, Vol. 85-86, Figs. 2 and 4, pp. 256 and 260.]

until the acquisition of thorium surface concentrations by the Lunar Prospector spacecraft. It now appears that the Moon possesses a fundamental asymmetry, stemming from the time of initial differentiation, with KREEP-rich rocks and mare volcanism having been concentrated on the Moon's Earth-facing hemisphere. Curiously, the elevations of the nearside hemisphere are about 2 km less than that of the far side. No matter the origin of the asymmetric distribution of KREEP-rich rocks, it appears that their associated high heat production fundamentally affected the post-magma-ocean magmatic history of the Moon's near side.

The above description of the magma-ocean model is admittedly simplified and is discussed in far more detail in Chapter 4. Nonetheless, the model in its generic form has held up remarkably well over the past thirty or so years. The concept of the Moon possessing distinct geologic terranes is the most recent contribution to the lunar magma-ocean concept, and this will be more fully discussed in Section 5.

2. THE CRUST

The lunar crust provides us with the most direct evidence for a major differentiation event early in the Moon's history. Because the crust is easily accessible to both remote-sensing techniques and sample analyses, much is now known of its composition and the processes by which it formed. Although these two lines of study are only applicable to rocks that now reside at the surface, processes associated with impact cratering have brought once deep-seated rocks to the surface, allowing the deep crust to be investigated at certain locales as well. Geophysical investigations, including analysis of the Apollo seismic data and the Moon's gravity and topography, are also sensitive to properties of the crust.

The most important questions that will be addressed in this section are related to the composition of the crust, any lateral or vertical compositional variations that might be present, and its thickness. When used in combination, these pieces of information can be used to constrain the bulk composition of the crust, and hence place constraints on its mode of origin and the extent of lunar differentiation. At the end of this section a brief review will be given of our current knowledge of the lunar crust.

2.1. Samples of the crust

Rock samples collected during the Apollo and Luna missions and the identification and characterization of lunar meteorites provide first-hand information about the mineralogy and lithology of the Moon's principal crustal rock types. These can be related to remotely sensed information, and their global distribution (lateral and vertical) can be inferred through consideration of mixing models (chemical and physical) and geologic processes. The samples include several varieties of intrusive igneous rocks, basaltic lavas and volcanic glasses, and a wide range of breccias formed by impact melting and ballistic sedimentation. Even though the samples represent a spatially restricted subset of lunar rocks, there are good reasons to think that the existing rock suites represent fairly well the global crustal rock types with but a few exceptions. First, because of the lateral and vertical redistribution of materials by large impacts, and the assembly of diverse rock components into impact breccias, many lithologies of potentially widely separated sources may be combined as clasts into a single breccia. The same argument applies to the diversity of materials and potential sources for small rock fragments found in the unconsolidated regolith. Second, because the Moon is essentially anhydrous, and there are no aqueous sedimentary or alteration processes to mechanically sort minerals, the mineralogy of lunar rocks is greatly restricted (Chapter 2). Third, even though large impacts may have exhumed deeply buried rocks, high-pressure mineralogy is restricted because of the low lunar pressure gradient (~ 5.3 MPa per km or 1 kbar per 19 km). Fourth, because the Moon cooled early in its history compared to larger bodies such as Mars, Venus, and Earth, most lunar rocks have not been extensively reprocessed (metamorphosed or melted repeatedly) except as associated with impacts. Thus, big surprises in terms of new lunar rock types are not likely to be encountered in future exploration. As discussed below, however, rocks from deep within the lunar crust (and mantle, as in mantle xenoliths) are not well represented among the samples (or not at all) and the full range of basalt types has not yet been sampled.

The Lunar Sourcebook subdivided lunar igneous rocks into “mare basaltic lavas and related volcanic rocks” and “pristine highland rocks” (Taylor *et al.* 1991). This scheme was generally followed in *Planetary Materials* (Papike *et al.* 1998). It is not our intent here to

revise the classification scheme. Instead, the focus is on the makeup of the crust and mantle of the Moon and on relating rock types to geochemical or mineralogical signatures at the surface of the Moon (Chapter 2). Thus, while the grouping of major rock types in this chapter differs somewhat from groupings associated with some previous classifications, it is essentially the same as that adopted by Warren (1993). This section focuses on the *crustal* rock types, including the ferroan anorthositic, magnesian and alkalic intrusive suites, KREEP basalts, and polymict breccias produced by impact mixing of the primary rock types. Mare basalts and volcanic glasses are covered in more detail as samples of the mantle in Section 3.1 and in Chapter 4. Herein, we refer to the glasses as “volcanic glasses,” but this is essentially the same as referred to elsewhere as “pyroclastic” glasses, and in those cases where MgO contents are sufficiently high (~15 wt% or greater), we also use the term “picritic” glasses.

The crustal igneous rocks, also referred to as “pristine igneous” rocks (Warren 1993; Papike et al. 1998), are almost exclusively plagioclase rich, and the plagioclase is almost exclusively calcic, with anorthite (An) contents typically much greater than 50%, and most greater than 90% (Fig. 3.2). The major mafic silicate minerals are pyroxene and olivine, with pyroxene dominated by the orthorhombic, low-Ca variety. Thus the major rock types are anorthositic (*sensu stricto* >90 vol% plagioclase), norite, troctolite, and rarely (at least among the samples) gabbro (see Table 3.1). The nomenclature of Stöffler et al. (1980) incorporates intermediate rock types and is followed here. Rarer rock types include spinel troctolite, feldspathic lherzolite, dunite, granite or felsite (fine-grained texture, granitic assemblage), monzogabbro, and quartz monzodiorite (QMD). Although the plagioclase anorthite (An) content typically exceeds 50%, which dictates use of the term “gabbro” (Streckeisen 1976; Le Maitre 1989), “quartz monzodiorite” has heritage in previous lunar studies, and thus the term is retained for lunar samples that have been described previously as QMD. The use of the word “pristine” refers to the set of characteristics that distinguish a rock as having originated by magmatic processes related to the intrinsic thermal properties of the Moon and not as a result of impact-induced melting. The key distinguishing characteristic is very low siderophile-element concentrations because these elements are added in high concentration by most impacting materials and provide an effective tracer of the impact process. Other characteristics include compositions that are consistent with an igneous process as opposed to mixtures of disparate rock types of known composition. The pristine designation represents a means to restrict the lunar igneous rock sets to those rocks that truly formed by internally generated magma processes. The distinction, however, becomes blurred in light of the possibility that large impact-melt bodies associated with the largest impact basins may have been many kilometers thick and may have differentiated (e.g., Sudbury, see Chapter 5). In zones that cooled slowly and where gravitational differentiation occurred, sinking metal might have effectively scavenged siderophile trace elements. Recognizing a sample as being pristine is important in order to assess processes related to the internal igneous differentiation of the Moon.

The crustal igneous rocks have been subdivided into suites according to their major mineral compositions, and in some cases other characteristics such as trace-element signatures and isotopic systematics correspond to these subdivisions. Objections to calling the subdivisions “suites” may be raised on the grounds that the term “suite” implies a petrogenetic relationship (Papike et al. 1998) and such may not be the case. Here, the term “suite” is retained for major groupings and objections are addressed in the following sections. The ferroan-anorthositic suite includes those rocks whose plagioclase is highly calcic (An content generally >94) and whose mafic silicates, either pyroxene or olivine, have relatively high Fe/Mg values (Fig. 3.2). The magnesian suite includes rock types whose mafic silicate minerals have high values of Mg/Fe and whose plagioclase compositions cover a range of An contents that are correlated with their Mg/Fe values. Rocks of the magnesian suite have high values of Mg/Fe relative to their An contents, but they are not all necessarily “magnesium rich” (see rock compositions in the online RIMG supporting materials at www.minsocam.org, Tables A3.1–A3.12). The

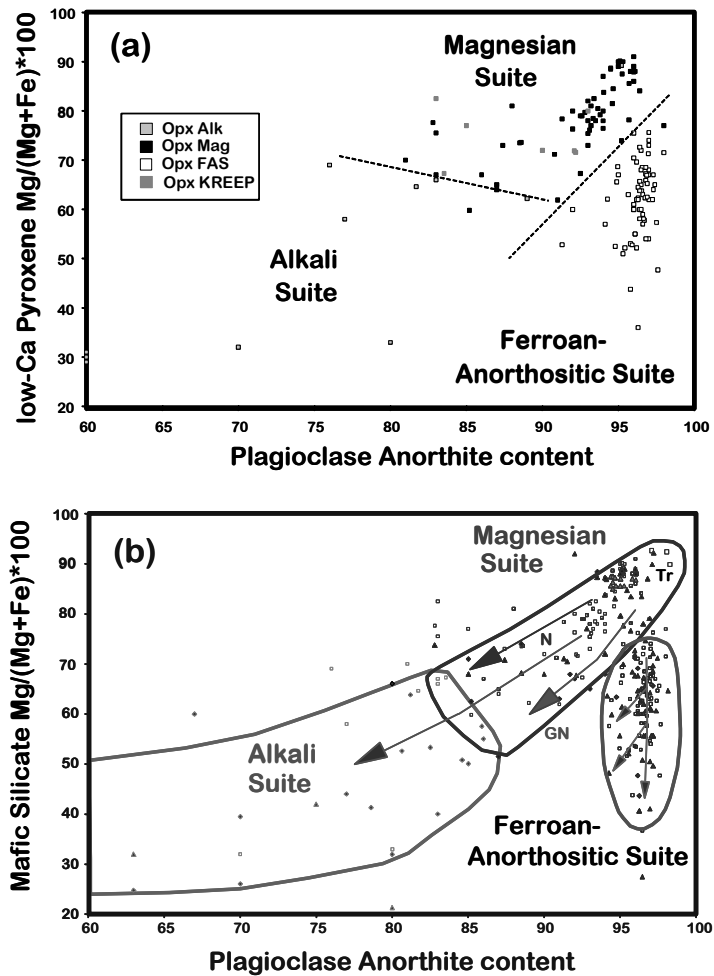


Figure 3.2. $Mg/(Mg+Fe)$ in mafic silicates vs. anorthite content, $Ca/(Ca+Na+K)$, of coexisting plagioclase in lunar crustal igneous rocks. (a) Orthopyroxene $Mg/(Mg+Fe)$ vs. coexisting plagioclase An content, showing rock types divided into a ferroan-anorthositic suite (high An content and relatively ferroan orthopyroxene), magnesian suite (high Mg at high An, ranging to lower Mg at lower An), and alkali suite (plagioclase relatively enriched in Na and K, and relatively ferroan mafic silicates). Dashed lines represent values typically used to distinguish groups. Data are from the compilation by Warren (1993), supplemented with additional data from Papike et al. (1998). (b) $Mg/(Mg+Fe)$ for all mafic silicates (olivine, low- and high-Ca pyroxene) vs. coexisting plagioclase An content for the intrusive igneous rock suites and KREEP basalts. Typical trends resulting from fractional crystallization (arrows) suggest a possible relationship between the magnesian- and alkali-suite rocks. The overall trend from upper right to lower left is similar to trends observed for rocks of terrestrial layered mafic intrusive bodies and is the general trend of fractionation of the minerals of KREEP basalt as determined from early crystallizing cores to late rims. The ferroan-anorthositic and Mg suites are difficult to relate through a common magmatic process. The near-vertical trend of the ferroan-anorthositic suite requires a more complex petrogenetic scenario (Herbert et al. 1978; Longhi and Boudreau 1979; Raedeke and McCallum 1980). Specific groups within the magnesian suite such as the norites (N) and gabbronorites (GN) appear to differ petrogenetically from each other and thus are shown associated with different fractionation trends (arrows) (e.g., James and Flohr 1983). Mineral compositions of troctolite (Tr) tend to be at the magnesian and anorthitic end of the trend.

Table 3.1. Nonmare pristine rocks according to mass and landing site, Apollo samples.

Igneous Rock Suite		grams	A11	A12	A14	A15	A16	A17
Ferroan	<i>sum, >1 g, pristinity >5</i>	9474	0	0	0	280	9186	8
Anorthosite Suite	anorthosite	9174	0	0	0	279	8887	8
	noritic anorthosite	174	0	0	0	1.1	173	0
	troctolitic anorthosite	6	0	0	0	0	6	0
	anorthositic norite	120	0	0	0	0	120	0
Magnesian Suite	<i>sum, all listed samples</i>	2593	0	1.4	17	222	10	2342
	norites (> 0.5 g)	1563	0	0	1.6	212	0	1350
	gabbronorite	310	0	0	0.4	0	8	301
	troctolite	656	0	0	14	3	0.7	636
	spinel-troctolite	9.2	0	1.3	0.01	7.5	0.4	10
	ultramafic	56	0	0.1	0.4	0	0	55.2
Alkali Suite	<i>sum, all listed samples</i>	14.3	0	1.7	7.8	3.7	0.5	0.6
	Alkali anorthosite	3.9	0	0.45	3.33	0.10	0	0
	alkali norite	2.8	0	0.08	1.60	0.04	0.45	0.60
	alkali gabbronorite	0.2	0	0	0.23	0	0	0
	alkali troctolitic anorth.	0.2	0	0	0.23	0	0	0
	felsite (granite)	3.6	0	1.20	2.32	0.01	0	0.02
	monzogabbro (QMD)	3.6	0	0	0.06	3.54	0	0
KREEP Basalt	sum, all listed samples	17.9	0	0	0.02	15.1	0.04	2.7

Footnotes: Values are derived from data in Planetary Materials, RiM-G Vol. 36 (Papike et al. 1998). Pristinity refers to grading scale as developed and applied by Warren (1993). Spinel troctolite in Apollo 17 samples estimated from descriptions of large clasts in 72395 and 72435 (Dymek et al. 1976).

“alkali” suite includes rock types for which Na and K contents are high compared to those of the magnesian suite. A growing body of evidence points to a relationship between KREEP basalt and members of the magnesian and alkali suites (Jolliff et al. 1993; Snyder et al. 1995b), thus these are discussed in succession. The following sections refer to Table 3.1 to illustrate the distribution of igneous rock types as a function of landing site and, broadly, their spatial location and abundance relative to major geochemical provinces or “terranes.” This table contains a sample selection bias in that it derives from well-known (published) analyzed samples, thus igneous rocks that occur as clasts in breccias are under-represented. However, the compilation points to trends that appear to be robust, such as the high concentration of ferroan anorthosite at Apollo 16. When combined with global remotely sensed data and data from the lunar meteorites, information derived from this simple tabulation provides important constraints for the distribution of these important rock types.

In the following sections, descriptions of rock distribution and chemical compositions are intended to focus on those aspects relating to the integration of sample and remote-sensing information. For example, chemical compositions are discussed according to their FeO, TiO₂, and Th content so as to highlight possible relationships to global compositional maps and variations in concentrations of these relatively well-determined elements.

2.1.1. Ferroan-anorthositic suite. The ferroan-anorthositic rocks are chemically and mineralogically distinct from other lunar igneous rock groups (see also Chapter 2). Although rare in the Apollo 11, 12, 14, and 17 samples, rocks of this suite were found among the Apollo 15

samples and they dominate the Apollo 16 and Luna 20 samples. The two key aspects of the ferroan-anorthositic suite (FAS) embodied in the name provides the motivation for grouping these rocks together and for inferring a specific petrologic relationship. First, the majority of samples of FAS rocks are highly anorthositic, that is they contain very little other than plagioclase. Of the large rocks listed in the compilation of Warren (1993), only a handful of the FAS rocks contain more than 10% of the mafic silicates pyroxene and olivine. The FAS rocks contain few to none of the common minor or accessory minerals such as ilmenite, spinel, phosphates, or zircon. The modal mineralogy of the FAS rocks coupled with relatively coarse relict grain size and cumulus texture, where such texture is preserved, clearly indicate formation by a cumulus igneous process. The very high plagioclase content of the FAS rocks (>90%) is a defining characteristic of the suite. Nevertheless, at the end of this section we review the possibility that not all FAS rocks throughout the crust, laterally and with depth, are so highly anorthositic.

The second major aspect embodied in the title of “ferroan anorthositic suite” is that the mafic silicates are ferroan in composition, that is, the mafic silicates have a relatively low (atomic) Mg/(Mg+Fe) ratio. This characteristic is not simply a matter of definition because among the demonstrably igneous lunar rocks, there exists a gap in the Mg/(Mg+Fe) values at high plagioclase An content (see Fig. 3.2a). Furthermore, several other key geochemical signatures discussed below correspond to the low Mg/(Mg+Fe) values. There is petrologic significance to the combination of highly calcic plagioclase (anorthite) and ferroan mafic silicates. Experience from terrestrial layered mafic rock bodies suggests that simple igneous differentiation that produces rocks such as troctolite, norite, and gabbro would give a trend with a positive slope on a plot of the Mg/(Mg+Fe) ratio of coexisting mafic silicates vs. plagioclase An content, such as shown in Figure 3.2b. As crystallization proceeds, plagioclase compositions progress from calcic to sodic and coexisting mafic silicate compositions, from magnesian to ferroan. What sets the FAS rocks apart is the consistently high Ca content of plagioclase with little regard for variations in the Mg/(Mg+Fe) values of the coexisting mafic silicates. Such a trend (or lack of a trend) requires special petrogenetic explanations. Raedeke and McCallum (1980) showed that rocks of the terrestrial Stillwater Complex, which includes thick anorthosite layers, also show a vertical trend at high An, similar to the lunar FAS rocks. They attributed these trends to a process of equilibrium crystallization of intercumulus melt in a plagioclase-rich mush. Longhi and Ashwal (1985) proposed a two-stage formation and emplacement process that would further explain the separation of plagioclase-rich rocks from co-crystallizing mafic silicates and trapped melt. In general, this characteristic of FAS rocks and the history and processes of their emplacement have been the focus of much study (e.g., Longhi 1977, 1980; Longhi and Boudreau 1979; Raedeke and McCallum 1980; Longhi and Ashwal 1985; James *et al.* 1989; Jolliff and Haskin 1995; Floss *et al.* 1998) and remain among the outstanding questions of lunar petrology.

Mineralogy and mineral modes. Most of the FAS samples are indeed rich in plagioclase, with a mass weighted average of about 96%. However, some rocks consist of over 20% pyroxene (the range for samples greater than one gram is 77–99% plagioclase). Pyroxene is typically more abundant than olivine in the FAS rocks and, in some samples, high-Ca pyroxene is present as well as pigeonite and hypersthene (see Table 3.2). Because of ferroan bulk compositions, pigeonite (or inverted pigeonite, see below) is also common. At more magnesian compositions [Mg/(Mg+Fe) > 0.7], high- and low-Ca pyroxenes are found, but not pigeonite. Of the large rock samples, only one is olivine rich (62237; 62 g). The major mineral assemblage is important because it constrains the composition of the melt that crystallized these minerals to lie generally along the plagioclase-pyroxene cotectic. This constraint in turn is important for petrologic models of the crystallization of magma systems to produce FAS rocks. According to models of magma-ocean crystallization, much of the magma ocean solidified as olivine plus pyroxene cumulates, but by the time plagioclase began to crystallize, the dominant mafic silicate would have been pyroxene, not olivine.

Table 3.2. List of ferroan anorthosites with mass exceeding 1 gram.

Sample	Rock type	estimated mass (g)	~modal % feldspar	weighted % feldspar		Main reference
				all	w/o 60015	
60015	anorthosite	4600	99	48.069		Ryder & Norman (1979, 1980)
60025	anorthosite	1836	90	17.442	33.904	James et al. (1991)
62255	anorthosite	800	97	8.191	15.922	Ryder and Norman (1979)
62275	anorthosite	443	93	4.349	8.453	Warren et al. (1983a)
60215c30	anorthosite	300	97	3.072	5.971	Rose et al. (1975)
61015	anorthosite	300	96	3.040	5.909	James et al. (1984)
65315	anorthosite	285	99	2.963	5.760	Ebihara et al. (1992)
15415	anorthosite	269	99	2.811	5.464	Ryder (1985)
60135	norite	120	77	0.975	1.896	Ryder and Norman (1980)
64435c210A	anorthosite	100	98	1.034	2.011	James et al. (1989)
65325	anorthosite	65	99	0.676	1.314	Warren and Wasson (1978)
62237	noritic anorthosite	62	85	0.560	1.088	Ebihara et al. (1992)
62236	noritic anorthosite	57	86	0.520	1.011	Nord and Wandless (1983)
67075c17	anorthosite	50	96	0.507	0.985	Haskin et al. (1973)
67915c12-1	noritic anorthosite	50	85	0.449	0.872	Taylor and Mosie (1979)
60055	anorthosite	36	98	0.367	0.714	Ryder and Norman (1980)
60515	anorthosite	17	95	0.170	0.331	Warren et al. (1983a)
60056	anorthosite	16	95	0.160	0.312	Warren et al. (1983a)
60639c19	anorthosite	10	99	0.104	0.203	Warren and Wasson (1978)
67635	anorthosite	9.1	92	0.088	0.172	Stöffler et al. (1985)
65327	anorthosite	7.0	99	0.073	0.141	Warren and Wasson (1978)
77539c15	anorthosite	6.2	99	0.065	0.125	Warren et al. (1991)
64435c239	troctolitic anorth.	6.0	83	0.053	0.102	James et al. (1989)
15295c41	anorthosite	5.3	99	0.056	0.108	Warren et al. (1990)
15362	anorthosite	4.2	98	0.043	0.084	Ryder (1985)
67636	anorthosite	3.2	97	0.033	0.064	Stöffler et al. (1985)
67035c26	gabbroanorthitic anorth.	2.3	80	0.019	0.038	Warren (1993)
67637	anorthosite	2.3	96	0.023	0.045	Stöffler et al. (1985)
65767c3	anorthosite	2.0	98	0.021	0.040	Dowty et al. (1974)
67016c346	anorthosite	2.0	95	0.020	0.039	Norman and Taylor (1992)
67455c30	anorthosite	1.7	95	0.017	0.033	Ryder and Norman (1978)
73217c35	anorthosite	1.7	95	0.017	0.033	Warren et al. (1983a)
67539c7	anorthosite	1.5	96	0.015	0.029	Stöffler et al. (1985)
15437	troctolitic anorth.	1.1	80	0.009	0.018	Ryder (1985)
67915c26	noritic anorthosite	1.0	85	0.009	0.017	Marti et al. (1983)
67535	anorthosite	0.99	93	0.010	0.019	Stöffler et al. (1985)
Sum		9473.8		96.03	93.23	
Sum w/o 60015		4873.8				

Source of data: Papike et al., 1998; Planetary Materials, Warren, 1993 (pristinity index >5).

Taking the modal proportion of plagioclase weighted according to mass, then of the listed large FAS rocks, the average proportion of plagioclase is about 96%. Owing to the fact that 60015 contains nearly half the mass and is estimated to contain 99% plagioclase, the mass-weighted average may be biased. Excluding 60015, the mass-weighted average proportion of plagioclase drops to 93%.

FAS summary by Apollo landing site (g):

A15	280
A16	9180
A17	8

Minor or trace minerals found in the ferroan anorthositic rocks include ilmenite, aluminous Cr spinel, troilite, Fe-Ni metal, and an Si phase (Papike *et al.* 1998). Minerals that would signal the presence of trapped melt such as the phosphates, zircon, and K-feldspar are not found in these rocks. Their absence indicates a cumulus formation process that very efficiently excluded late-stage trapped melt (e.g., Morse 1982). Recrystallization textures or subsolidus annealing is evident in many FAS samples, leaving open the possibility that low-melting accessory minerals might have been lost during a metamorphic episode (Phinney 1994).

Compositions. The FAS rocks are compositionally distinctive. Because most are rich in calcic plagioclase, most compositions are highly aluminous. Some of the distinguishing geochemical traits include very low incompatible-element concentrations (Taylor *et al.* 1991), high Sc/Sm (typically >10 ; Norman and Ryder 1980), 0.6-1.0 ppm Eu concentrations (Korotev and Haskin 1988; Jolliff and Haskin 1995), and low Cr/Sc (see Table A3.1 and Norman and Ryder 1980). High Sc concentrations are consistent with the abundance of ferroan pyroxene because in lunar rocks, Sc correlates closely with Fe^{2+} . Low Cr/Sc is consistent with formation of these rocks following extensive crystallization of mafic cumulates, including chromite and Cr-bearing pyroxenes (i.e., upper-mantle cumulates). Owing to the low oxygen fugacity, evidenced by the stability of Fe-metal, Eu is predominantly divalent and is enriched in plagioclase relative to the trivalent REEs. Since incompatible trace elements are so low in concentration in FAS rocks, whole-rock compositions exhibit large positive Eu anomalies.

The very low incompatible-trace-element concentrations are consistent with the virtual absence of late-stage accessory minerals. Calculated equilibrium melt compositions during the interval of plagioclase crystallization from the magma ocean have trace-element concentrations within about a factor of ten to fifty times chondritic values (Snyder *et al.* 1992b; Jolliff and Haskin 1995; Papike *et al.* 1998), indicating their formation from relatively unevolved melt (i.e., other than fractionation associated with the crystallization of olivine and pyroxene from a magma ocean beginning with trace-element concentrations at several times chondritic). Among the elements well determined by remote sensing, surface FeO concentrations span a range from the extremely low values of <1 wt% of nearly pure anorthosite to 15 wt% in ferroan norite, but the average

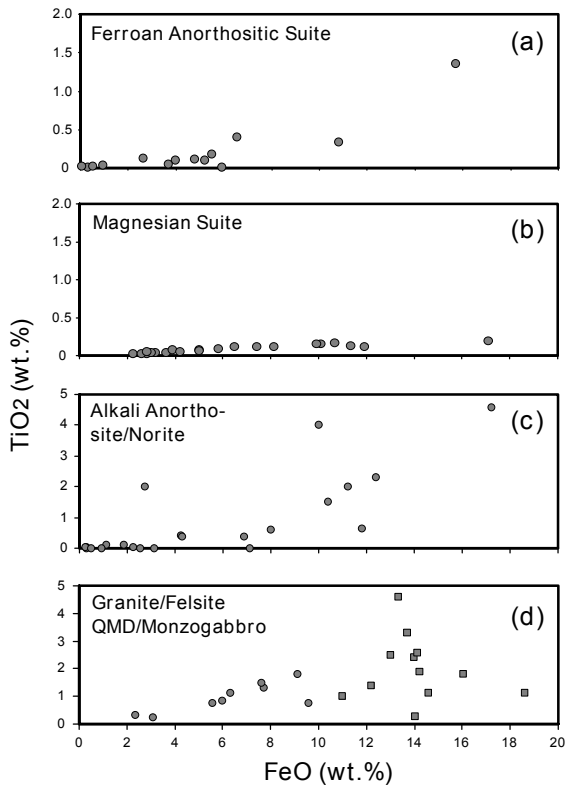


Figure 3.3. TiO_2 vs. FeO for crustal igneous rock suites. In (d), compositions with >10 wt% FeO have been arbitrarily considered to be QMD or monzogabbro (squares), even though some of those with <10 wt% FeO may have too much FeO and too little SiO_2 to be considered granite. Note different TiO_2 scales between the upper two and lower two plots.

concentration (excluding mare basalts) is around 4 wt%. Concentrations of TiO_2 and Th are extremely low in all of the FAS rocks (see Figs. 3.3 and 3.4).

Age relationships. The FAS rocks are isotopically very primitive and extremely old. Values of $^{87}\text{Sr}/^{86}\text{Sr}$ are nearly as low as primitive meteorites and indicate formation from an unfractionated reservoir. Although age determinations using different isotopic systems vary, Sm-Nd internal isochrons for two rocks yield ages of 4.44 and 4.54 Ga (see Fig. 3.5), providing a firm link between formation of the FAS rocks and the early differentiation of the Moon. Recent determinations of Sm-Nd isochron ages of 4.29 and 4.4 Ga (Norman et al. 1998; Borg et al. 1999; Norman et al. 2003) might imply that FAS rocks formed (or remained very hot) over an extended period of perhaps two hundred million years or more, or that the younger of the FAS ages were somehow disturbed or reset. Some of the FAS samples also appear to have extremely positive ε_{Nd} values ($\varepsilon_{\text{Nd}} = +3.1$ for 62236) indicating that these could have formed from reservoirs previously depleted of light rare-earth elements (standard magma-ocean crystallization models predict $\varepsilon_{\text{Nd}} \sim 0$). Alternatively, Norman et al. (2003) have suggested that the plagioclase fractions may have been affected by subsequent reequilibration, whereas the mafic fractions of the ferroan anorthosites define a crystallization age of 4.46 ± 0.04 Gyr. If the positive ε_{Nd} of 62236 is real, then its relatively young age combined with the recrystallized nature of some of the ferroan

rocks may record an event such as recrystallization associated with remobilization of FAS cumulates, or perhaps underplating of anorthositic materials by later-formed magmas. The magmatic evolution of FAS rocks is addressed in detail in Section 3 of Chapter 4.

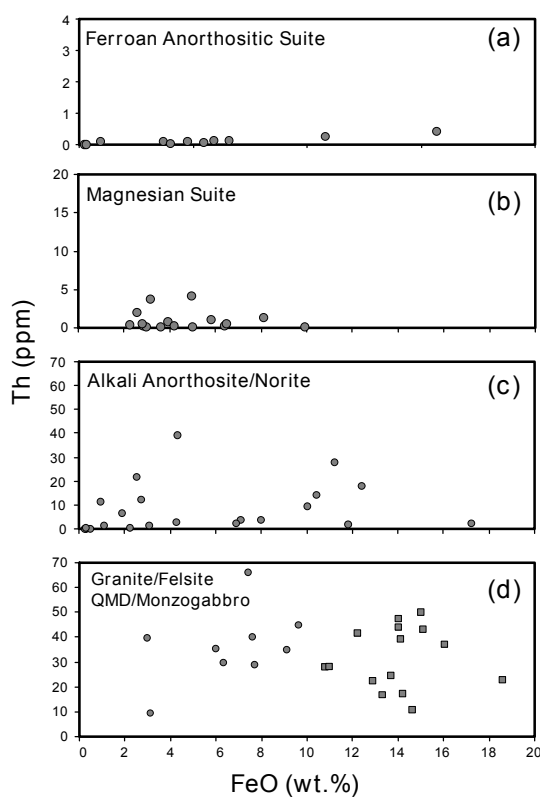


Figure 3.4. Th vs. FeO for crustal igneous rock suites. In (d), compositions have been arbitrarily assigned to granite for those samples with $\text{FeO} < 10$ wt% and QMD/monzogabbro for $\text{FeO} > 10$ wt% (squares). Note different Th scales.

Depths of origin. The textures and mineralogy of FAS rocks indicate that they crystallized at least in part slowly and over a range of depths. Major mineral compositions are well equilibrated, and elements that can be enriched during rapid crystallization such as Al in pyroxene and Ca in olivine are low in concentration in these minerals. In terrestrial rocks, Al can also be incorporated in pyroxene as a result of high pressure, but other characteristics of the rocks would permit distinguishing such effects. Pyroxene grains in FAS rocks are typically exsolved (low-Ca and high-Ca separation), and in some samples, plagioclase contains exsolved grains of pyroxene and other minerals (e.g., Jolliff and Haskin 1995; Norman et al. 2003). Unfortunately, there are no direct and sensitive mineralogical indicators of pressure in the FAS rocks, so the next best method to assess

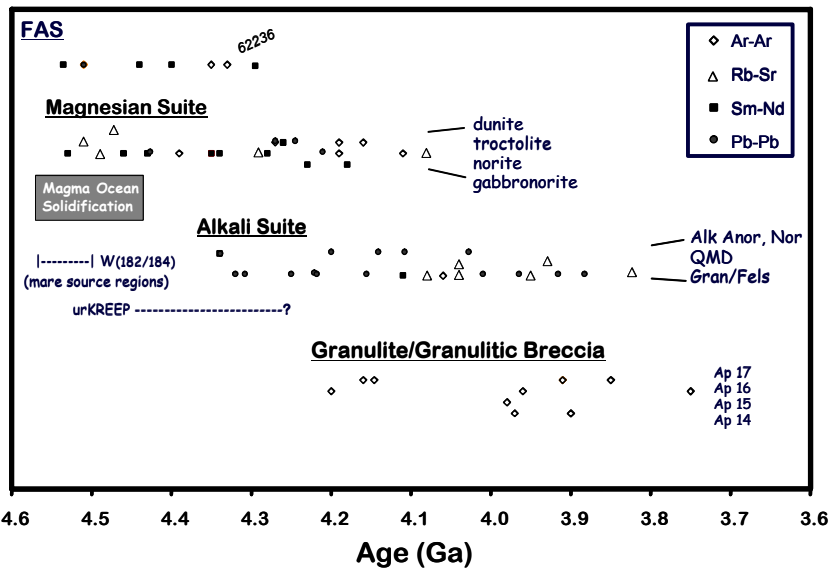


Figure 3.5. Crystallization ages of selected crustal rock suites. Time spans indicating magma-ocean solidification and the extended period for urKREEP crystallization are interpretive. The time span for development of the mare source regions based upon W(182/184) systematics is meant to indicate a rapid magma-ocean crystallization of the mare source (see Chapter 4). The Sm-Nd age of sample 62236 (Borg et al. 1999) is surprisingly young (see discussion in text). For other ages and data sources, see Chapter 5, Table 5.6.

depth of formation is to estimate cooling rates from features such as compositions and widths of exsolution lamellae or the ordering of cations in pyroxene (McCallum and O'Brien 1996). Of the samples studied so far, none indicate depths of origin exceeding 25 km (McCallum and O'Brien 1996). On the basis of exsolution features in FAS rocks from North Ray Crater, Apollo 16, Jolliff and Haskin (1995) inferred a two-stage cooling and depth history that was initially slow and deep, and later rapid and shallow, as postulated by Longhi and Ashwal (1985). McCallum and Schwartz (2001) suggested a two-stage process of solidification at 4.5 Ga and partial melting at 4.3 Ga, coupled with the removal of melt bearing a high Sm/Nd component, to explain the isotopic characteristics of rock 67215.

Distribution. Because the Apollo 16 site, where FAS rocks are so abundant, was thought early in post-Apollo studies to be representative of the feldspathic lunar highlands, a logical inference was that rocks of the ferroan-anorthositic suite should be the main component of the feldspathic highlands. Global remote sensing, mainly of FeO and Th concentrations, showed that the Apollo 16 site was, however, not as representative of the feldspathic highlands as once thought. Concentrations of FeO and Th in regolith at the Apollo 16 site are higher (5.5 wt% FeO, 1.8 ppm Th) than much of the feldspathic highlands of the lunar far side (4.5 wt% FeO, <1 ppm Th). Examination of the Apollo 16 regolith shows that this difference results largely from the presence of mafic impact melt, delivered to the site probably as part of ejecta deposits related to the Imbrium, Serenitatis, and/or Nectaris events (Haskin et al. 2002). The question remains as to just how anorthositic the pre-basin substrate at this site might have been. After subtraction of the impact-melt component and exotic mare basalt components (Korotev 1997), the remaining Cayley Plains regolith composition apparently has <4 wt% FeO and ~30 wt% Al₂O₃, but an Mg/(Mg+Fe) of ~0.7, somewhat higher than expected if the soil is composed predominantly of FAS components. Stöffler et al. (1985) did a similar mixing model and cast the results into

the following rock components: 86–87% anorthosite, 6–8% magnesian gabbronorite, 4% ferrogabbro, ~2% dunite, ~1% feldspathic lherzolite, and a trace of spinel troctolite.

Samples of regolith from the ejecta deposits of North Ray Crater are poor in mafic impact-melt components and are more directly representative of typical feldspathic highlands materials (Stöffler et al. 1985; Norman et al. 1995, 2003). The North Ray Crater regolith and the large feldspathic fragmental boulders strewn about its rim appear to be more dominated by FAS components (see also Jolliff and Haskin 1995; Korotev 1996, 1997; Norman et al. 2003) than the Cayley regolith, and the most ferroan regolith compositions are very similar to the most ferroan feldspathic lunar meteorites (see also Chapter 2).

2.1.2. Magnesian suite. The magnesian-suite rocks include pristine lunar rocks for which $Mg/(Mg+Fe)$ values (Mg') of mafic silicates range from about 0.95 to 0.6, coupled with systematic variations in the An content of coexisting plagioclase from about 98% to 84% (see Fig. 3.2). As implied by the term “magnesian,” these rocks have relatively magnesian compositions for their plagioclase anorthite content, compared to the other major igneous suite, the FAS rocks. All members of this suite, however, are not necessarily *magnesium rich*, especially the more anorthositic members (see Table A3.2). Although the general trend of decreasing Mg' with decreasing An content resembles trends observed for different rock types of terrestrial layered intrusives (Raedeke and McCallum 1980), inclusion of the diverse members within the magnesian suite does not necessarily imply a petrogenetic relationship among all members. On the contrary, subgroups exist that appear to be unrelated to one another (e.g., James 1980; Papike et al. 1998). For this reason, the magnesian-suite rocks have been considered to represent intrusions into the early lunar crust, which is presumed to have been ferroan anorthositic.

Mineralogy, mineral modes, rock types. The major minerals of the magnesian-suite rocks are plagioclase, low-Ca pyroxene, and olivine, plus minor amounts of high-Ca pyroxene, and, in some cases, pleonaste (Mg-Al) spinel. The most common accessory minerals include ilmenite, the phosphates apatite and RE-merrillite (whitlockite), troilite, zircon, baddeleyite, chromite, and rarely cordierite, silica, K-feldspar, niobian rutile, zirconian armalcolite, zirconolite, and Fe metal (see Table A3.2). The main rock types are norite, troctolite, spinel troctolite, and gabbronorite, plus more feldspathic variations, such as noritic anorthosite (or, in terrestrial rock nomenclature, leuconorite). Several “ultramafic” assemblages are found among the Apollo samples that are rich in pyroxene and/or olivine (see Table 3.3), but of these, most are tiny rock fragments with the notable exception of a dunite (72415-8, with a total mass of 55 g) collected at the Apollo 17 site. Others of the very small rock fragments listed in the table may not represent the modal mineralogy of their parent rocks. Of the samples listed by Warren (1993), norites are the most abundant according to mass, followed by troctolites and gabbronorites, however, in all cases, the sample masses are dominated by a few large rock samples collected at the Apollo 17 site (Papike et al. 1998). The proportions of rock types present at a given landing site can also be determined by coupled analyses of the soils and rock fragments contained therein (e.g., Bence et al. 1974; Jolliff et al. 1991b, 1996). Lithologic proportions determined in this way reflect the same general systematics of rock distribution as indicated by the larger samples, including the predominance of the magnesian suite among the nonmare igneous rock types found at the Apollo 17 site.

Compositions. Major-element compositions of the magnesian-suite rocks vary widely, as shown in Table A3.2. This variation results partly from the fact that most samples are small, and many are unlikely to be representative of the larger rocks from which they were derived. Among the rocks listed in Table A3.2, MgO , for example, ranges from 7 wt% (an anorthositic norite) to 45 wt% (dunite) and Al_2O_3 ranges from <2 wt% (dunite) to nearly 29 wt% (troctolitic anorthosite). Because of the small and potentially unrepresentative sample sizes, mineral assemblage and mineral chemistry have been used as the main criteria for classification, as described above. Still, numerous compositional features serve also to distinguish members of

Table 3.3. List of magnesian-suite intrusive rocks.

Sample	mass (g)	~Plag An mol%	~Low-Ca ppxroxene Mg#	~Olivine Mg#	~Modal % feldspar	Main reference
Troctolite						
76335	465	96	88	87	77	Warren and Wasson (1978)
76535	155	96	86	88	50	Ryder and Norman (1979)
76536	10.3	—	86	83	70	Warren and Wasson (1979)
14321c1020	9.2	95	89	86	70	Lindstrom <i>et al.</i> (1984)
15455c106	3.0	95	85	83	71	Warren and Wasson (1979)
73146	3.0	95	88	86	85	Warren and Wasson (1979)
14303c194	2.0	95	—	88	70	Warren and Wasson (1980)
76255c57("U5B")	2.0	96	91	89	77	Ryder and Norman (1979)
12071c10	1.3	70	—	—	—	Warren <i>et al.</i> (1990)
14304c95("a")	0.9	94	—	87	55	Goodrich <i>et al.</i> (1986)
60035c21	0.7	96	89	88	57	RD Warner <i>et al.</i> (1980)
14172c11	0.7	94	—	87	65	Warren and Wasson (1980)
14179c6	0.7	94	—	87	70	Warren <i>et al.</i> (1981)
14321c1024	0.7	95	—	80	85	Warren <i>et al.</i> (1981)
73235c127	0.7	96	86	83	60	Warren and Wasson (1979)
14305c264	0.2	70	—	—	—	Warren and Wasson (1980)
14305c279	0.2	85	—	—	85	Warren <i>et al.</i> (1983)
sum mass	655.5					
Spinel-troctolite						
15445G (F?)	4.0	—	—	90	50	Ryder and Norman (1979)
15445c71-A	1.5	92?	—	92	35	Ridley <i>et al.</i> (1973), Ryder (1985)
12071c10	1.3	97	—	>78	70	Warren <i>et al.</i> (1990)
65785c4	0.3	96	84	83	65	Dowty <i>et al.</i> (1974b)
67435c77	0.1	97	—	92	40	Ma <i>et al.</i> (1981b)
14304c109("q")	0.0003	94	—	87	?	Goodrich <i>et al.</i> (1986)
15455 H	2?	96	91	92	25	Baker and Herzberg (1980)
15295 c	—	93	—	91	75	Marvin <i>et al.</i> (1989)
72435	—	96	70	73	~80	Dymek <i>et al.</i> (1976)
73263 particles	—	96	90	90	~70	Bence <i>et al.</i> (1974)
76503 particles	—	96	90	90	~70	Bence <i>et al.</i> (1974)
77517c disagg	—	97	90	90	—	RD Warner <i>et al.</i> (1978b)
sum mass	9.2					
Ultramafic						
72415/8 Dunite	55.2	94	87	87	4	Ryder and Norman (1979)
12033;503 Harzburgite	0.1	—	91	89	—	Warren <i>et al.</i> (1990)
14161;212,1 Peridotite	<0.1	—	87	85	1	Morris <i>et al.</i> (1990)
14161;212,4 Dunite	<0.1	—	—	85	—	Morris <i>et al.</i> (1990)
14304c121("d")	0.1	—	—	89	—	Warren <i>et al.</i> (1987)
14305c389 Pyroxenite	<0.1	—	91	90	1	Shervais <i>et al.</i> (1984a)
14321c1141 Dunite	0.1	—	—	89	2	Lindstrom <i>et al.</i> (1984)
sum mass	55.5					
Norite						
77075/77215	840	91	71	—	55	Ryder and Norman (1979)
78235/78255	395	93	81	—	47	Warren and Wasson (1979a)
15455c228	200	93	83	—	70	Ryder (1985)
77035c130	100	93	79	—	60	Warren and Wasson (1979)
15445c17("B")	10	95	82	—	63	Shih <i>et al.</i> (1990)
72255c42	10	93	75	—	40	Ryder and Norman (1979)
78527	5.2	93	80	77	50	Warren <i>et al.</i> (1983b)
14318c146	1.5	87	73	71	55	Warren <i>et al.</i> (1983b)
15361	0.9	94	84	—	40	Warren <i>et al.</i> (1990)
15360;11	0.7	93	78	—	65	Warren <i>et al.</i> (1990)
14318c150	0.5	83	78	74	65	Warren <i>et al.</i> (1986)
78236,3	—	—	—	—	—	Blanchard and McKay (1981)
sum mass	1563.8					
Gabbronorite						
76255c82("U4")	300	87	65	—	41	Warren <i>et al.</i> (1986)
67667	7.9	91	78	71	24	Warren and Wasson (1979a)
73255c27,45	0.9	89	74	—	53	James and McGee (1979)
61224;6	0.3	83	67	—	34	Marvin and Warren (1980)
14311c220	0.2	85	60	—	75	Warren <i>et al.</i> (1983c)
76255c72("U5A")	0.1	86	67	—	39	Ryder and Norman (1979)
14161;7044	<0.1	88	64	—	60	Jolliff <i>et al.</i> (1993)
14304c114("h")	<0.1	89	—	68	40	Goodrich <i>et al.</i> (1986)
sum mass	309.5					

Troctolites and norites listed for those samples larger than 0.5 g; for others, all samples documented by Warren (1993) and Papike *et al.* (1998) are listed. All of the "ultramafic" rocks except the Apollo 17 dunite are tiny rock fragments or clasts. Whether they actually represent larger ultramafic rocks is not certain. Sample 67667 also referred to as feldspathic lherzolite (Stöffler *et al.* 1985).

this rock suite. TiO_2 values are typically low, rarely exceeding 1 wt% and averaging less than 0.5 wt% (Table A3.2). Values of $\text{Mg}/(\text{Mg}+\text{Fe})$ vary systematically and correlate positively with $\text{Ca}/(\text{Ca}+\text{Na}+\text{K})$. Among the trace elements, the magnesian-suite rocks are distinguished from FAS rocks by low Sc/Sm and high Cr/Sc ratios. Most of the magnesian-suite rocks are cumulates that do not contain representative proportions of trapped melt, so bulk incompatible-element concentrations tend to be fairly low, albeit significantly higher than FAS rocks by 1–2 orders of magnitude. Some, however, have high incompatible element concentrations, and ion-microprobe analyses of REE concentrations in magnesian-suite silicates, especially pyroxene and plagioclase, have shown relatively high concentrations for these minerals (Papike et al. 1994, 1996; Shervais and McGee 1998).

In fact, much has been made in the past decade about the apparent trace-element enrichment of the magnesian-suite rocks (or their parent melts) despite the fact that most have very small trapped-melt components. Early studies of rocks such as troctolite 76535 (e.g., Haskin et al. 1974) recognized that the varied accessory mineral accompaniment and trace-element contents (trapped-melt components) signaled a more evolved equilibrium melt (and inferred parent melt) than the ferroan anorthosites. However, the trace-element-rich accessory minerals could also be explained as a result of metasomatic alteration or addition of the accessory components at some later time. The application of the ion microprobe to determine trace-element contents of the major silicate minerals, coupled with equilibrium mineral/melt distribution coefficients, showed that the cumulus minerals themselves had relatively high concentrations of incompatible elements. This argued against metasomatism and led to the recognition that indeed many of the magnesian-suite cumulates, even those lacking a trapped melt component, must have formed from trace-element-rich equilibrium melts (Papike et al. 1994, 1996; Shervais and McGee 1998), in particular, ~0.7 to 2 times high-K KREEP, which corresponds to ~15–45 ppm Th. Even the group 2 “trace-element poor” Apollo 17 norites cited by James (1980) were shown by Papike (1996) to have high REE concentrations in plagioclase and orthopyroxene that, when combined with distribution coefficients, indicate equilibrium melts with REE concentrations 200–1000 times CI chondrites. That many of these rocks lack abundant accessory minerals means that trapped melt was effectively excluded from them when they crystallized.

Despite finding significant trace-element enrichment in many of the magnesian-suite norites and presumably, in their parent melts, it remains to be proven that all magnesian-suite rocks had such parentage.

Age relationships. Isotopic data for the magnesian-suite rocks are considered in detail in Chapter 4, especially as they relate to the magmatic evolution of crustal rocks. Here, we summarize the age data and some of the inferences that can be made with respect to the distribution of these rocks within the Moon’s crust. Several important points can be made with respect to the age data, which are shown in Figure 3.5. First is the partial overlap of the magnesian-suite rocks ages with those of the FAS rocks. In particular, some of the oldest magnesian-suite rocks are nearly as old as the oldest FAS rocks, which means that they formed at essentially the same time as the formation of crust from the magma ocean, and not necessarily as later remelting and intrusion events into an already solid ferroan-anorthositic crust. Second is the extended range of ages from >4.5 Ga to about 4.1 Ga, suggesting that the processes that led to magnesian-suite intrusive activity occurred over a prolonged interval relative to the ferroan-anorthositic rocks. We will return to this point in the discussion of ages of the alkali-suite rocks.

Depths of origin. The application of thermobarometry to lunar samples is difficult because of the low-pressure gradients in the Moon and the paucity of minerals whose compositions are sensitive to low-pressure variations. Only a few rock types have appropriate assemblages of coexisting minerals for such determinations. Among these are symplectite-bearing troctolites such as 76535 (Gooley et al. 1974) and spinel cataclasites such as breccia clasts from 72435

(Dymek et al. 1976; Herzberg 1978) and 15295 (Marvin et al. 1989). McCallum and Schwartz (2001) have recently reevaluated the depths of origin of several of the magnesian-suite rocks using updated thermodynamic data and advances in quantifying the energetics of crystalline solid solutions to calculate pressures and temperatures of equilibration. For troctolite 76535, assuming local equilibria in the vicinity of the symplectites, which consist of clinopyroxene + orthopyroxene + Cr-spinel surrounded by olivine and plagioclase, McCallum and Schwartz computed temperatures for the recrystallization of about 800–900°C and pressures of 220–250 MPa, corresponding to 42–50 km depth. For the spinel cataclasites, the relevant reaction involves olivine + cordierite and orthopyroxene + spinel (Herzberg 1978; Herzberg and Baker 1980). Temperatures are estimated from olivine-spinel equilibria (Sack and Ghiorso 1991) and Al_2O_3 in orthopyroxene (Herzberg 1978). For three samples studied by McCallum and Schwartz (15445, 77517, 73263), equilibration temperatures fall within the range of 600–900°C with minimum pressures of 100–200 MPa, corresponding to 20–40 km depth. Crustal thickness modeling that utilizes gravity, topography and seismic constraints suggests that the lunar crust is on average between 40 and 50 km thick (see Section 2.7). Thus, if the thermobarometry results are taken at face value, they imply that the magnesian-suite rocks originate from the lower half of the crust.

Distribution. Magnesian-suite rocks are found among the samples from all of the Apollo landing sites, even Apollo 11 (Korotev and Gillis 2001). They are most abundant, however, at the Apollo 14 and 17 sites (see Tables 3.1 and 3.3), especially the latter, and specific groups of rock types tend to be found mainly at one or two specific sites. For example, troctolites are common as clasts in Apollo 14 breccias and as rocks at the Apollo 17 site. Magnesian-suite norites also occur as clasts in Apollo 14 breccias and as rocks at the Apollo 15 and 17 sites. Gabbronorites occur as clasts and small rocks at the Apollo 14 site and as clasts and rocks at the Apollo 16 and 17 sites. Samples of like rock types at a given site, such as the Apollo 16 gabbronorites, are more likely related to one another by mineral and trace-element compositions than they are to the samples of like rock types from other sites (James and Flohr 1983). This similarity suggests petrogenetic links between samples at one site, but not between sites, and led to the idea that the magnesian-suite rocks represent distinct intrusive bodies into the early crust, which was presumed to be a more-or-less global ferroan-anorthositic shell. That most of the reported ages of magnesian-suite rocks are younger than the ferroan anorthosites supports this interpretation, but the overlap between the youngest ferroan anorthosites and the oldest magnesian-suite samples means that the process that formed the sampled magnesian-suite rocks must have been operative very early, even before the initial differentiation was complete globally (see also Chapter 4).

The results of studies of depths of equilibration and burial of magnesian-suite rocks indicate that at least some of them last equilibrated in the middle to lower crust. In the past, it was assumed that the process of magnesian-suite emplacement into early FAS crust was a global phenomenon, and that they were only excavated by the largest basin impact events. Early on, however, in lunar sample studies, attention was called to the so-called east-west dichotomy relative to Apollo and Luna landing sites whereby rocks of the magnesian and ferroan anorthositic suites seemed to be more abundant among nonmare samples of the western and eastern sites, respectively (e.g., Hunter and Taylor 1983; Stöffler et al. 1985; Shervais and Taylor 1986).

The assumption of a global distribution of the magnesian suite within the crust is also challenged on the basis of the components of the feldspathic lunar meteorites, which are mostly dominated by ferroan-anorthositic materials (Jolliff et al. 1991b; Korotev 1996; Korotev et al. 2003a). This observation, coupled with recent global remote sensing (FeO as indicated by Clementine and Lunar Prospector data), indicates that these meteorites may represent a vast portion of the feldspathic highlands (see also Chapter 2). One could also argue, however, that where the crust is thicker beneath the feldspathic highlands, basin impacts may have been less likely to penetrate deeply enough to exhume magnesian-suite intrusives. In this regard, analysis

of the materials exhumed by the South Pole-Aitken basin, whether by return of samples or remote sensing of Mg, would be a key test of the global distribution of magnesian-suite rocks. At present, the global distribution of magnesian-suite intrusives within the crust is not known, although recent studies coupling the magnesian suite to KREEP-rich parent magmas (Snyder et al. 1995a,b; Korotev 2000) makes it likely that their primary occurrence (aside from impact redistribution) is controlled by the early distribution of KREEP, which appears to be concentrated in the regions of mare Imbrium and Oceanus Procellarum (see Section 5.1).

Although the magnesian-suite rocks are discussed here as a group, it is with recognition that various subgroups can not be related directly to one another through a common parent magma (see James and Flohr 1983). It also appears to be the case that igneous rocks containing two or more of the different rock types (e.g., a norite and a troctolite) as might be found in a sample from an igneous contact of a layered intrusion, are not found among the samples. Moreover, impact breccias in the sample collection are not found that represent simple fragmented mixtures of two or more of the magnesian-suite rock types. Thus, direct evidence that layered intrusions or other composite igneous bodies exist that contain two or more of these rock types is lacking among the samples (Papike et al. 1998). Thus, one of the key unresolved issues is how the different magnesian-suite lithologies are related to one another.

Remote sensing studies of central peaks of large craters, which could have depths of origin up to ~30 km below the surface, may provide some clues to the distribution of rock types in the crust (e.g., Tompkins and Pieters 1999; Wieczorek and Zuber 2001a). With the 100–200 m resolution of the Clementine multispectral data, distinct rock types can be discerned on the slopes of central peak mountains, which are steep enough to prevent buildup of thick regolith deposits. Rock types such as anorthosite, norite, and troctolite are observed together and a common inference is that these assemblages represent uplifted magnesian-suite intrusive rock bodies. However, the observation that mafic crustal igneous rocks (norite, gabbro, troctolite) in the sample collections are commonly of the magnesian suite and that rocks rich in olivine and pyroxene are rare among the FAS samples leads to a potentially erroneous inference (e.g., Heiken et al. 1991) that mafic crustal rocks observed remotely are necessarily of the magnesian-suite variety. Commonly, when remote sensing indicates a relatively mafic crustal rock, the assumption has been made that the exposure is of a magnesian-suite lithology and composition. On the other hand, several lines of argument support the possibility that such exposures may be mafic *ferroan* rocks instead. First is the observation that mafic varieties of FAS rocks do occur in the sample collection and share many of the distinguishing trace-element geochemical signatures of the more plagioclase-rich FAS samples. Second is the observation that most of the feldspathic lunar meteorites, which may be argued on the basis of statistical reasoning to represent the vast feldspathic highlands that constitute the northern lunar far side, are dominated by ferroan-anorthositic lithologic components. If the rocks of central peaks are uplifted from depths as great as 30 km, they could represent ferroan mafic rocks that are the deep-seated complement to the ferroan anorthosites.

2.1.3. Alkali suite. Compared to the ferroan-anorthositic and magnesian-suite rocks, the alkali suite is minor by mass (see Table 3.1) and occurs mainly as small rock fragments or clasts in impact breccia. These rocks are distinguished by their alkali-rich bulk compositions and by the combination of relatively ferroan mafic silicates and plagioclase that is less calcic than plagioclase of the magnesian suite. The alkali suite comprises a variety of assemblages including anorthosite, troctolitic anorthosite, norite, gabbronorite, gabbro, felsite (fine-grained granite), and monzogabbro. The majority of these rocks by mass occur in the Apollo 12, 14, and 15 samples, especially Apollo 14 (see Table 3.1); however, traces of alkalic igneous rocks have been reported in samples from all of the Apollo sites except Apollo 11. In most cases, rock samples are small (<1 g), with but a few exceptions (see Tables 3.4 and 3.5). The largest specimens amount to only a few grams each, such as a 1.7 g alkali anorthosite clast in 14047 (Warren et al. 1983a), a 1.8 g granite clast in 14321 (Warren et al. 1983c), and a 2.5 g quartz monzodiorite

Table 3.4. List of alkali-suite anorthosite and norite.

Sample	mass (g) (if avail.)	~Plag An mol%	~Modal % feldspar	Main reference
Alkali Anorthosite				
12003,179/210	0.10	82	100	Warren <i>et al.</i> (1990)
12033,425/501	0.13	83	99	Warren <i>et al.</i> (1990)
12033,550/532	0.02	83	96	Laul (1986), Simon and Papike (1985)
12033,97.7	0.10	88	100	Hubbard <i>et al.</i> (1971b)
12037,178/177	0.02	~92	~97	Laul (1986), Simon and Papike (1985)
12073c120/122	0.08	79	99	Warren and Wasson (1980)
14160,106/105	0.19	82	100	Warren and Wasson (1980)
14161,7245	0.04	83	90	Jolliff <i>et al.</i> (1991)
14304c122"b"	0.49	82	98	Warren <i>et al.</i> (1987)
14305c283WhtA	0.14	85	95	Warren <i>et al.</i> (1983c)
14305c400	0.67	76	99	Shervais <i>et al.</i> (1984a)
14321c1060WhtA	0.14	86	96	Warren <i>et al.</i> (1983c)
15405c181	0.10	84	99	Lindstrom <i>et al.</i> (1988)
Alkali Noritic or Troctolitic Anorthosite				
14047c112/113	1.65	81	84	Warren <i>et al.</i> (1983b)
14066c49/51	0.01	81	85	Shervais <i>et al.</i> (1983)
14160,197/217		~70	80	Snyder <i>et al.</i> (1992)
14305c91	0.14	86	90	Hunter and Taylor (1983)
67975,131N		85	85	James <i>et al.</i> (1987)
Alkali Norite and Gabbronorite				
12033,555/534	0.07	81	49	Laul (1986), Simon and Papike (1985)
12042,280/281		~85		Laul (1986), Simon and Papike (1985)
14303,44		86		Hunter and Taylor (1983)
14304c86"g"	0.23	82	14	Goodrich <i>et al.</i> (1986)
14311,96		85		Hunter and Taylor (1983)
14311,220	0.23	85	75	Warren <i>et al.</i> (1983c)
14313c70WhtA	0.03	83	50	Warren <i>et al.</i> (1983c)
14316,6/12	0.002	84	60	Warren <i>et al.</i> (1981)
14318,146/149	1.20	87	55	Warren <i>et al.</i> (1983b)
15405c170	0.04	89	70	Lindstrom <i>et al.</i> (1988)
67915,163	0.23	63	43	Marti <i>et al.</i> (1983)
67975,14		88	50	James <i>et al.</i> (1987)
67975,44Nm		86	21	James <i>et al.</i> (1987)
67975,44Nf		~70	63	James <i>et al.</i> (1987)
67975,62		85	38	James <i>et al.</i> (1987)
67975,86		82	15	James <i>et al.</i> (1987)
67975,117N			50	James <i>et al.</i> (1987)
67975,136N		~70	42	James <i>et al.</i> (1987)
67975,42N		85	48	James <i>et al.</i> (1987)
77115c19	0.60	95	70	Winzer <i>et al.</i> (1974)

clast in 15405 (Ryder 1985). The occurrence of an 82 g breccia composed mostly of granitic and monzogabbroic materials (12013), however, suggests that larger rocks or rock bodies composed mainly of alkali-rich materials may exist. The KREEP-rich impact-melt breccia 15405 (513 g), which contains clasts of quartz monzodiorite, indicates a spatial, if not petrogenetic, link between some of the alkali lithologies and KREEP basalt. Such relationships are also observed in smaller impact breccias, especially in samples from the Apollo 12 and 14 sites.

Mineralogy and mineral modes. Minerals of the alkali suite include plagioclase, low-Ca and high-Ca pyroxene, K-feldspar, a silica phase, apatite, merrillite, ilmenite, Cr-spinel, fayalite, zircon, baddeleyite, troilite, and Fe-Ni metal. Plagioclase typically is more sodic than

Table 3.5. List of alkaline-suite QMD/monzogabbro and granite/felsite.

Sample	mass (g) (if avail)	high-Ca pyroxene Mg#	Olivine Mg#	Plag An mol%	Modal % feldspar	Main reference
Quartz monzodiorites (monzogabbro)						
15405c56	2.50	—	—	46	—	Ryder (1985)
15434,12	0.62	33	80	40	—	Ryder and Martinez (1991)
15434,14 bx	0.15	—	80	40	—	Ryder and Martinez (1991)
15434,10	0.12	—	60	30	—	Ryder and Martinez (1991)
15459c315	0.10	29	60	59	—	Lindstrom et al. (1988)
15403,24,7001	0.04	32	70	50	—	Marvin et al. (1991)
14161,7069	0.023	35	70	41	—	Jolliff (1991)
14161,7264 bx	0.020	62	71	50	—	Jolliff et al. (1991)
14161,7373	0.018	49	70	28	—	Jolliff (1991)
15403,71a	0.005	30	60	50	—	Marvin et al. (1991)
15403,71c	0.001	—	20	60	—	Marvin et al. (1991)
15403,71b	<0.001	30	—	30	—	Marvin et al. (1991)
15403,7002	<0.001	31	60	45	—	Marvin et al. (1991)
15403,23c	—	—	—	—	—	Marvin et al. (1991)
Granite/Felsite						
12013 bx	—	—	—	—	—	Quick et al. (1977)
14321c1028	1.80	5	2	—	60	Warren et al. (1983a)
12033,507	1.20	—	8	50	55	Warren et al. (1987)
14303c204	0.17	40	42	75	60	Warren et al. (1983a)
14004,94 glass/bx	0.15	—	—	—	40	Snyder et al. (1992)
14004,96 glass/bx	0.10	—	—	—	35	Snyder et al. (1992)
14161,7269 glass/bx	0.04	50	—	67	50	Jolliff (1991)
14001,28,2 bx	0.03	—	—	80	45	Morris et al. (1990)
73215c43,3	0.02	35	19	60	50	James and Hammarstrom (1977)
14001,28,3 bx	0.02	—	—	80	45	Morris et al. (1990)
14001,28,4 bx	0.02	—	—	80	45	Morris et al. (1990)
12070,102-5	<0.01	30	13	50	—	Marvin et al. (1991)
73255,27,3	<0.01	—	—	—	—	Blanchard and Budahn (1979)
15403,71c	—	45	—	—	—	Marvin et al. (1991)

bx = brecciated, not strictly monomict

An_{86} (Warren 1993) and low-Ca pyroxene is more ferroan than En_{70} (Snyder et al. 1995b). Samples rich in plagioclase, i.e., > 80 vol%, occur primarily among Apollo 12 and 14 materials. Some of these are clasts in breccias and some are small rocks or rock fragments. A variety of more pyroxene-rich assemblages also have been found at these sites, and these have been referred to mainly as alkali norite, or in a few cases, gabbronorite or monzogabbro. Similarly alkalic and ferroan assemblages also occur in a few Apollo 15, 16, and 17 samples, but these are less common than in Apollo 12 and 14 samples. Some of the rocks that have relatively sodic plagioclase and ferroan pyroxenes also have modally significant silica and K-feldspar, and have been referred to as quartz monzodiorite (QMD) (Ryder 1976) or as monzogabbro (Jolliff et al. 1999). Some of these have high proportions of phosphates, as high as 10 wt% (Jolliff 1991), although the small size of most of these rock fragments casts uncertainty on whether their modes might be representative of larger rocks or outcrops. Rock assemblages that are rich in K-feldspar and silica, commonly occurring in a granophytic intergrowth, are found among non-mare samples from most sites. Like other alkali-suite samples, these are most common among Apollo 12 and 14 samples, and are more numerous than reflected in Tables 3.4 and 3.5. Masses of several samples exceed a gram, and among the samples in these tables, the QMD-monzogabbro and granite groups each have summed masses comparable to the alkali-anorthosite and alkali-norite groups.

Compositions. Bulk compositions of the alkali-suite rocks are distinctive (see Table A3.3). Sodic plagioclase and the presence of K-feldspar are reflected in Na- and K-rich compositions. Trace-elements follow Na and K, with enrichments in Eu, Ba, Rb, and Cs. Bulk compositions are relatively ferroan, with Mg/(Mg+Fe) of alkali anorthosites and alkali norites averaging about 0.6, and granite and QMD-monzogabbro, ~0.4.

The alkali anorthosites differ from the other rock types in this group in their alkali-element proportions and trace-element signatures. The hallmark of the alkali anorthosites is their high Na₂O concentrations, averaging about 1.6 wt%, which are not necessarily accompanied by commensurately high K₂O (their average K₂O wt% is ~0.3). Enrichment in Eu is also a signature of this rock type, with Eu ranging from ~3 to 8 ppm and averaging ~6 ppm, as compared to average concentrations in FAS rocks of ~0.8 ppm and in magnesian-suite rocks, of ~1.2 ppm. The more mafic alkali norites, on the other hand, have lower Na₂O (with an average of 1.25 wt%) and higher K₂O (~0.5 wt%). In these rocks, Eu follows Na, and both correlate to plagioclase content. Barium follows K and is typically enriched in the more mafic norites by about a factor of 3 relative to the alkali anorthosites. Other incompatible trace elements such as the REEs, Zr, and Th do likewise. These variations are consistent with the norites containing a higher proportion of trapped melt.

In terms of the three elements sensed most accurately from orbit (FeO, TiO₂, and Th), compositions of these rocks cover a broad range (see Figs. 3.3 and 3.4). The alkali anorthosites typically have concentrations of FeO <4 wt% and very low TiO₂, averaging <0.5 wt%. The alkali norites have FeO concentrations ranging to 17 wt% with an average of ~10 wt%, and TiO₂ concentrations range to nearly 5 wt% with an average of ~2 wt%. Concentrations of Th are variable, averaging 5 ppm in the alkali anorthosites and 12 ppm in the alkali norites and alkali gabbronorites, but with maximum values near 40 ppm.

The QMD-monzogabbro and granite samples have been distinguished generally on the basis of mineralogy, with most workers referring to samples with abundant silica and K-feldspar as granite, and those with abundant silica, K-feldspar, and pyroxene, as QMD or monzogabbro. The granitic samples typically have SiO₂ contents of 65–75 wt%, FeO <10 wt% and K₂O >3 wt% ranging up to ~8 wt% (Table A3.4). The monzogabbros typically have >10 wt% FeO, ranging to over 16 wt%, and K₂O <3 wt%. Concentrations of TiO₂ are higher in the monzogabbros, averaging about 2 wt% compared to ~1 wt% in the granites. The trace-element signature of the monzogabbros is an extreme enrichment in REE concentrations and high field-strength elements such as Zr and Hf. The granite compositions show extreme enrichments in the alkali elements (K, Rb, Cs) and Ba, as well as in Nb, Ta, Th, and U. They also typically have a distinctive “V”-shaped REE pattern at about 100–300 times chondritic, with enrichment of both the lightest and heaviest REEs. The incompatible elements in these rock types do not follow a typical KREEP-like pattern, and this has been attributed to fractionation involving merrillite and other late-stage trace-element-rich minerals, and immiscible silicate-liquid segregation that occurred during late-stage crystallization (Jolliff 1991, 1998; Snyder *et al.* 1995b).

Recent studies have supported a relationship between the alkali-suite and magnesian-suite rocks (e.g., Snyder *et al.* 1995a; Shervais and McGee 1999). The trend among mineral compositions shown in Figure 3.2b suggests that fractional crystallization of a KREEP basalt-like magma could produce both the magnesian- and alkali-suite rocks (see also Chapter 4, Fig. 4.20). Most of the magnesian-suite rocks appear to be cumulates that were effectively separated from the bulk of their residual-melt component. The alkali suite could represent other, more chemically differentiated products of the same magmas. Alkali anorthosites might have originated as perched or flotation cumulates within intrusive magma bodies and alkali norite and gabbronorite could represent mafic cumulates that retained their trapped-melt components. Granite and monzogabbro would represent segregations of late-stage

residual melt. One of the problems with this scenario is that members of these two rock suites (magnesian- and alkali-suite) are not typically found together in crystalline rocks or breccias.

Age relationships. Isotopic characteristics are also not clear on the relationship between the alkali and magnesian suites. While crystallization ages overlap, the alkali suite extends to younger ages (see Fig. 3.5). Ages extend from a little over 4.3 Ga to nearly 3.8 Ga (Meyer et al. 1989), with the apparent cut off at ~3.8 Ga likely resulting merely from the absence of younger impact basins that were large enough to excavate significant quantities of subsurface rocks. Other isotopic systematics indicate relationships between the alkali-suite rocks and KREEP basalt. Additional details of the isotopic systematics of alkali-suite samples are given by Snyder et al. (1995b; 2000).

Depths of origin. Mineral compositions and textures of members of the alkali suite so far are consistent with fairly rapid cooling associated with shallow emplacement and crystallization (see McCallum and O'Brien 1996; McCallum 1998; Jolliff et al. 1999). Even samples containing fairly coarsely exsolved pyroxene (coarse, at least, for a lunar rock) appear to have been emplaced in the shallow crust, within one or two kilometers of the surface. This is in contrast to some members of the magnesian suite that appear to have depths of origin deeper than 20 km.

Distribution. Perhaps the key questions regarding the alkali suite are related to their extent and distribution. Clearly these rock types are more abundant at the western landing sites, Apollo 12, 14, and 15, and Lunar Prospector results suggest a general confinement of concentrations of these materials to the Procellarum KREEP Terrane. What is not known is whether the alkali-suite rocks form extensive outcrops or separate intrusive bodies. Small sizes suggest that they could simply be the broken, trapped-melt-rich parts of overall more magnesian rocks. Remote sensing, however, points to several locations as places where such rocks may be more common, if not making up large outcrops or volcanic exposures, such as the domes and other volcanic constructs observed in parts of Oceanus Procellarum (e.g., Hawke et al. 2003a), and exposed by impacts such as Aristarchus, Kepler, and Mairan. A very curious Th-rich compositional anomaly occurs at the Compton Belkovich region (Gillis et al. 2002) that is associated with a low FeO abundance (as sensed remotely) suggesting the possibility of an alkali-anorthosite exposure at this locale. Some of the more mafic rocks that would be expected to occur with such an anorthosite have not yet been observed, however.

2.1.4. KREEP basalts. Although KREEP-bearing materials occur among samples from all of the Apollo sites, volcanic KREEP basalts are found primarily among the samples from Apollo 15. Apollo 17 samples have yielded one significant occurrence of KREEP basalt and a few small clasts or rock fragments occur in the Apollo 12, 14, and 15 samples (Table 3.6). Among these, only the Apollo 15 KREEP basalts appear to have a demonstrably local source (e.g., Spudis 1978; Ryder 1994). The term “KREEP basalt” refers strictly to the rocks that can be shown to have formed as a result of internal melting, not impact processes. Nevertheless, some of the KREEP basalts are almost identical in composition to known impact-melt rocks, especially those from the Apollo 14 site. Most of the texturally and compositionally similar rocks found at the Apollo 14 site have been shown to contain clasts or to have too much plagioclase to represent basaltic liquids.

A breccia containing clasts of an apparently volcanic KREEP basalt was found at the Apollo 17 site, and these have widely been referred to in the literature as “Apollo 17 KREEP basalt.” It should be emphasized, however, that these clasts all occur in a single boulder from Station 2 (72275) (Ryder et al. 1977) and that they differ compositionally from those found at the Apollo 14 and 15 sites (e.g., different FeO, Al₂O₃, and trace element concentrations; see Salpas et al. (1987) and Table A3.5). No rock fragments of this KREEP basalt type have been found in the rock fragments of the Apollo 17 regolith (Bence et al. 1974; Jolliff et al. 1996),

Table 3.6. KREEP basalts.

Sample	mass (g)	~modal % feldspar	Main reference
15386	7.50	43	Ryder (1985)
15382	3.20	41	Ryder (1985)
72275c91	2.73	40	Salpas <i>et al.</i> (1987)
15434,18	0.74	45	Ryder and Sherman (1989)
15434,16	0.44	45	Ryder and Sherman (1989)
15434,189	0.41		Ryder and Sherman (1989)
15434,8	0.32	42	Ryder and Sherman (1989)
15304,6	0.31	49	Ryder and Sherman (1989)
15434,29	0.30		Ryder and Sherman (1989)
15264,4	0.28		Ryder and Sherman (1989)
15434,21	0.22	32	Ryder and Sherman (1989)
15024,11	0.21		Ryder and Sherman (1989)
15434,17	0.20	48	Ryder and Sherman (1989)
15404,5	0.17		Ryder and Sherman (1989)
15564,16	0.16		Ryder and Sherman (1989)
15434,25	0.14		Ryder and Sherman (1989)
15314,34	0.11	47	Ryder and Sherman (1989)
15434192	0.10		Ryder and Sherman (1989)
15405c68	0.08	40	Ryder (1985)
15007,290/291	0.06		Warren <i>et al.</i> (1983c)
15434194	0.05		Ryder and Sherman (1989)
67015c310	0.043	72	Marvin <i>et al.</i> (1987)
15007,292/293	0.030		Warren <i>et al.</i> (1983c)
15007,302	0.021		Warren <i>et al.</i> (1983c)
14161,7048	0.020	55	Jolliff <i>et al.</i> (1991)
15007,304	0.015		Warren <i>et al.</i> (1983c)
15007,294	0.011		Warren <i>et al.</i> (1983c)
Sum mass	17.9		
Average modal % feldspar	49		

which is consistent with this rock type having come from elsewhere and not being a common derivative of a local source. The Station 2 boulder (72275) may well be a fragment of distal ejecta, perhaps from Imbrium and almost certainly with a provenance different from the main Apollo 17 impact-melt breccia formations thought to be from Serenitatis.

Mineralogy and mineral modes. Minerals of the KREEP basalts include pyroxene (mostly pigeonite and augite, with minor orthopyroxene) and plagioclase as the main minerals, with lesser amounts of K-feldspar, phosphates, ilmenite, zircon (and other Zr-bearing phases including baddeleyite, zirconolite, zirconian armalcolite), K-feldspar, fayalite, silica (cristobalite), troilite, and Fe-metal. Mineralogically, the absence of magnesian olivine, higher plagioclase and low-Ca pyroxene proportions, and the presence of abundant late-stage mesostasis, distinguish these basalts from the mare basalts. Mineral compositional variations are consistent with fractional crystallization such that plagioclase and pyroxene cores are calcic and magnesian, with their rims being sodic and ferroan, respectively. These mineral-compositional variations constitute one of the lines of evidence linking KREEP basalts to magnesian- and alkali-suite rocks.

Compositions. KREEP basalts are typically aluminous (13–16 wt% Al_2O_3 and 9–15 wt% FeO , Table A3.5), and their defining characteristic is an incompatible trace-element enrichment at about 100–150 times chondritic concentrations. The compositions of Apollo 15

KREEP basalts are very similar to one another, but the Apollo 17 KREEP basalt composition differs significantly from these. The 72275 compositions are more ferroan ($Mg/(Mg+Fe) \sim 0.5$ compared to 0.6), they have lower TiO_2 concentrations (see Fig. 3.6), they have incompatible-trace-element concentrations 1/2 to 1/3 of those of Apollo 15 KREEP basalt, and they have higher Sc, V, Co, and Ni concentrations. Figure 3.7 illustrates the differences in FeO and Th concentrations. Salpas et al. (1987) concluded that the Apollo 15 and Apollo 17 KREEP basalts are not related to each other in any direct petrologic way. The 72275 KREEP basalt is intermediate between Apollo 15 KREEP basalt and mare basalts, and is most similar to the Apollo 14 “group 5” aluminous basalts (Dickinson et al. 1985).

A key aspect of the geochemistry of volcanic KREEP basalts is their rather magnesian bulk composition given their strong trace-element enrichment. This characteristic seems to require mixing of mantle-derived magnesian melts with KREEP-rich magma-ocean residua (urKREEP) or sinking of urKREEP into the mantle with subsequent remelting (see Warren 1988) (summarized recently by Papike et al. 1998).

The volcanic KREEP basalts have somewhat lower incompatible-element concentrations than some of the Apollo 14 and 15 impact-melt rocks (see below). Nevertheless, the incompatible trace elements (e.g., K, Ba, Rb, Cs, trivalent REEs, Zr, Hf, Nb, Ta, Th, U) occur in remarkably similar inter-element ratios in all the KREEP basalts as well as the KREEP-bearing mafic impact-melt breccias. On the basis of remotely sensed compositions, volcanic KREEP basalt cannot be distinguished from mafic impact melt—geologic and morphologic relationships are required (Spudis 1978).

Age relationships. Crystallization ages of the Apollo 15 KREEP basalts are well determined by analyses of multiple isotopic systems to be 3.82–3.86 Ga (summarized by Papike et al. 1998), presumably shortly after the Imbrium impact event (Ryder 1994). KREEP basalt fragments from 72275 yield slightly older crystallization ages (3.93–4.08 Ga). Isotopic systematics (ϵ_{Nd}) suggest a relationship between KREEP basalts and magnesian- and alkali-silicate rocks (Shih et al. 1992).

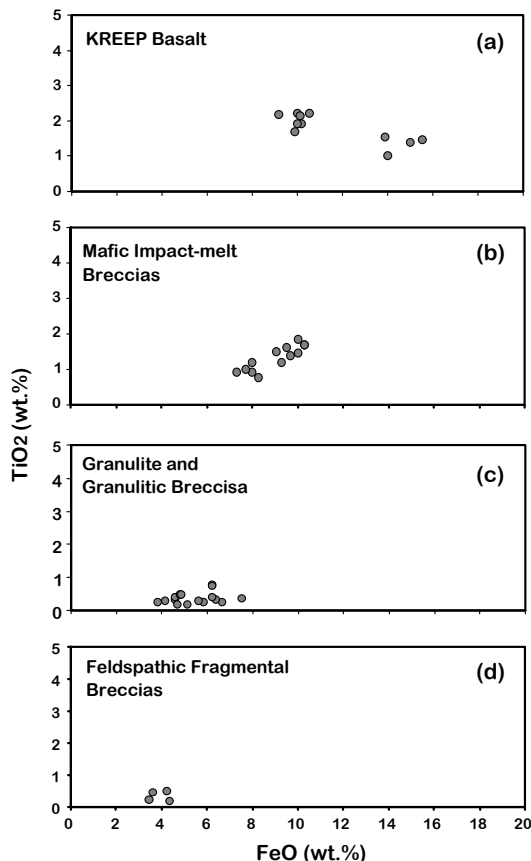


Figure 3.6. TiO_2 vs. FeO for KREEP basalts, mafic impact-melt breccia groups, granulites and granulitic breccias, and feldspathic fragmental breccias. For KREEP basalts, the cluster at $\sim 10\%$ FeO is from Apollo 15 samples and the cluster at $14\text{--}16\%$ wt% FeO is from a single Apollo 17 sample, 72275. Decreasing FeO and TiO_2 concentrations from (a) to (d) is probably a complex function of compositional stratigraphy of the crust with depth as well as wide-scale lateral variations associated with major geochemical terranes (see also Fig. 3.8).

Distribution. Recent remote sensing and photogeologic analysis reveal several locations where KREEP basalts may occur on the surface the Moon. Two such places occur near the Apollo 15 site, where KREEP basalt is a common component of the regolith. The Apennine Bench has been cited as a likely location for KREEP basalt flows (Hawke and Head 1978; Spudis 1978), and Clementine and Lunar Prospector data suggest the presence of KREEP basalt in the target region of the Aristillus crater, located just to the west of the Apollo 15 site (Gillis and Jolliff 1999; Blewett and Hawke 2001). KREEP basalts do not appear to make up any of the extensive mare flows in the Procellarum-Imbrium region, but they could be a significant buried component or a component of nonmare materials in the Procellarum KREEP Terrane. The absence of KREEP basalt among rock fragments in regolith of the Apollo 17 site (Jolliff et al. 1996) indicates that KREEP basalt is most likely not a local component there, and its occurrence as a clast component in the station 2 boulder is consistent with a remote origin (e.g., Spudis and Pieters 1991).

Most of the materials at the Apollo 14 site that are mineralogically and geochemically similar to KREEP basalt are probably clast-free/poor, crystalline impact melt. The high Th concentration of KREEP basalts coupled with the observed global distribution of Th suggests that their occurrence is restricted to the Procellarum KREEP Terrane (see Section 5).

2.1.5. Mafic impact-melt rocks and breccias. Detailed descriptions of the different lunar breccia (polymict) groups can be found elsewhere and constitute the subject of a voluminous literature and extensive investigations. In particular, the major groups of polymict breccias are described and summarized in *The Lunar Sourcebook* (Heiken et al. 1991) and in Chapter 5 of *Planetary Materials* (1998). In this and in subsequent sections, we focus on key characteristics of several of the main lunar breccia types as indicators of specific crustal components or geologic provinces of the Moon. As their compositions are more mafic than typical lunar highlands surface materials, they are thought to have formed mainly as ejected impact melt from basin-sized impacts that penetrated deep enough into the lunar crust to encounter rocks more mafic than observed at the surface.

Mafic impact-melt breccias from the Apollo landing sites, particularly Apollo 14, 15, 16, and 17, are abundant and form compositionally distinct groups. These groups exhibit a range of major-element compositions and incompatible-element enrichments. While concentrations of incompatible elements span a significant range, inter-element ratios vary little and have been

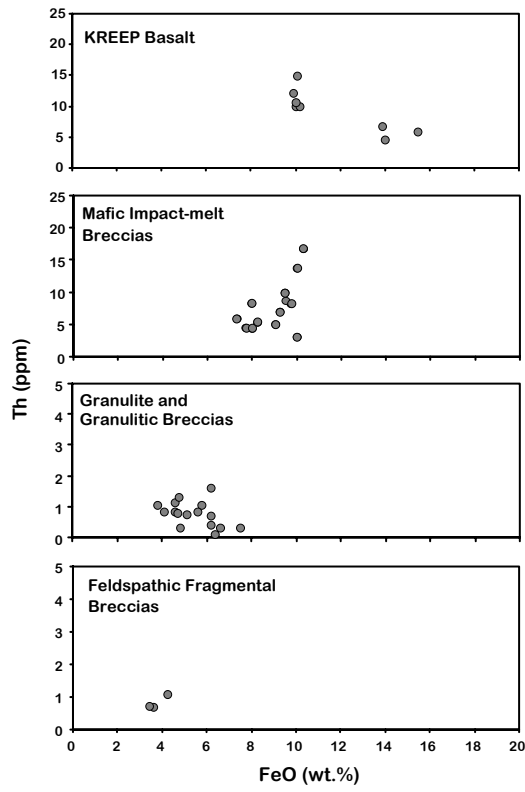


Figure 3.7. Th vs. FeO for KREEP basalts, mafic impact-melt breccias, granulitic breccias, and feldspathic fragmental breccias. Note the difference in thorium scales between the upper and lower plots.

used to infer a common lunar KREEP component. This discussion of mafic impact melt breccias draws upon groupings defined by numerous past studies (e.g., Ryder and Wood 1977; Spudis and Ryder 1981; Korotev 1994; Jolliff et al. 1996). These groupings are the same as those presented by Korotev (1998) in which he presented average concentrations of several of the key elements sensed remotely by the Lunar Prospector gamma-ray spectrometer. These groups were also used by Jolliff (1998) and the compositions listed in Table A3.6 are from that paper.

Mineralogy and mineral modes. The mafic impact-melt breccias have also been referred to as basaltic impact melts, and depending on their specific textures, they have been called crystalline-matrix breccias, “dimict” breccias, poikilitic breccias, or aphanitic-matrix breccias (see Stöffler et al. 1980). The mineralogy of the mafic impact-melt breccias is very similar to that of the KREEP basalts, except that clasts are as variable as the known lunar rock types. Importantly, clasts tend to be of relatively calcic plagioclase and magnesian mafic silicates when compared to the matrix, and the matrix usually contains fine-grained accessory minerals that provide the incompatible-element enrichment.

Compositions. The mafic impact-melt breccia groups have concentrations of $\text{FeO} > 7 \text{ wt\%}$ and $\text{Al}_2\text{O}_3 < 22 \text{ wt\%}$ (Table A3.6). Though TiO_2 concentrations range only from ~1 to 2 wt% (Fig. 3.6), incompatible elements range from ~50 to >200 times chondritic values (Fig. 3.7). The key compositional characteristic of all the mafic impact-melt breccias is that the incompatible elements, regardless of concentration, occur in KREEP-like proportions with very little deviation.

The Apollo 14 melt breccias have a broad range of incompatible-element concentrations, but most have very similar inter-element ratios (Warren 1989; Jolliff et al. 1991b). The concentration of Th, for example, ranges from about 10–30 ppm, averaging ~17 ppm. Compositions of individual samples vary according to clast contents and the proportions of clasts and matrix. Jolliff et al. (1991b) selected a set of rock fragments of similar texture whose compositions form a very tight group to define an average impact-melt-breccia composition represented by the majority of Apollo 14 melt breccias; this composition is similar to the “average high-K KREEP” of Warren (1989).

Apollo 15 melt breccias were divided into 5 groups by Ryder and Spudis (1987) on the basis of compositional clustering of samples, and these groups have different levels of trace-element enrichment. Nevertheless, analyses of additional samples have revealed a continuum of compositions between the groups (Lindstrom et al. 1988). A common interpretation has been that distinctive group compositions indicate that members of a particular group originated in the same impact event, and that different groups require different origins. However, $^{40}\text{Ar}/^{39}\text{Ar}$ dating by Dalrymple and Ryder (1993; 1996) has shown that even within groups, compositionally similar samples apparently have different ages, thus interpretations relating a group of impact-melt breccias to a specific impact are not straightforward.

Of the five Apollo 15 groups, group A has the highest level of incompatible-element concentrations at about 70% of high-K KREEP, overlapping in part the high concentrations of the Apollo 14 group. Group B compositions have incompatible-trace-element concentrations at about 50% of high-K KREEP. Group C compositions are notably more aluminous and less mafic, and may simply be the more feldspathic extreme of compositional group B (Korotev 1994). Group D consists of well-studied impact-melt rocks 15445 and 15455, taken by Ryder and Spudis (1987) to be potential candidates for samples of the Imbrium melt sheet (as opposed to ejected melt or reworked Imbrium ejecta). Concentrations of incompatible elements in group D are relatively low, being about 20% of those of high-K KREEP.

Among the Apollo 17 samples, Spudis and Ryder (1981) distinguished two texturally and compositionally distinct groups: poikilitic breccias and aphanitic breccias. The poikilitic breccias are by far the more abundant of the two and form the large breccia boulders at the base

and on the slopes of the North and South Massifs. A third compositionally distinct group of breccias described by Jolliff et al. (1996) occurs among small rock fragments found in the massif soils. These small samples were distinguished as a group on the basis of their similar and high concentrations of incompatible trace elements. They are similar in trace-element composition to Apollo 15 group B and Apollo 16 group 1M, but have siderophile-element signatures more like the other Apollo 17 groups.

Among all of the mafic impact-melt breccia groups, incompatible trace elements exhibit extremely tight correlations, such as between Th and Sm (Fig. 3.8). These correlations form a key line of evidence that the impacts that produced these melt breccias tapped a common, deep reservoir. An inverse correlation exists between $Mg/(Mg+Fe)$ and Th contents (see Fig. 3.9), which suggests a relationship between Fe and incompatible-element enrichment. The Apollo 15 and 17 KREEP basalts do not adhere to this correlation.

Age relationships. The formation ages of numerous impact-melt breccias have been determined, principally using $^{40}\text{Ar}/^{39}\text{Ar}$ methods (e.g., Dalrymple and Ryder 1993, 1996). However, the dating method is difficult because of incomplete degassing of clasts and subsequent disturbances. Some of the Ar release patterns are simply too difficult to interpret unambiguously. Still, most of the dated mafic impact-melt breccias have ages in the range of $\sim 3\text{--}3.9$ Ga, so either most of the impact basins formed at about this time, or the samples are dominated by a small number of events. This topic is considered in more detail in Chapter 5. The important point here is that a source of KREEP enrichment was apparently not widespread until this time, judging by the compositions of other key breccia groups discussed below.

Depths of origin. Depths of origin are difficult to constrain in these breccias. Minerals that might record depths of melting generally don't survive the impact-melting process, and

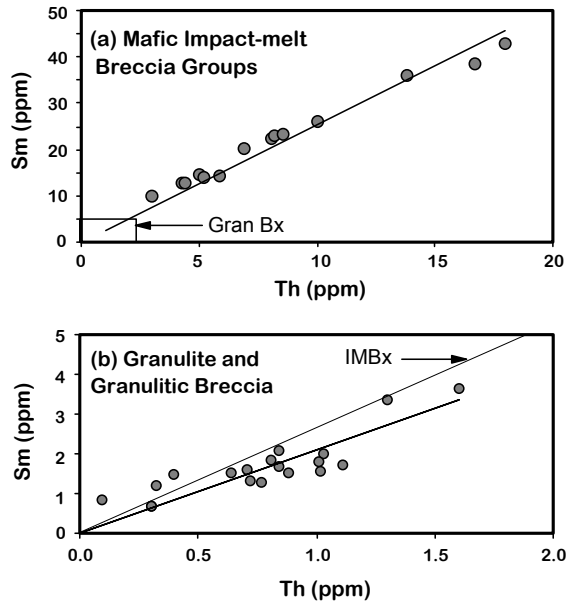


Figure 3.8. Sm vs. Th in mafic impact-melt breccias and in feldspathic granulites and granulitic breccias. Note different Sm scales between (a) and (b). Gran Bx and IMBx denote granulitic breccia and impact melt breccia, respectively.

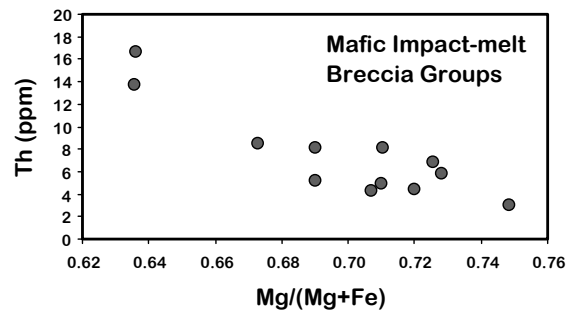


Figure 3.9. Th vs. molar $Mg/(Mg+Fe)$ in the mafic impact-melt breccias. Data are group averages from Table A3.6.

the clasts present may have been entrained in a different part of the target as the melt left the excavation cavity. Judging by mineral compositions and textures, most of the clasts in the sampled melt breccias appear to have relatively shallow origins. An argument based on compositions is that the breccia bulk compositions, and especially the matrix material, are difficult to match by mixing known rock compositions. The implication is that the melted component includes materials from depth that are not common or not found near the surface. That component is typically richer in FeO and incompatible elements than the clasts (Ryder and Wood 1977; Ryder 1979). The broad-scale inference is that the crust must become more mafic with depth. Although the ejecta of most large basins are more mafic than the most feldspathic parts of the upper crust, we now know from global remote sensing that broad lateral variations in composition exist in the crust. Thus, any layering that might be present locally may not be representative globally.

Distribution. Studies of melt rocks and breccias from terrestrial impact craters indicate that most small impacts very effectively homogenize target materials. A notable exception is the 100 km diameter Popigai crater where distinct compositional variability in impact-melt lithologies is found that is related to differences in target rock compositions (Kettrup et al. 2003). Regardless, the common interpretation of lunar impact-melt rocks is that specific compositional groups represent individual impacts. This interpretation, coupled with the observation that impact-melt groups from a given landing site bear more resemblance to other groups from the same site than they do to groups from other sites, has led to the paradigm that the impact-melt breccias originate from the nearest large basin. This approach has been challenged in recent years on several grounds (e.g., Haskin et al. 1998). One argument is that the very large impacts that formed basins likely struck targets that were heterogeneous on a scale large enough to prevent total homogenization, especially in the clast content entrained by melt exiting different regions of a basin as has been demonstrated for the Popigai crater (Kettrup et al. 2003). Another is that isotopic age data are difficult to interpret and are not entirely consistent with the nearest-basin paradigm. Finally, impact ejecta modeling (Haskin 1998; Haskin et al. 2003) suggests that ejecta from one or two of the latest and largest of the nearside basins (Imbrium and Serenitatis) may dominate the mafic impact-melt breccias sampled at all of the Apollo sites.

A common interpretation of the KREEP trace-element similarity of the diverse mafic melt-breccia groups is that the impacts that formed these tapped a common source of very incompatible-element-rich material, presumably a deep global KREEP layer sandwiched between the crust and mantle. Global remote sensing by Lunar Prospector shows, however, that such KREEP rich material was strongly confined to the Procellarum KREEP Terrane and was not excavated by all large basins (especially notable are the Crisium and South Pole-Aitken basins).

2.1.6. *Granulitic breccias.* The feldspathic granulites and granulitic breccias are found at most of the landing sites and within the nonmare lunar meteorites (e.g., Dhofar 026, Cohen et al. 2004) as small rocks, rock particles in regolith, and lithic clasts in breccias. Their textures suggest heating and recrystallization, and compositional as well as shock features in some indicate a relationship to impact processes. However, in many cases, the geologic setting in which this metamorphism occurred remains unclear. These rocks have compositions that are similar to estimates of the bulk lunar crust, and many are clearly mixtures of different precursor rock types, yet they are not easily explained as chemical mixtures of the known igneous rocks (Korotev and Jolliff 2001).

Mineralogy and mineral modes. The mineralogy and textures of granulitic breccias are described in Bickel et al. (1978), James and Hammarstrom (1977), Warner and Phinney (1977), Bickel and Warner (1978), Lindstrom et al. (1986), Cushing et al. (1999), and Cohen et al. (2004). These rocks form a continuum between fine-grained igneous textures, impact-melt textures (e.g., poikilitic-poikiloblastic), and metamorphic textures (granoblastic). In terms of normative mineralogy, these rocks typically have about 80 vol% plagioclase and

most contain olivine, orthopyroxene, and clinopyroxene. The magnesian granulites typically have olivine > pyroxene, and the ferroan ones have pyroxene > olivine. From their normative mineralogy, these all lie near the boundary between troctolitic anorthosite, noritic anorthosite, and anorthositic norite.

Compositions. Meteoritic siderophile-element contamination indicates impact involvement in the origin of these rocks. Average compositions cover a relatively restricted range; for example, the range of Al_2O_3 is 25–29 wt% averaging 26.8 wt%, MgO is 4–9 wt% averaging 7 wt%, and FeO is 3.8–7.5 wt% averaging 5.4 wt% (see Table A3.7). Incompatible element concentrations are extremely low; for example, the range of Th is 0.1–1.6 ppm averaging 0.8 ppm, and Sm is 0.7–3.7 ppm averaging 1.7 (see Fig. 3.8). The most common interpretation of these compositions is that they represent upper-crustal materials uncontaminated by the excavation of KREEP-rich materials from the Procellarum KREEP Terrane by impacts such as Imbrium and Serenitatis.

The granulites and granulitic breccias can be divided into magnesian and ferroan varieties (Lindstrom and Lindstrom 1986) and for some elements, such as FeO and Sc , the compositions appear to form two distinct groups. Both groups, however, are found at a given landing site and the significance of the variation and grouping in $\text{Mg}/(\text{Mg}+\text{Fe})$ is not known. The magnesian group has $\text{Mg}/(\text{Mg}+\text{Fe})$ ranging from 0.72 to 0.78 with an average of 0.75, whereas the ferroan group ranges from ~0.5 to 0.7 with an average of 0.62. It is important to note that the designation of one of these groups as “magnesian” does not necessarily imply any relationship to the magnesian-suite igneous rocks, especially those magnesian-suite rocks that have been shown to have a trace-element-rich lineage (Korotev and Jolliff 2001). At the Apollo 17 site, for example, the magnesian granulitic breccia compositions do not correspond to the magnesian-suite norites, troctolites and troctolitic anorthosites that are also found at the site.

Age relationships. Age data are difficult to determine on these rocks (see Cohen et al. 2004) but for those that have been reported (all of which are based on the $^{40}\text{Ar}/^{39}\text{Ar}$ chronometer), ages range from about 3.8 to 4.2 Ga. The younger of these ages may have been reset by the impacts that exhumed the breccias (Papike et al. 1998). The formation of most of these rocks appears to predate the formation of the large, late basins such as Imbrium and Serenitatis.

Depths of origin. While textures of the granulitic breccias indicate burial and thermal metamorphism, some disagreement exists as to the depth of burial and duration of annealing needed to produce these (Cushing et al. 1999). Although textures and mineral compositions reflect annealing processes, these do not necessarily require deep burial and slow heating/cooling. In some cases, but not all, mineral compositional zoning is minimal, suggesting equilibration. Judging by FeO concentrations, typical compositions are similar to highlands compositions sensed remotely, which suggests that the granulitic breccias might be representative of the near-surface and upper crust.

Distribution. The granulites and granulitic breccias are found at all Apollo and Luna landing sites, but they are most common in samples from the eastern nonmare sites. The low incompatible trace-element concentrations further suggest an origin away from the Procellarum KREEP Terrane. Ages and textures are consistent with formation in large impacts, burial coupled with heating beneath either a thick ejecta blanket or an impact-melt sheet, and later excavation to the surface. The clustered compositions (such as high Al_2O_3 and low FeO) of the granulitic breccias suggest that they might be fairly representative of the average compositions of significant areas of the ancient upper crust of the Moon.

2.1.7. Feldspathic fragmental breccias. Fragmental breccias are a common product of impact processes and they occur at all Apollo landing sites (e.g., Lindstrom et al. 1977; James 1981; Lindstrom and Salpas 1981; Norman 1981; Stöffler et al. 1985). Because the fragmental breccias consist of a diversity of rock types mixed together, they potentially record

information about the target areas of large impacts. When a group of such breccias is found to have a common composition, that composition takes on added significance as potentially representing an especially broad area. Such is likely to be the case for the plagioclase-rich fragmental breccias, which occur most abundantly at the Apollo 16 site. In recent years, the similarity between their composition and the compositions of many of the feldspathic lunar meteorites has led to the conclusion that these may best represent vast expanses of the feldspathic highlands surface far from the influence of mixing with more mafic ejecta from the large and late nearside basins such as Imbrium and Serenitatis. Key clast types found in these breccias include granulitic breccia, cataclastic anorthosite, and fragment-laden feldspathic impact melt (Papike et al. 1998). The compositions of these breccias provide a key constraint on the composition of the Feldspathic Highlands Terrane and the feldspathic regions of the Moon's upper crust.

Compositions and mineral modes. Of the major breccia groups, the feldspathic fragmental breccias are the most aluminous, with typical Al_2O_3 concentrations of 29–31 wt%, which corresponds to noritic anorthosite (see Table A3.8). The group from Apollo 16, North Ray Crater, has ferroan bulk compositions and components are dominated by ferroan-anorthositic-suite lithologies. They have extremely low incompatible-element concentrations (e.g., TiO_2 <0.5 wt% and Th <1 ppm, see Figs. 3.6 and 3.7), and their compositions are very similar to the most feldspathic of the lunar meteorites (see Table A3.9).

Age relationships. The Apollo 16 breccias contain no clasts younger than 3.9 Ga, which is taken to be approximately the age of their formation. They have so little KREEP that it is reasonable to assume that they were assembled prior to the widespread distribution of KREEP by the Imbrium and other impact basins in the Procellarum KREEP Terrane.

Distribution. The feldspathic fragmental breccias are most common at the Apollo 16 site, specifically, in the ejecta of North Ray Crater. Stöffler et al. (1985) argued that the materials excavated from North Ray Crater represent the Descartes Highlands, which are, in turn, part of the ejecta deposit of Nectaris (see also Bussey and Spudis 2000). At the Apollo 16 landing site, the Descartes Formation is buried beneath the Cayley Formation, which is considered to be largely an Imbrium-produced deposit. Remote sensing indicates that the distinctive composition of materials excavated by North Ray crater as reflected by breccias such as 67455 (highly feldspathic and ferroan) is widespread to the east, towards and beyond Nectaris. In fact, the feldspathic fragmental breccias from North Ray Crater, along with the feldspathic lunar meteorites (see next section) provide the most plausible match for the vast anorthositic region of the Feldspathic Highlands Terrane on the lunar farside north of the equator.

2.1.8. Lunar meteorites. The lunar meteorites now constitute a large enough group of samples that they form a statistically significant data set. At the time of writing, the number of stones is in excess of 80 and the number of distinctly different sources, counting likely pairs (pieces of the same rock or different rocks likely to have come from the same crater) as a single source, is about 30 (see Tables 3.7 and 2.1). Because these are likely to represent more randomly sampled locations on the Moon than the six Apollo and 3 Luna sample locations, the distribution of rock types and compositions represented by the meteorites provide an important comparison to global compositional and mineralogical data sets. The range and distribution of compositions of the lunar meteorites contrast with those of the Apollo and Luna samples and reflect both the abundance of highly feldspathic highlands and of low-Ti basalts.

The meteorites fall into three broad groups, which are reflected on compositional plots of TiO_2 vs. FeO and Th vs. FeO (see Fig. 3.10, and Tables A3.9 and 2.1): (1) feldspathic regolith and impact-melt breccias, (2) mixed mare-highland breccias, and (3) mare basalts and gabbros. The feldspathic breccias form the most numerous group, accounting for ~62% of the samples both by number and by mass. The clustering of compositions of the feldspathic

Table 3.7. List of lunar Meteorites according to likely source pairs.

Designation	Lithology	mass (g)	mass all	TiO ₂	Al ₂ O ₃	FeO	Mg	Th (ppm)	Reference
Dhofar 081 (plus 280, 490, 910, 1084)	Fsp Fig Bx	174	459	0.15	30.5	2.93	2.82	63.1	Warren et al. (2001); Russell et al. (2004)
Dhofar 026	Fsp Gr Bx	148	0.22	29.6	4.06	3.92	63.3	0.4	Cohen et al. (2004)
Northwest Africa 482	Fsp IMBx	1015	0.16	29.4	3.80	4.28	66.8	0.2	Korotev et al. (2003b)
Dhofar 302, 305-307, 309-311, 489, 730-731, 908, 909, 911, 925, 1085	Fsp Rbx	1068	29						Russell et al. (2002); Nazarov et al. (2002, 2004), and Denitova et al. (2003)
QUE 93069 (plus 94269)	Fsp Rbx/IMBx	21	25	0.25	28.9	4.44	4.53	64.5	Korotev et al. (1996)
Dar al Gani 400	Fsp Rbx/IMBx	1425	0.18	28.9	3.70	4.88	70.1	0.3	Korotev et al. (2003b); simple average
Dar al Gani 262	Fsp RBx	513	0.20	28.4	4.47	5.50	68.7	0.4	Korotev et al. (2003b)
MAC 88105 (plus MAC88104)	Fsp RBx	663	724	0.23	28.1	4.28	4.05	62.8	Jolliff et al. (1991)
Yamato 86032 (plus 82192/3)	Fsp Fig Bx	648	712	0.23	27.5	4.82	5.32	66.4	Lindstrom et al. (1991a); simple average
“Achondrite 1153”	Fsp Rbx	???	0.18	27.4	5.20	3.89	57.1	Yanai and Ueda (2000)	
Yamato 791197	Fsp Rbx	52	0.40	27.3	5.71	5.76	64.3	0.3	Korotev et al. (2003b)
Northeast Africa 001	Fsp Rbx	262	~27					0.2	Haloda et al. (2005); Korotev and Irving (2005)
Dar al Gani 996	Frg Bx	12							Russell et al. (2003)
Dhofar 025 (plus 301, 304, 308)	Fsp RBx	751	772	0.29	26.9	4.90	7.10	72.1	Korotev et al. (2003b)
Pecora Escarpment (PCA) 02007	Fsp RBx	22	0.28	26.5	5.90	6.69	66.9	0.4	Korotev et al. (2004)
Dhofar 733	Fsp Gr Bx	98							Russell et al. (2003)
Allan Hills 81005	Fsp Rbx	31	0.27	25.7	5.47	8.17	72.7	0.3	Korotev et al. (1993)
Meteorite Hills (MET) 01210	North-bearing Bas Bx	23							Antarctic Meteorite Newsletter (Feb 2004)
Yamato 983885	Fsp RBx w/ bas	290		22.0					Warren and Bridges (2004)
Calablong Creek	Fsp RBx w/ basalt	19		0.80	20.9	10.9	5.14	45.7	Kaiden and Kojima (2002); Warren and Bridges (2004)
Yamato 981031 (plus 793274)	Mixed Bas/Fsp RBx	186	195	0.58	17.7	12.8	8.54	54.5	Hill and Boynton (2003)
QUE 94281	Mixed Bas/Fsp RBx	23	0.60	16.0	13.2	9.10	55.1	1.0	Korotev et al. (2003a); simple average
Sayh al Uhaymir (SatU) 169	KREEP IMBx w/ Reg	206	221	15.9	10.7	11.1	64.9	32.7	Jolliff et al. (1998)
EEI 87521 & 96008	Bas/Gab Fig Bx	84	0.53	14.8	16.2	8.91	49.3	1.0	Gnos et al. (2004)
Northwest Africa 3136	North-bearing Bas Bx	95							Korotev et al. (2002, 2003a); simple average
Yamato 793169	Low-Ti Basalt	6		2.11	11.8	20.7	5.58	32.5	Kuehner et al. (2005); Korotev and Irving (2005)
Northwest Africa 773 basaltic matrix	Bas RBx w/ Ol-Gab	633	0.78	10.6	17.3	13.2	57.6	0.7	Korotev et al. (2003a); simple average
Northwest Africa 773 Ol-cumulate	Ol-Cab cumulate			0.24	3.100	18.1	27.1	2.2	Fagan et al. (2003); and Jolliff et al. (2003)
Asuka 881757	Low-Ti Basalt/gabbro	442		2.42	10.0	22.6	6.04	1.6	Korotev et al. (2003a); simple average
LAP 02205 (plus LAPxxxx)	Low-Ti Basalt	1226	1875	3.23	9.9	22.3	6.34	33.6	Anand et al. (2004); Jolliff et al. (2004)
Northwest Africa 032 (plus 479)	Low-Ti Basalt	300	456	3.21	9.0	22.6	8.21	39.3	Fagan et al. (2002)
Dhofar 287	Basalt w/ RBx	154	2.86	8.1	22.2	12.3	49.7		Taylor et al. (2001)

Mass (g) column is the mass of the first meteorite listed. “Mass all” is the combined mass of the group if more than one meteorite is listed. Pairing as suggested by Korotev (see note below).

Fsp RBx = feldspathic regolith breccia; IMBx = impact-melt breccia; Gr Bx = granulitic breccia; Fig Bx = fragmental breccia; Bas = basalt; Gab = gabbro

EET: Elephant Moraine; LAP: LaPaz Icefield; MAC: MacAlpine Hills; QUE: Queen Alexandra Range (Antarctic locales).

An up-to-date, though subject-to-frequent-change resource at time of writing: http://epsc.wustl.edu/admin/resources/meteorites/moon_meteorites_list.html (maintained by R. Korotev)

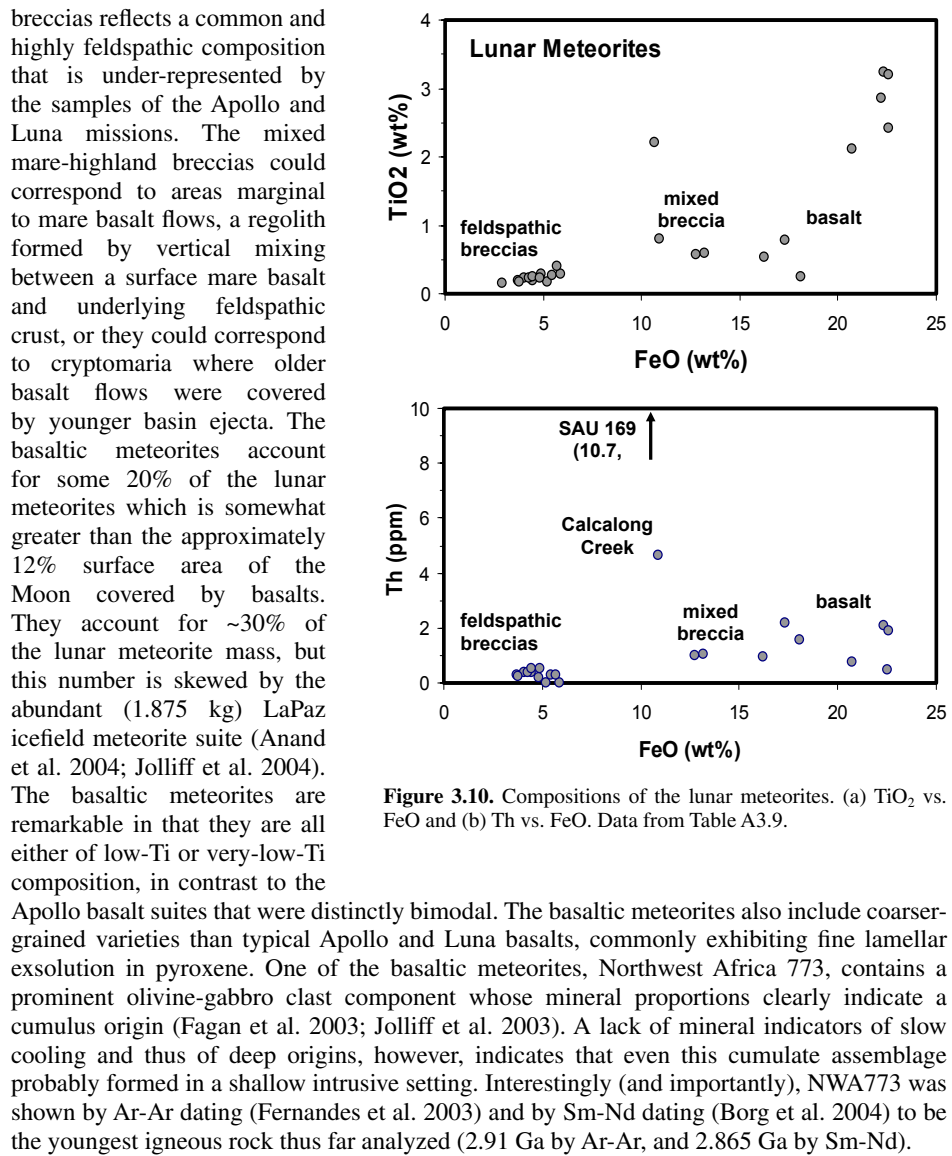


Figure 3.10. Compositions of the lunar meteorites. (a) TiO_2 vs. FeO and (b) Th vs. FeO . Data from Table A3.9.

The lunar meteorite groups correspond broadly to the major geologic terranes as expressed at the Moon's surface, with one apparent exception. The feldspathic breccias correspond well to the Feldspathic Highlands Terrane, with FeO concentrations of 3–6 wt% matching well with the peak of global values, especially over the northern far-side highlands. The percentage of feldspathic breccias among the meteorites is remarkably consistent with the proportion of the Moon's surface that falls in the range of "feldspathic" according to its FeO content (i.e., less than ~6 wt%). The low and very-low-Ti basaltic meteorites correspond to the abundant low-Ti basalt regions of the Moon as indicated by the global distribution of Ti (Giguere et al. 2000; Lucey et al. 2000; Gillis et al. 2003). Even the Procellarum KREEP Terrane is now represented by at least two of the meteorites, Calcalong Creek (Hill and Boynton 2003) and Sayh al Uhaymir 169 (Gnos et al. 2004), which have elevated concentrations of incompatible

elements. The only major terrane apparently not represented among the meteorites is the South Pole-Aitken basin, which is expected to yield samples that are relatively mafic but not necessarily basaltic. Although several of the meteorites (Yamato 981031, Yamato 793274 and QUE 94281) have bulk compositions that are intermediate in composition (e.g., ~13 wt% FeO), these are composed of bimodal mixtures of feldspathic and basaltic components (Lindstrom *et al.* 1991; Jolliff *et al.* 1998; Arai and Warren 1999).

2.2. Seismology

Of all the geophysical methods used to study the Earth's structure, seismology is uniquely suited to determine many parameters that are critically important to understanding its dynamic behavior. For this reason, NASA deployed seismometers on the lunar surface during each of the Apollo missions. Four of the passive seismic stations that were installed came to operate concurrently from Dec. 1972 to Sep. 1977, at which point the transmission of data was suspended because of a lack of funding. These stations were placed in an approximate equilateral triangle with distances between corners being about 1100 km and two of them, Apollo 12 and 14, placed only 180 km apart in one corner. In the 8-year period beginning with Apollo 11 when the experiment was underway, more than 12000 events were recorded (see Table 3.8). These events were found to differ in signal characteristics and were grouped into four categories: deep moonquakes, shallow moonquakes, meteoroid impacts and thermal moonquakes (see reviews by Toksöz *et al.* 1974, Nakamura *et al.* 1982, Lognonné and Mosser 1993, and Lognonné 2005).

In comparison to the Earth, the moonquakes are very small magnitude events with the largest, the shallow moonquakes, having Earth-equivalent body-wave magnitudes of about 5 (Goins *et al.* 1981b). The deep moonquakes are by far the most numerous events and generally have magnitudes less than 3. Stress drops associated with the shallow events are about 40 MPa (400 bars), whereas stress drops associated with the deep moonquakes are much smaller, being only about 10 kPa (0.1 bar). This manifests itself in a significant difference in the level of seismicity between the Earth and Moon. The annual seismic energy release from moonquakes was estimated to be about 10^{10} J, whereas it is $\sim 10^{18}$ J for the Earth (Goins *et al.* 1981b). The reason that such small events were observable at all is because the Moon's surface is very quiet in comparison to the Earth, with no oceans or an atmosphere to produce micro-seismic background noise.

The types of seismicity observed on the Moon are distinguishable from those that we observe on the Earth. Subsets of the deep moonquakes have nearly identical waveforms, implying a common origin in a small hypocentral region (Nakamura 1978), and occur monthly (Lammlein *et al.* 1974) deep within the Moon (~700-1200 km). These events were originally classified as belonging to 109 distinct hypocentral regions (Nakamura *et al.* 1982), and was recently updated to at least 166 (Nakamura 2003). The monthly intervals at which deep moonquakes occur suggest a strong relationship between them and the tides raised on the Moon by the Earth and the Sun. A large percentage of the seismic events observed on the short period components of the Apollo seismic experiment are very small moonquakes that occur with great regularity. These are believed to be natural seismic occurrences generated by small near-surface moonquakes less than about 1.5 to 4 km away that are triggered by diurnal thermal variations (Duennebier and Sutton 1974). Shallow moonquakes (~50 to 220 km depth, Khan and Mosegaard 2002) are the most energetic seismic sources observed on the Moon, although they are less abundant than the other types of seismic events, with an average of only

Table 3.8. Catalogued seismic events (Nakamura *et al.* 1982; Nakamura 2003).

Type	Number of events
Artificial impacts	9
Meteoroid impacts	1743
Shallow moonquakes	28
Deep moonquakes	7245
Unclassified	3533
Total	12,558

5 events occurring per year (Nakamura 1977). Shallow moonquakes are the only events that are believed to be related to tectonic activity (Nakamura et al. 1982).

The seismic events due to meteoroid impacts provide important information on the interplanetary medium, and the impacts detected correspond to meteoroids having estimated masses in the range from 100 g to 1 t or greater (Duennebier et al. 1975; Dorman et al. 1978; Oberst 1989). In addition, Earth-crossing cometary and asteroidal objects have been identified from the seismic data with the former occurring in clusters related to known meteor showers (Oberst and Nakamura 1991).

The lunar seismic signals were found to differ from terrestrial ones in their anomalously long continuance and high frequency content. For instance, the signal from the S-IVB impact continued for up to 4 hours. First arrivals typically are small, with slowly building amplitudes obscuring much of the information usually present in terrestrial seismograms. These characteristics are believed to be due to intense scattering in the highly heterogeneous and porous lunar regolith coupled with a low level of attenuation. The lunar crustal Q -value is an order of magnitude greater than the Earth's and is ascribed as being due to the absence of water and volatiles in the Moon (Latham et al. 1970a) (Q^{-1} is proportional to the fraction of energy that is dissipated in the lunar interior per loading cycle). This apparent complexity together with the small number of usable seismic events, the paucity of stations and their locations set certain limits on the amount of information that could be extracted from this dataset.

It has, nevertheless, been possible to retrieve a set of first arriving P- and S-waves that constitute the primary source of data from which several models of the lunar velocity structure have been obtained. Using linear inversion techniques (Toksoz et al. 1974; Goins et al. 1981a; Nakamura et al. 1982), the gross structure of the lunar interior has been delineated. Khan et al. (2000) reanalyzed the same dataset using a non-linear inversion technique, obtaining a more realistic view of the inherent resolution associated with the lunar seismic velocity profile. Lognonné et al. (2003) have further performed a complete reanalysis of the original data records which, when compared with the previous analyses, offers an assessment of the ambiguities in picking lunar arrival times.

Finally, we note that the information content of the Apollo seismic data has not yet been completely exhausted. As an example, the technique of using seismic-receiver functions has recently been shown to be viable in detecting converted phases at the crust-mantle interface (Vinnik et al. 2001). Additionally, waveform cross-correlation techniques have recently been used by Nakamura (2003) as a tool to reclassify and group the lunar seismic events. This study has discovered an additional 88 deep moonquake nests, and has further shown that 31 of the original 109 deep nests were incorrectly classified. While arrival times for these new deep moonquake sources have not yet been picked, they would aid in refining the seismic velocity structure of the deep lunar interior. It is further possible that some of these new sources have a far-side origin, allowing the question of whether or not the Moon possesses a core to be addressed (Nakamura 2005).

2.2.1. The crust-mantle interface. The Earth's internal structure can be thought of as a series of concentric shells, each of which transmits seismic waves at a different speed. The boundaries between shells are marked by seismic discontinuities at which the speed of transmission makes a sudden jump. The shallowest seismic discontinuity that is global in its extent is known as the Mohorovicic discontinuity, or Moho for short, and the terrestrial crust is almost always defined as the region above this discontinuity. The Moho was defined by Steinhart (1967) as the level where the compressional wave velocity first increases rapidly or discontinuously to a value between 7.6 km/s and 8.6 km/s. In the absence of a recognizable steep gradient, it is taken as the level where the P-wave velocity first exceeds 7.6 km/s. This definition was also employed in delineating the crust-mantle interface of the Moon (i.e., the "lunar Moho").

Geometrical ray theory has proven to be the most successful technique in tackling the lunar seismograms. Using this method, the crustal structure beneath the Apollo seismic stations, in particular stations 12 and 14, has been investigated using the artificial impact data set (this includes impacts of the lunar module ascent stage and the upper stage of the Saturn rocket). Epicentral distances range from 9 to 1750 km, although not all of these events have been recorded due to their limited energy and the sequential emplacement of the stations.

Several studies have reported crustal velocity profiles beneath the Mare Cognitum region near the Apollo 12 and 14 landing sites by inverting travel times of first P-wave arrivals (S-wave arrivals from the artificial-impact events are highly indistinct and accordingly were not used in these studies). Using linear inversion techniques, these models generally found that the seismic velocity gradually increased from the surface to a depth of \sim 20 km, at which point a seismic discontinuity was found. Below this depth, the velocity was found to be approximately constant down to the crust-mantle interface. Estimates for the thickness of the crust at this locale varied from 65 km (Toksöz *et al.* 1972), over 55 km (Toksöz *et al.* 1974), and finally 58 ± 8 km (Nakamura *et al.* 1982). It should additionally be mentioned that Goins *et al.* (1981c) obtained a crustal thickness of 75 km beneath the Apollo 16 site based on their identification of secondary phases that were interpreted as reflections off the lunar Moho. An additional reflected phase suggested to them that a 20-km discontinuity was present at this site as well. The data presented as evidence of these purported reflected and refracted arrivals, however, are not entirely convincing and await a reanalysis.

Figure 3.11 shows the seismic velocity model of the lunar crust and upper mantle as obtained by Khan *et al.* (2000). This model was constructed using a Bayesian inversion technique, and their seismic model is presented as a series of 1-D marginal probability distributions at 1-km depth intervals. As the contours in this image correspond to the likelihood of obtaining a given velocity at a given depth, it should be noted that the most probable velocity as a function of depth does not necessarily correspond to the most probable velocity profile. The construction of this profile used two arrivals at the Apollo 15 station and one at

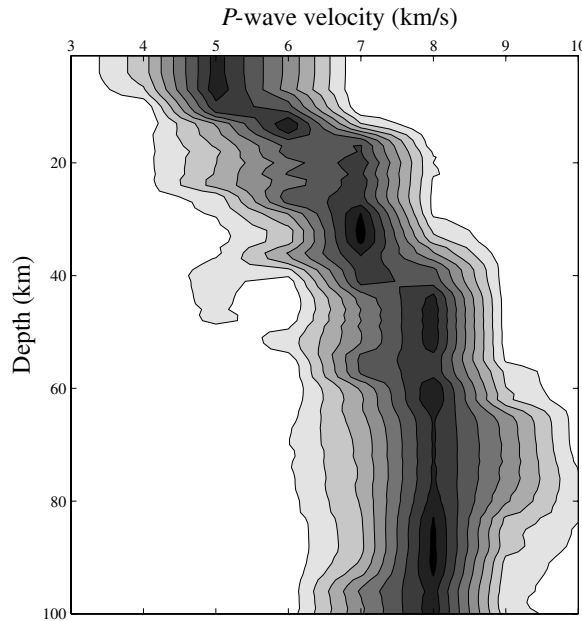


Figure 3.11. P-wave velocity model of the upper 100 km of the Moon derived from the non-linear Bayesian inversion of Khan *et al.* (2000). The marginal probability of the seismic velocity is plotted at one-kilometer depth intervals, and the contours define nine equally sized probability intervals.

the Apollo 16 station, with the remainder coming from stations 12 and 14. Hence, this velocity profile should be considered as representative of the Mare Cognitum region near the Apollo 12 and 14 landing sites. Of particular importance in this figure are the sharp increases in velocity that occur near 20 and 45 ± 5 km below the surface. The latter of these velocity increases is interpreted as representing the crust-mantle interface, and is designated by a P-wave velocity increase between the crust and upper mantle of ~ 1.0 km/s. Using Bayesian hypothesis testing to further distinguish between a thin or thick crust led to the result that a 35–45 km thick crust is highly favored to a crust 50–70 km thick. If the thin crust hypothesis is correct, then its thickness is 38 ± 3 km (Khan and Mosegaard 2002). An inversion by Lognonné et al. (2003), which is based upon an independent set of arrival times, also indicates that the crust at the Apollo 12 and 14 sites is thinner than previously assumed, possessing a thickness of only 30 ± 2.5 km. As will be shown in Section 2.6, estimates of the average crustal thickness based on inversions of gravity and topography data are more consistent with these recent thin-crust estimates than the Apollo era value of ~ 60 km.

2.2.2. The 20-km seismic discontinuity. The Apollo-era crustal velocity models beneath the Apollo 12 and 14 sites showed that the seismic velocity gradually increased from the surface to a depth of about 20 km, at which point a seismic discontinuity was observed. Beneath this depth to the base of the crust the seismic velocity was found to be relatively constant. The crustal velocity model of Khan et al. (2000) (as well as the preferred thin-crust model of Khan and Mosegaard (2002)) is also characterized by a sharp increase in velocity ~ 20 km beneath the surface. In this section, we assume that this feature is real and assess the possible origins that have been proposed for this seismic discontinuity.

The gradual increase in velocity with depth in the upper 20 km of the crust has been attributed to the closure of microfractures with increasing lithostatic pressure (e.g., Toksöz et al. 1972; Simmons et al. 1973). This interpretation is supported by the in situ measurement of seismic velocities for fractured lunar rocks as a function of increasing confining pressure, which shows a similar behavior (e.g., Todd et al. 1973; Wang et al. 1973; Simmons et al. 1975). The constant seismic velocity beneath a depth of ~ 20 km has been suggested to be representative of competent unfractured bedrock. While these interpretations are widely accepted, there is no consensus as to the origin of the sharp velocity increase that is observed ~ 20 km below the surface. Three possible explanations are that this feature is the result of (1) a fracture discontinuity, (2) a change in composition, or (3) a combination of the two.

Fracture discontinuity. It was recognized from investigations of the elastic properties of the returned lunar samples that the increase in lithostatic pressure with depth could not by itself produce a seismic discontinuity at ~ 20 km depth. Indeed, the confining pressure at a depth of ~ 60 km was shown to be insufficient to close all fractures in the lunar samples (Todd et al. 1973; Wang et al. 1973; Simmons et al. 1975). While Simmons et al. (1973) suggested that an increase in temperature with depth could have annealed fractures that were once present beneath a depth of ~ 20 km, this hypothesis has never been quantifiably tested.

Another hypothesis suggested by Simmons et al. (1973) for the intracrustal discontinuity is that the lower crust formed (i.e., crystallized from the magma ocean) after the major impact basins fractured the upper portion of the already solidified crust. However, since magma-ocean crystallization models at the time suggested that the entire crust probably formed in a relatively short time period of ~ 100 Ma (e.g., Solomon and Longhi 1977), this explanation never gained much popularity. Gamma-ray data obtained from the Apollo and Lunar Prospector missions (Lawrence et al. 1998, 2000), though, show that KREEP-rich rocks are primarily located in the regions of Oceanus Procellarum and Mare Imbrium, and this observation has suggested to some that the crystallization of the lunar magma ocean may have been prolonged beneath this region (Wasson and Warren 1980; Jolliff et al. 2000a; Korotev 2000; Wieczorek and Phillips 2000). Regardless of whenever the lower portion of the crust solidified in this

region, the high abundance of incompatible elements that are present there could have given rise to atypically high crustal temperatures, possibly contributing to the progressive annealing of fractures with depth.

Compositional discontinuity. It has been suggested by some that the sharp increase in seismic velocity at 20-km depth could (partly) be the result of a change in chemical composition (e.g., Toksöz *et al.* 1972, 1974). The initial interpretation was that the upper 20 km of crust was basaltic in composition, whereas the underlying crust was anorthositic. Even though the basalt flows in the vicinity of the seismic network are now thought to be no more than a kilometer thick, it is important to note that seismic velocity alone can not uniquely distinguish between rocks of gabbro, anorthositic gabbro, and anorthositic compositions (Liebermann and Ringwood 1976). Nevertheless, there are some compelling reasons to suspect that the deep crust might be compositionally distinct from the upper crust. As is discussed more thoroughly throughout this section, these include the following observations: (1) the ejecta of some large impact basins is more mafic than the surrounding highlands (e.g., Reid *et al.* 1977; Ryder and Wood 1977; Spudis and Davis 1986), (2) the central peaks of some complex craters contain mafic lithologies (e.g., Tompkins and Pieters 1999), and (3) the floor of the South Pole-Aitken basin, interpreted to represent lower crustal materials, has a highly noritic composition (Lucey *et al.* 1995; Pieters *et al.* 1997, 2001). We emphasize that these studies cannot easily distinguish between a compositionally zoned and stratified crust.

Compositional and fracture discontinuity. Aspects of the above two interpretations can be combined in two possible ways. First, Wieczorek and Phillips (1997) suggested that if the crust was initially stratified in composition, this might conspire to generate a fracture discontinuity as well. The rationale was that during the formation of an impact crater, a density contrast at depth would cause only some portion of the shock energy to be transmitted into the lower crustal layer, possibly inhibiting the formation of shock-related microfractures there. A second possible interpretation is that the crust within the region of Oceanus Procellarum is indeed stratified, with the upper crust being anorthositic and the lower layer being composed of Mg-suite plutonic rocks. Since the Mg-suite rocks generally have high abundances of incompatible elements, it is possible that the lower crust in this region was hotter than typical, causing fractures in the lower crust to completely anneal.

2.3. Gravity and topography datasets

2.3.1. Gravity. Because of a the relative velocity between the Earth and a spacecraft, a radio signal transmitted to or from the Earth will have its frequency shifted as a result of the Doppler effect. This phenomenon was first used by Muller and Sjogren (1968) to map the gravitational field of the Moon in the line-of-sight direction between the Lunar Orbiter spacecraft and the Earth. A surprising outcome of this pioneering work was the discovery of positive gravity anomalies over the depressions associated with the nearside impact basins. Since a surface depression that is isostatically compensated should possess a near-zero gravitational anomaly, these regions were inferred to contain some quantity of material that is not compensated. These inferred “mass concentrations” have ever since been referred to as “mascons.” This peculiar gravity signature has generally been interpreted as being the combined result of the uplift of the lunar crust-mantle interface beneath these impact basins, and/or the later flooding of mare basalts onto a thick and undeformable lithosphere (e.g., Wise and Yates 1970; Sjogren and Smith 1976; Phillips and Lambeck 1980; Phillips and Dvorak 1981). Mascon basins are also found on Mars (e.g., Yuan *et al.* 2001).

The collection of radio tracking data from the Apollo 15 and 16 sub-satellites and the Clementine and Lunar Prospector missions has subsequently greatly improved our knowledge of the lunar gravity field. The modeled gravitational-potential, U , has traditionally been expressed as a sum of spherical harmonic functions

$$U(r, \theta, \phi) = \frac{GM}{r} \sum_{i=1}^2 \sum_{l=2}^{L_{\max}} \sum_{m=0}^l \left(\frac{R}{r} \right)^l C_{ilm} Y_{ilm}(\theta, \phi) \quad (3.1)$$

where G is the gravitational constant, M is the mass of the planet, and (r, θ, ϕ) is the location of a point in space referenced to the center of mass of the body with $r > R$. Here, l and m are the degree and order of the spherical harmonic function Y_{ilm} , the corresponding spherical harmonic coefficient referenced to a radius R is C_{ilm} , and L_{\max} is the maximum degree of the expansion. The spherical harmonic functions are defined by

$$Y_{ilm}(\theta, \phi) = P_{lm}(\cos \theta) \begin{cases} \cos m\phi & i=1 \\ \sin m\phi & i=2 \end{cases} \quad (3.2)$$

where P_{lm} is an associated Legendre function, and are normalized such that the integral of the square of each spherical harmonic over the entire sphere is 4π . A useful visualization property of the spherical harmonic functions is that they have $2m$ zeros in the ϕ direction (longitude), and $l-m$ zeros in the θ direction (co-latitude). The effective wavelength of a given spherical harmonic can be approximated by $\lambda = 2\pi R/l$. The gravitational acceleration exterior to R is given by

$$\vec{g} = \nabla U \quad (3.3)$$

and the height of an equipotential, or level, surface (the geoid) with respect to a radius R is given to first order by

$$N(r, \theta, \phi) = R \sum_{i=1}^2 \sum_{l=2}^{L_{\max}} \sum_{m=0}^l C_{ilm} Y_{ilm}(\theta, \phi) \quad (3.4)$$

In center-of-mass coordinates the $l=1$ terms in the above sums are identically zero. The C_{1lm} and C_{2lm} terms are often referred to as C_{lm} and S_{lm} , respectively, and the C_{10} coefficients are typically referred to as $-J_1$ (see Lambeck (1988) and Kaula (1967; 2000) for further details). The J_2 term is affected by the rotational flattening of the Moon, and both the J_2 and C_{22} terms are affected by deformations caused by the gravitational attraction of the Earth.

The latest model of the lunar gravity field (Konopliv et al. 2001) includes the processing of tracking data obtained from the Lunar Prospector extended mission where the spacecraft sometimes approached the surface to within 10 km. While the nearside gravity field is now known to a good accuracy of ~ 30 mgals, because a spacecraft cannot be tracked much beyond the limbs of the Moon, the farside gravity field is only poorly determined, being uncertain by as much as ~ 200 mgals. As a spacecraft in orbit about the Moon can be tracked about 20° over the limb, the poorest gravity resolution occurs in an $\sim 60^\circ$ shadow zone centered on 0°N and 180°E . Gravity anomalies that are present within this shadow zone, however, do affect the long-term evolution of an orbiting spacecraft, and because of this it is possible to infer the gravity field within this region. Globally, though, the spherical harmonic gravity model is only accurate to approximately degree 15. Interpretation of farside gravity anomalies that are present within the shadow zone must be treated with caution as it is possible that their amplitudes have been muted and/or laterally offset.

The most recent JPL gravity model (LP150Q, Konopliv et al. 2001) has been determined up to degree and order 150, and possesses an effective half-wavelength spatial resolution of ~ 36 km. As the gravity field becomes increasingly noisy beyond approximately degree 100, and since the topography of the Moon is only known globally to less than degree 90 (with a half-wavelength resolution of ~ 60 km), we plot this gravity field in Color Plate 3.1 truncated at degree 90. This figure shows the familiar gravity highs over the major impact basins and the more poorly determined and noisy farside field. Even though direct tracking data does not

exist over most of the farside, many anomalies there are found to correspond to actual geologic features, such as the Hertzsprung, Korolev, and Mendeleev impact basins. Color Plate 3.2 shows the lunar geoid as determined from this gravity model. When the elevation of the Moon is referenced to the geoid (as opposed to a spheroid), lava flow directions should accurately track elevation changes (i.e., lava will flow “downhill”). We emphasize that the lunar geoid varies by almost a kilometer within the nearside maria, and that the gridded Clementine topography data is not referenced to the full geoid (see Section 2.3.2).

One of the more surprising discoveries from the Lunar Prospector based gravity fields is that some mascon basins do not appear to be associated (or only marginally) with mare basalts. A few of the most convincing non-mare mascon basins include Schiller-Zucchius (56°S , 44.5°W), Bailly (67°S , 68°W), Schrödinger (75°S , 134°E), Lorentz (34°N , 97°E), and Hertzsprung (1.5°N , 128.5°W) (e.g., Konopliv *et al.* 1998, 2001). While the interiors of some of these impact basins might contain mare deposits that were subsequently buried by impact ejecta from nearby craters (i.e., Schiller-Zucchius), it is unlikely that “cryptomare” is the entire origin of the gravity anomalies associated with these basins. Modeling of the thickness of the lunar crust has shed some light on the origin of the largest mascon basins. Neumann *et al.* (1996) found that the crust-mantle interface beneath some impact basins was uplifted above its isostatic position. Wieczorek and Phillips (1999) further found that some nearside basins were in a superisostatic state, even after the load associated with the mare basalt fill was removed. As was originally suggested by Neumann *et al.* (1996), this could be the result of the basin floor rebounding above its isostatic level during the impact event, and subsequently being frozen in place. This topic will be discussed in Section 5.1.2.

Finally, we note that the orientation of the Moon is controlled by differences in its principal moments of inertia, and that these moments completely determine the degree-2 gravity field. The minimum energy configuration of the Moon is a state in which the maximum moment of inertia lies along its rotational axis and where the axis of its minimum moment of inertia coincides with the Earth-Moon direction. We note that both the present orientation of the Moon, and one that is rotated by 180° about its rotation axis, are equally stable. The direction of the Moon’s center-of-mass/center-of-figure offset (which is a degree-1 feature) is unrelated to its current orientation.

2.3.2. Topography. The topography of the lunar surface has been measured in a number of ways, including the use of laser altimetry, stereo-photogrammetry, radar interferometry, radar sounding, and limb profile data. Prior to the Clementine mission, though, the highest resolution datasets were primarily restricted to the Earth-facing hemisphere and equatorial ground tracks of the Apollo command and service modules (see Bills and Ferrari 1977a and references therein). Data from the Clementine Lidar have since greatly improved our knowledge of the global shape of the Moon (Zuber *et al.* 1994; Smith *et al.* 1997). While this instrument was originally designed for military purposes, through careful in-flight programming of the ranging process, and judicious filtering of the returned data, near-global surface elevation data were obtained from this mission. However, because of the short time in lunar orbit (~ 2 months), and the high spacecraft altitudes over the poles, significant gaps in coverage exist.

During the first month of the Clementine mission, topographic profiles were obtained from 79°S to 22°N , and during the second month from 20°S to 81°N . The Lidar had an intrinsic range resolution of ~ 40 m, though absolute surface elevations may be uncertain by ~ 130 m as a result of uncertainties in the spacecraft orbit and orientation. The laser spot size on the lunar surface when the spacecraft was at perapse is ~ 200 m, and the minimum along-track spacing of shots is about 20 km. Over the rougher highlands many spurious returns were ultimately discarded, yielding a more typical along-track spacing of about 100 km. The cross-track spacing of the orbit tracks is approximately 60 km at the equator ($\sim 2^{\circ}$ of longitude; 1° of lunar longitude corresponds to 30.3 km).

Because of the non-optimal design of the Clementine Lidar, it is necessary to be aware of some possible artifacts in the data. Electronic noise and background solar radiation caused the Lidar to detect multiple returns for each laser shot. In order to determine which return (if any) was from the lunar surface, the data were filtered in two ways. First, up to four returns that occurred within an expected predefined range window were recorded. Second, a stochastic and fractal model of surface topography was used to construct a sequential filter to track the surface along a given profile (see Smith et al. 1997 for details). Filtering the data in this manner ultimately led to the acceptance of 72,548 range measurements.

All of the accepted elevations from the Clementine Lidar are plotted in Color Plate 3.3. Of particular notice are the uneven coverage and data gaps, especially over the poles. Elevation data is always reported with respect to some reference surface, and the data in this figure (as well as the $0.25^\circ \times 0.25^\circ$ gridded data on the PDS site) are referenced to a spheroid with an equatorial radius of 1738 km and a flattening of 1/3234.93 that corresponds to the J_2 portion of the lunar geoid. We emphasize that these data are not referenced to the full geoid; hence basalt flow directions inferred from this representation of the data may be erroneous, especially near the mascon basins.

The Clementine elevation measurements have been expanded in spherical harmonics up to degree and order 90 (GLTM2c) using the expression

$$h(\theta, \phi) = \sum_{ilm} H_{ilm} Y_{ilm}(\theta, \phi) \quad (3.5)$$

In contrast to the gridded dataset, the elevations are referenced to a sphere with a radius of 1738 km. The elevation of the lunar surface from this model, referenced to the full geoid, is plotted in Color Plate 3.4. Clearly visible in this image are the major impact basins and farside South Pole-Aitken basin. Also of note is the fact that the Moon possesses a 1.9 km displacement of the center of figure with respect to the center of mass toward the backside direction of 8°N and 157°W . The origin of this will be discussed in Section 2.7, and here we only note that this causes the average elevation of the nearside to be ~ 1.9 km less than that of the far side.

Another significant global feature of the Moon is its degree-2 shape. The Moon currently possesses an ~ 2.2 km polar flattening (related to the spherical harmonic term J_2), and a longitudinal ellipticity of 800 m (related to the spherical harmonic terms C_{22} and S_{22}) with the maximum amplitude occurring at $\sim 40^\circ\text{E}$. As a result of the combination of tides raised by the Earth and the rotation of the Moon, if the Moon were ever in a state of hydrostatic equilibrium, its expected shape and gravity field would be composed almost exclusively of J_2 and C_{22} terms, corresponding to a tri-axial ellipsoid. The measured values, however, are many times greater than what is expected for the current Earth-Moon separation. A popular explanation for the origin of the degree-2 shape and gravity field is that these terms were “frozen” into the lithosphere when the Moon was much closer to the Earth and was rotating more rapidly (e.g., Jeffreys 1970). Lambeck and Pullan (1980) estimated that the present shape of the Moon was similar to the equilibrium shape corresponding to an Earth-Moon separation of about 25 Earth radii (the Earth-Moon separation is currently about 60 Earth-radii). This interpretation is potentially problematic as the lunar orbit should rapidly evolve to a distance of ~ 30 Earth radii in less than 100 My (e.g., Webb 1982). It is alternatively possible that the degree-2 shape of the Moon is a result of primordial crustal thickness variations.

The fidelity of the Clementine altimetry data can be assessed by comparing it to independently obtained measurements. Using the technique of radar interferometry, Margot et al. (1999b) determined absolute elevations for the region of Tycho crater with a spatial and vertical resolution of about 200 and 30 m, respectively. Comparing this data set with the 87 Clementine measurements that occur in this region, two important differences were noticed. First, the Clementine data for this region appear to be shifted in latitude by ~ 3 km.

Second, while the RMS difference between the two data sets is only \sim 90 m, up to three of the Clementine measurements could be in error for this region. This latter result suggests that about 3–4% of the accepted Clementine range data could be erroneous.

Finally, two techniques have been used in an attempt to fill the polar data gaps of the Clementine altimetry data. Similar to the Tycho study above, Margot *et al.* (1999a) used radar interferometry to determine elevations poleward of 87.5° . Because of the Earth-Moon viewing geometry, these data were primarily obtained over the lunar nearside. These measurements have been used to constrain the elevations of those regions that are permanently shadowed and that might possess near-surface deposits of ice (see Chapter 2). An alternative method for determining polar topography is to use Clementine stereo imagery. Using these data, Cook *et al.* (2000) constructed digital elevation models poleward of 60° that possess a 1-km spatial resolution. These relative elevation determinations were tied to the absolute Clementine altimetry data, but while relative vertical elevations could be as good as 100 m, absolute elevations far from the Clementine tie-points might be in error by as much as a kilometer. The combination of elevation measurements obtained from stereo-imagery and radar-interferometry studies should ultimately be able to improve the current 90-degree spherical harmonic representation of the shape of the Moon. This would be of particular importance in modeling the high-resolution line-of-sight nearside gravity data obtained from the extended portion of the Lunar Prospector mission.

2.4. Thickness of the mare basalts

Knowledge of the thickness of extruded mare basalts is key to understanding the Moon's thermal history, lithospheric thickness, gravity field, and the effect of vertical impact mixing on regolith composition. Basic approaches for determining mare thicknesses make use of a flooded crater's morphology, the composition of crater ejecta, and subsurface reflections observed in the Apollo 17 radar sounding experiment. The interpretation of gravity anomalies can also be used to constrain the thickness of a mare deposit, though solutions based on this method are not unique. Using orbital images, the first two methods have been applied regionally, whereas the Apollo 17 radar sounding data are only applicable to swaths across the Serenitatis and Crisium basins, and Oceanus Procellarum. In this section, we review the results of these three approaches.

By assuming that a crater forms with a characteristic shape, the thickness of mare basalts within the rim of a partially flooded crater can be estimated (e.g., Baldwin 1970). The first depth estimates were made by Eggleton *et al.* (1974), using wrinkle ridges that were presumed to represent the crater rims of shallowly buried craters. Later, De Hon (1974; 1977; 1979) and De Hon and Waskom (1976) systematically mapped the thickness of the nearside maria using flooded and embayed crater relationships. In doing so, they found that the eastern maria averaged 200 to 400 m in thickness and that the western maria were closer to 400 m. Isolated regions thicker than 1 km were found to occur where basins and large craters are superposed on the floor of the Procellarum region and in the central portion of some of the larger impact basins. Individual basalt flows (where recognizable) vary considerably in thickness, but are generally in the range of 30 to 60 m (e.g., Schaber 1973; Schaber *et al.* 1976; Hiesinger *et al.* 2002). Thus, the above inferred basalt thicknesses imply the superposition of multiple discreet flows.

The accuracy of mare-thickness maps using the partially flooded crater method, however, is difficult to assess because of the few partially embayed craters that are present within the maria. Additional uncertainties are also inherent in the method for individual craters. For example, Hörrz (1978) concluded that the craters used to measure basalt thickness were more degraded prior to mare flooding than De Hon had originally assumed. Between the time of crater formation and mare inundation, crater profiles likely became shallower as a result of impact erosion, infilling by crater ejecta, and/or rebound of the crater floor. The net result of a shallower initial crater profile is an overestimation of mare thickness. On the basis of this

argument, Hörz (1978) reduced the depth of mare deposits obtained by De Hon by a factor of two. Another limitation to the method is that it can only measure the thickness of basalts deposited since the time the impact crater formed. If mare basalts were emplaced before the crater formed, then the actual basalt thickness could be considerably greater.

The above crater morphology studies could only determine mare thicknesses up to ~ 2 km, as a greater basalt thickness would completely bury any medium sized crater. A similar morphological technique was applied to large impact basins by Williams and Zuber (1998) that extended the maximum measurable basalt thickness up to ~ 7 km. Using Clementine altimetry, these authors determined the depth/diameter relationship for unflooded impact basins. Basins that possessed maria were found to be shallower than the depth-to-diameter trend predicted, and this shallowing was attributed to the thickness of mare basalts. The inferred mare thicknesses from this study are the following: Grimaldi (3.5 km), Humorum (3.6 km), Orientale (0.6 km), Nectaris (0.8 km), Smythii (1.3 km), Crisium (2.9 km), Serenitatis (4.3 km), and Imbrium (5.2 km). These values are in general thinner than previous studies that predicted basalt thicknesses up to 10 km (e.g., Solomon and Head 1980). We note that some of these thickness estimates may still be overestimated because some impact basins may have been partially shallowed by viscous relaxation (such as Imbrium and Serenitatis; see also Section 5.1.2). Thus, it seems likely that the basalts within the large impact basins are probably no thicker than about 4 km.

Clementine multispectral data, along with the relationship between the depth and diameter of a crater's excavation cavity (e.g., Croft 1980), have additionally been used to measure the thickness of mare basalts. In this technique, if impact craters excavate highland materials beneath the maria, the ejecta composition can be utilized to estimate the depth of the mare/highland interface. Specifically, a crater that penetrates the mare/highland contact at depth should excavate feldspathic materials that are spectrally distinct from the surrounding mare basalts. In general, these measurements are more robust than those of the crater infilling model because they offer an increased number of control points with which to contour basalt isopach maps. Moreover, the crater drill-core method is not sensitive to the amount of crater degradation prior to mare flooding, or whether these craters are perched on top of older mare deposits. The method does, however, rely on the accuracy with which highland materials can be detected in the ejecta of the observed craters, and this shortcoming will cause a slight overestimate of the mare thickness. In comparing the crater excavation method of measuring mare thicknesses with those previously determined by De Hon and Hörz for similar areas—Oceanus Procellarum (Heather and Dunkin 2002), Mare Humorum (Budney and Lucey 1998), and Mare Smythii (Gillis and Spudis 2000) it appears that in most instances thickness values are closer to those of Hörz (1978), thus supporting his lower thickness estimates for the maria.

The poor image quality of the lunar farside prior to the Galileo and Clementine missions prevented the measurement of farside mare thicknesses. Recent thickness measurements have been made using the methods discussed above, along with shadow measurements of flow fronts, and partially buried topography (Yingst and Head 1997, 1998, 1999; Gillis 1998; Gillis and Spudis 2000). These measurements yield basalt thicknesses of ~ 200 to 300 m on average, approximately half as thick as their nearside counterparts. There are a few deposits on the farside that approach or exceed 1 km in thickness, and these occur as isolated deposits within the South Pole-Aitken basin (e.g., Ingenii, Jules Verne, Leibnitz, and Von Kármán), Mare Orientale, and Mare Moscovense.

Another method of mapping the thickness of mare basalts comes from an analysis of data collected from the Apollo 17 radar sounding experiment (Phillips et al. 1973). After transmitting an energy pulse towards the Moon, this instrument measured the time delay between any reflected energy. In addition to detecting the initial signal reflected from the surface, reflections were often observed from subsurface horizons as well. Within the mare,

these horizons were found to be approximately parallel to the surface, and were interpreted to represent a partially developed regolith that was buried by subsequent lava flows (Maxwell and Phillips 1978; Peeples *et al.* 1978).

Within Mare Serenitatis, two nearly continuous buried horizons were observed, one at a mean depth of 0.9 km and the other at a mean depth of 1.6 km. The regolith horizon is required to be at least 2 m thick to be detectable, and several hundred million years are probably necessary to form such a layer (Sharpton and Head 1982). This suggests that at least two distinct major phases of mare volcanism occurred within this basin. While the deepest reflector in this basin most likely represents pre-mare “bedrock” (Sharpton and Head 1982), it is also possible that it might represent the top of another thick sequence of lava flows. Unfortunately, radar-sounding data over the Serenitatis basin was only obtained for the southern portion of this basin, leaving open the possibility that the basalts could be considerably thicker in the basin center. Nonetheless, these results imply that the basalts in this basin are on average at least 1.6 km thick, which is less than half of the 4.3 km value as determined by Williams and Zuber (1998). In Mare Crisium, only one nearly continuous reflector was observed at a mean depth of 1.4 km below the surface. In contrast to the Serenitatis basin, this profile passed through the center of this basin. If this subsurface reflector represents pre-mare bedrock, then the inferred average basalt thickness of this basin is again about half of the 2.9 km value as obtained by Williams and Zuber (1998). Alternatively, it is possible that this reflector might represent the surface of an older basaltic flow (Head *et al.* 1978). A subsurface horizon was also found in the central portion of Oceanus Procellarum (Cooper *et al.* 1994). These data show that the maria are about 1 km thick just east of Grimaldi, and decrease in thickness to ~0.6 km near the crater Kepler.

Integrating the above methods for measuring mare thickness indicates that the mare basalts are a volumetrically minor component of the crust. The average mare thickness on the nearside is generally less than 400 m with the basins containing up to 4 km of basalt fill. Mare thicknesses on the far side are comparatively thinner, with the average thickness being close to 200 to 300 meters. Even in the areas where the crust is thinnest on the far side (e.g., in South Pole-Aitken basin) mare thicknesses rarely exceed 500 m. One estimate of the total volume of extruded mare basalts is 10^7 km³ (Head and Wilson 1992). As these authors used mare thicknesses that were about twice that of De Hon’s measurements, this number should probably be viewed as an upper limit. Assuming an average thickness of 0.3 km yields a total mare basalt volume of 2×10^6 km³. Assuming that the lunar crust is on average 50 km thick, the mare basalts only represent about 0.1–0.5% by volume of the crust.

2.5. Lithospheric thickness and mascon tectonics

The elastic lithosphere defines the strong outer rind of a planetary body. Because the lithosphere must be relatively cold to maintain its strength, its thickness provides information on the temperature of the shallow portions of the Moon and thus can constrain thermal history models (see Chapter 4). In this section, we focus on the principal methods that have been used to infer lunar lithospheric thicknesses—faulting around mascons—and critically examine what work remains to be done. We briefly mention how gravity and topography studies have also been used to estimate the lithospheric thickness of the Moon.

Mascons are excess concentrations of mass that act as loads on the lunar lithosphere, causing it to flex under the applied force (e.g., Melosh 1978). If the stress within the lithosphere exceeds a critical value (the yield stress) the material will fracture, possibly resulting in visible faults on the surface of a planet. Around many of the mascon basins, faults are indeed visible as concentric or linear rilles (interpreted as grabens), and within the mare as ridges (i.e., “wrinkle” ridges interpreted to be thrust faults (e.g., Golombek 1985)). Many have assumed that these faults formed when the flexural stresses within the lunar lithosphere exceeded the yield stress, and that the location and width of the faulted zones can be related to the thickness

of the lithosphere at this time (e.g., Comer et al. 1979; Solomon and Head 1979, 1980; Freed et al. 2001). It is important to note that since the lithosphere is in reality not perfectly elastic, the obtained values should be considered as an “effective” elastic thickness (Burov and Diamant 1995; Kohlstedt et al. 1995). The effective elastic thickness is, furthermore, likely to differ from the lithospheric thicknesses as defined by thermal considerations (e.g., McNutt 1984).

The method of matching flexural topographic profiles from a load to the location and width of zones of faulting is well established and has been used on all of the terrestrial planets (e.g., Thurber and Toksöz 1978; Solomon and Head 1980; McGovern and Solomon 1993, 1998; Albert et al. 2000). In interpreting these results, though, it is important to consider the limitations of the present models and our ignorance of the rheology of the outer layers of planetary bodies. Plate-flexure models that have been applied to the Moon generally assume that the lithosphere behaves purely elastically (see Zhong and Zuber 2000 for a visco-elastic treatment). Once the stress exceeds the yield stress, however, the material is no longer elastic and is assumed to behave plastically. This means that fractures or faults relieve some of the elastic stress and change the stress distribution within the lithosphere (Schultz and Zuber 1994). No models of mascon tectonics to date have yet modeled this inelastic rheology correctly (Albert and Phillips 2000; Albert et al. 2000), so models are really only able to predict how the material initially fails. Pre-existing faults (perhaps caused by the basin-forming impact) might also affect the distribution of stress within the lithosphere and how the material fails. The state of stress before the mascon load was applied is additionally poorly constrained. Some indication of the state of isostasy before mare emplacement is provided by the lunar gravity and topography fields (Neumann et al. 1996; Konopliv et al. 1998, 2001 Wieczorek and Phillips 1999), and these studies suggest that while some basins might have been in a pre-mare isostatic state, others were probably not.

The plate flexure models also require specific knowledge about the load, such as the temporal and spatial distribution of the mare load, and how much of the load is from the top and bottom (e.g., mare basalts vs. volcanic intrusions, respectively). The plate flexure model also requires a knowledge of the elastic properties of the lithosphere (rigidity and Poisson’s ratio), but the vertical and lateral variations of these parameters within the lunar lithosphere are not well constrained. In order to understand how the stresses induced by flexure causes faulting, a rock-failure criteria must be used, and different criteria can yield different results (Freed et al. 2001).

Many of the uncertainties mentioned above have important or unknown effects upon calculated estimates of the lithospheric thickness. Important first steps in exploring this parameter space have been made by Solomon and Head (1980), Pullan and Lambeck (1981) and Freed et al. (2001). Even with the above-mentioned uncertainties, much can be learned by modeling the locations of compressional and extensional features. Solomon and Head (1980) looked at 8 different basins and found that the extensional rilles formed when the lithosphere was thin (less than about 70 km) and that the ridges formed later when the lithosphere was thicker (more than 100 km). The ridges are mostly younger than the rilles, so the thicker lithosphere associated with the younger features is consistent with the lithosphere cooling and thickening with time. Solomon and Head (1980) also found that some basins with the same age have different lithospheric thicknesses at the time of rille formation, but that the thickness at the time of ridge formation was more uniform. They interpret this to mean that there was shallow thermal heterogeneity in the Moon during rille formation, but that with time, thermal conduction or convection evened out the shallow temperature differences.

Although simple plate flexure models can explain the origin of concentric rilles and radial ridges, a major problem is that the early models predicted that there should be strike-slip faulting between these two regimes. No significant strike-slip faulting is visible anywhere on the Moon, and this discrepancy has been called the “strike-slip paradox.” Several potential

resolutions of this paradox have been proposed. Solomon and Head (1980) postulated that global expansion and contraction related to the lunar thermal evolution (e.g., Solomon and Chaiken 1976) modified the local stress field around the mascons and inhibited strike-slip faulting. If true, the timing and location of faulting at the mascons provides a stringent constraint on lunar thermal histories. Golombek (1985) noted that strike-slip faulting is not likely to occur where faults actually nucleate, several kilometers beneath the surface, especially if the stress distribution in the megaregolith is not isotropic. Schultz and Zuber (1994) further noted that (1) because the load was not placed instantaneously, the history of loading and faulting must be considered, and (2) the mode of failure is non-unique in that it could be strike-slip or tensional jointing. Freed *et al.* (2001) have recently shown that lunar curvature, certain initial stress distributions, and certain failure criteria reduce, and perhaps eliminate the zone of strike-slip faulting.

While the strike-slip paradox has been given much attention in the literature, there is another aspect of lunar tectonics that until recently has remained just as paradoxical. Namely, plate flexure models predict that radial compressive faults should preferentially form in the central portion of the mare basalt load (e.g., Melosh 1978), whereas geologic mapping of the mascon basins shows that the majority of ridges within the mare filled basins are in fact concentrically oriented (e.g., Solomon and Head 1980). In the study of Freed *et al.* (2001), it was shown that by taking into account a putative global compressive stress field, as well as the temporal history of basaltic eruptions in a basin, that it is possible to form both concentric and radial ridges within the basin. While this is one possible explanation, an analysis of their figures reveals two other explanations that we consider to be equally plausible. First, the geometry of the load was shown to influence where radial and concentric ridges should form. In particular, if the mare basalts were much thicker in the central portion of the basin than near its periphery, then radial ridges were favored to form. In contrast, if the basalts in the basin had a more uniform thickness (as is the case for at least Mare Crisium; see Section 2.4), then the formation of concentric ridges would be favored. In addition, the pre-mare isostatic state of the basin was shown to influence the distribution of radial and concentric ridges. If the basin was initially sub-isostatic, and the basin floor subsequently rebounded after mare flooding, then the formation of radially oriented ridges would be favored. In contrast, if the basin was initially super-isostatic, then basin subsidence after mare volcanism would be enhanced and the formation of concentrically oriented ridges would be favored. As many basins are predicted to have been in a pre-mare super-isostatic state (Neumann *et al.* 1996; Konopliv *et al.* 1998, 2001; Wieczorek and Phillips 1999), this latter explanation is particularly compelling.

Considering the simplifications used in relating mascon tectonics to lithospheric thickness, it is useful to consider methods based on gravity and topography data for constraining this quantity. It is important to realize, though, that the lithospheric thickness recorded by the formation of rilles and ridges might be from a time that is different than those recorded by a basin's current gravity and topography fields. Using the Apollo data, Kuckes (1977) found the elastic lithospheric thickness at several basins to be around 50 to 100 km. Using Clementine gravity and topography data and a thin elastic spherical shell formulation Arkani-Hamed (1998) found the elastic thickness to range from about 20 to 60 km beneath the nearside mascon basins. Using Lunar Prospector gravity data, Aoshima and Namiki (2001) reported that for at least the Orientale and Serenitatis basins, the lithospheric thickness was not well constrained, casting doubt on whether gravity and topography will be as useful as mascon tectonics in determining lithospheric thickness at the time of mare basalt loading. In an investigation by Sugano and Heki (2004), the gravity signatures of the major basins were modeled by assuming an initial basin topographic profile, and then comparing the flexural deformation of the Moho with mass deficits inferred from their present Bouguer anomalies. Lithospheric thicknesses were generally found to lie between 20 and 60 km, with Serenitatis and Imbrium possessing smaller values. However, the employed crater diameters were taken

from Wilhelms (1984), and if the excavation cavity diameters of Wieczorek and Phillips (1999) were used instead, elastic thicknesses close to zero would be obtained for most basins (T. Sugano, personal communication 2005). This would imply that these basins were in a pre-mare isostatic state before the emplacement of the mare basalts. Elastic thickness estimates were also reported in a study by Crosby and McKenzie (2005), but their model admittance spectra were not windowed in the same manner as the observations (see Pérez-Gussinyé et al. 2004). In comparing the above studies, it should be clear that there is no consensus concerning the thickness of the elastic lithosphere based on gravity and topography methods.

In the final analysis, there is still much work to be done in determining the lunar lithospheric thickness and how it varies both spatially and temporally. A more complete exploration of the parameter space of mascon tectonic models is needed and more sophisticated models that include inelastic effects need to be applied. As for inversions based on gravity and topography data, the major impediment is the lack of a suitable loading model that correctly takes into account the basin forming process (which may include acoustic fluidization of the crust (Melosh 1979) and near-instantaneous Moho uplift), the initial surface and Moho relief, the loads associated with ejecta exterior to the basin, and the spatial and temporal loading history of mare volcanism. Without such a model, gravity and topography data in this regard will probably be limited to determining the degree of compensation of a basin at the present time, and before the commencement of mare volcanism.

2.6. Gravity and topography admittance studies

If the density structure of a planet were completely known, then it would be straightforward to compute the gravitational attraction at any point in space by employing Newton's law of gravitation. Unfortunately, as a result of the non-uniqueness of potential modeling, it is conversely not possible to uniquely invert for the density structure of a body by using gravity and topography information alone. This non-uniqueness of potential modeling, however, can be overcome by invoking reasonable assumptions about the interior structure of a planet.

In this section, we describe two general techniques that have been used to place constraints on the thickness of the lunar crust. One method relies upon the relationship between the lunar geoid and topography in the space domain, whereas the other relies upon the relationship between these fields in the spectral (wavelength) domain. Both techniques are roughly consistent in suggesting that the lunar crust is on average about 50 km thick. A summary of the various methods that have been used to constrain the average thickness of the crust is given at the end of this section.

2.6.1. Geoid to topography ratios. Both spatial and spectral techniques have been used to invert for the average thickness of the crust for planetary bodies, with each technique possessing its own merits and caveats. Both methods first assume that the crust is compensated by a specific model (i.e., Airy, Pratt, or elastic support), and then adjust the parameters of this model in order to best match the observed relationship between these two fields. One of the strengths of investigating the relationship between the lunar geoid and topography in the space domain is that certain regions can be excluded from consideration if they appear to be inconsistent with the assumed compensation model. For instance, it is reasonable to assume that the lunar highland crust might be compensated by an Airy mechanism, in which surface topography is supported by a crustal root. As the lunar mascon basins are clearly inconsistent with this hypothesis, these regions can be simply ignored in the analysis.

One spatial inverse technique that relates isostatically compensated topography to its associated geoid anomaly was developed by Ockendon and Turcotte (1977) and Haxby and Turcotte (1978). If the crust is compensated by an Airy mechanism, the local geoid to topography ratio (GTR) was shown to be proportional to the average crustal thickness. A more accurate approach was developed in spherical coordinates by Wieczorek and Phillips (1997)

who showed that the previous technique incurred errors on the order of 10 km for small planets such as the Moon and Mars (see also Wieczorek and Zuber 2004).

In an investigation by Wieczorek and Phillips (1997), geoid to topography ratios of the nearside highland crust were determined after excluding the maria and removing the degree-2 terms from the lunar gravity and topography fields. We have redone these calculations here using the updated gravity model of Konopliv *et al.* (2001) and obtain an average GTR of 26.7 ± 6.9 m/km. If the lunar crust is compensated by an Airy mechanism, then this value corresponds to a globally averaged crustal thickness of 49 ± 16 km. In comparing this value to the seismically constrained crustal thickness near the Apollo 12 and 14 sites, the difference in elevation between these sites and the mean planetary radius must be considered. If we assume that the degree-2 portion of the lunar topography is entirely the result of rotational and tidal flattening (see Section 2.3.2), and hence ignore these terms, then the average elevation of these sites is about 1.6 km below the mean planetary radius. Assuming reasonable values for the density of the crust (2710 – 2885 kg m $^{-3}$) and mantle (3200 – 3335 kg m $^{-3}$) the crustal thickness at the Apollo 12 and 14 sites based upon the above GTR analysis is predicted to lie between 16 and 56 km. (If the degree-2 topography were retained in the above analysis, then the average elevation of the Apollo 12 and 14 sites would be about 1.0 km below mean planetary radius, and the inferred crustal thickness there would be slightly greater.)

The Apollo-era seismic velocity profile beneath the Apollo 12 and 14 sites (e.g., Toksöz *et al.* 1974) suggested that the crust there was about 60 km thick. As this is outside the range inferred from the above study, Wieczorek and Phillips (1997) suggested that the highland crust was more consistent with being partially compensated at an intra-crustal interface, as opposed to solely at the crust-mantle interface. The simplest interpretation was that the upper crust was “floating” on a more-mafic lower crust, and in support of this hypothesis they noted that a seismic discontinuity appears to exist about 20 km beneath the surface that could be compositional in origin (see Section 2.2.2). Reanalyses of the Apollo seismic data by Khan and Mosegaard (2002) and Lognonné *et al.* (2003), however, forces us to re-evaluate this hypothesis. In contrast to the Apollo-era models, these recent studies imply that the crust beneath the Apollo 12 and 14 sites is between 27 and 50 km thick. As this is within the range of 16 to 56 km as predicted by the above Airy compensation model, the seismic and gravity data can now be considered consistent with the hypothesis of an Airy compensated uniform density crust.

In addition to the above single layer compensation model, Wieczorek and Phillips (1997), also considered models in which the surface topography was compensated at both intracrustal and crust-mantle interfaces. In one model, the upper crust was constrained to have a constant thickness while the lower crustal thickness varied, whereas in a second model the inverse was assumed. Using the crustal thickness constraints of Khan *et al.* (2000) we find that the highland GTRs and inferred Apollo 12 and 14 crustal structure are only consistent with the model in which the upper crustal thickness varies while possessing a constant thickness lower crust. This model is consistent with the expectation that impact cratering would primarily redistribute upper crustal materials, leaving the lower crust of the highlands relatively untouched.

If it is assumed that the crust is entirely compensated by lateral variations in density (i.e., topographic highs correspond to lower crustal densities as in the model of Pratt) then the average crustal thickness derived from the above calculated GTRs is constrained to lie between 53 and 96 km. As this model predicts the crustal thickness of the Apollo 12 and 14 sites to be greater than 52 km, this model is inconsistent with the recent seismic velocity models. Wieczorek and Phillips (1997) have further shown that the composition and density of the highland crust (as inferred from the Clementine-derived iron abundances of Lucey *et al.* (1995)) are not significantly correlated with elevation, suggesting that Pratt compensation is not of regional importance. As is discussed in Section 2.7.1, though, it is still possible that a portion of the Moon’s center-of-mass/center-of-figure offset could be caused by hemispheric variations in crustal density.

We note briefly that two other studies have used geoid-to-topography ratios to constrain the thickness of the lunar crust. Using the Cartesian method of Ockendon and Turcotte (1977) and Haxby and Turcotte (1978), Arkani-Hamed (1998) obtained an average crustal thickness of 52 km (no error bar quoted) for the region encompassing the South-Pole Aitken basin. While this value is in agreement with those presented above, the assumption of Cartesian geometry may have biased this number by ~ 10 km. Furthermore, as will be discussed in Section 2.8.4, the floor of the SPA basin is more mafic and dense than the surrounding highlands, complicating the interpretation of this result. The gravity and topography coverage of this basin is also less well known than that of the nearside. Konopliv et al. (1998) have also attempted to place constraints on the thickness of the lunar crust by using the same Cartesian method. The average crustal thickness from their study, however, varies from less than zero to more than 200 km, and we suspect that this unphysical behavior is in part the result of not removing the mascon basins prior to computing regional geoid to topography ratios.

2.6.2. Spectral admittance studies. A different approach to modeling the relationship between the gravity and topography fields of a planet is to work in the spectral domain. In contrast to the spatial approach described above, in which a single admittance (GTR) is calculated for a given region, spectral approaches result in admittance and coherence functions that are wavelength dependent. One of the benefits of using a spectral approach is that the form of these functions can give clues to the compensation mechanism that is operating in the study region. If multiple compensation mechanisms are locally present, then it may be possible to isolate the effects of each by analyzing different wavelength bands. In addition, since an individual admittance and coherence is calculated for each wavelength under consideration, it is in principle possible to invert for multiple model parameters.

While spectral approaches are often superior to the interpretation of a single spatially derived geoid to topography ratio, they have their associated caveats as well. A primary drawback is that the methods so far employed could only investigate regions that are either square in Cartesian studies (e.g., Forsyth 1985; Simons et al. 2000) or circular in spherical studies (Simons et al. 1997; Wieczorek and Simons 2005). Hence, if one wishes to investigate a region that is compensated by a single mechanism, this restriction will often place strict constraints on the size of the study region, and hence the maximum wavelength that can be analyzed. As an example, the largest nearside highlands region that can be studied while avoiding the lunar maria and mascon basins is about 1000 km wide. In this case, the longest wavelength that could be analyzed would correspond to about degree 10. In contrast, GTR studies for the Moon are most sensitive to degrees less than this; spatial and spectral studies are thus seen to provide complementary information. We note that a recent method developed by Simons et al. (2006) allows for the spectral analysis of irregularly shaped regions on the sphere, and this somewhat mitigates the drawbacks associated with applying spectral admittance studies to the Moon.

Simons et al. (1997) have developed a technique in which spectral admittance and coherence functions are estimated for localized regions on a sphere. In this approach, the gravity and topography fields are multiplied by a windowing function (which is expanded in spherical harmonics up to a maximum degree L) that isolates a particular region. The optimal windows for this procedure are described in Wieczorek and Simons (2005). As the multiplication of two fields in the spatial domain is analogous to the convolution of their spherical harmonic coefficients in the spectral domain, a complementary tradeoff was shown to exist between spatial and spectral resolution. In particular, since the gravity and topography fields are spectrally truncated at a maximum degree L_g , the maximum degree that can be analyzed is $L_g - L$. Hence, the more that one localizes the data (i.e., the sharper the window and the greater L), the fewer the number of degree-dependent admittances that can be analyzed.

This localized spectral analysis technique was applied by Aoshima and Namiki (2001) to the nearside mascon basins in order to place limits on the average crustal thickness and elastic

thickness. As the thickness of the mare basalts in these basins is not well constrained, this was estimated by assuming that these basins were in a state of Airy isostasy prior to the commencement of mare volcanism, and that these loads are presently supported by the elastic lithosphere (see also Bratt *et al.* 1985). Their results are presented in Table 3.9. Wieczorek and Phillips (1999) have shown that this pre-mare isostatic assumption is probably valid for those basins that formed within the Procellarum KREEP Terrane (see Section 5.1.2; Imbrium, Serenitatis, Humorum, and Grimaldi), and for Serenitatis and Humorum, an average crustal thickness of 50 ± 10 and 50 km was determined, respectively. These values are consistent with those from the highland GTR analysis presented in the previous section. The interpretation of the other basins in their study is less certain as the validity of the pre-mare isostatic constraint is questionable.

In another study, Arkani-Hamed (1998) used a Cartesian admittance modeling approach to investigate the region encompassing the South Pole-Aitken basin. Assuming that this region is compensated by an Airy mechanism, he discarded those wavenumbers that did not show a positive correlation between the gravitational potential and topography. This spectral editing procedure improved the spectral correlation between the two fields and a reference crustal thickness of 54 km (no error bar quoted) was obtained. However, as the spectral admittance function was not explicitly shown, it is difficult to assess the uncertainty associated with this number. It is also not clear as to whether the lack of topographic data poleward of 80°S , the low fidelity of the farside gravity field, or the Cartesian approximation in this analysis biased this crustal thickness determination. This value is, nevertheless, consistent with the above-mentioned studies.

2.6.3. The average thickness of the lunar crust. The above admittance studies place constraints on the average thickness of the lunar crust that are independent of the Apollo seismic data. As is summarized in Table 3.9, these studies are in general agreement. Assuming that the crust is compensated by an Airy mechanism, the highland geoid to topography ratios imply

Table 3.9. Reference thickness of the lunar Crust.

Region	Reference Crustal Thickness (km)	Comments
<i>Extrapolating Apollo 12/14 seismic constraints to mean planetary radius</i>		
[†] Nearside highlands	65 – 76	Airy compensation; Toksöz <i>et al.</i> (1974)
[†] Nearside highlands	45 – 66	Airy compensation; Khan <i>et al.</i> (2000)
[†] Nearside highlands	33 – 48	Airy compensation; Lognonné <i>et al.</i> (2003)
<i>Geoid to topography ratios</i>		
Nearside highlands	49 ± 16	this study
[§] South Pole-Aitken	52	Arkani-Hamed (1998)
<i>Localized admittance modeling</i>		
Serenitatis	50 ± 10	Aoshima and Namiki (2001)
[*] Crisium	35 – 40	Aoshima and Namiki (2001)
[*] Nectaris	50 ± 5	Aoshima and Namiki (2001)
[*] Orientale	70 ± 5	Aoshima and Namiki (2001)
Humorum	50	Aoshima and Namiki (2001)
[*] Humboldtianum	55 ± 5	Aoshima and Namiki (2001)
<i>Cartesian spectral admittance modeling</i>		
[§] South Pole-Aitken	54	Arkani-Hamed (1998)

[†]Includes the cases where the degree-2 topography is assumed to be compensated and uncompensated.

^{*}These basins may not satisfy the pre-mare isostatic assumption.

[§]Based on farside gravity data.

that the average crust is 49 ± 16 km thick. Using localized spectral admittance functions, the two basins that are likely to satisfy the pre-mare isostatic assumption give a reference crustal thickness of 50 ± 10 km and 50 km for the Serenitatis and Humorum basins, respectively (Aoshima and Namiki 2001). A Cartesian admittance analysis of the South Pole-Aitken basin also suggests that the average crustal thickness is about 54 km (Arkani-Hamed 1998).

As was discussed in Section 2.2, the crust beneath the Apollo 12 and 14 sites was determined to be about 60-km thick during the Apollo era, whereas the reanalyses of Khan et al. (2000), Khan and Mosegaard (2002) and Lognonné et al. (2003) suggest a thinner crustal thickness of 45 ± 5 km, 38 ± 8 km, and 30 ± 2.5 km, respectively. We can now compare these thick and thin seismic estimates with the results of the above gravity-topography admittance studies. In doing so, we will assume that the Apollo 12 and 14 sites are compensated by an Airy mechanism and extrapolate the seismically derived crustal thickness to the mean planetary radius. For the following calculations, we will include the cases where the degree-2 topography of the Moon is compensated and where it represents the Moon's equilibrium shape that was frozen into the lithosphere when the lunar orbit was closer to the Earth (e.g., Lambeck and Pullan 1980). If the crust at this locale was 60-km thick, then using a plausible range of crustal and mantle densities (see Section 2.6.1) the average thickness at mean planetary radius would lie between 65 and 76 km. We note that this value is inconsistent with the estimates inferred from the gravity and topography admittance studies. In contrast, if we assume that the thickness of the crust beneath the Apollo 12 and 14 sites is 45 ± 5 km, then the average crustal thickness at mean planetary radius would lie between 45 and 66 km. Assuming yet a thinner value of 30 ± 2.5 km yields the range of 33–48 km. The limits of the above two thin-crust extrapolations are nearly identical to those of the GTR analysis of Section 2.6.1, and we therefore advocate an average lunar crustal thickness of 49 ± 16 km.

2.7 Crustal thickness models

It was recognized very early that the lunar gravity and topography fields are highly correlated with the large impact basins. The large positive gravity anomalies that were found over these topographic depressions led to the hypothesis that these were the result of both uncompensated basalt flows and relief along the crust-mantle interface (e.g., Wise and Yates 1970; Sjogren and Smith 1976; Phillips and Lambeck 1980; Phillips and Dvorak 1981). Based on higher resolution gravity and topography data, the mascons associated with some basins have been suggested to be the result of superisostatic uplift of the lunar mantle (Neumann et al. 1996; Konopliv et al. 1998, 2001; Wieczorek and Phillips 1999).

A number of attempts have been made to constrain globally the crustal thickness variations of the lunar crust using both gravity and topography data (e.g., Bills and Ferrari 1977b; Thurber and Solomon 1978; Bratt et al. 1985; Zuber et al. 1994; Neumann et al. 1996; von Frese et al. 1997; Arkani-Hamed 1998; Wieczorek and Phillips 1998). While the approach of each study is slightly different, a commonality among them is the assumption that the observed gravity field is the result of surface topography, mare basalts, and relief along the crust-mantle interface. Some of these studies have additionally attempted to take into account the effects of impact brecciation (Phillips and Dvorak 1981; von Frese et al. 1997), or the effects of density stratification within the crust (Wieczorek and Phillips 1998). As gravity modeling is non-unique, these crustal thickness models have traditionally been anchored to the seismically constrained crustal thickness of 60 km (e.g., Toksöz et al. 1974) at the Apollo 12 and 14 sites. Recent seismic inversions, however, suggest that the crustal thickness at these two sites is probably considerably thinner than once thought; in particular 45 ± 5 km (Khan et al. 2000), 38 ± 8 km (Khan and Mosegaard 2002), and 30 ± 2.5 km (Lognonné et al. 2003). In this section, we construct new crustal thickness models that utilize these new seismic constraints and the latest gravity model of Konopliv et al. (2001).

While there are many complications in constructing a crustal thickness model, the general approach is relatively straightforward. First the gravity field that results from the surface topography is computed (the Bouguer correction). This contribution is subtracted from the observed free-air gravity field of the planet, resulting in the Bouguer anomaly. Finally, the Bouguer anomaly is interpreted as relief along a subsurface density interface. The first complication is related to how one computes the gravity field of relief along a density interface. Standard first-order potential theory predicts the spherical-harmonic gravity and topography coefficients to be linearly related. Neumann *et al.* (1996), however, emphasized that the large crustal thickness variations inferred for the Moon invalidate this approximation. Using the higher-order Cartesian method of Parker (1972), they showed that the first-order method under-predicted the crustal thickness of large impact basins by about 10 to 20 km. Using spherical geometry, Wieczorek and Phillips (1998) derived an analogous higher-order method for calculating gravity anomalies due to finite-amplitude relief on a sphere. (See Thurber and Solomon (1978), Bratt *et al.* (1985) and von Frese *et al.* (1997) for alternative approaches in the space domain).

The next complication is related to how one inverts for the subcrustal relief given the Bouguer anomaly. In doing so, the Bouguer anomaly must be downward continued to the average depth of the crust-mantle interface, and this is a process that amplifies noise. The amplification of noise in the lunar gravity field is particularly destructive in the spectral domain as a result of the lack of farside tracking data. To counteract this problem on the Moon, Neumann *et al.* (1996) used the Cartesian downward continuation filter of Phipps Morgan and Blackman (1993) to stabilize their inversion, and Wieczorek and Phillips (1998) developed an analogous filter for use in the spherical-harmonic domain. The amount of filtering to be applied is a subjective decision, being controlled by the degree at which the filter is assigned a value of 0.5. For the crustal thickness inversions presented below, these were found to be unstable if this degree was greater than 40. In this study, the filter was chosen to have a value of 0.5 at degree 30 in order to offer a subjective compromise between retaining a high nearside spatial resolution versus the damping of unreasonable farside short-wavelength undulations.

Our individual inversions, described separately below, differ only slightly from those of Wieczorek and Phillips (1998). As was originally noted by Neumann *et al.* (1996), the short-wavelength power in the gravity fields of Lemoine *et al.* (1997) and Konopliv *et al.* (1998) was found to be inconsistent with predictions based upon the observed topography. This artifact was attributed to the stabilization procedures used to counteract the lack of farside tracking data in constructing these gravity models. Because of this, it was necessary to filter the Bouguer correction so that high frequency noise would not be introduced into the Bouguer anomaly. The LP150Q gravity field of Konopliv *et al.* (2001) used here, however, is consistent with predictions from the surface topography up to about degree 65. Hence, in this study, we truncate both the gravity and topography fields at this degree.

We describe below three plausible crustal thickness models of the Moon. The first two models assume that the crust is uniform in composition (excluding a thin veneer of mare basalts), whereas the third model assumes that the crust is stratified into upper anorthositic and lower noritic layers. The salient features unique to each model are discussed below, whereas the general aspects of the crustal models are discussed in the following section. We emphasize here that none of these models assume that the lunar crust is isostatically compensated.

Model 1 (LP150Q). This is the canonical model in which the lunar gravity field is assumed to be solely the result of surface topography, a thin veneer of dense mare basalts, and relief along the crust-mantle interface. For this model, as well as the two that follow, the gravitational attraction of the mare basalts within the nearside mascon basins was taken into account using the mare thickness model of Solomon and Head (1980) modified by the maximum thickness constraints of Williams and Zuber (1998).

A density of 2900 and 3300 kg m^{-3} was assumed for the crust and mare basalts, respectively (see Table 3.10). Given the known mass of the Moon, and a crust that is on average 55-km thick, the density of the mantle can be no greater than 3400 kg m^{-3} . For this model, a density of 3320 kg m^{-3} was assumed for the upper mantle, which results in an approximately zero-km thick crust (excluding the mare fill) beneath the Crisium basin. Because the density of the mare basalts and mantle are approximately the same, the assumed mare thickness model does not significantly affect the inverted total thickness of the crust. The crustal thickness at the Apollo 12 and 14 sites was constrained to be 45 km, and the globally averaged crustal thickness for this model is 53.4 km, consistent with the limits derived from gravity and topography admittance studies. The total crustal thickness for this model is shown in Color Plate 3.5.

Model 2 (LP150Q). This model is similar to the previous one, but with one major exception. Here we allow for the possibility that the degree-1 shape of the Moon (i.e., the 1.9 km center-of-mass/center-of-figure offset) might not be the result of crustal thickness variations. Particularly, after computing the Bouguer anomaly, the degree-1 terms were set to zero. In this model, the degree-1 Bouguer anomaly could either be the result of lateral density variations within the crust and/or mantle. We chose the density of the mantle for this model to be 3400 kg m^{-3} in order to give a zero crustal thickness beneath the Apollo basin that lies within the larger farside South Pole-Aitken basin. The globally averaged crustal thickness for this model is 43.4 km, consistent with the limits derived from the gravity and topography admittance studies. The total crustal thickness is shown in Color Plate 3.6.

Model 3 (LP150Q). As is discussed throughout Section 2, there are some compelling reasons to suspect that the lunar crust might either be vertically zoned or stratified in composition. In particular, a model in which the upper crustal thickness varies, while the lower crustal thickness remains constant, was found to satisfy the highland geoid to topography ratios (see Section 2.6.1). Here, we construct a dual-layered crustal thickness model of the Moon using this general structure. By strictly employing this model, however, it is not possible to satisfy the lunar gravity field over many of the large impact basins. Wherever this occurred, we allowed the lower crust to vary in thickness as well. The densities of the upper crust, lower crust, and mantle in this model were assumed to be 2820, 3040, and 3350 kg m^{-3} , respectively (see Section 2.8.4 for a discussion of the density of the lower crust). The upper crustal and total crustal thicknesses for this model are displayed in Color Plate 3.7. The globally averaged thickness of the crust for this model is 52 km, consistent with the limits derived from the gravity and topography admittance studies, and the average thickness of the upper crust is 26.9 km. We note that this dual-layered model is different in detail than the favored dual-layered model presented in Wieczorek and Phillips (1998).

Table 3.10. Crustal thickness model parameters.

Parameter	Model 1 (single-layered)	Model 2 (single-layered)	Model 3 (dual-layered)
Reference crustal thickness, km	53.4	43.4	52.0
Reference upper crustal thickness, km	—	—	26.9
Hemispheric crustal thickness difference, km	16.7	2.0	13.1
Density of upper crust, kg m^{-3}	2900	2900	2820
Density of lower crust, kg m^{-3}	—	—	3040
Density of mantle, kg m^{-3}	3320	3400	3350
Density of mare basalts, kg m^{-3}	3300	3300	3300

2.7.1. Implications

The center-of-mass/center-of-figure offset. One noticeable feature of the shape of the Moon is that its center of figure is displaced 1.9 km away from its center of mass in the direction of 8°N and 157°W. A popular explanation for this observation is that it could be the result of the lunar farside crust being significantly thicker than that of the nearside (e.g., Kaula *et al.* 1972; Kaula *et al.* 1974). In our crustal thickness models that assume constant density crustal layers, we indeed find that the farside crust is on average 17 km thicker than the nearside for our single-layered model (Model 1), and 13 km thicker for our dual-layered model (Model 3).

A thicker farside crust, however, is not the only possible explanation for the center-of-mass/center-of-figure offset of the Moon. In particular, it is possible that this feature could be the result of the degree-1 variations in either crustal and/or mantle density, as is implicitly assumed in our Model 2. As an example, in the strict case of Pratt compensation, the crust-mantle interface lies at a constant depth below the surface; in order for there to be a constant pressure along this interface, the crust must be denser than average at low elevations, and less dense than average at high elevations. Solomon (1978) and Thurber and Solomon (1978) emphasized that some portion of the lunar crust could be regionally or globally compensated by crustal density variations. This was based in part on observed correlations between the remotely sensed surface composition (Al/Si, Th, and Fe) and elevation in the limited Apollo data. Using the near-global iron abundance data of Lucey *et al.* (1995) derived from the Clementine mission, though, Wieczorek and Phillips (1997) have since shown that no significant regional correlation exists between density and elevation for the highlands. While this implies that Pratt compensation is regionally unimportant, they could not rule out a Pratt origin for the global degree-1 shape of the Moon. For example, the 1.9 km center-of-mass/center-of-figure offset could be accounted for if the nearside crust was on average 115 kg m⁻³ denser than that of the farside. This would correspond to about an ~4 wt% difference in iron content between the two hemispheres (Wieczorek and Phillips 1997). Additional studies of how crustal composition varies with elevation are needed before a Pratt origin can be ruled out for the long-wavelength shape of the Moon. Even if it turns out that density differences do not exist between the near- and far-side crust, it is possible that they might yet exist within the lunar mantle (e.g., Wasson and Warren 1980). In support of this, we note that the high-Ti basalts erupted exclusively on the lunar nearside, implying a higher TiO₂ content of the nearside mantle.

Impact basins. A feature common to all three crustal thickness models is that the crust is significantly thinned beneath many of the large impact basins. This dramatic feature was noted in previous models (e.g., Bratt *et al.* 1985; Neumann *et al.* 1996; Wieczorek and Phillips 1998) and has been interpreted as being the result of the large amount of material that is excavated in the cratering process. Most of these basins are also surrounded by an annulus of thickened crust, and this feature is most likely attributed to the thick ejecta deposit of the basin and/or to the lateral displacement of crustal materials that occurs during the excavation stage of the cratering process (Neumann *et al.* 1996; Wieczorek and Phillips 1999).

The large impact basins also exhibit some notable asymmetries based on their inferred crustal structure (see online RIMG supporting material at www.minsocam.org for crustal thickness images of the major basins). For instance, the excavation cavity of the Imbrium basin is not located at the geometric center of its main topographic rim, but rather is displaced towards the northwest (see also Spudis 1993). Furthermore, many nearside impact basins appear to possess a symmetry axis that might be indicative of having formed by an oblique impact (e.g., Serenitatis, Humorum, Crisium, and Nectaris). The crustal structure of the Nectaris basin is particularly odd with its northwest-southeast elongation. This structure could be the result of two closely spaced and unrelated impact basins, a double impact basin formed by two related bolides, or the result of a single highly-oblique impact.

Exposures of the mantle. Even though the crust is inferred to have been thinned dramatically beneath many of the large impact basins, these crustal thickness models predict that exposures of the lunar mantle should be rare to non-existent. Depending upon the assumed crustal thickness model, there are only two possible regions where we might expect to find evidence for mantle materials exposed near the surface. If we assume that the degree-1 shape of the Moon is a result of lateral density variations in the crust and/or mantle (Model 2) then this model predicts the mantle to be exposed beneath the Apollo basin that lies within the larger South Pole-Aitken basin. In contrast, if we assume that the degree-1 shape of the Moon is a result of crustal thickness variations (Models 1 and 3) then the only place where the crust is predicted to be entirely absent (excluding the mare fill) is beneath the Crisium basin. The possibility that the Crisium basin might have excavated into the lunar mantle was originally noted by Wieczorek and Phillips (1998), and the thinner seismic crustal thickness constraints (Khan and Mosegaard 2002; Lognonné et al. 2003) only strengthen the case that this indeed might have happened.

Given that the Apollo and Crisium basins have been partially flooded by mare basalts, it is unclear whether these putative mantle deposits would be presently visible at the surface. It is possible, though, that a mantle geochemical signature might be detectable in the ejecta blanket surrounding these basins. Alternatively, a mantle signature might be associated with younger craters that formed within the mare deposits of these basins. Two particularly interesting candidates are the craters Pierce and Picard that are located within Mare Crisium. X-ray fluorescence data obtained from lunar orbit over these craters have shown that they possess anomalously high concentrations of magnesium, and Andre et al. (1978) originally interpreted this as being the result of these craters having excavated into a buried Mg-rich basalt flow. In support of this interpretation, they noted that some of the Luna 24 samples from eastern Mare Crisium (which were presumed to be volcanic) similarly had high abundances of magnesium. Wieczorek and Phillips (1998) alternatively suggested that the high magnesium concentrations associated with these two craters might be the result of having excavated into either the underlying mantle, or an impact melt sheet that was partially derived from the mantle. A reassessment of the Mg-rich Luna 24 samples might be worthwhile in light of this suggestion.

Exposures of the lower crust. If the lunar crust is vertically stratified into upper anorthositic and lower noritic layers, then our dual-layered crustal thickness model (Model 3) makes specific predictions as to where we might find exposures of the lower crust. Similar to the dual-layered crustal thickness model of Wieczorek and Phillips (1998), our model predicts that the entire upper crust should be absent beneath many of the large impact basins, including Imbrium, Serenitatis, Crisium, Smythii, Humboldtianum, Orientale, Humorum, Nectaris, and South Pole-Aitken. Additionally, the upper crust is predicted to be less than 5 km thick beneath Mendel-Rydberg, Moscovense, Freundlich-Sharonov, and a portion of eastern Mare Frigoris. Unfortunately, mare basalts have extensively flooded most of these regions, obscuring these putative lower crustal exposures. A major exception to this is the South Pole-Aitken basin where mare deposits are relatively scarce (e.g., Wilhelms 1987; Yingst and Head 1997). The remotely-sensed composition of the floor of this basin appears to be composed of relatively mafic noritic materials (Pieters et al. 1997; 2001), in agreement with the predictions of this dual-layered crustal thickness model. As will be discussed more in Section 2.8.4, this model can also be used to predict whether the central peak of a complex crater is derived from either the upper or lower crust.

Other features. The crustal thickness models possess other notable features, a few of which will be mentioned here. First, the crust beneath the Aristarchus Plateau and Marius Hills is thickened by ~10 km with respect to the surrounding maria. Since these regions have been inferred to be unique long-lived volcanic centers (e.g., Wilhelms 1987), this may be related to a thick shield-like volcanic pile of extrusive and intrusive volcanic rocks. Second, the crust beneath the Apennine Bench is also seen to be thickened by ~15 km. This could similarly be attributed to

extensive volcanism, or perhaps to some process associated with the deposition of the Imbrium and Serenitatis ejecta. Though some portion of this unit may have formed by post-Imbrium KREEP-basaltic volcanism (e.g., Hawke and Head 1978; Spudis 1978), it is not clear whether the bulk of this thickened crust formed before, after, or during the Imbrium impact. Finally, a localized region of highly thickened crust is seen to lie west of the Orientale basin and northeast of the South Pole-Aitken basin. As this region is located on the farside of the Moon, this feature might (partially) be an artifact of the poor resolution of the gravity field in this region.

2.8. Crustal stratigraphy

2.8.1. Spectral reflectance studies of central peaks. Probing the composition of the crust at depth can be accomplished by using a unique property of complex impact craters. Typically, lunar craters larger than 35 km in diameter have peaks at their center that are believed to represent rocks that have been uplifted from beneath the surface during crater formation. While the exact depths from which these central peaks are uplifted are not exactly known, most estimates range between 0.1 and 0.2 times the crater diameter (e.g., Dence 1968; Roddy 1977; Melosh 1989). As an example, the crater Copernicus with a diameter of ~98 km may contain rocks from pre-impact depths of ~10–20 km exposed in its central peak. Most recently, Cintala and Grieve (1998) have made use of models that take into account both the excavation of crustal materials and the extent of impact melting to predict the amount of uplift in lunar central peaks. Assuming that the materials that constitute these peaks are derived from beneath the maximum depth of impact melting, their depths of origin were found to be approximately given by $0.109 D^{1.08}$, where D is the final rim diameter of the crater in kilometers. This depth of peak origin corresponds to almost twice the maximum depth of excavation of the crater.

Although no rocks were collected during the Apollo missions that directly sampled the central peak of a crater, spectral-reflectance remote sensing techniques can provide estimates of their composition. In particular, at visible through near-infrared wavelengths, crystal field transitions of Fe and Ti cause diagnostic absorption bands in reflectance spectra (see Chapter 2) allowing mafic minerals such as olivine and pyroxene to be identified. Until the 1990s, though, this type of remote sensing was confined to the acquisition of individual spectral measurements from Earth-based telescopes. While telescopic based spectra offer excellent spectral resolution, each measurement is an average over an area approximately 2 to 10 km in diameter.

Over the past 30 years, a database of high-resolution, telescopic near-infrared reflectance spectra has been acquired for numerous locations across the lunar nearside (e.g., McCord et al. 1981; Pieters 1993). Spectra of impact craters have been particularly fruitful as they expose fresh material from beneath the surface. Pieters' (1986) summary of the compositions of nearside craters based on these telescopic spectra revealed a crust with a surprisingly varied composition. Central peak rocks spanned the range of compositions found among pristine lunar highland rock samples, including troctolites, gabbros, norites, and anorthosites. These initial central peak studies led to several key conclusions for lunar geology. First, the peak compositions indicated potential gaps in the lunar sample collection (suggesting, for example, a greater abundance of gabbroic rocks than found among the samples (Lucey and Hawke 1989). Second, several of the central peaks might have tapped mafic plutons, potential sources for the Mg-suite samples (Lucey et al. 1986; Pieters 1991). And third, central peaks in many locations exposed anorthosite, allowing this rock type to be mapped across the lunar nearside and compared to the predictions of the magma-ocean theory.

Although the high spectral resolution of telescopic measurements allow detailed assessments of mineralogy, only spatial variations on the order of kilometers could be detected. Data collected from lunar orbiting spacecraft, in contrast, offer increased spatial resolution, but significantly less spectral information. In 1994, the Clementine mission returned global multispectral images of the Moon, including large portions of the lunar farside whose composition was previously unknown. Clementine's UVVIS camera provided high-spatial

resolution (100–400 m/pixel) images at five wavelengths, allowing first-order mineralogical determinations (see Chapter 2) at scales sufficient for detailed geologic mapping. Rather than measuring a single average composition for a central peak as with telescopic studies, multiple compositions within the peaks were distinguishable.

Using the Clementine data, Tompkins and Pieters (1999) conducted a global survey of central peaks in order to estimate the compositional variability of the lunar crust beneath the megaregolith. The craters ranged in diameter from 40 to 180 km, and the depths of origin of their central peaks were believed to range from approximately 5 to 30 km. Representative five-color spectra from spectrally and spatially distinct areas within the peaks were selected and classified on a relative scale, from which mineralogical abundances were estimated. These were then translated to rock types based on the classification scheme of Stöffler et al. (1980) (see Fig. 3.12). The lithologies found in these central peaks are shown in Color Plate 3.8.

From this survey, a more complete picture of the global trends emerged. Given the observed central peak compositions, the lunar crust is observed to be extremely anorthositic, gradually increasing in mafic content with depth. The crustal composition ranges from predominantly “pure” anorthosite to anorthositic norite. In general, these results are considerably less mafic than earlier estimates and predictions. Isolated mafic outcrops occur throughout the Moon, though true mafic rocks are rare among the surveyed craters; only ~10% of the central peaks contain mafic rocks such as gabbro or norite, and about half of the peaks are composed of

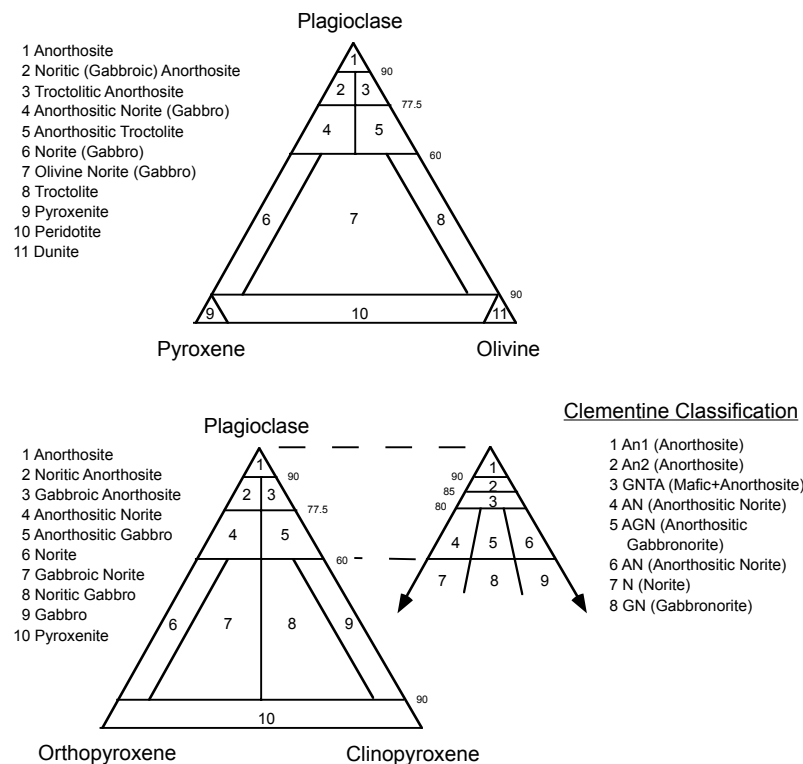


Figure 3.12. Classification scheme of lunar rocks based on Stöffler et al. (1980), and its relationship to the classification scheme used in Tompkins and Pieters (1999). Lower figure after Tompkins and Pieters (1999).

rocks that contain more than 85% plagioclase. The mafic lithologies identified among the central peaks are typically more anorthositic than the average value for large Mg-suite samples (Warren 1990). Nonetheless, central peaks that were identified as gabbro, norite, troctolite, gabbro-norite, anorthositic troctolite, anorthositic gabbro, and anorthositic gabbro-norite (following the Stöffler et al. classification scheme) were considered to be potential candidates for magnesian-suite plutons. This method, however, has no way of distinguishing Mg', so identifications of more mafic rock types could also reflect exhumation of relatively mafic ferroan anorthositic rocks.

2.8.2. The distribution of anorthosite. During the 1980s and early 1990s, analyses of telescopic near-infrared reflectance spectra revealed outcrops or patches of anorthosite on the order of tens of square kilometers in plan dimension on the lunar nearside, principally associated with uplifted blocks on the inner rings of impact basins such as the inner Rook Mountains of the Orientale basin and in parts of the inner ring of the Grimaldi basin (Spudis et al. 1984; Hawke et al. 1991, 1993, 2003b). Other exposures of anorthosite were found near the outer rings of basins such as Grimaldi, Humorum, and Nectaris, but in these cases, the anorthosites were found in central peaks and walls of superposed impact craters. (e.g., Hawke et al. 1993). Anorthosite has further been identified in the central peaks of Alphonsus and Petavius (Pieters 1986; Coombs et al. 1990) which are located near major rings of ancient impact basins, and in plains units of the northern highlands that were affected by large Copernican craters (Thales and Anaxagoras). In general, these anorthosite deposits appear to have been exposed from beneath a slightly more mafic surface layer. Locations where anorthosite has been identified using Earth-based reflectance spectra are shown in Figure 3.13 (see also Color Plate 3.9).

Clementine UVVIS spectra have subsequently been used to search for anorthosite globally using remotely sensed estimates of FeO abundances (Hawke et al. 2003b). In these studies, a surface iron abundance less than 4 wt% FeO, which likely corresponds to more than 90% plagioclase, was used as a criterion for detecting this rock type. In addition to exposures

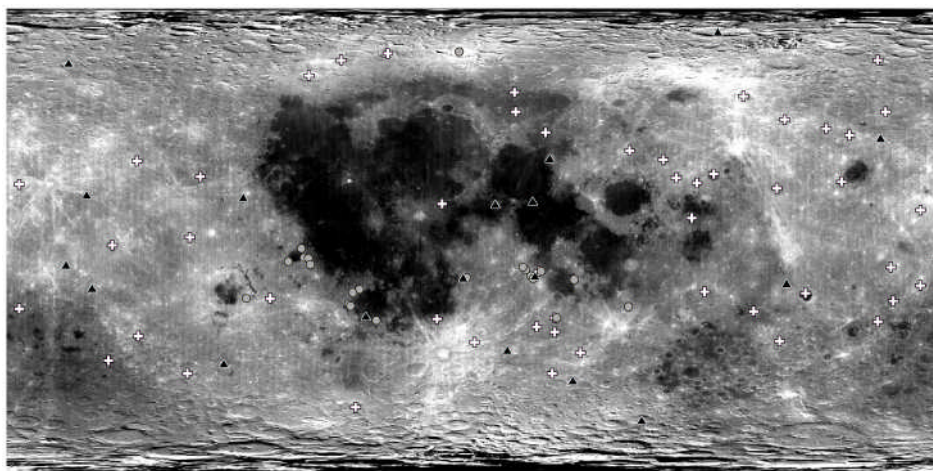


Figure 3.13. Anorthosite distribution superposed on the Clementine 750 nm global albedo basemap. Circles represent locations of outcrops of anorthosite observed with telescopic near-infrared spectra (Hawke et al. 2003b), triangles represent locations within central peaks of craters where Tompkins and Pieters (1999) identified anorthosite (An1), and crosses represent locations within central peaks of craters where anorthosite plus one or more additional rock types were identified. The base map is projected in a simple cylindrical projection. See also Color Plate 3.9.

identified previously, anorthosites were found in the inner rings of basins such as Hertzsprung, Korolev, Grimaldi, Humorum, Nectaris, and Orientale. Tompkins and Pieters (1999) further found numerous central peaks with exposed anorthosite which were presumably derived from depths ranging from 5 to 20 km below the surface (these occurrences are listed in Table A3.10). One should be aware, however, that as the mafic absorption features of these spectra rely on ferrous iron-bearing silicates, the possibility exists that feldspathic magnesian rocks could be misclassified as anorthosite, even if they contained more than 10% mafic silicates.

The exposures of anorthosite reported by Hawke and coworkers are especially noteworthy because many appear to contain less than 2 wt% FeO, which likely corresponds to a rock being composed of nearly 95% or more plagioclase. Some of these exposures, which can extend for more than 150 km, are even more anorthositic than the farside feldspathic highlands terrane, whose composition is typically 3.5–5% wt% FeO (Jolliff et al. 2000a; Lawrence et al. 2002). These nearly pure anorthosite exposures are particularly significant as they may represent remnants of the ancient anorthositic upper crust. As such, their distribution may provide an indication of the extent and stratigraphic position of positively buoyant anorthositic cumulates that formed during the primary crustal differentiation event of the Moon.

Anorthosite exposures are most common in the feldspathic highlands terrane where basin impacts have excavated through a slightly more noritic megaregolith that is on the order of a few kilometers to ~10 km thick (Spudis et al. 1984; Hawke et al. 1991, 2003b; Bussey and Spudis 2000). For example, the Hertzsprung and Korolev basins in the farside highlands probably excavated as deep as ~20–30 km, and abundant anorthosite exposures are found in the ring mountains of these basins. Such deep excavations would probably have been sufficient to breach a putative thick ejecta deposit from the South Pole-Aitken basin, which appears to be more mafic than the underlying anorthosites (Hawke et al. 2003b). Anorthosite is also exposed within the South Pole-Aitken basin in blocks uplifted by the Apollo and Ingenii basins, as well as in the Leibnitz and von Kármán craters (e.g., Pieters et al. 2001). It is possible that these deposits represent ancient feldspathic crustal materials that underlie the South Pole-Aitken impact melt sheet.

Anorthosite exposures are less common in the highlands of the southern nearside and in the region encompassing the Imbrium basin and Oceanus Procellarum (the Procellarum KREEP Terrane). Their paucity in these regions may partially result from obscuration by basalt flows and thick mafic ejecta deposits from the large nearside impact basins, or alternatively, a continuous anorthositic layer may never have existed within this region of the crust. While anorthosites have been identified in the central peaks of Eratosthenes and Aristarchus (McEwen et al. 1994; Tompkins and Pieters 1999; Hawke et al. 2003b), elevated thorium concentrations associated with these craters suggest that these exposures might be of an alkali variety, possibly associated with KREEP-rich intrusives, and may not be related to a primary ferroan anorthositic crust. Moreover, impact breccias found at the Apollo 14 site, thought to be predominantly Imbrium ejecta or remnants of older upper crust of the Procellarum KREEP terrane (Haskin et al. 2000), mostly lack ferroan anorthosite as clasts or chemical components (Jolliff et al. 1991b; Spudis et al. 1991). Nevertheless, exceptions to this general rule do exist (Shervais et al. 1983; Warren et al. 1983a). Finally, we note that anorthosites are also present in the inner ring of the Humorum basin which lies on the boundary between the Procellarum KREEP and Feldspathic Highlands Terranes (Hawke et al. 1993; Bussey and Spudis 2000).

A key question that has yet to be resolved is whether or not these anorthosite deposits are the remnants of a once globe-encircling layer as is predicted by simple models of magma-ocean crystallization. Even if ferroan anorthosites never existed within the Procellarum KREEP terrane, their lateral and depth distribution within the Feldspathic Highlands terrane could be used to test more complex anorthosite formation scenarios (e.g., Longhi and Ashwal 1985; Jolliff and Haskin 1995; Longhi 2000).

2.8.3. Composition of basin ejecta. Just as exposures of anorthosite in the rings of impact basins and central peaks of complex craters represent materials uplifted from depth, the composition of ejecta from impact basins similarly can provide a window into the subsurface crust. While the current depth of most lunar impact basins is generally fairly shallow (a few kilometers at most), this structure is the result of crustal rebound following the crater excavation stage as well as a variety of post-impact degradational processes (e.g., Melosh 1989). In contrast to the shallow observed depths of the large impact basins, ejecta blankets are derived from that portion of the crater that was ballistically excavated during the cratering process (i.e., the excavation cavity), and this is known to be appreciably deeper.

A wide variety of sources—including computational studies, laboratory experiments, and the inferred structure of lunar and terrestrial impact craters (e.g., Croft 1980; O’Keefe and Ahrens 1993; Wieczorek and Phillips 1999)—suggest that the excavation cavity is roughly parabolic in shape, possessing a depth/diameter ratio of approximately 1/10. Unfortunately, diameters of the excavation cavity of craters are in general not known, as post-impact slumping of the rim destroys its initial morphology. Nevertheless, for small craters the observed diameter and excavation diameter are comparable, and if desired, various methods can be employed that relate one to the other (e.g., Croft 1980). For the largest basins, the issue is more complex as it is sometimes difficult to determine which basin ring most closely corresponds to its excavation cavity (e.g., Wieczorek and Phillips 1999).

As two examples, consider the Imbrium and Serenitatis basins, whose excavation cavity diameters have been estimated at 744 km and 657 km, respectively, based on crustal thickness modeling (Wieczorek and Phillips 1999). These two basins should have excavated to a maximum depth of ~70 km, likely including the entire crustal column and portions of the upper mantle. However, because the excavation cavity has a parabolic shape, most of the material ejected would come from the upper parts of the crust. In particular, the upper 30% by depth contributes about half of the ejecta, whereas the deepest 10% by depth contributes only ~1% (e.g., Spudis 1993; Haskin *et al.* 2003). Finally, it should be noted that when the primary ejecta is ultimately deposited on the surface, it will mix with the local substrate (e.g., Haskin *et al.* 2003).

Caveats notwithstanding, basins of different sizes can be used as probes into the lunar crust, allowing an investigation of how the composition varies both laterally and vertically (e.g., Spudis *et al.* 1984; Spudis and Davis 1986). With the acquisition of global compositional datasets, Clementine and Lunar Prospector data have been used to estimate FeO concentrations of ejecta deposits (Spudis *et al.* 1996; Bussey and Spudis 1997, 2000; Blewett and Hawke 2001; Jolliff *et al.* 2002). Using these data, Bussey and Spudis (2000) advocated a general three-layer compositional model of the crust based on a study of the ejecta deposits of Orientale, Humorum, Nectaris, and Crisium (see also Hawke *et al.* 2003b). Ejecta-deposit compositions reveal a top layer of mixed feldspathic megaregolith that may extend to depths of ~10–20 km, and uplift structures in the form of basin inner-ring massifs exposed highly anorthositic rocks. While this anorthositic “layer” was presumed to overlie a more mafic lower crust, such as is likely exposed in the South Pole-Aitken basin (Pieters *et al.* 1997, 2001), for the most part, these basins did not excavate materials that were significantly more mafic than the upper feldspathic crust. In particular, a lack of mafic ejecta at the Orientale basin suggests the presence of a thick anorthositic upper crust at this locale. This case appears to be representative for most of the basins that lie within the Feldspathic Highlands Terrane (Jolliff *et al.* 2000a) where gravity and topography data imply a relatively thick upper crust (Wieczorek and Phillips 1998).

2.8.4. The composition of the upper and lower crust. The central peaks that were investigated in the Tompkins and Pieters (1999) study are approximately randomly distributed across the lunar surface (see Color Plate 3.8) making it is possible to investigate systematically lateral and vertical variations in crustal composition. These authors originally noted that the

central peaks of complex craters located within larger impact basins were generally more mafic than those that formed within the highlands. This observation was taken as being consistent with the hypothesis that large impacts excavate through the upper crust, bringing more mafic lower-crustal materials to surface. This was further quantified by Wieczorek and Zuber (2001a) who utilized a geophysically based crustal thickness model, and here we update their results using the updated model of this paper.

The dual-layered crustal thickness model presented in Section 2.7 assumes that the crust is stratified into upper anorthositic and lower noritic layers, with the thickness of the lower crust being approximately constant. By utilizing the composition of a complex crater's central peak and its associated pre-impact depth of origin, the validity of this geophysical model can be assessed. Specifically, if the depth of origin of a peak is predicted to be greater than the thickness of the upper crust at a given locale, then the peak should be composed of lower crustal (and hence noritic) materials. Using this approach, 91 of the 108 peaks in the Tompkins and Pieters (1999) study are predicted to be derived from the upper crust, whereas only 17 are predicted to have a lower crustal origin. Consistent with the geophysical crustal thickness model, those peaks that are exclusively composed of rocks containing more than 85% plagioclase (there are 51) are derived from the upper crust, whereas those peaks that contain some norite or gabbro-norite (there are only 6) have a lower crustal origin. Five of these mafic peaks are located within the South Pole-Aitken basin, whereas the remaining peak is from the crater Bullialdus, which lies near the Nubium basin (Pieters 1991). Peaks that have intermediate compositions do not show any clear correlation with being exclusively derived from either the upper or lower crustal layers.

If it is assumed that these central peaks are randomly distributed across the lunar surface and with depth, and that the dual-layered crustal thickness model is accurate, the bulk composition of the upper and lower crustal layers can be estimated. First, the average proportion of rock types that are present in the upper and lower crustal layers is summarized in Table 3.11 where it is seen that the upper crust is composed of 38% pure anorthosite. Furthermore, 89% of the upper crust is predicted to be composed of rocks that contain more than 80% plagioclase. The majority of the remaining material is composed of intermediate lithologies such as anorthositic norite, anorthositic gabbro-norite, anorthositic gabbro, and anorthositic troctolite.

Since only 17 central peaks are predicted to be derived from the lower crust of the Moon, its derived composition will be statistically less robust. Furthermore, because of uncertainties associated with the adopted crustal thickness model, as well as the modeled depth of origin

Table 3.11. Mineralogy of the upper and lower crust.

Rock type and assumed volume % plagioclase	Modal Abundance (%)		
	Upper Crust	Lower Crust	Most Mafic Lower Crust
anorthosite (95 ± 5)	38.3	22.1	0
An2 (87.5 ± 2.5)	34.3	17.6	4.2
GNTA (82.5 ± 2.5)	16.2	24.2	17.2
anorthositic gabbro (70 ± 10)	2.7	1.5	4.2
anorthositic gabbro-norite (70 ± 10)	2.9	4.6	7.5
anorthositic norite (70 ± 10)	3.0	15.4	29.7
anorthositic troctolite (70 ± 10)	1.6	1.5	0
gabbro (50 ± 10)	0.5	1.5	4.2
gabbronorite (50 ± 10)	0	6.1	17.2
norite (50 ± 10)	0	5.6	15.8
troctolite (50 ± 10)	0.4	0	0

of central peak materials, it is possible that a few upper crustal central peaks could have been misclassified as having a lower crustal origin. Recognizing this sampling problem, Wieczorek and Zuber (2001a) chose to analyze a subset of the lower-crustal central peaks that contain some gabbro and norite, and that might be representative of the “most-mafic lower crust.” This end-member composition (which is based only on six craters) lacks pure anorthosite and is composed of 33% norite and gabbro-norite and 30% anorthositic norite. When compared to the upper crust, the most-mafic lower crust is seen to contain a greater relative abundance of norite with respect to gabbro. For example, in the upper crust, anorthositic norite, anorthositic gabbro-norite, and anorthositic gabbro all occur in roughly equal proportions. In the most-mafic lower crust, though, anorthositic norite is approximately seven times more abundant than anorthositic gabbro and norite is approximately four times more abundant than gabbro.

Using the data in Table 3.11, the upper crust is found to be composed of $87 \pm 4\%$ plagioclase by volume and to have an Al_2O_3 content that lies between 28.5 and 32.2 wt%. The most-mafic lower crust is found to be composed of $65 \pm 8\%$ plagioclase and to have an Al_2O_3 content that lies between 18.2 and 24.7 wt%. The computed density of these crustal layers is listed in Table 3.12.

This bulk composition of the upper crust is comparable with, though slightly more feldspathic than, previous estimates. Pre-Clementine and Lunar Prospector estimates for the Al_2O_3 content of the upper crust were in the range of 26 to 28 wt% (e.g., Spudis and Davis 1986). Using Clementine derived iron abundances, Lucey *et al.* (1998a) found the lunar highland soils to be slightly more feldspathic, ranging from 27 to 29 wt% Al_2O_3 . Using the five most feldspathic lunar meteorites, Korotev (2000) estimated an Al_2O_3 abundance of ~ 28 wt% for the uppermost portion of the lunar crust. Finally, Jolliff *et al.* (2000a) obtained an Al_2O_3 abundance of ~ 29 wt% for the most feldspathic portion of the highlands crust based on an empirical correlation between aluminum and iron concentrations in the Apollo sample collection. Central peaks, which are likely derived from beneath the megaregolith (Bussey and Spudis 2000; Hawke *et al.* 2003b), indicate that the feldspathic component may in some places be even greater, up to 32 wt% Al_2O_3 .

Table 3.12. Bulk properties of the upper and lower crust.

Parameter	Upper Crust	Lower Crust	Most Mafic Lower Crust
Plagioclase, vol%	87.4 ± 4.3	79.0 ± 5.8	65.4 ± 8.4
Al_2O_3 , wt%	28.5–32.2	24.4–29.2	18.2–24.7
density, kg m^{-3}	2858 ± 35	2927 ± 47	3038 ± 69

2.9. Summary

Geophysical, remote sensing, and sample analyses are all converging on a picture of the lunar crust that varies both laterally and vertically in composition. To a good approximation, the lunar highland crust can be thought of as being either compositionally zoned or stratified. The average composition of the upper portion of the crust is extremely anorthositic (here estimated at $\sim 87 \pm 4\%$ plagioclase or 28.5–32.2 wt% Al_2O_3), and pure exposures of anorthosite are commonly found beneath a surficial layer of mixed, slightly more mafic regolith materials. The anorthositic lunar samples have ferroan compositions and ancient ages (~ 4.45 Ga) consistent with being derived by plagioclase flotation in a near-global magma ocean. The lower portion of the crust, in contrast, appears to be more noritic in comparison to the upper crust. This is evident from both the noritic composition of some central peaks, as well as the noritic composition for the floor of the giant South Pole-Aitken basin. Unfortunately, we do

not possess samples of these important rock types, leaving open the question of whether the lower crust is “ferroan” or “magnesian” in composition.

Geophysical and seismic analysis both suggest that the crust is thinner than previously assumed, being about 30–45 km thick at the Apollo 12 and 14 sites in comparison to the Apollo-era value of ~60 km. When this value is extrapolated globally, the crust is found to be on average about 49 ± 16 km thick. While the gravity and topography fields of the Moon are consistent with a crust that is homogenous in composition, remote-sensing considerations suggest that this view is too simplistic. A model that satisfies both the geophysical and remote-sensing constraints is one in which the crust is stratified into upper anorthositic and lower noritic layers. The thickness of the upper anorthositic crust in this model varies, whereas the thickness of the lower crust is constant except beneath the large impact basins. Geophysical and remote-sensing techniques constrain each of these crustal layers to be on average ~25 km thick. While crustal thickness models predict that exposures of the lunar mantle should be extremely rare to absent, the lower crust should have been excavated beneath many of the large impact basins, and is probably currently exposed within the South Pole-Aitken basin.

One group of rocks in the Apollo sample collection that remains enigmatic are those that comprise what is commonly referred to as the magnesian-suite. These rocks have high abundances of incompatible elements (i.e., KREEP), and much higher magnesium numbers than those of the ferroan anorthositic rocks. Global thorium abundances collected from orbit suggest that the KREEP-rich rocks of this suite are confined to the region encompassing Oceanus Procellarum and Mare Imbrium (see Section 5 for further details). Most of these rocks appear to have formed as crustal intrusions at various depths within the crust. The large span of crystallization ages (from ~4.45 to 3.85 Ga) attest to an extended period of Mg-suite magmatism in this region. As the youngest of these plutonic rocks were likely excavated and brought to the surface by the Imbrium impact, it is likely that Mg-suite plutonism may have continued for a much longer time than the ages of these samples suggest.

3. THE MANTLE

As of yet, no samples of the lunar mantle have been unambiguously identified in either the sample collection or by remote sensing techniques. Thus, unlike the lunar crust, the mantle can only be studied through less direct means. One method described below includes the chemical and isotopic analysis of mare basalts and volcanic glasses. Although they are now exposed at the surface of the Moon, the origin of these materials is ultimately related to partial melting deep within the lunar mantle, and their compositions reflect that of the mantle at the time they formed. Basalt and volcanic glass compositions combined with experimental petrology can infer the depths of origin and compositions of the mantle source regions. The only other fruitful method that can be used to infer the composition and structure of the mantle comes from an analysis of the Apollo seismic data.

Key questions that are addressed below include the major and trace element geochemistry of the mare source regions, the depths of origin of the volcanic samples, and whether there is evidence for chemical heterogeneities within the mare basalt source regions. Seismic analysis suggest that a major discontinuity may exist about 500 km below the surface, and the origin of this feature is crucial to understanding the Moon’s thermal and magmatic evolution. Of key importance is whether this discontinuity represents the maximum depth of the magma ocean, or instead the maximum depth of melting within the mare source region.

3.1. Mare basalts and volcanic glasses

Almost all of the prominent mare basalts and related pyroclastic deposits are associated with the large nearside basins and Oceanus Procellarum. Basalts are comparatively rare on

the lunar farside but do occur in Mare Moscoviense, Mare Ingenii, Mare Orientale, and in patches within other basins such as Apollo and the South Pole-Aitken basin. However, the distribution of mare basalts is not simply a case of lavas flooding topographic lows or thinned crust as the deepest basin on the Moon, the South Pole-Aitken basin, was demonstratively less volcanically active than regions of thinned nearside crust (Lucey *et al.* 1994; Smith *et al.* 1997; Wieczorek *et al.* 2001). Although mare basalts are prominent in lunar images, they form a rather thin veneer on the older crust. Thicknesses are typically less than 1 km exterior to impact basins and probably not more than 4 km within the largest basins (see Section 2.4). While the ages of large mare basalt samples dated radiometrically range from ~3.9 Ga to 3.2 Ga, the duration of basaltic volcanism appears to be longer. An age of 4.2 Ga has been reported for aluminous basalt clasts in a nonmare impact breccia (Taylor *et al.* 1983), and crater-counting methods indicate that basalts in some unsampled areas have ages approaching 1 Ga (Schultz and Spudis 1983; Hiesinger *et al.* 2000; Hiesinger and Head 2003). Although the concentration of radiogenic heat sources appears to be enhanced within the nearside crust and mantle, the existence of basalts on the farside indicates that heat sources there were also capable of raising the mantle temperature locally above the solidus. Experimental evidence for the depth of mare source regions is discussed in Section 3.3.1 below.

3.1.1. Basalt and volcanic glass compositional groups—major elements. Many volumes and hundreds of research papers have been written about the lunar mare basalts. Our intent here is not to describe the groups *per se*; instead it is to relate key aspects of the mare basalts to what can be inferred from orbital remote sensing and to discuss new implications for lateral and vertical heterogeneity of mantle source regions. For many years, the remote-sensing community has been aware that despite the wide variety of basalt compositions known from the direct analysis of Apollo and Luna samples, many basalt types exist for which we have no samples (e.g., Pieters 1978). For example, crater statistics imply relatively young ages of ~1 Ga for basalt flows in some locations, but so far, the youngest radiometrically dated ages are ~3 Ga. Remote sensing has revealed the occurrence of extensive buried mare basalt regions, referred to as cryptomare, indicating that ancient mare volcanism (>3.8 Ga) may be more common than would be inferred from the samples. Studies of basalts in the Western Procellarum region suggest an olivine rich mineralogy (Staid and Pieters 2001) coupled with higher Fe and Th contents (Jolliff *et al.* 2001). Clearly, much is yet to be learned about the extents of mare basaltic volcanism in space and time, especially regarding their petrogenesis and geochemical variability.

The first-order classification of lunar mare basalts is traditionally based upon TiO_2 concentrations since the mare basalts and volcanic glasses span a huge range. Basalts with TiO_2 concentrations <1 wt% are called very-low Ti or VLT, those with TiO_2 of 1–4 wt% are low-Ti, those with 4–8 wt% are intermediate, and >8 wt%, high-Ti. A second order classification has been made according to other compositional parameters or major mineralogy. The aluminous basalts, found mainly as clasts in breccias at Apollo 14, have >11 wt% Al_2O_3 . High-K basalts from Apollo 11 have ~0.3 wt% K_2O , compared to <0.1 % in most others. The Apollo 14 very-high K basalts, however, have 0.6–0.8 wt% K_2O and are also aluminous. At Apollo 12, the three main basalt groups were distinguished on the basis of mineralogy: olivine basalts, pigeonite basalts, and ilmenite basalts.

The major mafic mineralogy (olivine, pyroxene, Fe-Ti oxides) of basalts can be determined from orbit and the concentrations of FeO and TiO_2 can be estimated as has been done with the Clementine UVVIS data (Chapter 2). FeO and TiO_2 as well as other elements such as Th have been determined by the Lunar Prospector gamma-ray spectrometer, but at a much lower spatial resolution than the Clementine data. The two key compositional parameters useful for distinguishing mare basalts in the lab or from orbit are FeO and TiO_2 . FeO concentrations of the main mare basalt groups from Apollo and Luna samples range from ~15.5 wt% in the aluminous basalts to ~23 wt% in the Luna 24 ferrobasalts and Apollo 15 olivine basalts, with

most being in the range of 18–21 wt%. Concentrations of FeO in the volcanic glasses are slightly higher, with a range of 16–24 wt%, and averaging ~21 wt%. Concentrations of TiO₂ range from <1 wt% to 13 wt% in the high-Ti basalts and to 17 wt% in the high-Ti volcanic glasses (Tables A3.11 and A3.12). Because the high-Fe and high-Ti basalts are endmember compositions, they are seen readily from orbit. Where mare surfaces contain admixed nonmare materials, the ejecta of small craters can be used to discern the degree of mixing and the composition of the basalt flows (Staid and Pieters 2000).

Using global compositional data derived from Clementine spectra, Giguere et al. (2000) showed that the TiO₂ contents of mare basalts form a unimodal distribution, with a peak at about 4 wt% and a long tail to high concentrations. This is in contrast to the samples, which show a distinctly bimodal distribution, with intermediate-TiO₂ compositions being rare. Gillis et al. (2003) showed that this is not an artifact of the remotely sensed data, but is related instead to the non-representativeness of the landing sites. In particular, Clementine data for just the basaltic landing sites reproduce the bimodal distribution as is seen in the samples. In comparing landing site and sample TiO₂ and FeO, Gillis et al. also showed that remotely sensed data were consistent with significant mixing of basalt and non-volcanic materials relative to the returned rock samples.

3.1.2. Trace-element signatures. Trace-element contents and signatures of mare basalts have been studied at length and are described in much detail elsewhere (see Basaltic Volcanism Study Project 1981; Papike et al. 1998; Shearer and Floss 2000 for summaries). Among the trace elements, the REEs have proven to be the most diagnostic and useful for discriminating relationships and petrogenetic processes. Recognition of the complementary patterns of chondrite-normalized REE contents of mare basalts and nonmare crustal materials was key to understanding the basic relationship between the crust and mantle of the Moon (e.g., Taylor 1975). The common characteristics of depletion of the light REEs (LREE), the relative enrichment of the heavy REEs (HREE), and the negative Eu anomaly were found to be consistent with the partitioning behavior between the minerals olivine and pyroxene, and melt. Basaltic melts represented by almost all the lunar basalt types and the picritic glasses share these characteristics, which were inherited from their deep mantle sources. The negative Eu anomaly has been attributed to the fractionation of divalent Eu from the trivalent REEs during plagioclase crystallization and extraction to form the crust, but studies of experimentally determined distribution coefficients show that the formation of a negative Eu anomaly can also occur from the crystallization of mafic silicates (e.g., McKay et al. 1990). Thus the shallow negative Eu anomaly of the picritic glasses does not necessarily imply plagioclase separation, but likely reflects the olivine and pyroxene cumulate nature of their source region. The general variations in REE patterns between the mare basalts, feldspathic crustal lithologies, and KREEP-rich materials are consistent with the simple magma-ocean scenario. Significant variations in REE concentrations and patterns in the mare basalts are taken to reflect variations in their sources, but the degree of melting associated with formation of a specific basalt, assimilation of crustal material during emplacement, and fractionation during solidification can impart additional variations. These factors must be taken into account before appealing to source-region variations to explain differences between basalt groups. Because minerals fractionate trace elements when they crystallize, the volcanic glasses have proven to be the most useful for study of mantle source-region variations. Such variations are discussed further in Section 3.3.1 and in Chapter 4, and were reviewed recently by Papike et al. (1998).

Elements other than the REEs that behave incompatibly in lunar basaltic systems include the large alkalis (K, Rb, Cs), Sr, Ba, Zr, Hf, Nb, Ta, Th, and U. In general, these elements occur in low concentrations in lunar basalts and volcanic glasses either because their source regions were intrinsically low (undifferentiated or depleted) or because the source regions are cumulates composed largely of minerals that do not readily incorporate them. Some of these

elements are geochemically similar pairs that are difficult under common petrologic processes to fractionate from one another, such as Rb-Cs, Zr-Hf, Nb-Ta, and Th-U. In such cases, significant differences in trace-element abundance patterns signal specific processes. For example, the presence of garnet, if a component of a mantle source residue following partial melting, would have the effect of retaining preferentially the HREEs and so would impart a negative slope to the REE pattern of the basaltic liquid formed during partial melting. The lack of such patterns among the crystalline mare basalts was taken early on as evidence that garnet was not a significant component of basalt source regions, although it may be in some volcanic glasses (Neal 2001). Another example is the formation of ilmenite and other Ti-rich oxides, which can fractionate Hf from Zr. Scandium, which is incompatible in olivine, is enriched in pyroxene (especially high-Ca pyroxene), thus variations between Sc and the compatible trace element Cr correspond well to variations associated with the proportions of the major silicate minerals. Taken together, the patterns of trace elements, which are usefully compared between groups when normalized to an average composition or to chondritic compositions, are very useful discriminators of process and source variations.

Not all mare basalts are depleted of incompatible trace elements. Several groups such as the Apollo 14 very-high-K basalts, some of the Apollo 14 and Luna 16 high-alumina basalts, and the Apollo 11 high-K basalts have incompatible-trace-element enrichments that indicate either assimilation of some trace-element rich crustal component or enrichment of their source regions in incompatible elements. These processes can be difficult to distinguish and can be aided by isotopic studies. Recent investigations comparing trace-element patterns of the volcanic glass groups, enabled by secondary-ion mass spectrometry (SIMS), provide the best look at trace-element variations that relate to source regions (Shearer *et al.* 1996; Shearer and Floss 2000).

The divalent and trivalent trace transition metals (ferromagnesian trace elements) are generally compatible in mare basalts. Chromium tends to be enriched in basalts that have the highest Mg/(Mg+Fe) and that contain magnesian olivine and spinel, and its concentration decreases in basalts with progressively higher Fe/Mg ratios. Concentrations of Cr are higher in the volcanic glasses (2000-8000 ppm) than in the crystalline basalts (1000-6500 ppm) (Tables A3.11 and A3.12). Nickel and Co tend to correlate inversely with the incompatible elements and are in highest concentration in the most “primitive” olivine-rich basalts, reaching concentrations of ~90 and 70 ppm, respectively (Karner *et al.* 2003). The volcanic glasses have higher concentrations on average, reaching ~100 and 200 ppm for Ni and Co, respectively. Vanadium follows Ti and is enriched in the high-Ti basalts (up to 270 ppm). The range of concentrations of V in the crystalline basalts and the volcanic glasses is similar. Scandium also correlates with Ti and is enriched most in pyroxene-rich basalts. It typically occurs in higher concentration in crystalline basalts (30-90 ppm) than in volcanic glasses (30-60 ppm). Although oxygen fugacities are low and some divalent Cr may be present in the upper mantle source regions, Fe and Ni are mostly divalent. Reduction of iron and crystallization of Fe metal in basalts occurs late and such metal is low in Ni and Co content.

The Lunar Prospector mission results opened up a new frontier in lunar trace-element research with important implications for basalt generation. Two instruments provided data relevant to trace-element concentrations of surface materials, the gamma-ray spectrometer and the neutron spectrometer. The gamma-ray spectrometer provided data on the distribution of Th, U, and K (see Chapter 2), whereas the neutron spectrometer provided a means to infer the concentrations of Sm and Gd, two REEs with high neutron-absorption cross sections. In areas where vast expanses of basalt occur, the concentration of these elements in the regolith can be determined. Then, using simple mixing models with components derived from local geologic relationships, the concentration of these trace elements in the underlying basalts can be inferred. Using this approach, some basalts of the western Procellarum region, which were not sampled directly by any of the sample return missions, have been inferred to be

relatively enriched in the naturally radioactive, heat producing trace elements Th, U, and K. For example, whereas most of the Fe-rich mare basalts have Th concentrations less than 2 ppm (Korotev 1998), the gamma-ray data suggest that some of the basalts in western Procellarum may have Th concentrations as high as 6 ppm (Haskin et al. 2000; Jolliff et al. 2001). As these basalts cover vast areas, this trace-element signature is not likely to be a local phenomenon affected by assimilation or by crystallization processes, and their high iron content argues against vertical mixing with an underlying KREEP-rich substrate. If the mixing models are correct, this signature would represent a characteristic of the mantle source regions for these basalts, the significance of which is discussed below.

3.1.3. Mare basalt source regions. Basalts serve as probes of the composition, structure, dynamics, and thermal history of planetary interiors, and for the Moon and Mars, they represent the only samples derived from their respective mantles. The composition and depth of the source regions for mare basalts have been tied to models of lunar differentiation (i.e., the lunar magma ocean) and post-LMO mantle dynamics (cumulate overturn and assimilation). The mineralogy of the source region and the composition of the source, whether differentiated or undifferentiated, have tremendous consequences for the bulk composition and thermal history of the planet. In this section, we focus on observations that potentially constrain the depth and composition of the mare basalt source regions. Thermal evolution is the subject of Chapter 4.

Depth and mineralogy of the source. Two contrasting models for the depths of origin of the mare basalts are as follows. One is that mare magmatism represents melting over a wide range of depths from just below the lunar crust to deep in the upper mantle. The second model is that most of the mare basalts represent partial melts initiated deep within the lunar mantle and below a fairly rigid and cool lithosphere (>350 km). Both models have profound implications concerning the structure and thermal evolution of the Moon between 3.9 and 3.0 Ga when most of the mare basalts now visible at the surface erupted. Several lines of observation can be used to address this issue: high-pressure experiments on mare basalts, trace element characteristics of mare basalts, and geophysical observations.

Studies of high-pressure phase relations of mare basalts provide information about conditions under which melting occurred, including temperature, pressure (and thus depth), and the minerals involved in melting. A common method is to determine the pressure at which a given basaltic magma is multiply saturated; that is, possessing two minerals such as olivine and orthopyroxene on the liquidus. High-pressure experiments (e.g., Kesson and Lindsley 1976; Longhi 1992) indicate that (1) multiple saturation (predominantly olivine + orthopyroxene but also plagioclase \pm spinel \pm pigeonite \pm augite \pm ilmenite \pm armalcolite) for the mare basalts and volcanic glasses occurs over an extremely wide range of temperature and pressure conditions (<1200°C to 1460°C and <5 to 25 kbar), (2) the temperature and pressure of multiple saturation of the volcanic glasses (1410–1500°C and 17–25 kbar, corresponding to depths of 350–520 km) generally exceed those of the crystalline mare basalts (1200–1380°C and <5 to 12 kbar, corresponding to depths less than 250 km) (Longhi 1992, 1995), and (3) the pressure of multiple saturation for both the high-Ti and very low-Ti basalts overlap, suggesting that the mantle is not uniformly stratified in terms of composition, but maintains compositionally diverse regions at a given depth.

It is important to note that the depths of multiple saturation correspond to the depth of melting only if (1) two or more phases were indeed present in the source residue after melting, and (2) melting occurred at a single pressure. In the case of extensive melting, leaving just olivine in the residue, the depth inferred from the pressure of multiple saturation would be in error. Arguments based on observed volumes of basalt and the preservation of diverse compositional signatures, however, suggest that small degrees of partial melting (<20%) were probably the norm in the lunar mantle (Shearer and Papike 1993). Trace element and isotopic modeling also support modest degrees of melting (Hughes et al. 1989; Nyquist and

Shih 1992; Beard *et al.* 1998; Shearer and Papike 1999). Furthermore, Hess (1991; 1993) and Hess and Finnila (1997) showed that most of the basaltic magma compositions represented by the pyroclastic glasses surround and follow the olivine-orthopyroxene cotectic boundary, indicating multiple saturation with these two minerals. For crystalline mare basalts that have undergone changes in composition by assimilation or crystallization, multiple saturation experiments represent a minimum depth of melting, and the potentially wide range of depths that are inferred could be misleading. An important consideration for depth-of-melting experiments is that melting may have occurred over a range of depths as a partially molten diapir rose through the mantle.

That the mare basalts and the picritic glasses have different pressures of multiple saturation may be interpreted in two ways: (1) the parental magmas for the picritic glasses and mare basalts may be unrelated and in fact produced by melting at two different pressure regimes in the lunar mantle (parental magmas for the crystalline basalts at depths less than 350 km and the volcanic glasses at depths greater than 350 km), or (2) the multiple saturation depths for the mare basalts are an underestimation of their true depths of melting, and that the parental magmas for both the mare basalts and picritic glasses were generated at depths greater than 350–400 km. At issue are the depths at which melting occurred, as well as the compositional variations within the mantle both laterally and with depth. The volcanic glass experimental data may be interpreted as indicating that sources for high-Ti basalts and very low-Ti basalts both occurred at depths greater than 250 km. Such an arrangement would require disruption or overturn of the simple layered cumulate sequence that might result from static crystallization of a magma ocean (e.g., Hughes *et al.* 1988; Ryder 1991; Spera 1992; Shearer and Papike; Hess and Parmentier 1995). Given the limited spatial sampling of mare basalts, compositional variations within the lunar mantle remain poorly known.

Composition of mantle source regions. Mare basalts exhibit numerous distinct mineralogical, chemical and isotopic characteristics that reveal many characteristics of their mantle source. Within the context of terrestrial basalt classification, the normative mineral assemblage of mare basalts ranges from quartz to olivine. Most importantly, all of these mare basaltic magmas are non-tholeiitic (Longhi 1981; Hess 1998). The mineralogical (Fe metal) and chemical (reduced valence states for Fe, Ti, Cr) signatures of the mare basalts reflect extremely low oxygen fugacities (~IW buffer). They are depleted in alkali, volatile, and siderophile elements, and there is a complete absence of water and hydrous phases. The crystalline mare basalts and pyroclastic glasses have a ubiquitous negative Eu anomaly. In the crystalline mare basalts, the depth of the negative Eu anomaly increases with increasing TiO_2 . Also, from very low TiO_2 to the high TiO_2 mare basalts there is an increase in the abundances of incompatible-elements (REEs, Zr, Ba, Nb), and a decrease in the abundances of compatible elements (e.g., Ni). Sm-Nd and Lu-Hf isotopic compositions indicate that the mare basalt sources were fractionated with respect to chondritic compositions early in the evolution of the lunar mantle and have since remained isolated (Nyquist and Shih 1992; Beard *et al.* 1998). High-pressure experiments on near-primary basalts indicate that phases such as ilmenite, clinopyroxene, plagioclase, and spinel are not found on the high-pressure liquidus and therefore must have been consumed during melting. Olivine and orthopyroxene occur as high-pressure liquidus phases.

These observations constrain the mineralogical and chemical characteristics of the lunar interior. First, the isotopic data, incompatible-element enrichments and fractionation, the negative Eu anomaly, and the absence of plagioclase as a high-pressure liquidus phase for the near-primary basalts indicate that the source region had experienced early differentiation that resulted in a non-chondritic mantle, and that the individual source regions remained isotopically and mineralogically distinct. Isotopic closure of the systems could correspond to either crystallization of the magma ocean or subsolidus overturn of the LMO cumulate pile. Whether the non-chondritic nature of the lunar mantle is solely a product of lunar

differentiation or is instead a product of early differentiation of a non-chondritic bulk Moon is debatable. Second, the source region of the mare basalts is highly reduced, anhydrous and depleted in volatile and siderophile elements. Third, mineral assemblages making up the lunar mantle are dominated by olivine and orthopyroxene. This indicates that the source regions for the mare basalts are predominately harzburgitic rather than lherzolitic. Other phases such as ilmenite, clinopyroxene, plagioclase, spinel and perhaps garnet are heterogeneously distributed in the lunar mantle and were in most cases totally consumed during melting.

Trace element constraints on source regions. Understanding the trace-element contents of mare source regions is key for several reasons. One is that the naturally radioactive elements K, U, and Th provide long-lived sources that contribute to the buildup of heat needed to remelt mantle materials long after solidification of the magma ocean. Another relates to the trace elements whose abundance patterns can help to distinguish primitive unfractionated sources from sources that were fractionated by magma-ocean solidification processes. Related to these are the volatile elements that appear to have been associated with the eruption of volcanic glasses. Differences in the style of eruption of the volcanic glasses and mare basalts may be related to their volatile content, depth of origin, and whether or not the sources were undifferentiated and thus volatile-rich relative to the cumulate upper mantle. Volcanic volatiles are discussed in Section 3.1.4.

The low incompatible-element concentrations of most sampled basalts are consistent with being derived from generally depleted sources. Some portion of the trace elements in their source was likely incorporated as a trapped melt component in cumulates of the crystallizing magma ocean. However, small amounts of a component with a KREEP-like trace-element signature are indicated for some of the basalts and picritic magmas, and the main question is whether this signature is inherent to the mantle or is rather due to contamination during magma ascent.

The potential contamination of basaltic melts by trace-element-rich components is significant in relation to models of dynamic overturn of mantle cumulates. Early in lunar history, near the last stages of magma-ocean solidification, density instabilities may have mixed dense Fe-rich, late-stage cumulates formed near the crust-mantle boundary with deeper mantle cumulates. This mixing could have occurred either by sinking of the dense high-level cumulates or by diapiric rise of low-density magnesian mantle cumulates (e.g., Hess and Parmentier 1995). In either case, the end result could have been the incorporation of incompatible-trace-element enriched residua in various unrelated mantle source regions (see Chapter 4). In places where such processes occurred, the timing of mixing of different materials and the crystallization of late-stage minerals that can fractionate key trace elements may have produced some of the fundamental variations in composition observed between basalt groups. The most important example is the timing of crystallization of ilmenite and perhaps armalcolite. Titanium is an incompatible element in olivine, orthopyroxene, and plagioclase, yet it was effectively decoupled in lunar magma systems from the other incompatible elements and is not strongly enriched, for example in KREEP basalt and other materials with KREEP-like compositions. Likewise, the separation of a low-density Si-K-enriched melt following the crystallization of Ca-REE-phosphate in very late-stage LMO residua may have decoupled the REEs from K. Such a separation might lead to different mixing reservoirs with which rising basaltic liquids could interact.

Low-Ti mare basalt compositions exhibit generally chondritic ratios of high field strength elements (HFSE; Zr, Nb, Hf, Ta, Th) and Y, even though melting and crystallization of the magma ocean have processed their source regions. The ratios of these elements should not change significantly under low-pressure fractional crystallization processes (i.e., <18 kb), because unlike the terrestrial mantle, the lunar mantle has not experienced repeated processing after magma-ocean crystallization, which would tend to enhance the effects of slight differences in HFSE mineral partition coefficients. However, Ti-rich mare basalts and KREEP basalt generally exhibit non-chondritic ratios of these elements, which is probably

a result of Fe-Ti oxide addition (Ti-rich basalts) or removal (KREEP); the complement to the KREEP pattern is seen in the compositions of the high-Ti basalts (Fig. 3.14). Mare basalt compositions are consistent with an overturn model of the cumulate pile that would have incorporated excess ilmenite into the low-Ti basalt source (or possibly a KREEP component, as in the case of the Apollo 11 high-K basalts), thus disturbing a source region that had originally developed with chondritic HFSE (and Y) ratios (Neal 2001).

High-pressure phases in mantle source regions. Recent work suggests that some volcanic glasses may have source regions at depths below the differentiated cumulate mantle, and trace-element measurements suggest the possibility that garnet may occur in their residue (Neal 2001). In particular, if garnet were retained in the residue during partial melting, its influence on

magmatic compositions would be most noticeable in the heavy REE and Y concentrations because garnet has high mineral/melt partition coefficients for these elements. Retention of garnet in the residue would thus result in elevated LREE/HREE or incompatible-element/Y ratios in the corresponding partial melts. However, assimilation of late-stage cumulates and KREEP-rich materials to produce the high-Ti contents of some glasses, as well as the ubiquitous negative Eu anomaly (cf., Longhi 1992; Wagner and Grove 1997; Elkins et al. 2000; Neal 2001), can also lead to elevated values for these ratios. Therefore careful examination of the data is required to distinguish between the incorporation of fractionated material and the presence of residual garnet in the mantle source region.

The mare basalts generally exhibit chondritic Zr/Y ratios, whereas the volcanic glasses and KREEP-rich samples are suprachondritic (see Fig. 3.15). The Apollo 11 high-K and Apollo 14 basalts tend to exhibit suprachondritic Zr/Y, but these are probably due to the incorporation of KREEP (cf., Neal et al. 1988, 1989). While the Zr/Y database is small, the mare basalt and picritic glass groups are clearly distinguishable. In particular, the mare basalts and some glasses have Zr/Y ratios <4 , KREEP forms a tight group with Zr/Y ~ 4.5 , and some volcanic glasses have ratios in excess of the KREEP values (Fig. 3.15a). This is further emphasized when the slope of the REE profiles is considered as measured by the Sm/Yb ratio (Fig. 3.15b). Some volcanic glasses exhibit the steepest slope (highest Sm/Yb ratio of ~ 2), whereas the mare basalts and remaining glasses display Sm/Yb ratios between 1 and 1.25, with KREEP being intermediate. It is the glasses with Sm/Yb ratios greater than KREEP that are considered evidence that garnet was a residual component after the cessation of partial melting (Neal et al. 1988, 1989; Neal 2001). This result further requires these glasses to be derived from depths where Al-bearing garnet would be stable.

The geochemical evidence for garnet in the lunar mantle is consistent with both the predicted range of thermodynamically stable phase assemblages with depth and the lunar seismic data (e.g., Anderson 1975; Hood 1986; Hood and Jones 1987; Mueller et al. 1988). As an ex-

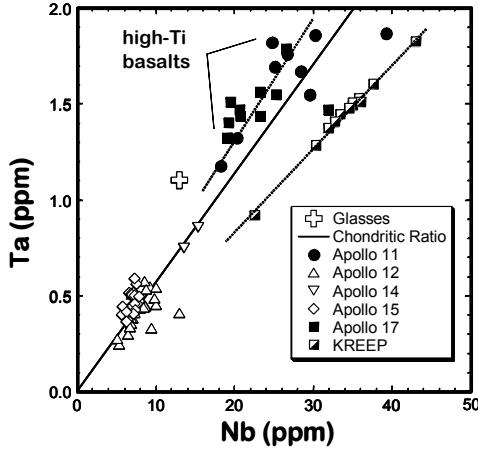


Figure 3.14. Plot of Ta vs. Nb for the mare basalts. Only one datum is available for the volcanic glasses (Shearer et al. 1990). Low-Ti basalts cluster around the chondritic ratio for Nb/Ta, whereas the high-Ti basalts have Ta/Nb ratios generally less than chondritic. Conversely, Ta/Nb ratios for KREEP are superchondritic. Modified after Neal (2001).

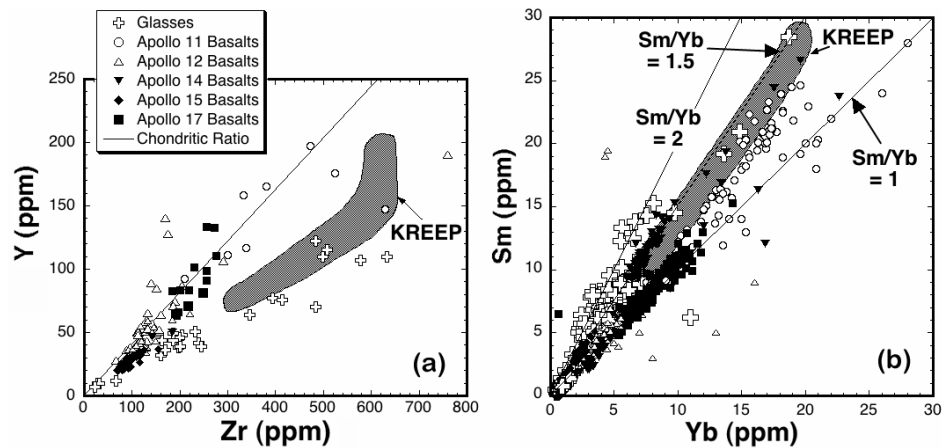


Figure 3.15. Two diagrams showing evidence for garnet being retained in the source regions of some volcanic glasses through increased Y/Zr (a) and Sm/Yb (b) ratios relative to KREEP. Modified after Neal (2001).

ample, Kuskov and Fabrichnaya (1994), Kuskov (1995; 1997), and Kuskov and Kronrod (1998) calculated the stable phases of a variety of compositional models by minimizing the Gibbs free energy. In comparing their predicted seismic velocities with the Apollo-era seismic velocity profiles, it was found that garnet should be a significant phase (8–13 mol%) in the lower mantle between depths of ~500 and 1260 km. For comparison, Neal (2001) modeled the high Zr/Y and Sm/Yb glasses using a source containing 5 vol% garnet. Although the coupled thermodynamic–seismic models imply that garnet is present in the lower mantle, garnet by itself is probably not responsible for the apparent 500 km seismic discontinuity, as is discussed in Section 3.2.3. We further note that garnet has been predicted to be thermodynamically stable in the mantle above the 500 km seismic discontinuity for certain compositional models and temperature profiles (Kuskov 1995, 1997; Khan et al. 2006). Based on the modeling of Kuskov (1995), up to 4 mol% garnet could be stable at a depth of 400 km, whereas Khan et al. (2006) find that ~15 wt% garnet may be present between depths of ~200 and 600 km. Thus, a garnet signature by itself should not be used as evidence for an origin beneath this discontinuity.

Despite the evidence articulated above for the presence of garnet in the lower mantle, whether this region escaped processing by the lunar magma ocean remains unknown. If the deep garnet-bearing source was “primitive” and “unprocessed” then it might have elevated siderophile- and chalcophile-element concentrations (e.g., Ir, Au, Cu, and Zn) for two reasons. First, these elements would not have been as efficiently scavenged from the primitive Moon during a core formation event as they would have been from a magma ocean. Second, the siderophile and chalcophile elements scavenged from the magma ocean by an immiscible sulfide melt (Neal and Ely 2002) would have to permeate through the solid primitive interior of the Moon, possibly enriching this region with these elements in the process. Simple elemental relationships show that at least some of the volcanic glasses possess higher siderophile and chalcophile abundances than the mare basalts, supporting the hypothesis that they were derived from a deep undifferentiated source (see Fig. 3.16). Although the database is not extensive, the glasses for which data are available (Anders et al. 1971; Morgan et al. 1972a; Morgan et al. 1972b; Ganapathy et al. 1973; Morgan et al. 1974) also have generally higher Ir and Au abundances relative to the crystalline basalts (see Neal 2001). Perhaps most significantly, the Cu and Zn data demonstrate that there are two groups of glasses; one with abundances greater than the basalts, and the other with abundances comparable to the mare basalts (Fig. 3.16). The former group contains glasses with chondrite normalized Sm/Yb > 1.5, consistent with being derived from a garnet-bearing, primi-

tive source. The latter group contains glasses with lower chondrite normalized Sm/Yb (<1.5) and higher Sc/Sm (>30) ratios, suggestive of being derived from a garnet-free source region in the lunar magma ocean cumulate pile, similar to the mare basalts (Neal 2001).

3.1.4. Volatile element content of the lunar mantle. Volatiles play a fundamental role in the evolution of a planet and exert an important influence on mantle processes (e.g., melting, dynamics, and heat transfer) and characteristics (e.g., mineralogy and melt composition). Unlike the Earth where estimates of juvenile volatiles can be made using a variety of approaches, the volatile budget of the lunar mantle can, at the present time, only be reconstructed from the record preserved in mare basalts and volcanic glasses. Several lines of observation can be used to reconstruct the volatile budget of the lunar mantle from mare basalt samples: mineral assemblage and composition, bulk volatile content, volatile coatings on mineral or glass grains, volatile element profiles in volcanic glasses, volatile element contents of volcanic glass beads within a well defined pyroclastic deposit stratigraphy, and distribution of volatile-driven pyroclastic eruptions. As in the terrestrial case, reconstructing the volatile content of the lunar mantle from basaltic melts is compromised by volatile degassing at the time the lavas erupted and subsequent contamination from external sources. Unlike terrestrial basalts where atmospheric and non-magmatic water add to the complexity, lunar-volatile contamination may be attributed to low-pressure condensation following impact, solar wind implantation, and assimilation or sublimation of cometary or meteoritic material.

To a first approximation, the presence of metallic iron or Ni-Fe alloys in mare basalts indicates that they crystallized at oxygen fugacities below the iron-wüstite buffer. Identification of an assemblage of Fe-rich olivine, cristobalite, and metal in the mesostasis of Apollo 14 basalts (El Goresy et al. 1972) constrain the f_{O_2} at the end of crystallization to be lower than the IW buffer and near the quartz-fayalite-iron buffer (QFI). These mineralogical observations are further corroborated by the total absence of ferric iron in both silicates and oxides, and the presence of reduced valance states of Cr and Ti (Haggerty et al. 1970). Intrinsic f_{O_2} determinations as well as those based on thermodynamic gas equilibria calculations show that the range of temperature and f_{O_2} for mare basalt crystallization is relatively small, varying from 10^{-13} at 1200°C to 10^{-16} at 1000°C (Wellman 1970; Sato and Helz 1971; Sato et al. 1973). Relative to standard buffer curves, these values are approximately 0.2 to 1.0 log units below iron-wüstite (IW) and above the univariant curve that defines the stability of ilmenite (see Fig. 3.17). An exception to this is the pyroclastic high-Ti basaltic glass, e.g., 74220. Sato (1979) showed that at temperatures between 1000 and 1100°C, the measured f_{O_2} for the high-Ti glass was approximately 0.15 to 0.3 log units above the IW buffer. However, extrapolating this relationship to the liquidus temperature of the high-Ti glass (>1325°C) shifts the estimate of f_{O_2} to approximately 0.3 log units below the IW buffer. Some lunar basalts show textural and mineralogical evidence for further subsolidus

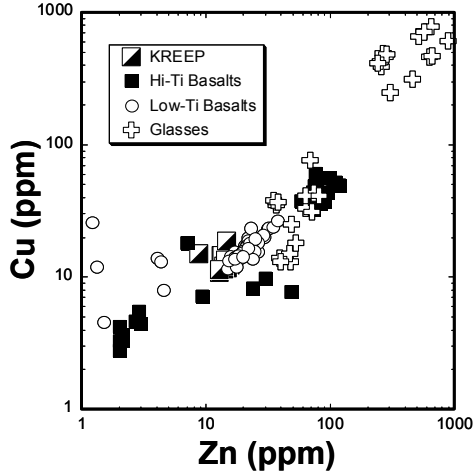


Figure 3.16. Plot of Cu vs. Zn for the volcanic glasses and mare basalts. Those glasses with elevated Cu and Zn abundances are inferred to originate in a deep primitive lunar mantle that escaped magma-ocean differentiation. Samples with elevated Cu and Zn abundances generally correlate with elevated Zr/Y and Sm/Yb ratios. [Used by permission of the American Geophysical Union, from Neal (2001), *Journal of Geophysical Research*, Vol. 106, Fig. 10, p. 27,881.]

reduction (summarized by El Goresy et al. 1976) taking place at a range of f_{O_2} below both IW and FIQ buffers.

Although the f_{O_2} conditions under which the mare basalts crystallized is restricted to below IW, it is unclear whether these reducing conditions reflect reducing crustal and mantle environments or reduction processes during magma transport and eruption. The oxidation state of the deep lunar mantle depends on the specific reactions that control the redox state. If the dominant redox controlling reaction in the lunar mantle were the uv-I-il buffer or a similar reaction, then the oxygen fugacity at constant temperature would rise with depth in the Moon at a rate of about 1 log-unit per 10–15 kbar (200–300 km). On the other hand, if the oxidation state in the Moon was controlled by the graphite-(CO+CO₂) system, the oxygen fugacity of the lunar mantle would increase at a greater rate with increasing depth, such that it would be near the fayalite–magnetite–quartz (FMQ) buffer at 400–500 km (Delano 1990).

Ringwood et al (1981) suggested that the reduced nature of the mare basalts was a surface phenomenon and that the lunar mantle was more oxidized (between the IW and Co-CoO buffers). They sited the late crystallization of metal in mare basalts and the depleted behavior of siderophile elements (W, Re) as lines of evidence. However, several direct and indirect lines of evidence do support a reduced mantle with f_{O_2} at or below the IW buffer. First, small metal inclusions of Fe-Ni metal in olivine phenocrysts in the Apollo 12 basalts indicate that the basalts were at or near metal saturation prior to extensive crystallization at the lunar surface (Brett et al. 1971). Second, Delano (1990) showed that the Cr content of liquids coexisting with spinel varies considerably with f_{O_2} , such that Cr is low (~1000 ppm) at the FMQ buffer and high (>2700 ppm) at the IW buffer. This is due to the lower solubility of Cr²⁺ in spinel at reducing conditions and therefore remaining in the melt. Delano pointed out that the Cr content of primitive lunar basalts (2700–6300 ppm) is significantly higher than similar terrestrial basalts (<1500 ppm). Therefore, if spinel was a residual phase in the lunar mantle and the Cr content was approximately chondritic, the high Cr content of the mare basalts suggests a reducing lunar mantle. Third, carbon solubility modeling by Fogel and Rutherford (1995) showed that the solubility of C is low at conditions 0.5 log units below the IW buffer and increases substantially above the IW buffer (>300 ppm). Therefore, the low concentration of dissolved C in mare basalts (~30 ppm) and volcanic glasses (<100 ppm) implies reducing conditions in the lunar mantle. Fourth, Weitz et al. (1997), in their examination of inclusions (olivine, metal, spinel) in Apollo 17 orange glass beads, concluded that metal-melt equilibria and the Cr content of the olivine and spinel indicated a pre-eruptive f_{O_2} of 1.3 log units below IW. They

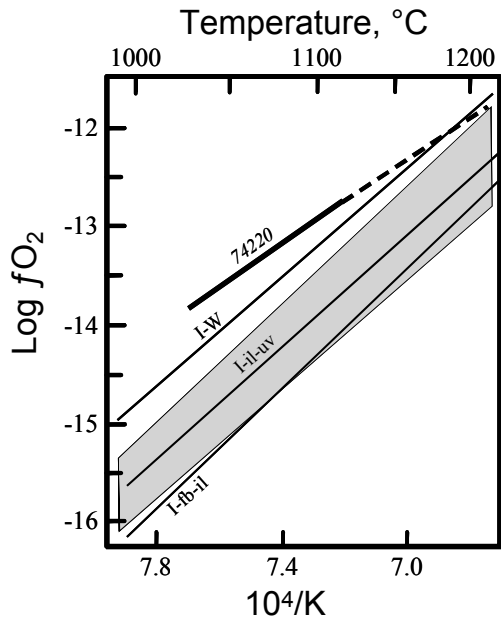


Figure 3.17. Oxygen fugacity as a function of temperature for several buffers relevant to the lunar interior: I-W, iron-wüstite; I-il-uv, iron-ilmenite-ulvöspinel; I-fb-il, iron-ferrobustamite-ilmenite. Although the intrinsic f_{O_2} curve for the Apollo 17 orange glass (74220) is at more oxidizing conditions than IW below 1175°C, the curve intersects its liquidus temperature at an f_{O_2} more reducing than IW. Patterned region represents the range of f_{O_2} corresponding to the crystallization of mare basalts.

also concluded that an episode of magma oxidation occurred during later stages of eruption. Finally, Fe metal is also present in intrusive igneous lunar rocks that bear no indication of reduction due to subsolidus reequilibration or volatile loss. By analogy to terrestrial basalts, the oxidation state of extrusive basalts and their intrusive equivalents ought to be similar (Basaltic Volcanism Study Project 1981).

Unlike terrestrial volcanic gases, those associated with lunar basaltic magmatism are devoid of H_2O . Judging from the samples, the lunar magmas also contained lower concentrations of gases. This finding has been interpreted as indicating that the lunar mantle is extremely dry and volatile poor. Hydroxyl contents for the Apollo 15 green and yellow volcanic glasses are below the detection limits of Fourier transform infrared spectroscopy (FTIR; ~10 to 50 ppm), and the absence of hydrous silicates such as amphibole and phosphates reflect their intrinsic low H_2O content. The bulk carbon content of analyzed mare basalt samples lies between 15 and 67 ppm (Gibson 1977), and this agrees with the more recent study by Fogel and Rutherford (1995) which demonstrated that the dissolved C species in lunar volcanic glasses is less than FTIR detectability (<50–100 ppm). The ratio of $\text{CO}:\text{CO}_2$ in Apollo 15 basalts ranges from 1:2 to 1:4 and appears to be dependent upon concentration (Gibson *et al.* 1975). Wellman (1970) calculated that the $\text{CO}:\text{CO}_2$ ratio should be approximately 1:2 at crystallization conditions experienced by lunar basalts in contrast to terrestrial volcanic glasses that have a CO_2 content that ranges from 0.05 to 0.43 wt% (Basaltic Volcanism Study Project 1981). The low C content of mare basalts has been attributed to the low C content of their source, the low solubility of C at reducing conditions (below the IW buffer), and volatile loss during eruption owing to diffusion and evaporation (Fogel and Rutherford 1995). Sato (1978; 1979), Wilson and Head (1981), Spera (1992) and Fogel and Rutherford (1995) suggested that the oxidation of graphite at relatively shallow depths (<4 km) was the mechanism for producing pyroclastic deposits on the Moon. In order for this process to be effective, though, graphite would need to be transported from the lunar interior by the basaltic magmas, and thus far, graphite has not been identified in mare basalts associated with pyroclastic deposits.

If CO was a major volcanic gas in lunar magmas, then carbonyl species such as COS , COCl , COCl_2 , FeCO_5 and others would have played a role in elemental transport (Colson 1992). The presence of carbonyls would favor the deposition of sulfides and possibly Fe metal with decompression, while liberating CO. Reactions involving carbonyls also may have played a role in the formation of vapor-deposited sulfides on volcanic glasses.

The sulfur concentrations of crystalline mare basalts range from an average of 400 ppm in some of the Apollo 15 low-Ti basalts to 2600 ppm in the high-Ti basalts from Apollo 17 (Delano 1986b, and references therein). The relationship between Ti and S content in the mare basalts, as shown in Figure 3.18, is partially attributed to increases in S saturation with increasing Fe and Ti content, with calculated S saturation in mare basalts ranging from 1500 to 3400 ppm. For comparison, pre-eruptive concentrations of S in terrestrial basalts range from 800 to 2500 ppm and generally exhibit a strong correlation with Fe (Basaltic Volcanism Study Project 1981). The S content of the bulk volcanic glasses ranges from 550 to 750 ppm for the Apollo 17 high-Ti glasses and averages 400 ppm for the very low Ti glasses. The individual glasses have been analyzed by both microprobe and ion probe methods (Delano *et al.* 1994; Shearer *et al.* 1997; Klein and Rutherford 1998) and the S concentrations of the individual glass beads are lower than both the crystalline basalts and the bulk glass beads (Fig. 3.18). The higher S content of the bulk beads relative to the individual beads reflects volatile-rich coatings on the glasses. Unlike the crystalline mare basalts, the glasses do not show a clear relationship between Ti and S content. The lack of the relationship between Ti and S and the overall lower S concentrations of the individual glass beads indicate substantial loss of S during pyroclastic eruptions. Fogel and Rutherford (1995) calculated that S loss by diffusion during fire fountaining would be significantly less than either CO_2 or Cl loss.

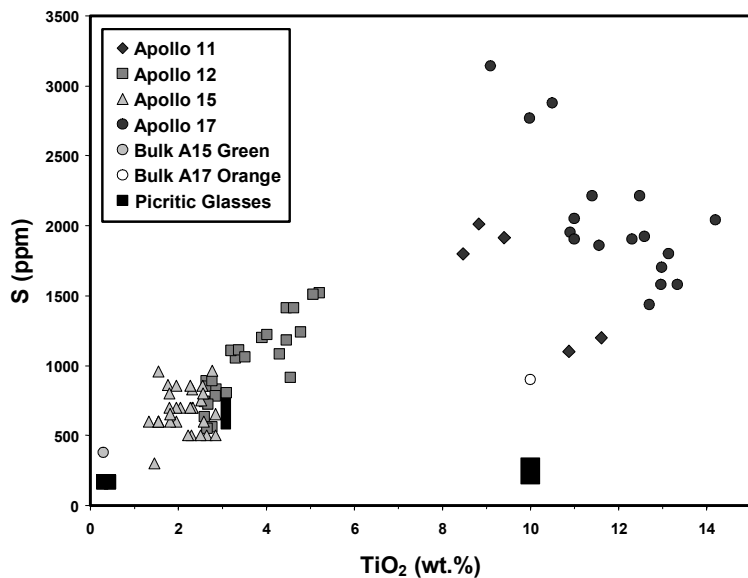


Figure 3.18. Sulfur concentrations in lunar picritic glasses and mare basalts. Data from Shearer et al. (1998), Agrell et al. (1970), Beatty and Albee (1978), Gibson et al. (1975, 1977), Gibson and Moore (1974), Rees and Thode (1972, 1974), and Wänke et al. (1975).

Clearly, abundant evidence suggests that the lunar magmas were reduced prior to eruption at the lunar surface (below IW-1) and that they were derived from a fairly reduced lunar mantle (below IW). All indications are that the lunar mantle was also anhydrous. It is more difficult to extract information concerning the nature of C and S in the lunar mantle. These volatiles were lost to various degrees during eruption of basaltic magmas at the lunar surface (highest loss during pyroclastic eruptions) and their solubility in lunar basalts was controlled by variables such as temperature, pressure, composition, and f_{O_2} . Although the solubility of C is low at the reducing conditions of lunar magmas, most models for lunar fire fountaining evoke the shallow oxidation of mantle-derived graphite that was entrained in the mare basalts.

3.2. Seismology

Besides the analysis of mare basalts, which are ultimately derived from the mantle, the only other detailed source of information about the lunar mantle comes through an analysis of the Apollo seismic data. However, because of the limited depth distribution of the deep moonquakes and the absence of identifiable quakes on the hemisphere opposite that of the seismic network, seismic velocity information was precluded from being inferred below a depth of ~ 1150 km.

Figure 3.19 depicts the seismic velocity model of Khan et al. (2000), which is based upon the first P- and S-wave arrival times of Nakamura and coworkers. This model was constructed using a Monte Carlo sampling of parameters within 56 variable thickness homogeneous layers, and the results were interpreted in terms of a Bayesian probabilistic framework. Plotted contours correspond to the probability of obtaining a given velocity at any given depth (see the discussion in Section 2.2). This inverse approach most faithfully addresses the inherent resolution of the data, as well as errors on estimated parameters (i.e., velocities, seismic discontinuities, etc.). However, as a relatively large number of layers were used, the range of acceptable velocities at any depth is fairly large, and thus not entirely useful for placing

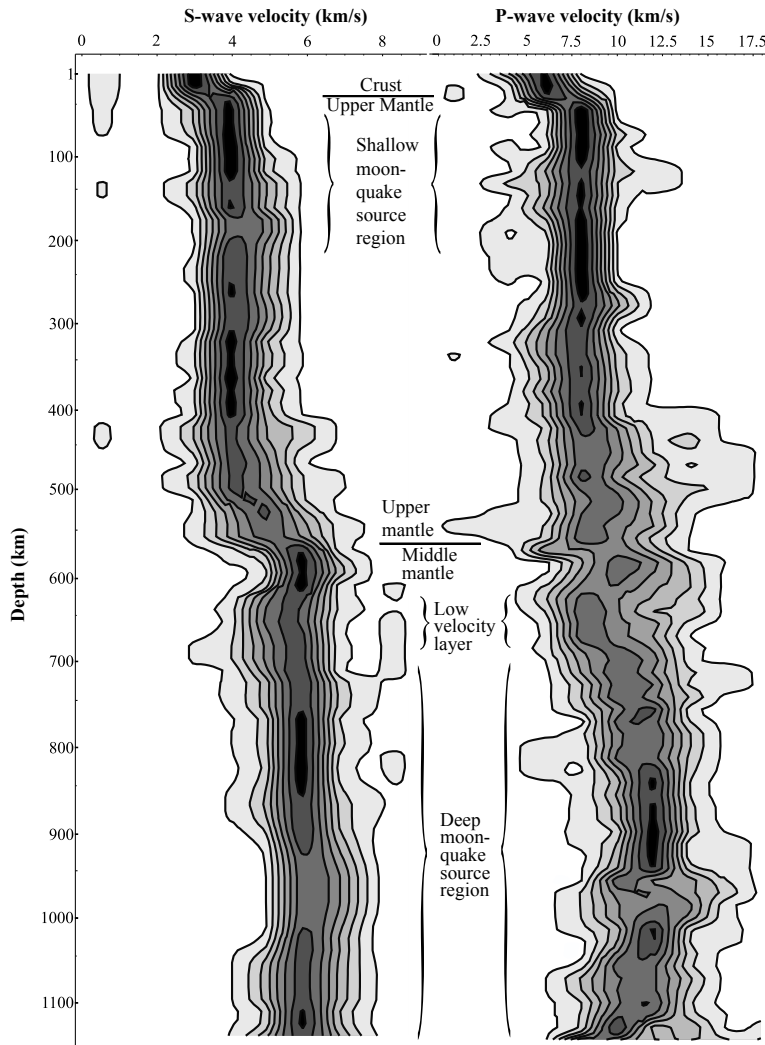


Figure 3.19. P and S-wave velocity profiles of the lunar mantle based on the Bayesian inversion of Khan *et al.* (2000). The marginal probability of the seismic velocity is plotted at one-kilometer depth intervals, and the contours define nine equally sized probability intervals. [Used by permission of the American Geophysical Union, from Khan *et al.* (2000), *Geophysical Research Letters*, Vol. 27, Fig. 1a, p. 1592.]

quantitative constraints on the geochemistry of the lunar interior. For this purpose, the models of Nakamura *et al.* (1982) Goins *et al.* (1981a) and Lognonné *et al.* (2003) would be more useful (see also, Khan *et al.* 2006).

Whereas earlier studies (e.g., Goins *et al.* 1981a; Nakamura *et al.* 1982) could not resolve the depth dependence of any velocity variations in the mantle (those present were introduced for computational convenience), quantifiable velocity variations are found in the Khan *et al.* (2000) model providing evidence for compositional stratification within the mantle. Specifically, their results suggest an almost constant velocity upper mantle from the base of the crust down to a depth of roughly 500 km. A slight decrease of S-wave velocity with depth

is indicated over this depth range (Khan and Mosegaard 2002, Fig. 14), consistent with the findings of previous studies (Nakamura et al. 1976; Goins et al. 1981a). Below a depth of 500 km both the P- and S-wave velocity structure indicate a gradual velocity increase toward the transition between the upper and middle mantle. At the base of this transition zone, at a depth of 560 ± 15 km, a substantial increase in velocity of the order of 1 km/s is found to occur (Khan and Mosegaard 2002, Figs. 9 and 13). A discontinuity at this depth was previously suggested by the Nakamura et al. (1982) velocity model. As a result of the large uncertainties of arrival times associated with the deep moonquakes, velocity variations within the middle mantle could not be unambiguously identified.

Relocalization of the shallow moonquake hypocenters showed these to be distributed in the depth range from 50 to 220 km (Khan et al. 2000), confirming earlier suggestions that the upper mantle is a source of tectonic activity (Nakamura et al. 1979). The high frequency content of seismic signals from the shallow moonquakes indicates large stress concentrations at their source. Stress drops associated with these quakes might exceed 100 MPa (Oberst 1987), consistent with a model in which thermoelastic strain within a thick lithosphere is released by an occasional shallow quake as the Moon cools. However, as only 28 shallow events were observed, definitive conclusions as to their origin cannot be drawn. Relocalization of the deep moonquake hypocenters indicates a well-defined source region with all quakes situated in the depth range of ~700 to 1150 km (see Fig. 3.20).

We note that some unresolved differences exist among the velocity models of Goins et al. (1981a), Nakamura et al. (1982), Khan et al. (2000), and Lognonné et al. (2003). Perhaps the most important is that the study of Goins et al. (1981a) found a decrease in velocity below a depth of ~480 km, in contrast to a velocity increase as found by Nakamura et al. (1982) and Khan et al. (2000). As these latter two studies relied upon the same data set, it should not be too surprising that they are in agreement. However, a complete independent analysis and inversion of the Apollo data by Lognonné et al. (2003) has found a significant P-wave velocity decrease to occur below a depth of 488 km, in agreement with the Goins et al. (1981a) model (see Fig. 3.21). Possible causes of this discrepancy include differences among these three datasets, as well as the different inversion techniques employed. We note that the inversions based upon the Nakamura et al. dataset have relied upon 41 deep moonquake sources whereas both Goins et al. (1981a) and Lognonné et al. (2003) have used 24. Lognonné et al. (2003) have also demonstrated that their lower mantle velocities are not robust to small changes in the number of utilized moonquakes. Indeed, when five of the deepest moonquakes were excluded in their inversion, a velocity increase below 500 km was obtained. We remark that in the coupled thermodynamic-seismic inversion of Khan et al. (2006), which is based on the Lognonné et al. (2003) first arrival data set, a seismic velocity increase below a depth of ~500 km has been found, consistent with the studies of Nakamura et al. (1982) and Khan et al. (2000).

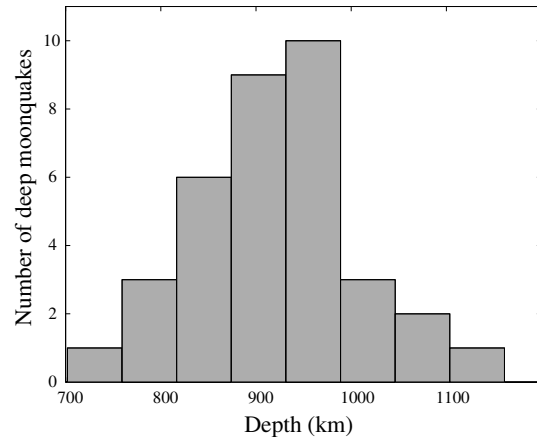


Figure 3.20. Depth distribution of the deep moonquakes. Data from Khan and Mosegaard (2002)

3.2.1. Evidence for a partially molten lower mantle. Information on the deepest structure of the Moon is relatively indirect since the seismic studies mentioned so far were limited to a depth of ~ 1150 km. The lack of knowledge deeper than this arises because of the distribution of the deep moonquake sources, where until recently, the only farside moonquakes that had been located came from a single focus that lies just over the eastern limb of the Moon (A33, Nakamura *et al.* 1973). Analysis of the signal characteristics from this sole farside focus showed clear onset of shear-wave arrivals at the two stations situated closest to the source, whereas at the furthest two stations none could be discerned. This is particularly telling, as the characteristic feature used in identifying the deep moonquakes is their prominent shear-wave and weak P-wave arrivals. At the two stations where S-wave arrivals were visible, their ray paths were found to have bottomed at depths of roughly 1000 km, while rays traveling to the two farther stations bottomed at about 1300 km depth. This observation led to the suggestion that the absence of shear wave arrivals at the two stations

farthest from the source was due to the rays having probed an attenuating region somewhere below a depth of 1000 km (or a radius less than ~ 740 km). As P-wave arrivals were observed, the attenuation must be relatively greater for shear waves. These observations are most easily explained by the presence of a high attenuation region, such as the presence of a partial melt, below a depth of ~ 1000 km (Nakamura *et al.* 1973).

A recent analysis by Nakamura (2005) has identified and located seven new moonquake nests that are either clearly on the farside, or, to within error, on the lunar limb. The distribution of these nests shows that there is a lack of moonquakes occurring within a radius of $\sim 40^\circ$ antipodal to the sub-Earth point. Given the observed asymmetric distribution of nearside moonquakes, as well as the asymmetric thermal evolution of the Moon (e.g., Wieczorek and Phillips 2000; Zhong *et al.* 2000; Parmentier *et al.* 2002), it is possible that this region might truly be aseismic. Nevertheless, of these seven nests, two were found to possess signal characteristics similar to the previously known farside nest, with clear S-wave arrivals being absent at the farthest stations in the seismic array. This strengthens the original suggestion of Nakamura (1973) that the deep lunar interior is highly attenuating to S-waves.

Lunar rotation studies indicate that the lunar interior is very effective in dissipating energy (e.g., Yoder 1981), with current estimates of the solid body tidal Q being very low (< 90 , Williams *et al.* 2001b). Since the seismic Q of the mantle has been found to be relatively high (> 4000 in the upper mantle, e.g., Nakamura and Koyama 1982) and about 1400–1500 in the lower mantle

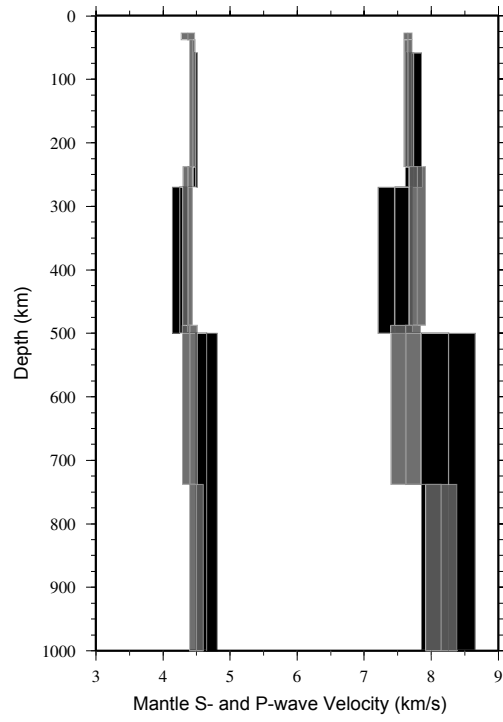


Figure 3.21. P- and S-wave velocity profiles of the lunar mantle based on the studies of Lognonné *et al.* (2003) (gray) and Nakamura *et al.* (1982) (black) with $1-\sigma$ uncertainties. Note the different velocity scale with respect to Figure 3.19.

(Dainty et al. 1976; Nakamura et al. 1976), the deeper interior must possess a significantly lower Q , possibly as a result of the presence of a partial melt. As noted by Nakamura (2005), a region possessing a seismic Q of 100 would attenuate P-wave amplitudes by a factor of 3 over a distance of 500 km, and those of S-waves by a factor of 6. Such a highly attenuating region could easily explain the near absence of detectable farside deep moonquakes, for even if they did exist, direct shear-wave arrivals would not be expected for these events.

3.2.2. Mineralogy and composition of the lunar mantle. A few studies have used the lunar seismic data to constrain the composition and mineralogy of the lunar interior. Initial investigations were limited to comparing the seismic velocity models of Goins et al. (1981a) and Nakamura et al. (1982) to those expected from a restricted suite of mantle mineral assemblages (Buck and Toksöz 1980; Hood and Jones 1987; Mueller et al. 1988). Later studies by Kuskov and coworkers (Fabrichnaya and Kuskov 1994; Kuskov and Fabrichnaya 1994; Kuskov 1995, 1997; Kuskov and Kronrod 1998, 2001; Kuskov et al. 2002) employed a thermodynamic approach to calculate stable mineral phases for a range of mantle compositions and temperature profiles, and then compared the obtained seismic velocities to the model of Nakamura et al. (1982). Finally, a recent study by Khan et al. (2006) used a similar thermodynamic approach, but instead of just comparing their results to a seismic velocity model, they inverted directly the first arrival time data set of Lognonné et al. (2003) for mantle composition and temperature using a Monte Carlo Bayesian inverse method.

Kuskov and Kronrod (1998) assumed that the mantle composition was constant in the three layers defined by the Nakamura et al. (1982) seismic velocity model (58–270 km, 270–500 km, and greater than 500 km), and parameterized the mantle temperature profile by an exponential function. For a range of chemical compositions and temperature profiles, thermodynamically stable mineral phases were determined, and the seismic velocity was calculated as a function of depth. In general, they found that the Nakamura et al. (1982) velocity model was best explained by an ~500 km orthopyroxenite upper mantle, and a garnet-bearing olivine and clinopyroxene mantle below this depth. Two best-fit models were presented, with each being constrained by a prescribed mantle density just beneath the crust. Concerning their upper mantle, one model contained about 95 mol% orthopyroxene and 4 mol% clinopyroxene between the crust and 270 km depth, and about 92 mol% orthopyroxene, 4 mol% clinopyroxene, 4 mol% olivine and 1 mol% garnet between 270 and 500 km. For this model, the magnesium number decreased from 84 at the base of the crust to 73.5 at a depth of 270 km. Their second model was somewhat less silica-rich above a depth of 270 km, possessing about 75 mol% orthopyroxene, 5 mol% clinopyroxene, and 19 mol% olivine. Between 270 and 500 km depth the composition was similar to the first model, being composed of approximately 96 mol% orthopyroxene and 4 mol% clinopyroxene. For this second model the magnesium number decreased from 87 at the base of the crust to 75 at a depth of 270 km. Both models gave nearly identical results for the mantle below 500 km. Here, a magnesium number of 86 was obtained and the mineral phases olivine, clinopyroxene, and garnet were found to be present in the molar proportions 56:35:9.

A recent study by Khan et al. (2006) similarly employed a thermodynamic approach and obtained results that are somewhat consistent with those of Kuskov and coworkers. As for the inverse approach, the most important difference between these studies is that Khan et al. (2006) directly modeled the first seismic arrivals, whereas Kuskov and coworkers compared the seismic velocities obtained from a thermodynamic model to the seismic velocity profiles of Nakamura et al. (1982), which is in itself a model. The first arrival data set of Lognonné et al. (2003) was used, and the Moon was assumed to be composed of a variable thickness and constant composition crust, upper mantle, and lower mantle. The bulk crustal composition was found to be consistent with the model of Taylor (1982), and the transition between the upper and lower mantle occurred near a depth of 600 km. The upper mantle was found to be

an orthopyroxenite containing ~75 wt% orthopyroxene, a relatively unconstrained amount of clinopyroxene, trace amounts of olivine, and depending upon depth, either plagioclase or garnet. Above a depth of about 200 km, plagioclase was stable with abundances less than about 10 wt%, and below this depth, garnet was present with abundances near 15 wt%. Below ~600 km depth, the mantle was found to be composed of approximately 60 wt% olivine and 40 wt% garnet. As for the magnesium number, this was found to increase from ~66 in the crust, to ~75 in the upper mantle, and finally to ~89 beneath a depth of 600 km.

While the overall mantle mineralogy of the Kuskov and coworkers and Khan *et al.* studies are similar, they differ in detail. Perhaps most importantly is that Khan *et al.* find relatively higher abundances of garnet in the upper mantle (~15 wt%) between depths of ~200 and 600 km, whereas Kuskov and coworkers only found approximately 1 mol% over a similar depth range. The lower mantle of Khan *et al.* is also more garnet rich, being composed of about 40% garnet by weight in contrast to about 9 mol% as obtained by Kuskov and coworkers. As a result of these differences, the Khan *et al.* mantle contains about twice as much aluminum as that of Kuskov and coworkers. Furthermore, clinopyroxene is predicted to be a rather minor phase by Khan *et al.* in the lower mantle, whereas this mineral is present with an abundance of ~35 mol% in the model of Kuskov and coworkers. While the magnesium number of the lower mantle is similar for these two models, this number is not easily comparable for the upper mantle as Kuskov and coworkers employed two compositional layers where Khan *et al.* used one.

One potential concern with the above studies is that neither has fully explored the consequences of possible titanium-rich phases in the mantle. While Kuskov and Kronrod (2001) and Kuskov *et al.* (2002) included titanium in their most recent thermodynamic modeling, its concentration was fixed to chondritic values. All other studies have neglected this element. As high-titanium basalts are somewhat common on the lunar nearside (with some containing up to 13 wt% TiO_2), high abundances of titanium (most likely present as ilmenite or ulvöspinel) are at least locally required in the nearside mantle beneath the Apollo seismic network. The presence of titanium-rich phases could possibly affect either the thermodynamic mineral stability fields, and/or have an effect on the seismic velocity of the mineral assemblage. It remains to be demonstrated as to whether this effect is significant or negligible.

3.2.3. Origin of the 500 km seismic discontinuity. Several seismic velocity models of the lunar mantle are characterized by a substantial velocity increase near a depth of ~500 km (Nakamura *et al.* 1982; Nakamura 1983; Khan *et al.* 2000; Khan and Mosegaard 2002). According to the Nakamura (1982) model, P-wave velocities here increase from 7.46 ± 0.25 km/s to 8.26 ± 0.40 km/s, whereas S-wave velocities increases from 4.25 ± 0.10 km/s to 4.65 ± 0.16 km/s. The recent thermodynamic-seismic inversion of Khan *et al.* (2006), which is based on the first arrival dataset of Lognonné *et al.* (2003), finds similar velocity increases across an interface located approximately 600 km below the surface.

As reviewed by Hood and Zuber (2000), previous work indicates that the large velocity increases near 500 km depth most probably require a change in composition in addition to a possible mineralogical phase transition (Hood and Jones 1987; Mueller *et al.* 1988; Kuskov 1997). When the allowed ranges in mantle temperature and the stability fields of appropriate mineral assemblages are considered, the spinel to garnet phase transition may occur at depths between approximately 300 km (20 kbar) to 550 km (25 kbar) (e.g., Green and Ringwood 1967; Kuskov 1995, 1997), or at depths as shallow as ~200 km (Khan *et al.* 2006). Although a spinel to garnet phase transition is consistent with the depth of the observed seismic discontinuity, this phase transition alone would result in only a small velocity increase (≤ 0.1 km/s for S-waves) for plausible mantle compositions (e.g., Hood and Jones 1987). In contrast, the Nakamura (1982) velocity model estimates probable S-wave velocity increases of 0.4 km/s, and such a large velocity increase can not be explained solely in terms of this, or any other known, phase transition. A change in composition is required and possibilities include a more aluminous composition

below 500 km depth, a higher Mg number of the lower mantle, or both (e.g., Hood 1986; Hood and Jones 1987; Mueller et al. 1988; Kuskov and Kronrod 1998; Khan et al. 2006).

Four possible explanations for the implied change in composition at 500 km depth may be considered. First, it is possible that the lunar mantle was initially compositionally homogeneous, but that melting and differentiation of a magma ocean occurred only to a depth of ~500 km. This would effectively transfer most of the aluminum from the upper mantle to the crust while the lower portion of the mantle would remain compositionally pristine. However, for plausible maximum bulk aluminum abundances (which determine the allowed amount of garnet in the lower mantle), the implied change in composition at this depth is still insufficient to explain the observed velocity increases (e.g., Hood and Jones 1987; Mueller et al. 1988). Furthermore, as was noted by Wieczorek and Phillips (2000), the gravitationally unstable nature of the post-magma-ocean mantle may have given rise to a global redistribution of mantle materials (Herbert 1980; Spera 1992; Hess and Parmentier 1995), obscuring any such putative compositional interface.

A second interpretation of the 500-km discontinuity is that the lunar mantle may have initially been compositionally zoned with more aluminous and/or magnesium-rich phases being present in the lower portion of the mantle. If the formation and differentiation of a lunar magma ocean to a depth of 500 km were to occur for this initial structure, then such a model could in principle produce velocity increases that are compatible with the Nakamura (1982) seismic velocity model (Hood and Jones 1987; Mueller et al. 1988). A lower mantle unaffected by magma-ocean differentiation containing higher abundances of aluminous and Mg-rich mineral phases could possibly be a consequence of the giant-impact origin of the Moon (see review of Hood and Zuber 2000). In particular, this model predicts that the Moon formed from a hot circumterrestrial silicate vapor cloud (e.g., Canup and Esposito 1996; Cameron 1997; Canup 2004), and fractional condensation of such a vapor would favor the earliest condensates to have a more aluminous and Mg-rich composition (Mueller et al. 1988). If these early refractory condensates accreted to form a small proto-Moon, then their subsequent remelting would have been inhibited because of their higher mean melting temperatures. The later accretion of less refractory condensates might thus have melted only the outer portion of the Moon.

While the 500-km seismic discontinuity is often cited as possibly marking the base of the lunar magma ocean, it is becoming increasing clear from giant impact simulations that the Moon could have formed in a completely molten state (e.g., Pritchard and Stevenson 2000; Canup 2004). A third interpretation of this feature is that it is directly related to the crystallization products of a deeper, near-global magma ocean. Though the exact crystallization sequence of a magma ocean is dependent upon several factors (such as its assumed bulk composition and the relative importance of fractional and equilibrium crystallization), it is generally agreed upon that the first ~40% of crystallization is dominated by olivine, and that the subsequent ~40% is dominated by orthopyroxene (e.g., Snyder et al. 1992b; Hess 2000; Shearer and Floss 2000). The magnesium number of these cumulates should further progressively decrease with increasing crystallization. As the mantle below a depth of 500 km corresponds to about 35% by volume of the Moon, it is conceivable that the 500-km discontinuity could represent the boundary between early olivine-rich and later orthopyroxene-rich magma-ocean cumulates. This mineralogical stratification is generally consistent with the thermodynamic-seismic inversions of Kuskov and coworkers (e.g., Kuskov 1995, 1997; Kuskov and Kronrod 1998), and more recently Khan et al. (2006) (see Section 3.2.2). The results of Khan et al. (2006) further imply that the magnesium number increases from ~75 in the upper mantle to ~89 in the lower mantle, consistent with the sequential emplacement of cumulates at the base of the magma ocean. Nevertheless, a potential problem with this scenario is that the post-magma-ocean cumulate pile is expected to be gravitationally unstable as a result of its progressively increasing iron content with radius (Hess and Parmentier 1995). If a large scale overturn were

to occur, then the magma-ocean cumulates might possibly end up in an inverted sequence, with high magnesium-number, olivine-rich cumulates residing in the upper mantle, and with low magnesium-number, orthopyroxene-rich cumulates in the lower mantle.

A fourth interpretation of the 500-km discontinuity is that it represents the maximum depth of melting of the mare source region. Motivated by the recognition that the crust beneath Oceanus Procellarum and Mare Imbrium is a unique geochemical province with high abundances of KREEP (e.g., Haskin 1998; Jolliff *et al.* 2000a; Korotev 2000; Wieczorek and Phillips 2000), Wieczorek and Phillips (2000) constructed a thermal-evolution model of the Moon that contained a large quantity of heat-producing elements within the Procellarum KREEP Terrane. They found that melting within the mantle primarily occurred beneath this province, and that the depth of melting increased with time, ultimately achieving a maximum depth somewhere between ~200 and 600 km. Based on this observation, as well as the fact that none of the picritic glasses have depths of multiple saturation (commonly interpreted to be depths of melting) in excess of 540 km (e.g., Longhi 1992; Elkins *et al.* 2000; Elkins-Tanton *et al.* 2003), they interpreted the 500-km discontinuity as possibly representing the maximum depth of melting beneath this nearside province. Because of the extraction of aluminous basaltic melts from the mare source region above ~500 km depth, the mantle below this depth would be expected to be relatively enriched in aluminous phase by perhaps up to 1 wt% Al_2O_3 . If this interpretation is correct, then the 500-km discontinuity is not a global feature of the Moon, but is rather only locally present beneath the Procellarum KREEP Terrane. Since three of the four seismic stations are located within this geochemical province, it is presently not a simple task to delineate the lateral extent of this feature.

3.3. Summary

As samples of the lunar mantle have not been identified within the lunar sample collection, information concerning its composition and structure can only come from indirect sources, such as the analyses of the mare basalts and volcanic glasses, and the Apollo seismic data. The sample data show that the lunar mantle is heterogeneous in composition, with low- to high-Ti sources at similar depths being required to account for the wide range of basaltic compositions. The mantle is depleted in alkali, volatile, and siderophile elements, and further possesses an extremely low oxygen fugacity near or below the iron-wüstite buffer. Some picritic glasses show evidence for garnet being present in their source, and high pressure experiments demonstrate that the mare basaltic magmas and picritic glasses are multiply saturated, usually with olivine and orthopyroxene, at pressures corresponding to depths less than 560 km. While these depths are often quoted as corresponding to depths of melting, other interpretations are possible. Crater counting studies suggest that mare volcanism extended over a large portion of lunar history (from >4 Ga to ~1 Ga), but was most active between about 3.9 and 3 Ga.

Most investigations of the lunar seismic data agree that there is a major seismic discontinuity at a depth between 500 and 600 km. It also appears that the deepest mantle (below a depth of ~1000 km) might be partially molten. Investigations of thermodynamically stable mineral phases that are consistent with the Apollo seismic data indicate that the upper ~500 km of the mantle is predominantly composed of orthopyroxene, with smaller abundances of olivine, clinopyroxene, plagioclase and garnet. In contrast, the lower mantle is predominately composed of olivine, with lesser quantities of garnet and possibly clinopyroxene. Whereas garnet is predicted to exist with high abundances in the lower mantle, it is also likely to be stable in the upper mantle as well between depths of ~200 and 600 km. Thus, the garnet signature seen in some picritic glasses does not necessarily imply an origin beneath the ~500 km seismic discontinuity.

The magnitude of the ~500-km seismic discontinuity requires that a change in composition occurs at this depth, and several hypothesis have been put forth to explain this feature. One possibility is that this depth represents the base of melting of the lunar magma ocean. However,

in order to explain the magnitude of the seismic discontinuity, the bulk composition of the Moon below this depth must be more Mg- and/or Al-rich than above it. Alternatively, if the lunar magma ocean was global in extent, and its cumulates were laid down sequentially and not subsequently disturbed, then this depth could mark the transition between early olivine-rich cumulates and later orthopyroxene-rich cumulates that are predicted to crystallize from a lunar magma ocean. If this scenario is true, then a large-scale post-magma-ocean overturn of the lunar mantle probably did not occur. Finally, it is possible that this discontinuity represents the maximum depth of melting in the mare source region. This is supported by thermal modeling which takes into account the high abundances of heat sources in the Procellarum KREEP terrane, as well as the fact that all mare basalts and picritic glasses possess multiple saturation depths less than 560 km. If this interpretation is correct, then the ~500-km seismic discontinuity might only be a local feature beneath the nearside mantle.

4. THE CORE

All of the terrestrial planets and many of the icy satellites have undergone a major differentiation event that resulted in the formation of a metallic core. Seismic data demonstrate that the central portion of the Earth is composed of a large iron-rich core whose size is about 55% of its radius. Venus is inferred to have approximately the same internal structure based on its similarity in size and mass, whereas the high bulk density of Mercury is suggestive of an iron-rich core that is about ~75% of its radius. Moment of inertia and mass constraints for Mars (e.g., Sohl and Spohn 1997; Bertka and Fei 1998) and Jupiter's moon Io (Anderson et al. 1996b) suggest that these bodies have iron-rich cores that are about half of their radius. By similar means, Ganymede and Europa are each inferred to have an iron-rich core, though their absolute size is not well constrained (Anderson et al. 1996a; 1998). In addition to the terrestrial planets and icy satellites, some of the asteroids apparently differentiated early forming iron cores that are sampled by the iron meteorites.

Because of the above observations, it is natural to suspect that the Moon should also possess a sizeable metallic core. However, as we describe below, several lines of evidence imply that if the Moon does have a core, it must be small (<460 km radius). The existence, size and composition of such a core is of fundamental importance in deciphering many aspects of the origin and evolution of this body. For example, it is widely believed that the origin of the Moon is related to a collision between the Earth and a Mars-sized object that ejected debris and vapor into circumterrestrial orbit (see Cameron 2000 and references therein). While the debris that accreted to form the Moon is predicted to be derived primarily from the silicate mantle of the impactor, current models do not uniquely constrain the amount of iron that would be entrained in this material. Knowledge of the size of the lunar core could thus be used to constrain the many unknown parameters associated with these models (Canup and Asphaug 2001). Secondly, if the Moon does possess an iron-rich core, then it is possible that it could have at one time generated a magnetic field. A lunar dynamo might help explain the curious magnetizations that have been measured in some of the Apollo samples, and the crustal magnetic fields that have been mapped from orbit. Thirdly, knowledge of the physical state of the core (liquid vs. molten) would help constrain its composition and temperature, and hence the thermal evolution of the Moon. Finally, the formation of an iron core may have had a noticeable effect on the composition of the lunar mantle, and subsequently on the composition of the mare basalts that erupted at the surface.

While most studies to date that have attempted to constrain the size of the lunar core presume that it is composed of metallic iron, in this section, we address the possibility, as suggested by Wieczorek and Zuber (2002), that the Moon might instead possess a molten, dense, iron- and titanium-rich *silicate* "core." Two reasons argue for the plausibility of this hypothesis. First, ilmenite is predicted to crystallize near the terminal stages of magma-

ocean crystallization, and because of its relatively high density, sink through the lunar mantle. This could plausibly result in the formation of a small dense silicate core possessing high concentrations of titanium and iron (Hess and Parmentier 1995). A second reason is tied to buoyancy considerations of lunar basaltic magmas. Because of the high iron and titanium concentrations that are found in some of these basalts, Delano (1990) realized that some magmas might have been negatively buoyant with respect to the deep lunar mantle. Specifically, he showed that if a basaltic melt with a titanium concentration greater than about 16 wt% was produced deep within the Moon, this melt would probably sink (see also, Circone and Agee 1996; Agee 1998). The absence of basalts with titanium abundances greater than this cut-off value was used as evidence in favor of this hypothesis.

Below we review the relevant information that bears on the size, physical state, and composition of the lunar core. Constraints on the core size come from the moments of inertia of the Moon, lunar laser ranging data, magnetic induction studies, and the abundance of siderophile elements in the mare basalts. We also discuss whether the lunar paleomagnetic data require the existence of a core dynamo, and whether the physical state of the core can be used to constrain its composition and current temperature.

4.1. Mass and moments of inertia

The mass and moments of inertia of the Moon are bulk properties that any lunar density model must satisfy. Differences in the principal moments of inertia are uniquely related to the second-degree gravitational harmonics of the Moon (e.g., Lambeck 1988) which have been measured to high precision by orbiting spacecraft. The rotation of the Moon is affected by its moments of inertia, and analyses of ranges to the lunar laser retroreflectors determine the independent librational parameters, which depend upon ratios of the principal moments (Dickey *et al.* 1994; Konopliv *et al.* 1998). By combining these pieces of information, the entire moment of inertia tensor of the Moon is now known to good accuracy. For studies of the lunar interior, one is generally only interested in the mean moment of inertia, which can be calculated by the expression

$$I = \frac{2}{3} \int_V \rho(r, \theta, \phi) r^2 dV \quad (3.6)$$

where r is radius, ρ is the position dependent density, and dV is the differential volume element.

While the moments of inertia do not uniquely determine the density structure of a body, they do give qualitative information as to whether or not the density increases with depth. For a homogeneous sphere, the moment of inertia normalized by MR^2 (where M and R are its mass and radius, respectively) is equal to 0.4. In contrast, the Earth, which has an iron core that is about half of its radius, has a normalized moment of inertia of about 0.33. Most recently, Konopliv *et al.* (1998) obtained a value of $I/MR^2 = 0.3931 \pm 0.0002$ for the Moon. This value was computed using a reference radius of 1738 km, and if the mean planetary radius were used instead, the normalized moment of inertia would be increased by 0.0004 (see Table 3.13).

As the mean moment of inertia of the Moon is seen to be very close to the value of a uniform density sphere, if the Moon possesses an iron core, it must be small. For instance, if one assumes that the density of the crust, mantle and core are uniform, then the lunar mass and moment of inertia can both be satisfied by either an ~330-km radius solid iron core ($\rho \sim 8.1$ g cm $^{-3}$) or an ~460-km radius liquid eutectic Fe-FeS core ($\rho \sim 5.2$ g cm $^{-3}$). In contrast, if the “core” were instead composed of a dense silicate material having a density less than 5.2 g cm $^{-3}$, then its radius would be larger. If the density of the lunar mantle increases with depth, as is suggested by the existence of the 500-km seismic discontinuity, then the above estimated core sizes should be viewed as upper limits. Indeed, plausible compositional models of the

Table 3.13. Properties of the Moon and its orbit.

Parameter	Value	Note
Semi-major axis (km)	384399	(1)
Orbit eccentricity	0.0549	(2)
Obliquity to orbit plane	6.688°	(1)
Orbit inclination	5.145°	(1)
Inclination of equator to ecliptic	1.543°	(1)
Orbital period (days)	27.321582	(2)
Mean planetary radius (km)	1737.103 ± 0.015	(3)
Polar flattening (km)	2.17 ± 0.11	(3)
Center-of-mass/center-of-figure offset (km)	1.90 ± 0.01 (8.1°N, 156.6°W)	(3)
GM_{Moon} ($10^9 \text{ m}^3 \text{ s}^{-2}$)	4902.801076 ± 0.000081	(4) (5)
Gravitational constant (G) ($10^{-11} \text{ kg m}^3 \text{ s}^{-2}$)	6.67259 ± 0.00030	(6)
Mass (10^{21} kg)	73.4767 ± 0.0033	
Mean density (kg m^{-3})	3346.45 ± 0.17	(7)
Normalized polar moment of inertia ($\text{C M}^{-1} \text{ R}^{-2}$)	0.3932 ± 0.0002	(8) (9)
	0.3936 ± 0.0002	(8) (10)
Normalized mean moment of inertia ($\text{I M}^{-1} \text{ R}^{-2}$)	0.3931 ± 0.0002	(8) (9)
	0.3935 ± 0.0002	(8) (10)
k_2	0.026 ± 0.003	(4)
	0.025 ± 0.003	(11)

Notes: (1) Williams et al. 2001b; (2) Yoder 1995a; (3) Smith et al. 1997; (4) Konopliv et al. 2001; (5) model LP150Q; (6) Bursa 1992; (7) assuming a sphere of mean planetary radius; (8) Konopliv et al. 1998; (9) $R = 1738 \text{ km}$; (10) $R = \text{mean planetary radius}$; (11) Williams et al. 2001a

lunar interior can be constructed that do not require the existence of an iron-rich core (e.g., Hood 1986). As one simple example, the measured moment of inertia and mass could be satisfied by a mantle that was linearly zoned in composition, with the top of the mantle and center of the Moon being composed of Fo_{95} and Fo_{61} , respectively.

The measured moment of inertia of the Moon by itself does not place any firm constraints on the existence or non-existence of a lunar core. However, as will be seen below, this parameter does offer important constraints on the interior composition when used in conjunction with the Apollo seismic data (Hood and Jones 1987; Mueller et al. 1988; Kuskov and Kronrod 1998, 2001; Khan and Mosegaard 2001) and k_2 Love number (Khan et al. 2006).

4.2. Seismology

The materials that might be expected to comprise a lunar core are characterized by relatively low P-wave seismic velocities (~5.5 km/s for solid iron, ~4 km/s for liquid iron, ~3 km/s for an Fe-FeS eutectic liquid, and ~2.5 km/s for a silicate magma). An ideal approach toward determining the size and composition of a putative lunar core would thus be to determine the seismic velocity structure of the deep interior. Some evidence for a 170 to 360 km radius low-velocity (3.7 to 5.1 km/s) core was tentatively suggested by Nakamura et al. (1974) on the basis of a single P-wave arrival from a farside meteoroid impact, but this observation is not definitive (e.g., Sellers 1992). Sellers (1992) further tentatively identified PKP arrivals from two additional farside impact events, and if these arrivals are ultimately deemed to be reliable, they are consistent with a 400 to 450 km radius core possessing a P-wave velocity of ~5 km/s (the sensitivity of the radius to the core velocity was not addressed). While these farside meteorite impacts may ultimately shed light on the existence and size of a putative lunar core, we consider these studies to be more provocative than definitive at the present time.

One indirect approach for investigating the size of a dense metallic core is to construct compositional models of the lunar crust and mantle that are consistent with the Apollo seismic velocity models. The mass of material below the limits of the seismic velocity profile can then be inferred from a knowledge of the known lunar mass, and the core size can be constrained by use of the known moment of inertia (Hood and Jones 1987; Mueller *et al.* 1988; Kuskov and Kronrod 1998, 2001; Kuskov *et al.* 2002). Because of the uncertainties in the velocity models, the mantle density profiles are only weakly constrained by the seismic data. Furthermore, these density profiles depend upon the assumed thermal structure of the mantle, which is also uncertain. Nevertheless, because of the relatively small density changes that are expected to occur in the mantle for plausible bulk compositions and temperature profiles, application of this approach has consistently indicated the likely existence of a small dense core. Hood and Jones (1987) found that a core radius of 200–450 km was implied for an iron composition, representing about 1–4% of the lunar mass. Mueller *et al.* (1988) similarly concluded that a metallic core at least 150 km in radius was necessary to reconcile the mass and moment of inertia constraints with the Nakamura (1982) seismic model. Kuskov and Kronrod (2001) have estimated the radius of the core to be 310–320 km for a pure iron composition and 430–440 km for a eutectic Fe-FeS composition, and the more recent analysis of Kuskov *et al.* (2002) gives a range between 330 and 530 km. We note that all of the above core sizes would be larger if the core was instead assumed to be composed of a less dense titanium- and iron-rich silicate composition.

4.3. Induced dipole moment

An alternate approach toward investigating the deep lunar interior consists of estimating limits on the electrical conductivity as a function of depth using surface and/or orbital magnetometer data (see the reviews of Sonnett 1982, Hood 1986, and Hood and Zuber 2000). This approach can, in principle, yield limits on the size of a high electrical-conductivity core. However, the composition of the core (e.g., molten silicate, metallic iron, metallic Fe-FeS) is not easily constrained by electromagnetic sounding data alone.

Limits on the mantle electrical conductivity profile were obtained using time-dependent measurements from a high-altitude orbiting magnetometer to monitor the input field and a surface magnetometer to monitor the sum of the input and induced fields. Application of this technique yielded bounds on the mantle conductivity profile and an upper bound of ~435 km on the radius of a high electrical-conductivity core (Sonnett *et al.* 1972; Dyal *et al.* 1976; Hood *et al.* 1982; Hobbs *et al.* 1983). The mantle conductivity was found to continuously increase from 10^{-4} – 10^{-3} S/m at a depth of 300 km to 10^{-3} – 10^{-2} S/m at a depth of 700 km to 10^{-2} – 10^{-1} S/m at 1000-km depth (e.g., Hood 1986). For this experiment, the electrical conductivity of a molten silicate core (~10 S/m) cannot be distinguished from that of a metallic iron core (~ 10^5 S/m) using Apollo data records with typical lengths under 100 hours (Hood *et al.* 1982). One difficulty with this time-dependent sounding technique is that two separate magnetometer data records are used and a very accurate intercalibration is required if the weak core signal is to be detected (Daily and Dyal 1979). Because the Explorer 35 orbital magnetometer and the Apollo 12 surface magnetometer that were employed were not perfectly intercalibrated, this error source essentially precluded an accurate determination of the core size via this technique.

A method for sounding the deep lunar interior that requires only data from a single magnetometer involves the measurement of the induced magnetic dipole moment of the Moon as it passes through the geomagnetic tail of the Earth (Goldstein *et al.* 1976). This method, while not capable of determining electrical conductivity bounds as a function of depth, has the advantage of being free of intercalibration errors and therefore allows more sensitive measurements of the weak induced fields expected from a small core. The method exploits the quasi-vacuum (i.e., nearly plasma-free) environment experienced by the Moon during its monthly traversals of the geomagnetic tail lobes. During these periods, the Moon is occasionally exposed to a nearly spatially uniform magnetic field for durations ranging from hours to

several days. This steady magnetic field slowly diffuses into the Moon, with the rate of diffusion being controlled by the material's electric conductivity. That portion of the lunar interior that is unaffected by the external field will give rise to an induced magnetic dipole moment oriented opposite to the applied field. Initially, the induced moment originates from electrical currents set up in the lunar mantle. However, after a decay period of ~ 5 hours or less, the external field diffuses through the mantle and induces currents on the surface of a high electrical-conductivity core, if one is present. At this point, the amplitude and time-dependence of the dipole moment is directly relatable to the core radius and its conductivity. If the core is a good conductor ($>10^2$ S/m), then the induced dipole moment should not significantly change during the few days time that the Moon spends in the geomagnetic tail lobe. However, if the core conductivity were representative of a silicate magma (~ 10 S/m) then the time-variability of the induced magnetic moment could be significant.

The first measurements of the lunar induced magnetic dipole moment in the geomagnetic tail were obtained using data from the Apollo 15 and 16 subsatellite magnetometers (Russell et al. 1981). After eliminating intervals when significant tail lobe plasma densities were present, the final estimated induced moment amplitude was $(-4.23 \pm 0.64) \times 10^{23}$ A m² T⁻¹. Assuming that mantle contributions to the induced moment were negligible, the corresponding radius of a high electrical-conductivity core is 439 ± 22 km. Additional measurements of the induced moment were reported by Hood et al. (1999) using data from the Lunar Prospector magnetometer. The selected data were obtained when the Lunar Prospector orbit plane was in an optimal orientation for induced moment measurements. Editing and averaging of individual orbit segments over a duration of about a day and a half yielded an estimate for the induced moment of $(-2.4 \pm 1.6) \times 10^{23}$ A m² T⁻¹. Assuming that mantle currents were negligible, the core radius was found to lie between 250 and 430 km for an electrical-conductivity typical of metallic iron. Alternatively, if the electrical-conductivity of the core were typical of a basaltic melt, then we find here that a core radius between 361 and 538 km would satisfy the average induced dipole moment.

Although the error estimates of the induced dipole moment of Hood et al. (1999) and Russell et al. (1981) overlap, the difference in the mean core radius estimates of nearly 100 km is an indicator of the difficulty of performing this measurement using a single magnetometer. Nevertheless, the fact that both sets of measurements yielded evidence for a small conducting core increases the likelihood that such a core actually exists in the Moon. In fact, a slightly larger core radius estimate would result if the positive paramagnetic and ferromagnetic induced moments of the crust and mantle were taken into account in the above calculations (Rochette 2000). However, this effect is small given the large measurement uncertainties associated with the induced dipole moment (Hood 2000).

4.4. Lunar laser ranging

The analysis of lunar laser ranges from stations on the Earth to corner-cube retroreflectors on the Moon can be used to determine the time-varying rotation of the Moon. The robustness of the measured lunar rotation depends upon the geometrical spread of the retroreflectors that were emplaced at the Apollo 11, 14, and 15 sites, and the Russian Lunakhod 2 site. At present, the accuracy of ranges to these retroreflectors is less than 2 cm. A review of the lunar laser ranging program up to 1994 is given by Dickey et al. (1994).

The rotation of the Moon can be characterized by two angles that describe the orientation of its polar principal axis, and a third angle that describes the rotation about this axis. Currently, the polar axis is inclined 6.69° to the orbit normal (the obliquity), the orbit plane is inclined 5.14° to the ecliptic plane, and the polar axis is tilted 1.54° from the normal to the ecliptic plane. However, in the past when the Moon was much closer to the Earth (~ 34 Earth radii away at ~ 4 Ga) the lunar obliquity could have been as high as 77° (Ward 1975).

Both the polar axis and the orbit normal precess with the same 18.6-year period about the normal to the ecliptic plane, but they are out of phase by nearly 180° . This rotational configuration, known as a Cassini state, describes the first-order rotational state of the Moon. Superposed on this configuration are small rotational oscillations about the polar axis, as well as small oscillations in the pole direction, that can be detected from an analysis of the lunar laser ranging (LLR) data. These deviations, referred to as physical librations, are mainly due to the differences between the principal moments of inertia and the low-degree static gravity field of the Moon. As described below, these and other rotational signatures can be used to infer the elastic properties of the Moon and the presence of a fluid core. In particular, a slight misalignment of the spin axis and orbit normal from the Cassini state has been observed, and this can be modeled as a result of energy dissipation within both the solid body of the Moon and along a liquid-core/solid-mantle interface.

4.4.1. Tides and the solid mantle. Solid-body tides are raised on the Moon by the gravitational attraction of the Earth, and the response of the Moon to these tides provides an opportunity to sample the elastic properties of its interior. The familiar response to the second-degree Earth tide is football shaped, with the elongated axis lying nearly along the Earth-Moon line. Higher-degree tides are also raised by the Earth, but the strength of these decrease by about two orders-of-magnitude for each increase in degree. For a spherically symmetrical body, the tidal response at each degree is proportional to three degree-dependent Love numbers. Here we concern ourselves only with the degree-2 terms. One Love number describes the change in the gravitational field of the Moon as a response to the Earth's tidal potential (k_2), another describes the vertical change in elevation of the surface (h_2), and the third describes the horizontal displacement of the surface (l_2). The Love numbers and their associated Q s (where Q^{-1} is a measure of the amount of dissipation that is incurred during a loading cycle) are bulk properties of the Moon that depend upon the interior structure and are therefore useful as constraints on models of the lunar interior. In particular, the degree-2 Love numbers depend most strongly upon the radial profile of the shear modulus, μ , or equivalently the S-wave velocity via the relationship $v_s = (\mu/\rho)^{1/2}$. In comparison to the shear modulus, the bulk modulus and P-wave velocity have relatively minor effects on the degree-2 love numbers. The presence of a dense liquid or solid core would change the k_2 Love number by a few percent.

The surface displacements of time-varying tides on the Moon are only about 0.1 m in height and about half of that horizontally. The time variations of these tides, which may be represented by a sum of periodic components, arise from variations in the distance and direction of the Earth as seen from the Moon. The two largest components have periods of 27.555 days (the anomalistic period, which is the time it takes for the Moon to go from perigee to perigee) and 27.212 days (the period with respect to the ascending node). Some additional tidal components have periods of 1/3 month, 1/2 month, 7 months, and 1 year. The precession periods for the lunar orbit are 6 years for the argument of perigee, 9 years for the longitude of perigee, and 18.6 years for the longitude of ascending node. In addition, the rotation of the Moon has motions such as the 75-year wobble of the pole direction. Because of these long dynamical time scales, the accurate interpretation of the rotation and orbit of the Moon via laser ranges requires the analysis of many years of data.

Time variations in the tidal field give rise to torques on the Moon, affect its moments of inertia, and influence its rotation. Tidal distortion of the second-degree gravity potential and moment of inertia tensor is proportional to the Love number k_2 . As the phase of the tidal response depends on Q^{-1} , tidal dissipation is proportional to k_2/Q (e.g., Segatz *et al.* 1988). However, when analyzing the rotation data, the mantle and core contributions to these numbers are not immediately isolated from one another. The oblateness of the core-mantle boundary influences the determination of the Love number k_2 and dissipation at this interface must be taken into account when the solid-body tidal Q is estimated. Fortunately, these core

and mantle effects can be separated as their influence on different periodic rotation terms is different. (The effects of core dissipation will be discussed separately in the following section.) A recent analysis of the LLR data yields a value of $k_2 = 0.025 \pm 0.003$ (Williams et al. 2001a), where most of the uncertainty in this value is a result of the uncertainty associated with the core flattening. (If the core flattening were set to zero, then LLR determination of k_2 would be larger by 14%.) LLR analyses also detect the tidal displacement Love numbers h_2 and l_2 , though k_2 is the most accurately determined among these quantities. If the displacement Love numbers could be improved sufficiently, then they would provide two additional constraints on the interior properties of the Moon. Time variations of the gravity field are measurable with accurate tracking of lunar orbiting spacecraft, and analysis of these data yield a concordant estimate of the Love number $k_2 = 0.026 \pm 0.003$ (Konopliv et al. 2001). Unfortunately, the uncertainty in these numbers is close to that which is required to distinguish between different models of the deep lunar interior. In particular, the uncertainty of k_2 is $\sim 10\%$, whereas the presence of an iron core would only affect this number by $\sim 5\%$.

The Apollo seismic experiment placed good constraints on the elastic properties of the upper layers of the Moon, but gave less definitive constraints for the lower mantle and possible core. When Love numbers are computed from these S-wave seismic profiles (Dickey et al. 1994), they are found to be similar (within about 20%), but not equal to the above values. Thus, the k_2 Love number offers the possibility of better constraining the S-wave velocity (and corresponding shear modulus) of the deep lunar interior where the seismically obtained values are less well determined (see Khan et al. 2006).

Imperfect elastic properties result in dissipation of energy whenever the Moon is flexed. Just as the k_2 Love number depends upon the radial profiles of elastic properties, the parameter k_2/Q for the whole Moon depends on the radial distribution of dissipation. In principle, the k_2/Q value may also depend on tidal frequency. Dissipative effects in the Moon cause a slight phase shift in the precessing polar axis with respect to the orbit normal axis from which the tidal Q can be determined (Yoder 1981; Williams et al. 2001b). In particular, a small advance in the polar axis of 0.26" from the Cassini configuration has been measured (e.g., Dickey et al. 1994; Williams et al. 2001b). The tidal solid-body Qs obtained from this number are extremely low and imply that a large amount of tidal dissipation is presently occurring within the Moon. For instance, the tidal Q for one month is found to be 37 whereas the annual Q is 60. While the bulk tidal Q of the Earth is smaller at ~ 12 (e.g., Burns 1986), this is primarily a result of dissipation within its oceans. Mars has been inferred to have a somewhat larger (though still relatively small) tidal Q between 50 and 150 from the acceleration of its satellite Phobos (e.g., Burns 1986). In contrast to the low whole-moon tidal Q , at seismic frequencies the Moon has a local Q of about 3000 to 3600 for the upper crust (Latham et al. 1970a,b), 4000 to more than 7000 for the upper mantle (Dainty et al. 1976; Nakamura et al. 1976; Nakamura and Koyama 1982), and 1400 to 1500 for the deep moonquake source region (Dainty et al. 1976; Nakamura et al. 1976). The Q has been inferred to decrease dramatically below the deep moonquake source region and this has been interpreted as possibly indicating the presence of a partial melt below this depth (Nakamura et al. 1973). Thus, given the high seismic Qs above a depth of ~ 1150 km, it appears likely that most of the solid body dissipation in the Moon occurs below this depth. In fact, if the tidal and seismic Qs are considered to be equivalent, then the average Q below ~ 1150 km depth is required to be less than 4 (Yoder 1981).

4.4.2. The core. While the presence of any significantly sized dense core will increase the Love numbers by a few percent, there are influences on the rotation of the Moon that are unique to the presence of a molten core. In particular, two torques arise from interactions at a solid-mantle/liquid-core boundary, and detection of the corresponding perturbations on the rotation would provide evidence for a fluid core. Because a fluid core will rotate independently from the solid mantle, a peak velocity difference of about 2 cm/s at the interface between the two should

exist. This velocity difference results in a local force, causes energy dissipation, and leads to a net torque over the whole surface of the core-mantle boundary. If this boundary is oblate, there will be a second force due to flow along this aspherical boundary. These two torques have different directions and their influences on the rotation are in principle distinguishable.

Analysis of the lunar laser ranging data has detected dissipation-caused phase shifts at four different rotation frequencies (Williams *et al.* 2001b). Solid-body tidal dissipation acting alone provides a poor match to these results, whereas dissipation due to both tides and an independently rotating core are able to satisfy these results. This analysis of the LLR data implies that about 34% of the dissipation-caused phase shift from the Cassini state is due to a liquid core. To obtain the core size from the strength of the core dissipation requires a model of the dissipation at the core-mantle boundary, and for this Yoder's (1981; 1995b) turbulent boundary layer theory has been used. In this model, the core size is primarily dependent upon its density, and only secondarily on its viscosity. The effect of viscosity on the core size would be more important if dissipation was a result of laminar flow, but laminar flow is only to be expected if the viscosity is in excess of ~ 10 Pa s (Yoder 1981). For the pressures and temperatures expected at the center of the Moon, the viscosity of a molten Fe-FeS metallic core is on the order of 10^{-2} Pa s (Dobson *et al.* 2000; Vocadlo *et al.* 2000), whereas the viscosity of a basaltic silicate magma would be slightly larger at $\sim 10^{-1}$ Pa s.

Assuming a kinematic viscosity of 10^{-6} m 2 s $^{-1}$ (7×10^{-3} Pa s for a density of 7 g cm $^{-3}$), the LLR analysis constrains the radius of a molten iron core to lie between 314 and 352 km. For a molten Fe-FeS eutectic composition ($\rho \sim 5.2$ g cm $^{-3}$) the core radius is constrained to lie between 334 and 375 km. Alternatively, if the core is composed of a dense iron- and titanium-rich silicate magma ($\rho \sim 3.5$ g cm $^{-3}$), then we find here that the core would be slightly larger, having a radius that lies between 363 and 407 km. These computed core radii are only slightly dependent upon the assumed core viscosity, where an order of magnitude increase in viscosity would only result in a decrease in core size by about 20 km. If the Moon possesses a solid inner and outer liquid core, then these core radii estimates would be overestimates as there would be two surfaces at which dissipation could occur.

Oblateness of the liquid-core/solid-mantle interface also influences the rotation of the Moon, and at present, the detection of the core flattening effect is about twice its uncertainty. This measurement provides an independent line of evidence for the fluid state of the core, and as the k_2 Love number is anticorrelated with the core flattening, its detection gives rise to a slightly smaller value of k_2 (see Williams *et al.* 2005). When used in combination with the core moment of inertia, this parameter can allow a computation of the resonant period of the free core nutation. If there is a solid inner core in addition to a fluid outer core, then this might also influence the rotation of the Moon. An aspherical inner core would experience gravitational torques from both the Earth and the lunar mantle, but the associated rotational signatures have not yet been tested against the available data.

Much of the rotation-derived lunar science information comes through forced terms, but there are also free rotational modes. The three solid-body free libration modes have been detected and their amplitudes and phases have been determined (Newhall and Williams 1997). Dissipation from flexing and fluid core interactions should cause lunar free librations to damp with geologically short time scales, so the finite amplitudes imply recent or active stimulation. Of particular interest to understanding the interior is the 75-year polar wobble, analogous to the Earth's Chandler wobble. It has been suggested by Yoder (1981) that this mode may be stimulated by eddies at the solid-mantle/liquid-core boundary. Both damping and active excitation may be observable in the future, and active excitation should cause temporal irregularities in this mode. There are also free rotational modes for a fluid core, and any core-mantle boundary flattening would give rise to a resonant free core nutation frequency.

Finally, we note that dissipation due to both tides and the core-mantle interaction deposits heat in the Moon. At present these are minor heat sources, but both could have significantly heated the Moon when it was closer to the Earth (Peale and Cassen 1978; Williams et al. 2001b). The amount of heating depends on the rate of expansion of the early lunar orbit due to the tidal dissipation that occurs in the Earth and its oceans. This early expansion rate is uncertain, and for a slow evolution, the early dynamical heating could have been comparable to the internal radiogenic heating. Furthermore, this energy might have been able to promote convection, and if the core was metallic, a dynamo. However, a faster orbital evolution would have less dramatic consequences. In addition to tidal heating, a large amount of heat would have been generated within a fluid core (if present) during a spin axis transition between two distinct Cassini states when the semi-major axis of the Moon passed through ~ 34 Earth radii (Ward 1975). At that time, the obliquity of the Moon is predicted to have switched from $\sim 26^\circ$ to a maximum of 77° , and then back down to $\sim 49^\circ$ on the order of $\sim 10^5$ years.

4.5. Lunar free oscillations

When a planet is abruptly perturbed, it oscillates with a distinct set of frequencies. As the amplitudes of these free oscillations depend upon various rheologic properties of the planet, they can be used to constrain its deep interior structure. An advantage of applying this method to a planetary body is that it is applicable even if seismic recordings from only one station are available. Since the state of the core affects the fundamental modes of free oscillations, identifying these are relevant to addressing the existence and physical state of the lunar core. Since the spheroidal free oscillations involve movement of the whole body, they are particularly sensitive to the density structure of the planetary body.

In a recent study, Khan and Mosegaard (2001) claimed to have identified excitations of lunar free oscillations associated with five large meteoroid impacts occurring in 1976 while the long-period instrumental response was extended to low frequencies. Only spheroidal modes were considered because of non-seismic interference in the horizontal component of the seismometers. Although a signal to noise ratio of ~ 1.9 was stated for the stacked normal mode amplitude spectra following these impacts, this has remained somewhat contentious. Gudkova and Zharkov (2002) have shown that the expected amplitudes from such events should be about two orders of magnitude below the detection limit of current broad-band seismometers. Furthermore, based on a synthetic seismogram of an impact with approximately the same energy as those used in the Khan and Mosegaard study, Gagnepain-Beyneix et al. (2006) have shown that the signal to noise ratio should be less than 0.01 over the frequency band that was investigated. They further noted that the stacking of individual amplitude spectra does not noticeably increase the signal to noise ratio as a result of the loss of phase information that is inherent in such a procedure.

While the detection of fundamental spheroidal lunar normal modes is unlikely to be realized with the current Apollo seismic data set, these should in principle be detectable following large shallow moonquake events using superconducting gravimeters (Lognonné 2005). Low-order torsional modes are also in principle detectable using modern broad-band seismometers (Gudkova and Zharkov 2002).

4.6. Thermal constraints on the physical state of the core

If one knew the composition of the lunar core, estimates of its temperature over time would place constraints on its current and past physical state. Thermal evolution models of the Moon, however, are highly variable, and this limits the uniqueness of this approach. Based on a variety of published thermal evolution models, the temperature at the center of the Moon at ~ 4 Ga may have been between about 1280 and 1750°C, and at present is predicted to be between about 1000 to 1480°C (see Chapter 4). Despite these large uncertainties, a few generalizations can be made.

For the pressures that would be encountered in a lunar core (~ 4 GPa), the melting temperature of pure iron is $\sim 1690^\circ\text{C}$ (e.g., Presnall 1995). If the core were composed of pure iron, then it could possibly have been in a molten state early in the geologic history of the Moon. However, current estimates of the internal temperature of the Moon all predict that such a core would have subsequently completely frozen. It is generally believed that the crystallization of the Earth's core is a contributing factor towards generating a dynamo (e.g., Roberts and Glatzmaier 2000). Therefore the gradual crystallization of a lunar iron core may similarly have powered a dynamo, possibly explaining the curious paleomagnetic signatures of the lunar rocks and magnetic anomalies as observed from orbiting magnetometers (see Section 4.7). However, as a presently solid core is incompatible with the LLR data, the hypothesis of a pure iron lunar core can probably be dismissed.

The addition of either carbon or sulfur to iron will act to lower its melting temperature. The Fe-C system exhibits eutectic melting behavior, possessing a eutectic composition of about 3.5 wt% carbon, and a eutectic melting temperature of $\sim 1175^\circ\text{C}$ (Hirayama and Fujii 1993). If only a small quantity of carbon was sequestered in the lunar core, then it is likely that some portion of it would have remained molten for most to all of lunar history. If the current temperature of the core were at or above the Fe-C eutectic temperature, then the Moon would currently possess both a solid iron inner core and a liquid Fe-C outer core. The Fe-FeS system similarly exhibits eutectic melting. In this system the eutectic composition at lunar core pressures is about 25 wt% sulfur, and the eutectic melting temperature is about 950°C (Fei *et al.* 1997). Thus, if a small amount of sulfur were present in the core, some portion of it would almost certainly be molten at the present time. If the core of the Moon is predominantly composed of metallic iron, then these temperature considerations highly suggest that it currently possesses both a solid inner and liquid outer core.

As an alternative to metallic compositions, it is also possible that the “core” of the Moon might be composed of dense iron- and titanium-rich silicate materials. The composition of such a material is not well constrained, and hence its liquidus and solidus temperature are also uncertain. A plausible composition might be similar to that of the Apollo 14 high-titanium black glass, as a magma of this composition is predicted to be more dense than the deep lunar mantle (Delano 1990; Circone and Agee 1996; Agee 1998). At core pressures, this composition has a liquidus temperature of $\sim 1570^\circ\text{C}$ (Wagner and Grove 1997). Though the solidus temperature is unknown, it seems likely that some portion of this material could remain in a molten state at the present time.

4.7. Paleomagnetism of the lunar samples

It has been known for some time from Apollo surface magnetometers and subsatellite data that the lunar crust possesses an intrinsic remnant magnetization. The central question of lunar magnetism is to determine the intensity, duration and, ultimately, the origin of the fields that magnetized the crustal rocks of the Moon. The answer to these questions would dramatically affect our understanding of the lunar interior and the physical environment of the early solar system. Unfortunately, while there have been a number of reviews of the subject (e.g., Collinson 1985, 1993; Fuller and Cisowski 1987; Hood 1995), little new paleomagnetic data on lunar samples has been published since the early 1980s (e.g., Collinson 1984; Chowdhary *et al.* 1987). Major advances have instead come in our understanding of the reliability and applicability of the various kinds of paleointensity experiments as well as in the growth and understanding of the terrestrial paleointensity database. The overall quality of the terrestrial data far exceed that of the Moon, and the analysis of these data have accompanied advances in our understanding of the dynamics of dynamo generation. In light of these advances, it is useful to reexamine the nature and quality of the lunar paleointensity experiments of two decades ago.

4.7.1. Paleointensity experiments on lunar samples. Paleomagnetic conglomerate tests on single Apollo breccias (Banerjee and Swits 1974) demonstrate that the remnant

magnetization of the lunar samples is of lunar origin and is billions of years old. However, as no outcrops of lunar bedrock were unambiguously sampled during the Apollo missions, the geometry of the paleomagnetic field of the Moon cannot be determined from the Apollo samples alone. As a result, nearly all work has focused on paleointensity measurements of the ancient field that magnetized the lunar rocks. Unfortunately, since the bulk of these experiments were completed in the late 1970s, it has become clear that most of these methods give results that could be inaccurate. (For critiques of the various paleointensity methods see Levi and Banerjee (1976), Bailey and Dunlop (1977), Collinson and Stephenson (1977), Sugiura (1979), Sugiura and Strangway (1980), Kono (1987), Tauxe (1993), Dunlop and Ozdemir (1997), Goguitchaichvili et al. (1999), and Herrero-Bervera and Valet (2000).)

Today, the Thellier-Thellier double-heating method (Coe et al. 1978) sets the standard for paleointensity studies because it progressively thermally demagnetizes the sample. In doing so, it provides an internal check that the magnetization is a primary thermoremanence, produces multiple independent field measurements for each sample, and can often yield accurate results even when the sample is altered during heating. A major improvement in the Thellier-Thellier experiment during the last twenty years has been the widespread incorporation of partial thermoremanent magnetism (pTRM) checks that can diagnose alteration of the ferromagnetic minerals during the experiment (e.g., oxidation of iron, change in grain sizes of magnetic minerals, and quenched phase transitions in kamacite). Since such alteration can lead to dramatically inaccurate paleointensities, the incorporation of pTRM checks leads to a significant improvement in the success rate of the Thellier-Thellier method. Although nearly all Thellier-Thellier experiments on terrestrial rocks today employ pTRM checks, these have never been used in any published lunar experiment.

Selkin and Tauxe (2000) have developed six criteria for judging the quality of Thellier-Thellier paleointensity experiments. Unfortunately, none of the paleointensity experiments ever performed on lunar rocks pass all six of these. In fact, even the most successful lunar experiments pass no more than three or four. Note, however, that these criteria are highly restrictive and were meant to select for data capable of demonstrating field intensity changes of a few tens of percent, whereas even an order-of-magnitude accuracy would be valuable for lunar studies. The reasons that the lunar paleointensity experiments do not pass these criteria are severalfold. To begin with, many samples were found to hold weak and/or unstable natural remanent magnetization. Secondly, fewer than twenty lunar experiments were investigated with the Thellier-Thellier method, and none of these used pTRM checks. Thirdly, magnetostatic interactions between ferromagnetic grains in the samples often resulted in wild swings in pTRM intensities at several different temperatures. Fourthly, heating-induced changes in the mineralogy destroyed the primary minerals carrying the remanent magnetizations. Finally, the scarcity of lunar materials has drastically limited access to samples and made it difficult to make repeated measurements on the same individual samples.

4.7.2. Evidence for time-varying paleointensities. The most significant development in lunar paleointensity experiments in the last twenty years was the saturation isothermal remanent magnetism (IRMs) normalization studies of Cisowski and coworkers (Cisowski et al. 1983; Cisowski and Fuller 1986; Fuller and Cisowski 1987). The basis of this method is to determine the ratio of the NRM to laboratory induced IRMs for each sample, which is intended to quickly measure the relative intensity of the paleofield by normalizing the sample's moment by the mass and mineralogy of its ferromagnetic material. Although these studies employed an empirically-derived calibration factor for the ratio between the IRMs and the absolute paleointensity, it has since been suggested that this factor may not be constant, but instead may be sample dependent because of its intrinsic dependence on crystal size (Fuller and Cisowski 1987; Tauxe 1993). On the other hand, recent work by several groups suggests that perhaps the factor relating paleointensity to the NMR/IRMs ratio may be constant after all (Kletetschka et al. 2003, 2004; Gattacceca and Rochette 2004).

The most reliable absolute and IRMs normalization paleointensity measurements are shown in Figure 3.22 as a function of age. Even with this select dataset there are a number of problems. (1) At any given age, the inferred paleofield often has a range of intensities. (2) The ages in this figure are either upper limits or are highly uncertain. This is because detailed $^{40}\text{Ar}/^{39}\text{Ar}$ thermochronology was not performed on any of the samples, and worse, some of the ages are based on the U/Pb isotopic system that is usually reset at much higher temperatures than the magnetization. Although metamorphic Ar-Ar ages were used for some samples (e.g., for breccias that were heated during lithification), there was little attempt to put thermal constraints on the samples using the Ar release pattern during stepped heating experiments. (3) In the absence of an external magnetic field, impact shock effects will tend to demagnetize a sample over time (Cisowski and Fuller 1978), which implies that paleointensity values from shocked samples are underestimates. And finally, (4) the temporal sampling of lunar paleointensities is very nonuniform with a substantial data gap occurring between 3.0 and 1.5 Ga, and few existing measurements from before 3.9 Ga.

While considerable care must be exercised when interpreting the lunar paleointensity data, the data in Figure 3.22 have been interpreted by some as evidence for a weak magnetic field prior to ~ 4 Ga, a rapid increase in intensity between 4.1–3.9 Ga to a value of $\sim 100 \mu\text{T}$ (or 1 Gauss in cgs units), followed by a return after 3.6 Ga to a value of $\sim 10 \mu\text{T}$ (e.g., Cisowski *et al.* 1983; Runcorn 1994, 1996). Much speculation has been published linking the temporally variable nature of these data to the evolution of a putative lunar dynamo. In particular, Runcorn (1994; 1996), and most recently Stegman *et al.* (2003), have argued that the apparent 4.1–3.9 Ga rise and subsequent fall in intensities could be the result of a late turn-on of the lunar dynamo and its subsequent demise. If true, such a late dynamo turn-on would constrain models of the initial thermal state of the Moon (e.g., Pritchard and Stevenson 2000; Stegman *et al.* 2003).

An alternative to the lunar dynamo hypothesis is that the lunar samples acquired a remanent magnetization by some process associated with impact cratering. Hood and Huang (1991) have shown that during a large impact, an expanding impact-generated plasma cloud could amplify ambient fields near the antipode of the basin. The rocks in these regions could then be magnetized by the process of shock remanent magnetization when seismic waves from the impact converged at this region (e.g., Hughes *et al.* 1977; Hood and Huang 1991; Watts

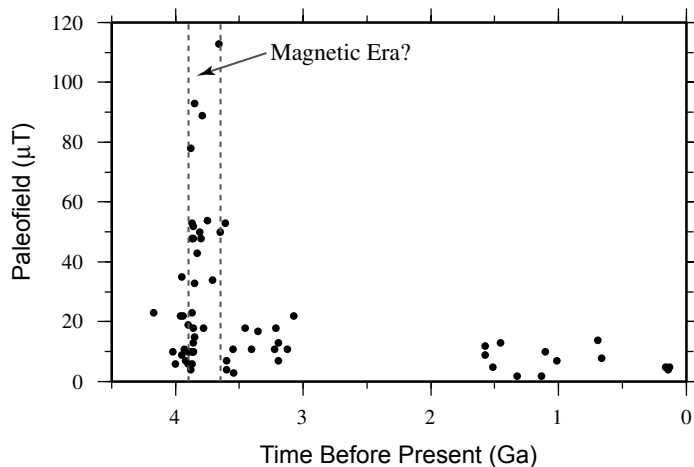


Figure 3.22. Absolute and IRMs normalization paleointensities of the lunar samples as a function of time. Data taken from Fuller and Cisowski (1987, Fig. 53).

et al. 1991; Wieczorek and Zuber 2001b). Consistent with this theory, the largest magnetic anomalies on the lunar surface as measured from orbit are in fact antipodal to many of the large basins (Lin et al. 1988, 1998; Hood et al. 2001). The field strengths in these regions may be as large as ~ 300 nT, whereas more typical fields of the Moon are only ~ 10 nT or less.

It is also possible that transient electrical currents set up in a plasma cloud close to an impact crater could have themselves generated a significant magnetic field (e.g., Martelli and Newton 1977; Srnka 1977; Srnka et al. 1979; Cerroni and Martelli 1982; Hood and Vickery 1984; Crawford and Schultz 1988, 1991; Hood and Huang 1991; Crawford and Schultz 1999). Measurements of surface fields by the Lunar Prospector electron reflectometer show that while basins possess low field strengths, basin ejecta is often strongly magnetized (Halekas et al. 2001, 2003; Richmond et al. 2003), consistent with such a process. As a lunar dynamo is unlikely to have operated during the past few Ga, the high paleofields measured from young lunar samples are most easily explained by impact processes. Finally, it is perhaps noteworthy that a large number of the high paleofield measurements occur near ~ 3.9 Ga, a time at which some models of the lunar cratering flux predict a large spike in the cratering rate (e.g., Cohen et al. 2000; Hartmann et al. 2000; Ryder et al. 2000).

While some temporal variations in the lunar paleointensity data may reflect real changes in field strength, it is important to assess the reliability and quality of the IRMs and absolute paleointensity data. Even the most reliable terrestrial Thellier-Thellier pTRM check paleointensity datasets show quite a bit of scatter. The Selkin and Tauxe (2000) dataset for just the last 300 My of Earth history has a ratio of variance to mean field equal to 0.7, which is actually not much less than that of the lunar IRMs and absolute paleointensity datasets (which have ratios of 1.0 and 1.6, respectively). Given that the terrestrial paleointensities show only a factor of two variation in mean intensity over the last 300 My (Selkin and Tauxe 2000), this begs the question of whether the apparent order-of-magnitude rise and fall of lunar paleointensity values with time is at all statistically meaningful.

An answer to this question can be obtained by use of the Kolmogorov-Smirnov (KS) test (Press et al. 1992, pp. 617-622), which assesses the probability that two datasets are drawn from the same underlying distribution. It does not make any assumptions about the nature of the underlying distribution, and is appropriate for even the smallest sample sizes (Lindgren 1993). It has also been used previously to analyze the significance of changes in the paleointensities of the Earth (Selkin and Tauxe 2000). We reject the null hypothesis that two sets of data are drawn from the same underlying distribution when the probability of this occurring is less than 5%.

We have applied the KS test to various subsets of the paleointensity database. These data were divided into three time periods (pre-3.9 Ga, 3.9–3.65 Ga, and post-3.65 Ga), and three different paleointensity techniques were considered (IRMs, the Thellier-Thellier subset of the absolute measurements, and all absolute measurements). These data were taken from the figures in Fuller and Cisowski (1987) and our results are summarized in Table 3.14. Using the IRMs database, it is seen that there is some statistical basis for saying that the IRMs data provide evidence for an increase in field strength around 3.9 Ga (there is a 3.8% chance that the pre-3.9 Ga and 3.9–3.65 data sets are drawn from the same distribution). There is an even better statistical basis for saying that the field strength decreased after ~ 3.65 Ga. It is also clear that there is no statistical difference between the pre-3.9 Ga and post-3.65 Ga IRMs normalization datasets.

Unfortunately, the absolute paleointensity measurements are not as definitive. Using all the absolute paleointensity measurements, we can similarly say that there is a good statistical basis for claiming that the field strength decreased after 3.65 Ga. However, the same is not true when only the Thellier-Thellier absolute paleointensity measurements are used (these are probably the most robust subset of the absolute measurements). Although we cannot reject the hypothesis that the 3.9–3.65 Ga and post-3.65 Ga periods of the Thellier-Thellier paleointensities are

Table 3.14. Kolmogorov-Smirnov (KS) tests on lunar paleointensity data.

Paleointensity Data Subsets	P	Reject Null Hypothesis?
Early (IRM) vs. Mid (IRM)	0.038	YES
Early (IRM) vs. Late (IRM)	0.25	NO
Mid (IRM) vs. Late (IRM)	1.0×10^{-5}	YES
Mid (TT) vs. Late (TT)	0.18	NO
Mid (A) vs. Late (A)	0.030	YES

P = Probability of the null hypothesis that the two distributions are drawn from the same underlying distribution.

IRM = Saturation isothermal remanent magnetism normalization dataset.

TT = Thellier-Thellier dataset.

A = Entire Absolute paleointensity dataset.

Early = pre-3.90 Ga, Mid = 3.90-3.65 Ga, Late = 3.65 Ga to present.

drawn from the same distribution, this discrepancy with the other datasets might be explained by the very small number of Thellier-Thellier measurements (the effective number of degrees of freedom for this test is significantly lower than that of any of the others).

4.7.3. What we know about lunar paleomagnetism. So what can we confidently take away from the lunar paleointensity work of the last thirty years? First, it is near certain that many of the lunar samples retain ancient (billions of years old) magnetizations. Second, it is likely that there were at least transient magnetic fields on the Moon that reached 10 μT and possibly as much as 100 μT . In particular, it is difficult to dismiss the 100 μT value from 62235 that has been reproduced in four separate experiments (two of which used the Thellier-Thellier technique) by two independent laboratories (Collinson *et al.* 1973; Stephenson *et al.* 1974; Cisowski *et al.* 1983; Sugiura and Strangway 1983). Given the uneven sampling of the lunar surface during the Apollo missions, it is highly probable that some lunar rocks might show evidence for an even higher field strength. Third, the lunar paleointensity data give statistically significant evidence for a strong rise in paleointensities around 3.9 Ga, followed by a weakening sometime after \sim 3.6 Ga. This evolution in intensity could be reflective of (1) a rising and weakening dynamo field, or (2) a time period in which impact-generated magnetic fields were more common, possibly as a result of a spike in the lunar cratering rate. And finally, the fact that (a) the paleointensities from more than a dozen samples younger than 1.5 Ga give fairly high values between \sim 1–10 μT (including a Thellier-Thellier value from the <200 Ma impact glass of 70019) and (b) large magnetic anomalies are associated with ejecta and the antipodes of large impact basins, we strongly suspect that impact events have had at least some role in magnetizing the lunar crust. Given the possibility that such impacts may have merely amplified a preexisting field, this does not exclude the possibility of an ancient lunar dynamo.

4.7.4. A lunar dynamo? If the observations of lunar paleomagnetism can be believed, then the intensity of the magnetic field was at one point as large as 100 μT at the lunar surface. If this were a result of an internal dynamo, then assuming a 375 km radius metallic core (which is the largest radius allowed by the LLR data), the field strength at the core-mantle boundary would be about 100 times greater (\sim 10 mT). This is more than 20 times greater than the field present at the core-mantle boundary of the Earth, and larger field strengths would be required if the lunar core was smaller. Is it possible for a convecting lunar dynamo to produce a field intensity of this magnitude? Such a question is important, because if a convecting lunar dynamo was present early in lunar history, it has implications for the early thermal state of the Moon and could potentially constrain lunar formation scenarios.

There is much uncertainty in using dynamo theory to estimate the strength of magnetic fields, but our current theoretical understanding (and using current planetary and satellite dynamos as analogs) makes a convecting lunar dynamo seem unlikely. A dynamo is formed when an electrically conducting fluid flows in the presence of a magnetic field, regenerating a self-sustaining magnetic field by induction (e.g., Busse 2000; Roberts and Glatzmaier 2000). Here we consider a fluid metallic iron core whose flow is generated by convective cooling. However, other conductive fluids (e.g., liquid silicates) or sources of flow (e.g. tidal effects) could possibly be relevant for the Moon.

When a dynamo is operating, its internal field strength can be estimated by use of the Elsasser number

$$\Lambda = \frac{B^2}{2 \rho \mu_0 \lambda \Omega} \quad (3.7)$$

where λ is the magnetic diffusivity ($\sim 2 \text{ m}^2 \text{ s}^{-1}$ for liquid iron), Ω is the angular rotation rate of the body, ρ is the density of liquid iron, μ_0 is the magnetic permeability of free space, and B is the internal intensity of the magnetic field at the core-mantle boundary (e.g., Stevenson 2003). Convection in the presence of rotation and the generation of a magnetic field is most efficient when the Elsasser number is close to unity, or perhaps between 1–10 (Zhang and Jones 1994; Stevenson 2003). Dynamos might exist for $\Lambda < 1$, but cannot exist when Λ is much greater than unity because large fields eliminate those aspects of the fluid motion that are favorable for dynamo generation. When the Elsasser number is near unity, the Coriolis and Lorentz forces are roughly balanced so that the buoyancy that promotes convection is less inhibited by the other two forces. Notice that the Elsasser number does not require either the core size or the relative importance of compositional versus thermal convection to be known. Dynamos that do not require convection (e.g., tidally or nutationally driven flows) are also expected to be limited by the condition $\Lambda \sim 1$, although this is less certain.

Letting Λ vary between 1 and 10, the present lunar rotation rate implies a maximum field strength between 300–1000 μT at the lunar core. When the Moon was closer to the Earth, say 30 Earth radii away, the field at the core would have been slightly larger with a strength of 500–1600 μT . Upward continuing the maximum of these values to the surface yields a maximum field strength of $\sim 16 \mu\text{T}$, which is smaller by a factor of six than the maximum paleointensity implied by the lunar samples. Moreover, this maximum estimate is based upon the strength of the internal toroidal field of the core, and it is generally understood that the poloidal field external to the core is generally smaller, possibly by a large factor (e.g., Hide and Roberts 1979).

The above analysis suggests that a lunar core dynamo would not have been able to generate a magnetic field of $\sim 100 \mu\text{T}$ at the lunar surface. However, considering the limitations in the above analysis, the existence of an early lunar core dynamo cannot be definitively ruled out. A better understanding of lunar magnetism will have to wait until the paleointensities of lunar samples are reassessed using modern measurement techniques. Advances in dynamo theory will further help elucidate whether or not 100 μT magnetic fields can be generated at the lunar surface.

4.8. Geochemical constraints on the presence of a lunar core from siderophile elements and short-lived isotopes

The siderophile (metal-seeking) elements comprise a suite of nearly 30 elements that are sensitive indicators to metal-silicate partitioning in planetary bodies. Because these elements should be extracted into metallic phases according to their metal/silicate partition coefficients during accretion, these elements may represent a chemical “fingerprint” of a planetary core formation. Over the past 30 years, estimates of siderophile elements in the lunar mantle have been used to argue for the presence of a small metallic core (0.1–5.5 lunar wt%; see Table 3.15),

Table 3.15. Summary of lunar core sizes based upon siderophile element concentrations.

Study	Core Mass Fraction (%)	Core Radius (km) [†]	Silicate Mantle Degree of Melting (%)	Core Ni Abund. (wt %)	Bulk Moon Comp.*
Newsom (1984)	2.0 – 5.5	369 – 517	2 – 9	12 – 25	CI
O’Neill (1991)	~1	~293	0	35 – 55	PUM, CI, H
Ringwood & Seifert (1986)	0.4	216	0	40	PUM
Righter & Drake (1996)	1	293	100	43	PUM/CI/H
Righter & Drake (1996)	5	500	100	8.3	PUM/CI/H
Righter (2002)	0.7 – 1.0	260 – 293	100	20.0 – 25.7	Proto-Earth/Impactor

*CI (CI chondrite); PUM (Primitive upper mantle); H (H chondrite).

†Assuming a core density of 7 g cm⁻³

based mainly upon experimental partition coefficients determined at low temperatures and pressures (1200–1300 °C and 1 bar; e.g., Ringwood 1979; Drake *et al.* 1984; Newsom 1984; O’Neill 1991). Recent experimental work has been carried out at higher pressures and temperatures, and this allows a re-examination of siderophile partitioning behavior for conditions that are likely to have endured shortly after the formation of the Moon. This section will describe how siderophile elements are estimated for the lunar mantle, outline the conditions under which the lunar core may have formed, and finally discuss the evidence and time interval of core formation as implied by short-lived radioisotopes.

4.8.1. Siderophile elements in lunar samples and mantle. Samples of the lunar mantle have not yet been recognized in the Apollo sample collection (even as xenoliths), so estimates of its siderophile-element concentrations must be derived entirely from crustal samples. Because impact processes have affected the lunar surface, surface materials often contain impact melts, and their original (or pristine) composition and mineralogy have thus been compromised. Impacting materials are commonly chondritic, and chondrites generally contain more than 10 times the siderophile-element concentrations of typical crustal and mantle rocks. As a result, distinguishing pristine from compromised siderophile-element concentrations can be challenging and has been contentious in the past (e.g., Anders 1978; Delano and Ringwood 1978).

The approach of looking for correlations between a siderophile element and a refractory lithophile element of equal compatibility (or incompatibility) has proven the most reliable and straightforward way to estimate siderophile-element concentrations in the lunar mantle. Siderophile elements, however, can be difficult to determine at the low concentrations typical of lunar basaltic rocks. For example, Mo and Sn are present at low ppb levels in lunar samples, and some of the highly siderophile elements (HSEs) such as Re, Os and Ir are in ppt levels. Data for highly siderophile elements in lunar rocks obtained to date have come almost exclusively from the highly sensitive technique of radiochemical neutron activation analysis (RNAA) (e.g., Wolf *et al.* 1979; Warren *et al.* 1986). Many early data, even from otherwise reputable labs, have been discredited (Wolf *et al.* 1979) as suspiciously high in comparison to later analyses of the same or closely similar samples. The most frequent cause of spurious data is probably laboratory contamination, a problem that is enhanced for the lunar basalts by their low concentrations of the HSEs, and by the small sample masses available for analysis.

When the lunar mantle is partially melted, elements can exhibit compatible, $D > 1$, or incompatible, $D < 1$, behavior, where D is the partitioning coefficient between the solid and liquid phases for that element. The relative depletions of an element in comparison to CI chondrites

can be used to estimate the original siderophile element abundances in the lunar and terrestrial mantle, and the abundances discussed below have all been estimated in this manner (see Newsom 1995 for a summary of this approach). Because this is an enormous field of literature, we do not review it here, but rather direct the reader to key articles by Jagoutz et al. (1979) and Palme and Nickel (1986) and recent reviews by Walter et al. (2000) and Righter et al. (2000).

A summary of siderophile-element concentrations and depletions are presented here in order to highlight differences between the Earth and Moon. Because the origin of the Earth and Moon are likely to be directly linked, the siderophile-element abundances for each body are compared and plotted in Figure 3.23 for the compatible elements and Figure 3.24 for the incompatible elements. The importance of these differences is discussed in the following paragraphs.

Ni and Co. Since both of these elements exhibit compatible behavior due to olivine and chromite fractionation, their concentrations in planetary mantles can be estimated by correlations with MgO and FeO (e.g., Wänke and Dreibus 1986) (see Fig. 3.23). Both Ni and Co for the lunar mantle are found to be approximately 5 times more depleted with respect to the terrestrial mantle.

Mo, W, Re. In many basalts from diverse planetary bodies, moderately siderophile elements (such as Mo, W, and Re) are incompatible and thus are positively correlated with other incompatible, refractory lithophile elements (such as Pr, Ba, Yb, La or Nd; see Fig. 3.24). This correlation line is found to be well below chondritic values, and this “depletion” is most likely due to metal-silicate equilibration (core formation) in that particular body (see the schematic illustration in Fig. 3.24a). The lunar mantle is substantially more depleted in Mo and Re than the terrestrial mantle (e.g., Newsom and Palme 1984; Newsom et al. 1996; Righter et al. 1998). However, the W depletions found in the lunar mantle are very similar to those found both in the terrestrial mantle and the eucrite parent body (Vesta) (e.g., Righter and Drake 1996), indicating that W may not be a very sensitive indicator of the pressure and temperature conditions of core formation.

P and Ga. Besides being siderophile, many elements such as P and Ga are also volatile. As a result of this, a measured depletion can be due to either core formation or volatility-controlled processes. In order to estimate the depletion of P and Ga due to core formation, these two elements must first be normalized to lithophile elements of nearly equal volatility. Good candidates for such a comparison are the alkali elements Na, K, Rb and Cs. Though it

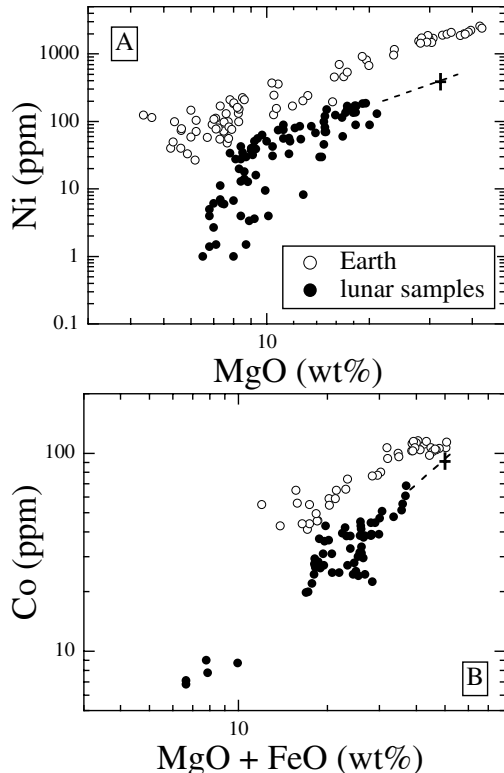


Figure 3.23. Compatible-element depletion diagrams for Ni-MgO and Co-(MgO+FeO) data. Data from Delano (1986a) and references therein. [Used by permission of Elsevier Science, from Righter (2002), *Icarus*, Vol. 158, Fig. 1, p. 2.]

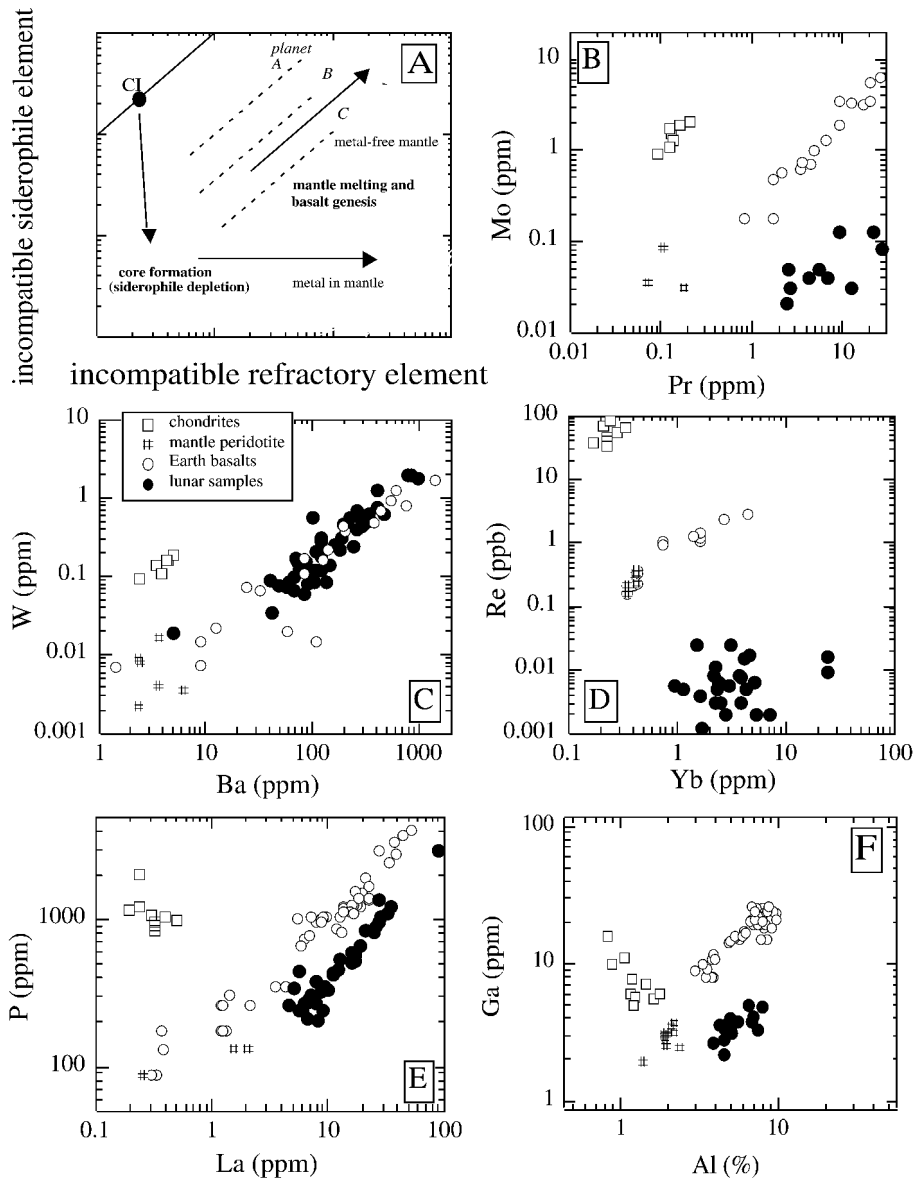


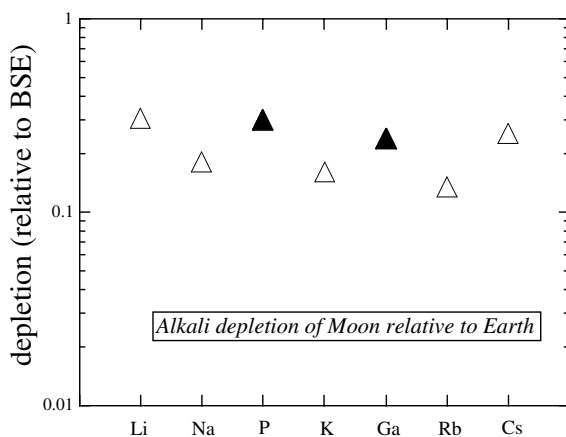
Figure 3.24. Siderophile-element depletion diagrams for Mo-Pr, W-Ba, P-La, Re-Yb, and Ga-Ti. Data sources: Lunar Mo and Pr: Taylor et al. (1971), Newsom and Palme (1984); terrestrial Mo and Pr: Newsom et al. (1986); Lunar P, La, Ga, Ti, W and Ba: BVSP (1981), Warren et al. (1986), Wänke et al. (1972), Wänke et al. (1974), Wänke et al. (1977), Palme et al. (1978); Terrestrial W and Ba: Newsom et al. (1996); terrestrial P and La: BVSP (1981), Newsom and Drake (1983) and references therein; Terrestrial Ga and Ti: Dickey et al. (1977), BVSP (1981); Norman and Garcia (1999), Frey et al. (1985). [Used by permission of Elsevier Science, from Righter (2002), *Icarus*, Vol. 158, Fig. 2, p. 3.]

has been recognized for some time that these elements are depleted in the lunar mantle relative to the Earth (e.g., Kreutzberger et al. 1986), Ga has been found to be no more depleted than Na in lunar highland feldspars (Norman et al. 1995). In fact, neither P nor Ga are depleted relative to the lithophile, volatile elements (Li, Na, K, Rb, Cs; see Fig. 3.25), suggesting that neither was depleted substantially by lunar core formation (e.g., Righter 2002).

Overall the siderophile elements show increasing depletion with increasing siderophility. Ni, Co, Mo and Re exhibit a further depletion over that in the Earth, whereas W depletions are similar to those in the Earth and eucrites. These observations argue qualitatively that the material that makes up the Moon has at some point undergone a metal-silicate differentiation event. We emphasize here, however, that this evidence does not necessarily imply that the Moon currently possesses a metallic core. In particular, if the giant-impact origin of the Earth-Moon system is correct, then the Moon is predicted to accrete from the material that was put in circumterrestrial orbit following this event. If the Earth and impacting body previously underwent a core-forming event, and if the core of the impacting body accreted to the Earth during this event, then a core-free Moon could form that nonetheless possessed the siderophile fingerprint of metal-silicate equilibration. In contrast, if a substantial amount of metallic iron was incorporated in the circum terrestrial disk during the giant impact, then it becomes possible that this material could have been reprocessed by a subsequent lunar core-forming event at lower pressures. Separating the consequences of these two putative core-forming events is not a simple matter, and depends upon knowing the composition and thermal history of the Moon, proto-Earth and impactor (Righter 2002).

4.8.2. Core formation models. Temperature, pressure, the fugacities of oxygen and sulfur, and silicate melt structure and composition all affect the partitioning behavior of an element between metal and silicate phases. Because of the relatively low pressures associated with the lunar core (~4 GPa), partition coefficients for typical pressures encountered at the core-mantle boundary have been obtained in the laboratory (Walker et al. 1993; Hillgren et al. 1994, 1996; Ito et al. 1998). From these experiments, metal/silicate partition coefficients have been parameterized for Fe, Ni, Co, Mo, W, P, Ga, Sn and Cu (Righter and Drake 1997, 1999, 2000). Using these expressions it is possible, for instance, to calculate metal/silicate partition coefficients along an adiabatic gradient in a deep magma ocean system (see Fig. 3.26). While the pressure at the base of a lunar magma ocean would only be ~4 GPa (or 40 kbar), if the Moon was derived from a much larger planet that collided with the Earth, the basal pressures of a magma ocean in this body could have been considerably greater.

Figure 3.25. Depletion of P and Ga in the lunar mantle relative to the alkali elements, Li, Na, K, Rb and Cs, normalized to the composition of the bulk silicate Earth (data from Jones and Palme 2000). [Used by permission of Elsevier Science, from Righter (2002), *Icarus*, Vol. 158, Fig. 7, p. 9.]



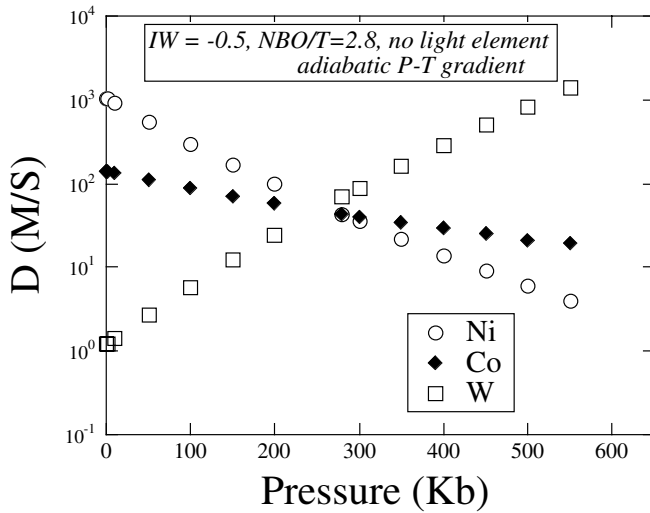


Figure 3.26. Effect of pressure and temperature on metal-silicate partition coefficients for Ni, Co and W using predictive expressions presented by Righter and Drake (1999). Conditions are an adiabatic temperature gradient with the oxygen fugacity fixed at 0.5 $\log f_{\text{O}_2}$ units below the IW buffer, a peridotite magma ($\text{nbo}/t = 2.8$), and no light elements in the metallic liquid.

Most previous work on lunar siderophile elements has concluded that the Moon has undergone metal-silicate equilibration, and therefore likely possesses a small metallic core. These models differ in the size of the core and its composition (e.g., Brett 1973; Wänke *et al.* 1977; Ringwood 1979; Drake *et al.* 1984; Newsom 1984, 1986; Ringwood and Seifert 1986; Wänke and Dreibus 1986; Hillgren 1991; O'Neill 1991; Righter and Drake 1996) and a summary of some of these models is presented in Table 3.15. Early models were based on the siderophile-element data reported by Wänke *et al.* (1977). Subsequent Mo and Re analyses of lunar materials were considered in the modeling of Newsom (1984), who accounted for the lunar Re and Mo depletions with a 2–5 lunar wt% metallic core if the Moon accreted directly from the solar nebula, or a 0.5–1 lunar wt% core if it formed from material coming from the terrestrial mantle. Later work by Ringwood and Seifert (1986), O'Neill (1991) and Hillgren (1991) all argued that the 3 times larger depletion of Ni in the lunar mantle in comparison to the terrestrial mantle could be explained by a Ni-rich lunar core. These conclusions were based primarily on the assumption that the Moon was made of material from the primitive upper mantle of the Earth. This latter assumption is now considered to be at odds with giant-impact models in which the Moon is predicted to be primarily derived from the object that collided with the proto-Earth.

While the thermal state of the Moon during and after its formation is not well known, it is likely that a large portion of it was at one time completely molten. Recognizing that metal-silicate partition coefficients change as both a function of pressure and temperature, Righter and Drake (1996) considered high pressure and temperature scenarios for the depletions of the lunar siderophile elements. They found that the siderophile-element depletions of the mare source region are consistent with a scenario in which a small metallic core (1–5 lunar wt%) equilibrated with an overlying molten mantle. Using a peridotite magma ocean, a best fit to the lunar depletions was obtained by using metal-silicate partition coefficients calculated for $T = 2200$ K, $P = 35$ kbar, $\Delta\text{IW} = -1$, and a core that contained 15 mol% sulfur. Again, these conclusions were based on the assumption that the Moon was derived from material like the primitive terrestrial mantle.

The issue of whether the Moon has a small metallic core has been re-examined by Righter (2002) in light of improved dynamical modeling of the giant-impact Moon-forming event and high temperature and pressure metal-silicate partition coefficients. In particular, he assumed that both the proto-Earth and impactor underwent an initial high-pressure core-forming event.

End-member initial conditions for these bodies assumed either that a molten core equilibrated with a totally molten mantle (“hot” initial conditions), or that metal equilibration occurred at the base of a magma ocean that coincided with the top of the perovskite stability field (“warm” initial conditions). Following the giant-impact event, the Moon was assumed to have formed exclusively from the mantle of either of these bodies. After the Moon accreted from this material, a second stage of metal-silicate equilibration was assumed to have occurred, but this time at the low pressures associated with the lunar molten-core/molten-silicate-mantle interface. Given reasonable compositions for the impactor and proto-Earth, a small metallic core (0.7–2 wt%) is predicted to have segregated and equilibrated with the lunar mantle following the giant impact event. The scenario in which the Moon is made from the mantle of a “hot” proto-Earth is the least likely of these models because the lunar mantle is predicted to be more depleted in W, P and Re than is observed. Discarding this scenario, the Moon is predicted to have an Fe-rich core that is 0.7–1 % of its mass. The results from this latest study eliminate previous geochemical objections to the Moon having a composition primarily derived from the impactor that collided with the proto-Earth.

While the recent modeling of Righter (2002) is consistent with the Moon possessing a small metallic core, he also investigated the possibility of whether core formation in the impactor alone could account for the observed lunar siderophile element abundances. In this scenario, if the core of the impactor completely accreted to the Earth, then the siderophile element data would not require the existence of a lunar core. It was found that if core formation in the impactor occurred at low temperature, pressure and f_{O_2} conditions, the abundances of Ni, Mo, P and Re could be accounted for. The abundances of Ga, Co, and W, however, were found to be slightly lower than observed. Given the uncertain composition, size, and thermal history of the impactor, it is possible that this might not be a fundamental objection to the hypothesis that the Moon does not possess an iron core.

Finally, we note that several factors have yet to be considered in the above models, including the kinetics of metal-silicate equilibration, the dynamics of metal-silicate differentiation, and the time scale of magma-ocean crystallization. In a study by Rubie et al. (2003) for the terrestrial magma ocean, it was shown that the timescale of metal-silicate equilibration between a layer of molten iron and an overlying silicate magma was about two orders of magnitude greater than the timescale of magma-ocean crystallization. This is particularly important because as soon as a solid silicate layer forms between the two, metal-silicate equilibration will effectively cease. If this result were applicable to the Moon, then metal-silicate equilibration would be favored to occur by the sinking of small metal droplets through a silicate magma ocean. This process, however, is sensitive to the dynamics of metal segregation from the silicate magma, and the “effective” pressure of equilibration could either over- or under-estimate the pressure at the core-mantle interface (Rubie et al. 2003).

4.8.3. Isotopic studies bearing on core formation. The short half life of ^{182}Hf (~9 My) as it decays to ^{182}W enables Hf-W isotope data to be used in examining planetary differentiation processes early in the history of the solar system. With Hf being lithophile and W siderophile, core formation should have dramatically increased the Hf/W ratio of the silicate mantle and reduced it in the core. If core formation occurred while ^{182}Hf was alive, differentiation would further produce positive and negative $\epsilon^{182}\text{W}$ anomalies relative to chondrites in the silicate mantle and core, respectively (Lee and Halliday 1995; Halliday et al. 1996; Jacobsen and Harper 1996). ($\epsilon^{182}\text{W} = [(^{182}\text{W}/^{183}\text{W})_{\text{sample}}/(^{182}\text{W}/^{183}\text{W})_{\text{standard}} - 1] \times 10^4$). Early differentiation in the solar system is witnessed by negative $\epsilon^{182}\text{W}$ anomalies in metal from iron meteorites and extremely positive anomalies in the eucrites (Lee and Halliday 1997).

Early tungsten isotopic measurements of mantle-derived terrestrial basalts showed that while they did not possess distinct $\epsilon^{182}\text{W}$ anomalies ($\epsilon^{182}\text{W} \sim 0$) (Halliday et al. 1996; Halliday 2000), they did possess a suprachondritic Hf/W ratio. As chondritic materials were thought

to have near-zero $\varepsilon^{182}\text{W}$ anomalies, these data were broadly interpreted to indicate that core formation for the Earth was “late” (>60 My). Even if a late veneer of chondritic material was added to the Earth, as may be required to account for the highly siderophile element abundances in the mantle (e.g., Morgan 1986; Morgan *et al.* 2001 though see Frost *et al.* 2004 for an alternative scenario), this would not be able to completely dilute a positive early-core forming $\varepsilon^{182}\text{W}$ signature back to zero (Halliday and Lee 1999). Recent studies, however, have found that the $^{182}\text{Hf}/^{180}\text{Hf}$ ratio at the start of the solar system was about three times lower than previously suggested, and this implies that the bulk silicate Earth has a resolvable ^{182}W excess of $\sim 1.9\varepsilon$ units relative to chondrites (Kleine *et al.* 2002; Schoenberg *et al.* 2002; Yin *et al.* 2002). These data imply that core formation occurred early for the Earth, within 33 ± 2 My of solar system formation.

Apollo samples analyzed for W isotopes show $\varepsilon^{182}\text{W}$ values ranging from zero to more than +6, although the Moon appears to have an approximately chondritic Hf/W ratio (Lee *et al.* 1997). Because of the highest measured $\varepsilon^{182}\text{W}$ anomalies, it was recognized that these analyses needed to be corrected for cosmic ray-induced neutron capture on ^{181}Ta (e.g., Jones and Palme 2000). It was demonstrated that the measured ^{182}W excess in mineral separates from some lunar basalts (specifically the high-Ti basalts) correlated with their Ta/W ratios, and this confirmed the theoretical predictions that the $^{181}\text{Ta}(n,\gamma)^{182}\text{Ta}(\beta^-)^{182}\text{W}$ reaction due to cosmic irradiation was indeed the cause of some of the excess ^{182}W . Lee *et al.* (2002) demonstrated that although such a correction reduced the magnitude of the $\varepsilon^{182}\text{W}$ anomalies, it did not remove them. In addition to this process, some of the excess ^{182}W can be attributed to silicate fractionation effects, since ilmenite, clinopyroxene, and garnet all fractionate Hf from W (Righter and Shearer 2003; Shearer and Righter 2003). Model ages based on these data suggest that lunar core formation occurred $\sim 53 \pm 4$ My after the formation of the solar system (Lee *et al.* 1997, 2002; Halliday and Lee 1999) and less than 70 My after solar system formation for the source of the high-Ti mare basalts (Lee *et al.* 2002). If the Earth and Moon possess identical Hf/W ratios, then the results of Kleine *et al.* (2002) suggest that core formation occurred earlier, between 24 and 35 My after solar system formation.

4.9. Joint inversions of several datasets

As has been highlighted in the preceding sections, the size, composition and physical state of the lunar core cannot be uniquely determined by the analysis of individual datasets in isolation. Each measurement can be interpreted in multiple ways, and both a metallic and dense molten-silicate core are defensibly permissible. One method that might further constrain the deep interior structure of the Moon would be to construct models that are not only consistent with a single measurement, but several. An investigation in this spirit has recently been performed by Khan *et al.* (2006) who jointly modeled the measured mass, moment of inertia, k_2 Love number, and tidal dissipation quality factor Q . As these four measurements are affected by the depth dependence of the lunar density, shear modulus, and local quality factor q , a joint inversion of these should be able to better resolve the attributes of the lunar core.

The approach taken in the aforementioned study was to first address the question as to whether the lunar core is either completely solid or molten, and then to use the most likely answer to place limits on its density and shear modulus. Assuming that the structure of the Moon could be adequately approximated by a series of five concentric homogeneous shells, a Monte Carlo method was used to sample values of the density, shear modulus, q , and thickness for each layer. The crust was restricted to have an average thickness between 30 and 60 km, and the shear modulus of the lowermost layer was constrained to be representative of either completely molten or solid materials. Using these sampled parameters, the mass, moment of inertia, Love number and tidal dissipation factor were computed, from which the misfit between the data and model was quantified. All results were then interpreted in terms of a Bayesian probabilistic framework.

Using the method of Bayesian hypothesis testing (by use of the Bayes factor), it was shown that the hypothesis of the Moon possessing a completely molten core is highly favored to that of a solid core by a very large factor. For the molten core scenario, its radius was found to have a nearly uniform probability distribution between about 70 and 450 km, and to be nearly zero exterior to this range. The probability of the core density was found to linearly increase from a value near zero at $\sim 3.5 \text{ g cm}^{-3}$ to a maximal value at a density near $\sim 7.5 \text{ g cm}^{-3}$ (densities greater than this were not sampled). While central densities typical of molten iron, an Fe-S eutectic melt, and a dense molten silicate core can be found that are consistent with the data, their results favor the denser side among these possibilities.

A few considerations should be borne in mind when interpreting these results. First, the value adopted for the k_2 Love number was taken from a recent LLR study (see Williams et al. 2005) that is smaller by one standard deviation than the independent determination based on radio tracking data of lunar spacecraft (Konopliv et al. 2001). Second, the above model results are based upon the premise that the Moon can be adequately described by five homogeneous layers. While this is a reasonable assumption, models with more layers are also defensible. In particular, if the Moon possesses a solid inner core (see Section 4.6), then a minimum of six homogenous layers would be required to describe its interior density and rheological structure (i.e., crust, upper mantle, middle mantle, lower attenuating mantle, liquid outer core and solid inner core; see Fig. 3.27). The inclusion of extra layers would, at a minimum, increase the variance of the solution parameters, and could affect the magnitude of the Bayes factor.

Finally, we note a possible difference in interpretation that could arise between Bayesian and non-Bayesian inverse approaches when the physical model is highly non-unique. Let us presume that the mass, moment of inertia, k_2 Love number, and quality factor of the Moon were perfectly known. (It is unlikely that higher precision measurements of at least the mass and moment of inertia would significantly improve models of the lunar interior.) As only four scalar numbers are being used to constrain how the lunar density, shear modulus, and quality factor varies with depth, a potentially large range of models might exist that could exactly fit these observations. In the Bayesian framework, the posterior probability distribution would be

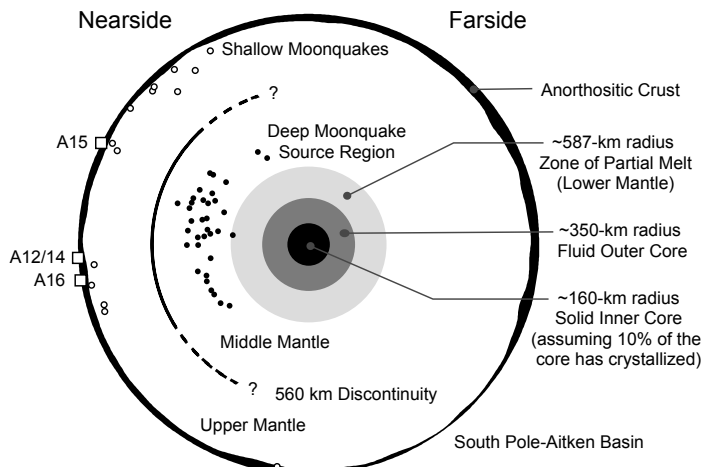


Figure 3.27. Schematic diagram of the internal structure of the Moon as revealed by various geophysical methods. The thickness of the crust is shown for a pole-to-pole profile at 0 and 180° longitude, and the shallow and deep moonquakes have been projected onto the nearside hemisphere as a function of depth and latitude. While the radius of a solid inner core is completely undetermined, thermal considerations suggest that at least some portion of the core has crystallized.

obtained simply by multiplying this model space by the prior probability distribution, as each model has the same zero misfit (i.e., the same likelihood, see Ulrych *et al.* 2001). In contrast to the situation where the likelihood function is somewhat peaked, the posterior probability distribution would be critically dependent upon the assumed prior probability distribution. A more conservative inverse approach might be to instead treat all physically reasonable models that satisfy perfectly known measurements as being possible solutions. If this criterion were to be used, it is unlikely that the data would be able to distinguish between the case of a pure liquid iron core and that of a dense molten silicate core.

4.10. Summary

The geophysical evidence presented above implies that the central portion of the Moon is molten (with or without a solid inner core), has a high electrical conductivity, and is denser than the overlying mantle. The precise composition of this “core,” however, is not well constrained by these studies. Indeed, the moment of inertia, the k_2 Love number, the quality factor Q , and lunar rotation and magnetic induction studies are all consistent with the core being composed of either a molten Fe-FeS-C metallic alloy with a radius less than 375 km, or a molten silicate composition that is slightly larger. If the lunar core is composed of molten silicate materials, then this composition must be enriched in both iron and titanium in order to be denser than the overlying silicate mantle. Thermal considerations suggest that some portion of the core, regardless of its composition, should have crystallized over the past 4.5 Ga, thus predicting that the Moon currently possesses a solid inner core as well.

Although the above geophysical methods for inferring the properties of the lunar core are not very sensitive to its composition, two additional pieces of information could be used to favor one hypothesis over the other. Firstly, modeling of the lunar siderophile-element abundances is consistent with the Moon possessing an iron-nickel rich core with a radius between 260 and 293 km (Righter 2002). While this range of core sizes is consistent with the range of core radii as implied by the geophysical techniques, it remains possible that core-free models could be constructed that are consistent with the measured siderophile-element abundances. Secondly, the paleomagnetic signature of the lunar samples, as well as the crustal fields as measured from orbit, imply that the magnetic field intensity of the lunar environment was once much greater than is currently observed. While this might be taken as being consistent with the Moon once possessing a dynamo (which would require the core to be metallic), these field strengths might also be consistent with transient magnetic fields generated during impact events. Indeed, the largest magnetic anomalies observed from orbit appear to be associated with the antipodes of the largest basins. Current dynamo scaling relations further suggest that a convecting iron core would not be able to generate the magnetic field intensities that are required by the paleomagnetic data.

A schematic illustration of what is known of the internal structure of the Moon is presented in Figure 3.27. This figure illustrates (1) the lateral variations in crustal thickness that are the result of impact cratering events (i.e., the SPA basin on the farside), (2) the existence of a seismic discontinuity at a depth of \sim 560 km, (3) the spatial distribution of the deep and shallow moonquakes, (4) the likely existence of a partially molten region beneath a depth of 1150 km, (5) and the existence of a molten outer core with a radius of \sim 350 km. As some portion of the liquid core is likely to have crystallized, a solid inner core is most likely present as well. An arbitrary core crystallization of 10% by volume would result in an inner core radius of about 260 km. While the 560-km seismic discontinuity may be a global feature of the Moon, this presumption cannot be tested using the limited spatial distribution of the Apollo seismic network.

5. CRUSTAL PROVINCES

The lunar maria and highlands have long been known to be fundamentally different based upon contrasts in their albedo, morphology, and spectral properties. For this reason it was, and

still is, common to broadly divide the lunar surface into these two distinctive terrains—where the term *terrain* refers to “an area of ground with a particular physical character” (Allaby and Allaby 1991). With the collection of geophysical and remote-sensing data from orbit, as well as the analysis of surface samples, it has become apparent that there are limitations with this mare/highland classification scheme. Equatorial gamma-ray data obtained from orbit during the Apollo missions showed that the highest abundances of thorium, and by inference KREEP, are in the Procellarum and Imbrium regions on the lunar nearside (e.g., Metzger et al. 1973). Laser altimetry data has shown that the Moon possesses a 2-km center-of-mass/center-of-figure offset (e.g., Kaula et al. 1972; Zuber et al. 1994), suggesting that the farside crust might be significantly thicker than that of the nearside. Furthermore, analyses of the Apollo samples suggest that the eastern and western landing sites are significantly different in composition (e.g., Shervais and Taylor 1986). Although the Apollo data were limited in coverage, some workers have suggested, or hinted at, the possibility that differences in geologic evolution between the near and far sides of the Moon may be more fundamental than the traditional dichotomy between the maria and highlands (e.g., Wasson and Warren 1980; Warren and Rasmussen 1987; Ryder 1994; Haskin 1998).

Global gamma-ray and neutron-flux data from the Lunar Prospector mission have since convincingly shown that the surface concentrations of Th and other incompatible elements are highly localized only within the Imbrium and Procellarum regions (Lawrence et al. 1998, 2000; Elphic et al. 2000). This distribution has led to the idea that the Imbrium-Procellarum region is a unique geochemical crustal province that possesses a distinctive geochemistry and thermal evolution (e.g., Haskin et al. 2000; Jolliff et al. 2000a; Korotev 2000; Wieczorek and Phillips 2000). Jolliff et al. (2000a) have further advocated dividing the Moon into three major crust-mantle *terrane*s: the Procellarum KREEP Terrane (PKT), the Feldspathic Highlands Terrane (FHT), and the South Pole-Aitken Terrane. In the terrestrial vernacular, a terrane is defined as a “fault bounded area or region which is characterized by a stratigraphy, structural style, and geologic history distinct from those of adjacent areas, and which is not related to those areas by unconformable contacts or facies changes” (Allaby and Allaby 1991). Although the fault-bounded aspect of this definition does not apply to the Moon because of its lack of plate tectonics, as will be seen in the following sections, the remainder of this definition is probably an accurate description for at least the Procellarum KREEP and Feldspathic Highlands Terranes. Though the surface properties of the region encompassed by the South Pole-Aitken basin are unique for the Moon, we consider it likely that this region simply represents an exposure of lower crustal rocks that may well be typical of the Feldspathic Highlands Terrane.

In this section, we first give a general description of the major terranes that have been proposed by Jolliff et al. (2000a). Our discussion here closely follows this paper as well as that of Wieczorek and Phillips (2000), Haskin et al. (2000) and Korotev (2000). Finally, using the inferred compositions of these lunar terranes, we place constraints on the bulk composition of the Moon.

5.1. The Procellarum KREEP Terrane

The Procellarum KREEP Terrane differs from other regions of the Moon primarily by its KREEP-rich geochemistry and extended volcanic history. Data from the Lunar Prospector mission shows that the surface abundance of incompatible elements (Th, K, Gd, Sm, and by inference the other elements that make up KREEP) are highly concentrated in a single region that encompasses Oceanus Procellarum, Mare Imbrium, and the adjoining mare and highlands (Lawrence et al. 1998, 2000; Elphic et al. 2000). It is by this surface enhancement of KREEP that the confines of this terrane are tentatively delineated in Color Plate 3.10. Whereas the mare exterior to the PKT (as derived from Lunar Prospector data) have Th abundances of only ~2 ppm or less, the mare regolith within the PKT has concentrations that lie between ~3 and 7 ppm. Highland regions that reside in the PKT are inferred to be dominated by Imbrium ejecta

and possess Th abundances that range up to \sim 12 ppm, consistent with samples that are believed to be derived from this impact basin (e.g., Korotev 1998).

Another defining characteristic of the Procellarum KREEP Terrane is its unique volcanic history. Outside of this terrane, the majority of mare basalts erupted within the confines of large impact basins where the low-density upper crust has been substantially thinned. In contrast to this behavior, Oceanus Procellarum represents the largest contiguous expanse of mare basalts, even though this region possesses a relatively thick crust and is not in an obvious basin setting (e.g., Wieczorek *et al.* 2001). While the PKT encompasses only about 16% of the surface area of the Moon, more than 60% of the mare basalts by area are located there. The only recognized lunar volcanic complexes are found within Oceanus Procellarum (e.g., Marius Hills, the Aristarchus Plateau, Rümker Hills, and Hansteen Alpha; see Whitford-Stark and Head 1977, 1980; Wilhelms 1987; Hawke *et al.* 2003a), and the vast majority of the young Eratosthenian and Copernican basalts appear to have erupted close to these complexes. Furthermore, even though only \sim 20% of the maria have TiO_2 abundances greater than 5 wt%, more than half of the basalts within the Procellarum KREEP Terrane have TiO_2 abundances that are at least this great (Haskin *et al.* 2000). The youngest lunar basaltic lava flows erupted within Oceanus Procellarum, possibly as recently as 900 ± 400 My ago (Schultz and Spudis 1983), and the oldest lunar basalt that has been dated (\sim 4.2 Ga) came from a clast within an Apollo 14 breccia that was likely derived from this terrane (Taylor *et al.* 1983). Most basaltic eruptions exterior to this terrane, in contrast, occurred primarily during the Imbrian period.

Although Lunar Prospector has demonstrated that the Procellarum KREEP Terrane has a high surface abundance of incompatible elements, we caution that the gamma-ray and neutron spectrometers only sense the upper meter of the regolith. A major question is whether the KREEP component within this terrane is solely surficial (as in a veneer of KREEP-rich mare basalts and Imbrium ejecta), or whether it extends deep into the underlying crust and/or mantle. In either case, the KREEP-rich geochemistry and extensive volcanic history of this terrane suggest that these two phenomena are genetically related (Wieczorek and Phillips 2000). In the following two sections we first present evidence that a large portion of the crust within the PKT is enriched in incompatible elements. Following this, we consider whether the mare basalts within this terrane have high abundances of incompatible elements, or whether this is merely the result of vertical mixing with an underlying KREEP-rich substrate. Finally, we speculate on the origin and evolution of this unique region of the Moon.

5.1.1. Crustal composition. On the basis of Apollo gamma-ray data, Haskin (1998) made the suggestion that the Imbrium basin may have formed in a unique KREEP-rich geochemical province and that the primary ejecta from this basin should hence be enriched in incompatible elements. By modeling the deposition of KREEP-rich Imbrium ejecta onto a KREEP-poor substrate, he argued that the distribution and concentration of thorium exterior to this province was consistent with having an Imbrium origin. In particular, the concentration of thorium in the highlands was found to gradually decrease with distance from the Imbrium basin and then to slightly increase near its antipode. Global thorium data obtained from Lunar Prospector have since confirmed this prediction (Lawrence *et al.* 1998). It is important to note that this distribution of Th would not be obtained if the Imbrium bolide impacted a target that only possessed a near-surface KREEP enhancement. Instead, quantitative modeling seems to require an average crustal composition that lies somewhere between 4 and 9 ppm Th (Haskin *et al.* 1999).

The uniqueness of the Imbrium target composition is illustrated by a comparison with the composition of ejecta from other large lunar impact basins. With the possible exception of Serenitatis (Wieczorek and Zuber 2001b), which is adjacent to Imbrium, no other impact basin possesses a Th-enriched ejecta blanket. Because other large impact basins are known to have excavated deep into the crust (e.g., Wieczorek and Phillips 1999), this implies that only the crust near the Imbrium basin is significantly enriched in incompatible elements. As the

confines of the Procellarum KREEP Terrane are not symmetric about the Imbrium basin, the ejecta from this basin cannot be the sole source of the Th enhancement within this terrane.

Modeling of the thickness of Imbrium's ejecta blanket has shown that a significant quantity of Imbrium-derived materials should be present at each of the Apollo landing sites (Haskin 1998; Haskin et al. 2003). On the supposition that only ejecta from this basin would be rich in incompatible elements, Haskin et al. (1998) have reevaluated the old hypothesis that all KREEP-rich impact melts in the Apollo sample collection have an Imbrium origin (e.g., Evensen et al. 1974; Tera et al. 1974; Reid et al. 1977; Schaeffer and Schaeffer 1977). If this were indeed true, then these samples would place a strict constraint on the composition of the Imbrium target. As an example, Korotev (2000) has shown that the composition of these mafic impact melts can be modeled to a good approximation as being a mixture of three components: (1) typical feldspathic upper crustal materials (82.5 vol% plagioclase or 28.4 wt% Al_2O_3), (2) a material very similar in composition to Apollo 15 KREEP basalt, and (3) highly forsteritic dunite (Fo_{90}). Though there exists considerable variability in the composition of the mafic impact-melt rocks, the average proportion of these components is 58% KREEP basalt, 29% feldspathic upper crust, and 13% dunite. As a basin the size of Imbrium should have excavated through the entire crust (e.g., Wieczorek and Phillips 1999), the dunite component may represent the upper mantle in this locale (Korotev 2000).

If the above model results can be extrapolated to the rest of the Procellarum KREEP Terrane, and if the dunite component has a mantle origin, then about 67% of the crust within this terrane has a composition similar to that of KREEP basalt, or its differentiated equivalent. Since KREEP basalt has an average Th concentration of about 12–13 ppm, this implies that a large portion of the incompatible elements of the Moon (~30%, Jolliff et al. 2000a) are sequestered within this relatively small region of the crust. The origin of the feldspathic upper-crustal component in these impact-melt breccias is less certain. One possibility is that this component was similarly derived from the Imbrium target. Under this scenario, the crust of the PKT might best be described as possessing compositionally distinct feldspathic and KREEP basaltic materials, perhaps stratified into the upper and lower crust, respectively. Consistent with this interpretation is the observation that many central peaks in this terrane have broadly anorthositic compositions (~60–90 vol% plagioclase, see Tompkins and Pieters 1999 and Section 2.8). We caution, however, that spectral studies cannot distinguish between ferroan and alkali lithologies.

Petrological studies of the mafic impact melts, however, suggest that ferroan-anorthositic materials might have been absent from both the Imbrium (Spudis et al. 1991) and Serenitatis targets (Ryder et al. 1997). If this is true, then the feldspathic upper-crustal component in these melt rocks as inferred by Korotev (2000) might instead represent locally derived substrate that was melted and mixed with the primary ejecta of these basins. In either case, this feldspathic chemical component would have been present within the confines of the Procellarum KREEP Terrane in some form or another. Alternatively, it is possible that the three-component mixing model of Korotev (2000) overly simplifies the composition of the Imbrium target, and that anorthositic materials may truly be absent from this region of the crust.

5.1.2. Viscous relaxation of impact basins. In support of the hypothesis that the Procellarum KREEP Terrane possesses a high abundance of heat-producing elements, of the two sites where the lunar heat flow was determined (Apollo 15 and 17) the heat flow of the site within the PKT was found to be the larger (Langseth et al. 1976). Unfortunately, these two landing sites are situated close to the boundary of this terrane and it is not certain if these measurements are representative of either the PKT or FHT. Nevertheless, other pieces of evidence seem to suggest that the crust was hotter than typical within this region, causing impact-induced topography to viscously relax faster than in the surrounding highlands.

The size and shape of the excavation cavity of the young large nearside impact basins was investigated by Wieczorek and Phillips (1999) using a gravity-derived crustal thickness

model. In concordance with craters that are orders of magnitude smaller in size (e.g., Croft 1980; O’Keefe and Ahrens 1993), it was found that the maximum depth of excavation was approximately 1/10th of their transient crater diameter. The Imbrium and Serenitatis basins, however, were found to be anomalous in that their reconstructed excavation cavities were tens of kilometers shallower than expected. One likely explanation for this observation is that these basins originally formed in concordance with the general scaling relationship, but that they were modified during, or after, the impact event. One possible form of post-impact modification is viscous relaxation, whose rate is highly dependent on temperature. Since the Imbrium basin lies within the confines of the Procellarum KREEP Terrane, and Serenitatis is just on its border, a higher than typical crustal temperature at these locales is a reasonable expectation as a result of the high abundance of radioactive elements found there. It is also possible that the apparent shallow structure of these basins is a result of their having been filled by lavas that possess a density similar to that of the lower crust. The only volcanic rock that meets this criterion is KREEP basalt (mare basalts have densities of ~ 3.3 g cm $^{-3}$ which is similar to the underlying mantle). While rare in the sample collection, KREEP basalts have been identified at the Apollo 15 and 17 sites. The composition of the mafic impact-melt breccias further implies that KREEP basalt may be a major chemical component within the crust of this region.

The second piece of evidence for higher crustal temperatures in the PKT comes from the isostatic state of large impact basins. As originally noted by Neumann *et al.* (1996), the inferred crustal structure of the large impact basins suggests that some of these are currently superisostatic (i.e., the crust-mantle interface has been uplifted above its isostatic level). This appears to be true even when the load of the mare basalts is accounted for (Wieczorek and Phillips 1999), and the existence of mascon basins that do not possess significant mare fill is similarly suggestive of their being in a superistostatic state (Konopliv *et al.* 1998, 2001). Only those basins that formed near the PKT (Imbrium, Serenitatis, Grimaldi, and Humorum) appear to have been in an isostatic state prior to the emplacement of their mare fill (Wieczorek and Phillips 1999), consistent with the suggestion that viscous stress relaxation was important only within the Procellarum KREEP Terrane.

The final piece of evidence for significant viscous relaxation within the PKT is a qualitative one. Haskin *et al.* (2000) recognized that there are very few highland structures that breach lava flows within this region, which is somewhat surprising as the thickness of the mare is inferred to be relatively thin (see Section 2.4). While these lavas would completely cover some ancient impact structures, if the pre-mare topography within the PKT were similar to that of the surrounding highlands, then highland exposures would still be expected. Since this is not the case, they reasoned that this initially high standing surface topography might have viscously relaxed as a result of high crustal temperatures.

5.1.3. Are the Procellarum basalts thorium rich? The evidence presented in the previous sections seems to suggest that a large portion of the crust within the Procellarum KREEP Terrane is enriched in incompatible elements. Lunar Prospector gamma-ray data further show that the upper meter of the mare regolith in this region has a moderate Th enhancement as well (~ 3 to 7 ppm in the most FeO-rich regions). Somewhat surprisingly, though, almost all of the crystalline mare basalts in the Apollo sample collection have Th abundances less than ~ 2 ppm, including those from the Apollo 12 mare site that lies within this terrane (e.g., Jolliff *et al.* 2001). All of the basaltic lunar meteorites for which data exist similarly have a low abundance of Th (recall that more than 60% of the mare basalts by area erupted within the 16% surface area of the PKT). A major question is thus whether some of the basalts in Oceanus Procellarum are enriched in a KREEP component, or if the surface enrichment as observed from orbit is merely the result of vertical mixing with an underlying KREEP-rich substrate. The resolution of this question has very fundamental implications for lunar magmatic processes. If it turns out that these basalts are indeed enriched in KREEP, then either the mare source region was

KREEP-rich as well, or these basalts assimilated a substantial quantity of incompatible elements as they traversed the crust. Alternatively, if the basalts in this region are similar to those collected by Apollo, then the heat source for their generation may have been from the overlying crust (Wieczorek and Phillips 2000).

Either side of this debate can be reasonably defended (see Haskin et al. 2000; Jolliff et al. 2000a; Wieczorek and Phillips 2000), and it may turn out that reality lies between these two extremes. Evidence in favor of the eruption of Th-poor basalts in this region includes the apparent paucity of Th-rich mare basalts in the Apollo, Luna, and lunar meteorite sample collections. Perhaps more telling, though, is the nature of samples returned from the Apollo 12 landing site. Orbital gamma-ray data imply a surface Th concentration of ~6 ppm for this site (Jolliff et al. 2000b), which is consistent with the soils that were collected there (see also Chapter 2). However, these soils were found to represent a mixture between locally derived Th-poor mare basalts and a KREEP-rich nonmare component (e.g., Hubbard and Gast 1971; Hubbard et al. 1971; McKay et al. 1971; Meyer et al. 1971; Evensen et al. 1974; Jolliff et al. 2000a). As the mare basalts at this locale are relatively thin, it is possible that local impact craters could have excavated this KREEP-rich component from the underlying crust (e.g., Wasson and Baedecker 1972), or incorporated material through vertical mixing of buried ejecta horizons produced by large nearby craters such as Lansberg and Reinhold (Jolliff et al. 2000b). Part of the KREEP component at the Apollo 12 site might also be derived from a ray of Copernicus (Wentworth et al. 1994).

Alternatively, two pieces of evidence give support to the view that the mare basalts in the Procellarum KREEP Terrane possess high abundances of incompatible elements. Firstly, remotely sensed data indicate that some of the basalts in this region have both high concentrations of FeO (~20–22 wt%) and Th (~5 ppm). Such a composition could in principle be derived by mixing atypically high FeO basalts (>23 wt%) with KREEP-rich materials such as monzogabbro (QMD) and/or granite (35–40 ppm Th). However, QMD and granite are rare in the Apollo sample collection and it is unlikely that they are abundant in any significant quantity underlying the expansive mare basalts in Oceanus Procellarum. Secondly, although crystalline KREEP-rich mare basalts are not common in the sample collection (with the exception of the Apollo 11 high-K group (3.3–4.8 ppm Th, see Section 3.1), this fact can not be used to conclude that basalts with higher concentrations are not common elsewhere. Some Th- and FeO-rich volcanic and impact glasses with basaltic compositions do occur in the Apollo samples (Delano et al. 1982; Jolliff et al. 1991b) suggesting that this putative crystalline rock might be more common than the Apollo and lunar meteorite collections imply.

5.1.4. Origin and evolution of the Procellarum KREEP Terrane. The enrichment of incompatible elements and the unique volcanic history of the Procellarum KREEP Terrane bear strongly on the origin and evolution of this province. In particular, the observation that KREEP-rich materials are only abundant within this region of the Moon seems to suggest that the final dregs of the lunar magma ocean ultimately accumulated within this region. While it is difficult to dispute that this happened, the process by which this occurred is not forthcoming (see Chapter 4). One possible explanation is that the crust in this region might have been thinner than typical, perhaps because of a now unrecognizable Procellarum impact event. Hydrostatic forces would then have caused a KREEP-rich magma sandwiched between the crust and mantle to accumulate beneath this region (Warren 2001). Alternatively, the last remaining dregs of the lunar magma ocean may have accumulated above a degree-1 downwelling of dense ilmenite cumulates (Parmentier et al. 2002).

If the mafic impact-melt breccias are representative of the crust within the PKT, and if we take the mixing-model results of Korotev (2000) literally, then one third of the crust in this region is composed of anorthositic upper crustal materials, with the remainder being of a composition similar to Apollo 15 KREEP basalt. Assuming an average crustal thickness of

40 km for this region, this translates to the equivalent of ~13 km of feldspathic upper crust and ~27 km of KREEP basalt. As a result of the high abundance of incompatible elements in KREEP basalt (~12.4 ppm Th), this material could have remained partially molten up until at least the time of the Imbrium impact (e.g., Solomon and Longhi 1977; Wieczorek and Phillips 2000; Hess and Parmentier 2001). This is consistent with the observation of Ryder (1994) that the Imbrium impact event induced KREEP-basaltic volcanism in this region, most likely by denuding a subcrustal KREEP-basalt magma chamber. The slow crystallization of this subcrustal KREEP-basalt layer could have given rise to the Mg- and alkali-suite rocks that were most likely exhumed by the Imbrium impact event (e.g., Snyder *et al.* 1995a,b). Additionally, the large range of crystallization ages for these rocks (~3.9 to 4.4 Ga e.g., Nyquist and Shih 1992; Snyder *et al.* 2000) are consistent with such a protracted period of crystallization. As the Imbrium basin was the last basin forming event to have excavated deeply into the crust of this region, we would not expect to find Mg- and alkali-suite rocks any younger than the ~3.84 Ga age of this basin. Indeed, it is very likely that Mg- and alkali-suite plutonism extended beyond ~3.9 Ga.

The high abundance of radioactive elements in the Procellarum KREEP Terrane also appears to be related to the voluminous and protracted volcanic history of this province. Wieczorek and Phillips (2000) demonstrated that the inferred heat production of this province was more than sufficient to melt the underlying mantle over the duration of observed mare volcanism. Similarly, Parmentier *et al.* (2002) have shown that if the magma-ocean ilmenite cumulates sank beneath the PKT, carrying with them a significant quantity of incompatible elements, melting of the mantle beneath this region would naturally occur as well. These models are discussed further in Chapter 4.

Finally, we note that extensive melting of the mantle beneath the Procellarum KREEP Terrane would have drastically altered its composition. In the most extreme case, massive melting would leave a residuum composed solely of olivine, with its Mg-number depending upon the degree of melt extraction. This appears to be consistent with the inference of Korotev (2000) that the mantle beneath this region is composed of a highly forsteritic dunite. Alternatively, it is possible that this high-magnesium dunite could be related to a possible overturn of magma-ocean cumulates (Hess and Parmentier 1995). Figure 7.5 (in Chapter 7) shows an interpretative and highly idealized cross section of the crust and mantle beneath the Procellarum KREEP Terrane.

5.2. The Feldspathic Highlands Terrane

The Feldspathic Highlands Terrane differs from the Procellarum KREEP Terrane primarily by its ancient age, feldspathic composition, limited post magma-ocean magmatism, and low abundances of incompatible elements (Jolliff *et al.* 2000a). Other representative characteristics include both its high albedo and extensively cratered terrain. The confines of this terrane are based primarily upon the Clementine-derived iron abundance data and, as is shown in Color Plate 3.10, span more than 60% of the surface area of the Moon. In contrast to the PKT, less than 10% of this area is covered by mare basalts, and those mare deposits that are present erupted primarily during the Imbrian period (Wilhelms 1987). With the exception of these minor mare deposits, the feldspathic Apollo samples and lunar meteorites that make up this terrane have crystallization ages of about 4.4–4.5 Ga (e.g., Nyquist and Shih 1992).

Based on surface FeO abundances, Jolliff *et al.* (2000a) have distinguished between a central anorthositic portion, and an outer slightly more mafic region of the Feldspathic Highlands Terrane. The central anorthositic portion has some of the lowest FeO abundances on the Moon, averaging ~4.2 wt% FeO, and is centered on the farside near 40°N and 180°E where the crust is inferred to be its thickest (see Section 2.7). Flanking this central region to both the west and east, the outer portion of this terrane is seen to be slightly more mafic, having an average FeO abundance of ~6 wt%. Since the outer portion of the Feldspathic Highlands

Terrane is inferred to have a thinner crust than the central portion, the ejecta blankets of large impact basins in the outer region are likely to contain a greater quantity of material derived from the lower crust, which is expected to be somewhat more mafic.

The composition of the upper crust of the Feldspathic Highlands Terrane has been estimated from both sample and remote sensing studies. Firstly, an average of the five most feldspathic meteorites, which are presumably derived from this terrane, imply that the upper crust is composed of ~28 wt% Al_2O_3 , or 82.5% plagioclase (Korotev 2000). Secondly, based on the Clementine-derived ~4.2 wt% FeO abundance for the central portion of this terrane, as well as an empirical correlation between FeO and Al_2O_3 in the Apollo sample collection (Korotev 1999), Jolliff et al. (2000a) estimated an Al_2O_3 abundance of ~29 wt%. Finally, based on the composition of central peaks, which are inferred to have an upper-crustal origin beneath a slightly more mafic surficial regolith (see Section 2.8.4; Wieczorek and Zuber 2001a), the abundance of Al_2O_3 is constrained to lie between 28.5 and 32.2 wt%, corresponding to a modal abundance of $87 \pm 4\%$ plagioclase.

The lower portion of the Feldspathic Highlands Terrane is likely to be more mafic than its upper portion. This inference is supported primarily by the somewhat more mafic composition of ejecta from large impact basins (e.g., Bussey and Spudis 2000), the mafic compositions of some central peaks (e.g., Tompkins and Pieters 1999) and the noritic floor of the South Pole-Aitken basin (e.g., Pieters et al. 2001). Based on central peak compositions and crustal thickness modeling, the lower portion of the crust appears to have a high abundance of noritic materials and a relatively low abundance of gabbroic materials (see Section 2.8.4, Wieczorek and Zuber 2001a). This implies that the lower portion of crust in this terrane does not contain a significant quantity of mare basaltic intrusions, which is consistent with the scarcity of basaltic lavas found there. The most-mafic portion of the lower crust from this study is inferred to have a composition of 18.2–24.7 wt% Al_2O_3 , corresponding to a modal abundance of $65 \pm 8\%$ plagioclase. Figure 7.4 (in Chapter 7) shows an interpretative and highly idealized cross section of the crust and mantle beneath the Feldspathic Highlands Terrane.

5.2.1. South Pole-Aitken basin. The South Pole-Aitken basin on the lunar farside is unique in terms of its surface composition and geophysical character, and it looms large in debates about the structure of the lunar crust. Although its precise age is not known, superposition relationships mark it as the oldest of the topographically well-preserved lunar impact basins. With a 2100–2500 km diameter and 12–14 km total vertical relief (Spudis et al. 1994; Wieczorek and Phillips 1999), it is the largest recognizable impact structure in the solar system.

The first studies using Clementine derived FeO and TiO_2 concentrations (Lucey et al. 1998b) indicated that upper-mantle materials were likely to be a part of the mixture making up the basin floor. However, absolute FeO abundances based on Lunar Prospector gamma-ray data (which lie between ~6 and 12 wt% FeO) have since shown that the Clementine derived abundances for this basin were overestimated. This is likely a result of this region possessing a mineralogy that differs from the Apollo and Luna sites, which were employed in calibrating the Clementine-based FeO determinations. In particular, it appears that higher proportions of orthopyroxene are present within this basin when compared to most of the Apollo sites where clinopyroxene and olivine are more significant (see Chapter 2). Investigations of South Pole-Aitken basin rock types using combined remotely sensed mineralogy and compositions derived from Lunar Prospector data indicate that the basin, despite its great size, probably penetrated mainly into a noritic lower crust (Pieters et al. 1997, 2001) and that if mantle rocks are present, or incorporated into the melt sheet, they are not abundant. However, the precise mineralogy of the basin floor is still debatable, as mineralogical mapping using Clementine multispectral data imply that clinopyroxene might be significantly more abundant than previously thought (Lucey 2004). If true, this may be suggestive of a widespread basaltic component mixed with noritic lower crustal materials.

Questions remain as to the nature of the lower crust of the Moon and its relationship to the materials exposed in the South Pole-Aitken basin. While this basin clearly differs from the Th-rich Procellarum KREEP Terrane, its abundance of Th is slightly enhanced compared to the surrounding highlands (~2–3 ppm vs. <1 ppm). Whether the exposed crust there is typical of the deep crust of the Feldspathic Highlands Terrane is not known, but we think that this is likely for several reasons. Firstly, geophysical crustal thickness modeling suggests that this basin did not excavate all the way into the mantle as approximately 25 km of crustal materials are predicted to underlay the floor of this basin (see Section 2.7). Secondly, the high-standing topography and inferred thickened crust northeast of this basin has been interpreted as representing the ejecta from an oblique SPA impact (Zuber *et al.* 1994; Schultz 1997). As this putative ejecta deposit has some of the lowest iron abundances on the Moon, it is unlikely that there is a significant mantle component within it (Wieczorek and Phillips 1999). Thirdly, the dual-layered crustal thickness model presented in Section 2.7 implies that the floor of this basin should be almost exclusively composed of lower crustal materials. And finally, the central peak of Bullialdus, which is inferred to have a lower crustal origin (see Section 2.8.4), has a composition similar to the floor of this basin.

While we can not dismiss the possibility that this basin might have excavated into the mantle (e.g., Lucey *et al.* 1998b), we think that the evidence is currently against this hypothesis (see Lucey 2004). Nevertheless, even if the material that is exposed in this basin is derived largely from the lower crust, we recognize that this impact event would likely have reprocessed this material in some manner. In particular, the floor of this basin could represent a giant impact melt sheet that might have partially differentiated (Morrison 1998). Even though the mantle was probably not excavated in this impact event, it is still possible that impact melting of the underlying mantle may have occurred.

5.2.2. Origin and evolution of the Feldspathic Highlands Terrane. The feldspathic composition and ancient age of materials that comprise the Feldspathic Highlands Terrane is consistent with it having a magma-ocean flotation-cumulate origin. Unlike the Procellarum KREEP Terrane, which has been heavily modified by post-magma-ocean magmatism, extrusive and intrusive volcanic products are comparatively rare within this terrane. Furthermore, the duration of mare volcanism within the Feldspathic Highlands Terrane seems to have been limited primarily to a relatively short period of time within the Imbrian period. Because this terrane dates to the time of primary differentiation, its surface has been affected heavily by numerous large impact events, including the event that created the giant South Pole-Aitken basin. Regardless, this terrane probably represents the best example of a primary differentiation crust within our solar system.

The available evidence seems to suggest that the crust of the Feldspathic Highlands Terrane becomes more mafic and noritic with depth. Furthermore, if the floor of the South Pole-Aitken basin is representative of lower crustal materials, then thorium abundances grade from <1 ppm in the upper crust to ~2–3 ppm in the lower crust. A major question regarding this terrane is the origin of this compositional zonation, and several hypotheses have been advanced to explain this observation. One hypothesis advocated by Head and Wilson (1992) is that the mafic character of the lower crust could be a consequence of numerous basaltic intrusions. However, as gabbroic lithologies are relatively rare in the lower portion of the crust (<5% by volume, see Section 2.8.4), this interpretation is probably not correct. Many investigators have also suggested that the deep crustal rocks of this terrane could be composed of Mg-suite plutonic rocks (e.g., Reid *et al.* 1977; Ryder and Wood 1977). However, most Mg-suite rocks appear to be genetically related to the petrogenesis of KREEP, and these rocks are most likely to reside exclusively within the Procellarum KREEP Terrane (e.g., Jolliff *et al.* 2000a; Korotev 2000; Wieczorek and Phillips 2000).

An alternative explanation for the mafic character of the lower crust is that this might

simply be a result of cumulate flotation in a chemically evolving lunar magma ocean (Wieczorek and Zuber 2001a). In particular, as the magma ocean crystallized, it should have become both increasingly FeO rich and dense (Warren 1990). In order for an assemblage of minerals to float in this magma and accrete to the underlying crust, its bulk density must be less than that of the surrounding magma. Thus, as the residual magma ocean became more dense, and the crust grew downward, the proportion of mafic cumulates that could be incorporated into floating mineral assemblages would have increased. Furthermore, since the magma ocean would have become increasingly enriched in incompatible elements as crystallization proceeded, the deepest flotation cumulates would be expected to contain a greater quantity of thorium and other incompatible elements.

Finally, it is possible that the observed chemical zonation of the crust could have been achieved by the mechanical separation of feldspathic and mafic phases after the crust was largely formed. As a result of high crustal temperatures early in lunar history, if anorthosites were present in extensive discontinuous bodies, they could have buoyantly rose through the crust while their mafic complements would have sunk (e.g., Longhi 1980; Longhi and Ashwal 1985).

5.3. Bulk composition: Th and Al mass balance

Based upon a number of assumptions that were not too controversial at the time, Taylor (1982) argued that the Moon is enriched in refractory elements when compared to the terrestrial primitive mantle by about a factor of two. In particular, Al_2O_3 and Th abundances of 6 wt% and 125 ppb were obtained, respectively, for the Moon, in contrast to 3.6 wt% and 64 ppb for the primitive terrestrial mantle. Though a similar conclusion was obtained by Drake (1986), Warren and Rasmussen (1987) later argued for a more terrestrial-like composition based upon revised globally-averaged heat-flow estimates. One commonality among these studies is that they are strongly dependent upon estimates of the average thickness of the crust, the composition of the highlands crust, and the present day mean heat flow. In light of results from the Clementine and Lunar Prospector missions, as well as reanalyses of the seismic data which point to a thinner crust, it is clear that some of the assumptions employed in these models may need revision. Indeed, due to the added complexity of the inferred structure of the Moon as portrayed in Color Plate 3.10, the bulk composition of the Moon is perhaps less agreed upon today than it was a decade or more ago.

The most significant recent development concerning the bulk composition of the Moon was the realization that the crust and mantle are not as uniform in composition as once thought. Some recent mass-balance calculations based on surface remote sensing data, and using the concept of distinct crustal terranes (Jolliff et al. 2000a; Jolliff and Gillis 2002; Taylor et al. 2002), have come to similar conclusions as Taylor (1982). On the other hand, others (Warren 2000; Warren and Humphrys 2003) have argued for a more nearly chondritic or terrestrial mantle-like composition. Given the lack of direct samples of the lunar mantle, our limited spatial sampling of lunar basalts, our current uncertainty in the average thickness of the crust, and the unfortunate locations of the Apollo heat flow measurements, it is perhaps not at all surprising that such divergences exists. Many of the parameters that are input into these bulk compositional models are educated guesses, and variations of nearly a factor of two can often be justified.

Given these caveats, it is probably more important to understand the greatest sources of uncertainty inherent in these calculations than it is to advocate one bulk compositional model over another. As the bulk Th and Al abundances are key to deciphering the bulk composition and origin of the Moon, a few simple examples will be given here that demonstrate how fundamental uncertainties associated with key model parameters affect these calculations.

5.3.1. Aluminum. Since a significant portion of the lunar aluminum budget resides in the crust, its bulk concentration will necessarily be dependent upon the assumed average crustal thickness. Recent reanalyses of the Apollo seismic data have revised the crustal thickness

at the Apollo 12 and 14 sites down from 60 km to 45 ± 5 km (Khan *et al.* 2000), 38 ± 3 km (Khan and Mosegaard 2002), and 30 ± 2.5 km (Lognonné *et al.* 2003). A global extrapolation of these numbers in geophysical crustal thickness modeling then requires the assumption that the density of the crust and mantle are uniform. Thus, any mean crustal thickness estimate should probably be considered to be uncertain by at least ± 10 km. For illustrative purposes, if we assume the crust to be composed of 29 wt% Al_2O_3 , then a reduction in the average crustal thickness of 10 km will reduce the bulk lunar Al_2O_3 content by about 0.4 wt%.

While the concentration of Al_2O_3 in the upper crust is somewhat agreed upon, it appears that the lower crust of the Moon is less feldspathic, and its composition is not as well known (see Section 2.8.4). Taking this into account, a reasonable uncertainty of 3 wt% for the bulk Al_2O_3 content of the crust (see for example Table 3.12) would correspond to an additional uncertainty of about 0.2 wt% in terms of the bulk lunar Al_2O_3 composition. If we assume a uniform composition crust with an average thickness of 30 and 60 km, then the contribution of the crust to the lunar bulk Al_2O_3 abundance could lie anywhere between about 1.2 and 2.2 wt%, respectively.

An additional complexity regarding the bulk Al concentration of the Moon concerns the deep lunar interior. Mantle Al_2O_3 abundances have been estimated by the thermodynamic-seismic investigations of Kuskov and coworkers (e.g., Kuskov and Kronrod 1998) and Khan *et al.* (2006), and we here take the differences between these studies as an indication of the uncertainty in this value. Kuskov and Kronrod (1998) presented two best-fit models (see Section 3.2.2) whose chemical compositions were defined to be constant within the three mantle seismic velocity layers of Nakamura *et al.* (1982) (58–270 km, 270–500 km, and greater than 500 km). Their abundances correspond to 2.5 and 2 wt% Al_2O_3 for the upper mantle, 3.3 and 3.1 wt% for the middle mantle, and 5.1 and 5.3 wt% for the lower mantle. In contrast, Khan *et al.* (2006) found abundances that are higher by a factor of ~ 2 , with a most probable value of ~ 6 wt% for the upper 600 km of the mantle and ~ 11 wt% for the lower mantle.

For the calculations to follow, we assume that the Moon possesses a 50 km thick crust, a metallic core of radius 350 km, and a constant density mantle. We find that the difference between the two mantle compositions of Kuskov and Kronrod (1998) leads to an uncertainty in the bulk lunar Al_2O_3 concentration of only ~ 0.3 wt%. In contrast, the difference between the models of Kuskov and Kronrod (1998) and Khan *et al.* (2006) is considerably larger at about 3.5 wt%. For the models of Kuskov and Kronrod (1998), the contribution of the mantle to the bulk Al_2O_3 abundance is about 3.3–3.6 wt%, whereas for the model of Khan *et al.* (2006) it is about 6.8 wt%.

These examples demonstrate that the largest uncertainty in calculating the bulk aluminum concentration of the Moon resides not in the thickness and composition of the crust, but in the composition of the mantle. Nevertheless, tentative conclusions can be made. By employing the minimum mantle Al_2O_3 abundance of Kuskov and Kronrod, as well as the minimum crustal abundance noted above, the minimum bulk lunar Al_2O_3 concentration should be ~ 4.5 wt%. This is greater than the value of ~ 3.6 wt% for the bulk silicate Earth (Taylor 1992), but is less than the value of 6 wt% that was advocated by Taylor (1982) for the Moon. If the results of Khan *et al.* (2006) are correct, then the Moon is likely to have a bulk concentration of Al_2O_3 that is even greater than the model of Taylor (1982).

5.3.2. Thorium. As a large portion of the lunar incompatible elements is sequestered in the crust, bulk compositional models for these elements are dependent upon the average crustal thickness and composition. As an example, consider the average thorium abundance for the Feldspathic Highlands Terrane. While the surface abundance of this element is well known as a result of the Lunar Prospector measurements, the thorium concentration with depth in this terrane is less certain. If the floor of the South Pole-Aitken basin is representative of the lower crust, then the thorium concentration grades from less than ~ 1 ppm in the upper crust to about

2 or 3 ppm in the lower crust. If we assume that the lower crust is uniform in composition with a thickness of 25 km, a 1 ppm uncertainty in its composition would result in a bulk Moon uncertainty of 30 ppb. Furthermore, if we assume an average 1 ppm thorium abundance for the entire crust, then a change in crustal thickness of 10 km would correspond to a change in the bulk Th abundance of ~10 ppb.

The situation is considerably worse when one considers the uncertainties associated with the Procellarum KREEP Terrane as both its areal extent and crustal composition are highly uncertain. While many of the highland exposures within this region are likely to be composed of Imbrium ejecta, it is not clear how representative this material is in terms of the average crustal composition there. A plausible range of bulk Th abundances for this terrane is between 4 ppm (similar to that used in Jolliff et al. 2000a) and ~7 ppm (corresponding to a 50-50 mixture of KREEP basalt and feldspathic materials). Assuming that the crust of the PKT is on average 40 km thick, and that it occupies 10% of the surface area of the Moon, an uncertainty of 3 ppm Th for the PKT would correspond to an uncertainty in the bulk Th abundance of the Moon of ~20 ppb. An uncertainty in the crustal thickness of 10 km would correspond to an additional uncertainty of ~5–10 ppb. In addition, if we were to assume that the PKT had a slightly greater surface area of 15%, then the bulk lunar Th abundance would be increased by about 10–20 ppb.

Although direct samples of the lunar mantle have not been found among the sample collections, its geochemistry can be estimated from the composition of the lunar basalts. If primary melts of the mantle could be identified, then melt-solid distribution coefficients could be employed to back out the composition of its mantle source. In practice, though, the abundance of Th in a typical primary melt (as obtained from the picritic glasses), as well as the appropriate distribution coefficients, are both uncertain by a factor of at least two. While mantle Th abundances are expected to be low, the large volume of the mantle compensates this. In particular, the difference between a mantle possessing 40 ppb (e.g., Jolliff et al. 2000a) vs. 25 ppb Th (e.g., Warren and Wasson 1979b) simply corresponds to a bulk Moon difference of ~15 ppb.

It is thus clear that the bulk Th abundance of the Moon, which is principally based upon remote-sensing measurements, could be uncertain by a large amount. Although it is probably unreasonable to presume that all of the above sources of error would add constructively, giving rise to a maximum error of ~100 ppb Th, it is probably equally unlikely to assume that these uncertainties are distributed in a Gaussian manner, in which case the expected error would be about 50 ppb. In any case, this exercise demonstrates the difficulties involved in estimating the bulk thorium concentration of the Moon, and suggests that such studies cannot distinguish unambiguously between Taylor's enriched model (125 ppb) and that of a terrestrial primitive mantle composition (64 ppb). Nevertheless, as both Al and Th are refractory lithophile elements, if the Moon is enriched in Al, as appears to be the case, then it would be reasonable to also expect a corresponding enrichment in Th.

6. MAJOR RECENT ADVANCES IN LUNAR SCIENCE, UNANSWERED QUESTIONS, AND FUTURE DEVELOPMENTS

Prior to the Apollo missions, little was known of the composition and internal structure of the Moon. The wealth of data collected during Apollo led to a rapid increase of understanding in this regard, showing that, like the Earth, the Moon also possesses a crust, a mantle, and possibly even a small metallic core. The feldspathic composition of the crust quickly gave rise to the idea that a large portion of the Moon was initially molten, and this magma-ocean concept has since been the guiding paradigm under which most data are now interpreted.

The Clementine and Lunar Prospector missions have similarly led to great advances in understanding of the structure, composition, origin, and evolution of the Moon. Though one

might presume that this was the result of collecting new types of data, these missions merely completed the orbital reconnaissance that was initiated during Apollo. Topography, gravity, gamma-ray, magnetometer, electron-reflectometer, and spectral reflectance data were all acquired during the Apollo era, but these were either limited to swaths near the equator or to the Moon's Earth-facing hemisphere. During the 1990s, these measurements were extended globally for the first time and have shown that the traditional dichotomous mare-highland classification is inadequate in describing the structure and geologic evolution of this body. Large regions were found to possess distinctive geological characteristics, and these are inferred to be the result of either asymmetries associated with a crystallizing magma ocean, or later large impact events.

Much of what has been reported on in this chapter is the result of data collected from Clementine and Lunar Prospector, the continued analysis of the lunar samples, and the reanalysis of key geophysical datasets. Below we list some of the key advances in lunar science that have been made since the Apollo era, and some of the key scientific questions that have yet to be resolved.

6.1. Major advances in lunar science

1. The origin and evolution of the lunar crust and interior can be best understood by dividing the crust and underlying mantle into three major geological provinces: the Procellarum KREEP Terrane, the Feldspathic Highlands Terrane and the South Pole-Aitken basin.
2. The Procellarum KREEP Terrane encompasses Mare Imbrium and Oceanus Procellarum and is characterized by its high abundance of incompatible and heat-producing elements, its temporally extended volcanic history (from ~4.2 Ga to <900 Ma), the nearly complete basaltic resurfacing of this region, and the prevalence of Ti-rich lava flows.
3. The Feldspathic Highlands Terrane is characterized by its ancient age (>4.3 Ga) and highly feldspathic composition. It probably represents the primary magma-ocean flotation crust of the Moon, and has been altered only by subsequent impact processes and minor quantities of mare volcanism. The available evidence suggests that the crust of this terrane becomes increasing mafic with depth.
4. The South Pole-Aitken basin is not only the largest impact structure recognized on the Moon, but also in the solar system, with a diameter slightly larger than that of the Hellas basin on Mars. However, even though this basin has a diameter of over 2100 km, it does not appear to have excavated all the way through the lunar crust. The basin floor is noritic in composition, and this likely reflects the composition of the deep crust within the Feldspathic Highlands Terrane.
5. Seismic data demonstrate that the Moon possesses substantial internal structure. At the Apollo 12 and 14 sites within the Procellarum KREEP Terrane, the crust is about 30 to 40 km thick, and there is some evidence for an intracrustal seismic discontinuity ~20 km below the surface. The upper 500 km of the mantle beneath the Procellarum KREEP Terrane appears to have a nearly constant seismic velocity, suggesting that this region has a relatively uniform composition. A major seismic discontinuity is located about 500 km below the surface that most likely represents a change in mantle composition. Beneath a depth of ~1150 km, the mantle may be partially molten.
6. Many pieces of evidence suggest that the Moon possesses some form of a dense, molten, and high-electrical-conductivity core whose radius is less than 400 km.

6.2. Unanswered questions

1. *Is the surface distribution of KREEP representative of the underlying crust?* Although gamma-ray data collected from orbit shows that the surface abundance of incompatible and heat-producing elements are concentrated within the Procellarum KREEP Terrane, it is possible that the subcrustal distribution of KREEP could be more widespread than these data suggest.
2. *What is the provenance of the magnesian-suite rocks?* Since most of the Mg- and alkali-suite rocks appear to have some form of genetic relationship to KREEP, these samples probably originated within the Procellarum KREEP Terrane. Nevertheless, using the available remote-sensing data, it is uncertain as to whether or not this suite of rocks (possibly with lower abundances of incompatible elements) will be found at other locales on the Moon.
3. *What is the composition and origin of the lower crust?* Though many lines of evidence suggest that the lower portion of the feldspathic crust is more mafic and noritic than its upper portion, we do not have any samples of this important rock type. Though a more mafic lower crust is compatible with cumulate flotation in a chemically evolving magma ocean, its origin can only be definitively answered by chemical analyses of these crustal rocks.
4. *What is the composition of the South Pole-Aitken basin?* The floor of the South Pole-Aitken basin has been inferred to be largely composed of noritic materials, though recent mineralogical mapping suggests that clinopyroxene abundances may be significantly higher than previously thought. Its composition might be representative of the lower crust of the Feldspathic Highlands Terrane, although at present it cannot be ruled out that its composition is unique, and that it might contain components from the upper mantle. As suggested by the recent NAS Decadal Survey (National Research Council 2003), a mission to sample and return materials from the SPA Terrane would probably answer this question. Although lunar meteorites provide several samples of the Feldspathic Highlands Terrane, none yet appear to sample materials of the SPA basin.
5. *What is the composition and depth of origin of the farside and young nearside basalts?* Many different types of mare basalts are represented within the sample collections, yet key mare deposits remain unsampled. The volcanic history of the Procellarum KREEP Terrane differs dramatically from that of the Feldspathic Highlands Terrane, and samples of basalts that erupted on the lunar farside would help elucidate at what depths melting there occurred, as well as the composition of the farside mantle. Samples of the youngest basalts within the Procellarum KREEP Terrane would help constrain how mare volcanic processes have evolved with time within this geologic province.
6. *What is the origin and lateral extent of the 500-km seismic discontinuity?* Seismic velocity profiles beneath the Procellarum KREEP Terrane imply that a major seismic discontinuity occurs ~500 km below the surface. Models of the lunar interior imply that this discontinuity is compositional in origin, with the deeper mantle containing a higher abundance of Al and/or Mg. One possibility is that this boundary could represent the maximum depth of the lunar magma ocean. Alternatively, if the magma ocean was global in extent, then this depth might mark the transition between early olivine- and later orthopyroxene-rich cumulates. Finally, it is possible that this discontinuity might correspond to the maximum depth of melting within the post-magma-ocean mare source. If the latter explanation is correct, then the discontinuity may only be locally present beneath the Procellarum KREEP Terrane.

7. *What is the size and composition of the core, and was there ever a core dynamo?* While the available data imply that the Moon has a dense, molten, and high electrical-conductivity core, we do not know the composition of this core. Though it may be composed of metallic iron (with some amount of alloying Ni, S, and C), the geophysical data can also be reconciled with a core composed of a dense molten Ti-rich silicate magma. In support of this latter hypothesis, some magmatic evolution models of the Moon suggest that late Ti-rich magma-ocean cumulates may have sunk through the mantle, possibly to the center of the Moon. It is presently unclear if the crustal magnetizations are related to an internal core dynamo, or to processes associated with impact cratering.

The above lists demonstrate that even though we appear to have a good understanding of the composition and internal structure of the Moon, fundamental questions of first-order importance remain unanswered. While the answers to some of these questions might be inferred by the continuing analyses of existing datasets, the next big leap forward in lunar science will certainly occur with the collection of additional data from both the surface and orbit.

Below we list what we think are the most important science objectives that should guide the future scientific exploration of the Moon. We divide these into two main categories. The primary science objectives will almost certainly lead to a dramatic, and possibly revolutionary, understanding of the Moon. These objectives will require the collection of samples from the lunar surface, and the emplacement of a network of geophysical stations. While these goals might be achievable by robotic means, human exploration would be desirable. In contrast, many of the other scientific objectives can be achieved either from lunar orbit or from advances in technology on Earth.

6.3. Primary science objectives

1. *Determine the composition of the South Pole-Aitken Basin.* Knowledge of the composition of the floor of this basin will address many questions: Did this basin excavate into the mantle? Is the basin floor composed of ferroan or magnesian rocks? Is the floor of this basin typical of lower crustal materials? If so, how does this composition relate to the lunar magma ocean? Although some progress in deciphering the character of the South Pole-Aitken basin could be achieved by acquiring higher precision spectral reflectance, gamma-ray, and X-ray fluorescence data, the questions above will only be definitively resolved by the collection and analysis of samples. Samples from locations interior to the basin may consist of impact-melt rocks formed by the SPA event, perhaps reworked and excavated from depth by later cratering, whereas samples from outside the basin may represent materials ejected from deep within the crust and/or mantle.
2. *Determine the global seismic velocity structure of the lunar interior.* The Apollo seismic network only spanned a small region of the Moon that straddled the Procellarum KREEP and Feldspathic Highlands Terranes. Thus, it is not clear as to whether the inferred seismic velocity structure beneath this network is representative of either of these regions. A network of about 10 short-period seismometers operating for close to a decade would provide data on which to base much improved estimates of the crustal thickness at diverse sites, constrain the size, composition and physical state of the core, and determine whether the seismic velocity structure of the mantle differs beneath the major geologic terranes. A single long-period seismometer or superconducting gravimeter operating for about a year might also be able to measure lunar free oscillations excited by shallow moonquakes and meteoroid impacts. Such data would increase our knowledge of both the density and rigidity structure of the Moon.
3. *Determine the heat flow at various locations within the major terranes.* The heat flow of the Moon was measured at the Apollo 15 and 17 sites. Unfortunately, these

two sites straddle the Procellarum KREEP and Feldspathic Highlands Terranes, and it is thus not certain if these values are representative of either region. Some thermal models suggest that the heat flow within the heart of the Procellarum KREEP Terrane may be many times greater than was measured at the Apollo 15 site. Heat flow determinations within representative regions of each of these terranes would dramatically improve our understanding of how radioactive elements are distributed within both the crust and mantle, and lead to a better understanding of how the magma ocean crystallized. Multiple heat flow probes in and around the Procellarum KREEP Terrane would additionally help delineate the boundaries of this terrane, and hence place better constraints on the bulk composition of the Moon.

A mission concept currently exists to return samples from the South Pole-Aitken Basin (Duke et al. 2000; Pieters et al. 2003) that follows from the recommendations made in the NAS Decadal Survey (National Research Council 2003). This mission would collect additional remote sensing data over the basin and would return samples from two locations, one interior to, and the other exterior to its excavation cavity. The main objectives would be to date the age of the basin, and determine the composition and mineralogy of the basin impact melt sheet, the lower crustal and/or upper mantle, and the basalts that subsequently erupted there. Samples from relatively homogeneous regions of the surface in this basin would also provide a ground truth for remote sensing studies within this major lunar terrane.

6.4. Other science objectives

1. *Obtain global high precision and high resolution major-element concentrations of the lunar surface.* The primary major elements that are needed to understand the makeup of the surface are Fe, Mg, Ca, and Al. These and other elements can either be measured by an orbiting gamma-ray spectrometer (GRS) or an X-ray fluorescence (XRF) spectrometer. The D-CIXS X-ray fluorescence spectrometer (Grande et al. 2003) onboard the European Space Agency's (ESA) SMART-1 mission is currently collecting data. Furthermore, both XRF and GRS instruments are slated for the Japanese SELENE mission that should be launched in either 2006 or 2007. The XRF instruments will obtain the first such global datasets with a spatial resolution of ~30 km. While the SELENE gamma-ray spectrometer has an approximately six times better energy resolution than the respective Lunar Prospector instrument (~2 keV in comparison to 17.6 keV), as a result of the ~100 km mapping orbit of SELENE, these data will only have a spatial resolution of ~100 km in contrast to ~30 km for the Lunar Prospector data.
2. *Obtain global high spectral-precision spectral reflectance data in order to more accurately infer surface mineralogy.* In combination with global absolute atomic abundances, high spectral-resolution reflectance data will help to more uniquely determine the mineralogy of the surface. An infrared spectrometer on the SMART-1 mission (Keller et al. 2001) currently in orbit about the Moon, is obtaining spectra from 900 to 2400 nm, with a 60 nm spectral resolution and 300 m spatial resolution. The Spectral Profiler onboard SELENE would collect similar data from 500 to 2600 nm, with a 6–8 nm spectral resolution and a 500 m spatial resolution. The Indian Chandrayan-1 mission, planned for launch in 2007, and the US Lunar Reconnaissance Orbiter (LRO), scheduled for launch in 2008, would collect additional multi-spectral data.
3. *Obtain global high-resolution topography.* Whereas the Clementine altimetry data greatly improved knowledge of the shape of the Moon, significant gaps remain in this dataset, especially over the lunar poles. A laser altimeter is expected to accompany the SELENE mission and is designed to acquire data with an along- and cross-track spacing of approximately 2 and 5 km, respectively. Such data would represent a significant improvement over the Clementine dataset that only has an along- and

cross-track shot spacing of ~60 and 20–100 km, respectively. High-resolution topographic data are necessary to interpret the high-resolution gravity data that are currently available over the nearside of the Moon, as well as to delineate where deposits of ice may be found at the poles. The LRO mission would also employ a laser altimeter.

4. *Obtain gravity tracking over the lunar farside.* Currently, there is no direct spacecraft tracking data within ~60° of the center of the lunar farside. This lack of tracking data greatly limits the resolution the global gravity field, lunar crustal thickness investigations, and gravity-topography admittance studies. The SELENE mission is expected to carry a relay subsatellite transponder that would for the first time obtain direct tracking data over the central farside region. Using these tracking data the inferred gravity field is expected to be globally determined to about spherical harmonic degree 70 (in comparison to approximately degree 15 for the current gravity field).
5. *Determine the thickness of the mare basalts.* Knowledge of the thickness of basaltic lava flows on the Moon is necessary to understand its thermal evolution. In addition, by measuring the thickness of basalts within an impact basin, the underlying basin structure is revealed as well. The SELENE Lunar Radar Sounder instrument should accomplish this goal.
6. *Improve knowledge of the lunar core and internal properties by continued LLR ranging and the emplacement of additional retroreflectors on the lunar surface.* With the exception of the collection of additional seismic data, the analysis of lunar laser ranging (LLR) data offers the next best opportunity to further our understanding of the deep lunar interior. As modeling of the lunar ranges requires long spans of data (on the order of six years), and the most accurate of these data were collected over the past few years, continued ranging to the lunar retroreflectors will continue to improve models of the deep mantle and core. The emplacement of additional retroreflectors (~4) would significantly improve the analysis of these data. A ranging station that is currently under assembly should be able to range to lightweight retroreflectors that are smaller than the Apollo arrays (either individual corner cubes or small arrays of corner cubes) with a much higher precision. Another approach using optical transponders could produce a bright signal that would be detectable by the many existing Earth satellite ranging stations that cannot presently range to the Moon. In the future, lightweight retroreflectors could be carried to the surface by small spacecraft while larger payload capabilities could accommodate the transponders needed for stronger signals.
7. *Sample the youngest volcanic rocks within the Procellarum KREEP Terrane and the farside volcanic rocks.* Sampling farside volcanic rocks would enable us to determine if magmatic processes varied beneath the two major geologic terranes of the Moon. At present, it is not certain if farside magmas were derived from a similar source composition and depth as the nearside basalts. Sampling the youngest basalts within the Procellarum KREEP Terrane would additionally elucidate how volcanic processes varied as a function of time within this terrane. Other sampling targets would be regions that possess “extreme” compositions, such as those present within the Aristarchus plateau, Apennine bench, and Compton-Belkovich thorium anomaly.
8. *Obtain global imagery at multiple spatial resolutions and multiple illumination angles.* The primary image data that is used for geologic mapping of the Moon is still the Lunar Orbiter photographs from the 1960s. These images are, however, nonuniform in both spatial coverage and resolution. The Terrain Camera of the SELENE mission is designed to globally image the Moon with spatial resolutions up to 10 meters. Images will be taken under low sun illumination (<30°) and stereo imagery will be useful for constructing high spatial resolution digital elevation

models. Narrow- and wide-angle imaging planned for the LRO mission will provide 0.5-m resolution panchromatic images over selected 5-km swaths and 100-m resolution multi-band imaging over a 100-km swaths, respectively.

Successful SMART-1, SELENE, Chandrayan, and LRO missions[†] may accomplish many of the above scientific objectives within the next few years. Within five years time, it is also likely that technological advances on Earth will improve the collection of laser-ranging data, although the emplacement of additional ranging sites is still highly desirable. The remaining major tasks in lunar exploration will thus be the construction of a global geophysical network that includes both seismometers and heat flow probes, as well as the robotic sampling of a few key rock types (SPA, farside basalts, young basalts) (see also Crawford 2004). With the accomplishment of these tasks, the next logical steps in lunar exploration will likely involve human return to the nearest celestial object in our solar system.

7. ACKNOWLEDGMENTS

We thank the various NASA programs, especially Planetary Geology and Geophysics, and Cosmochemistry, that have supported the research of individual co-authors. Klaus Mosegaard and Philippe Lognonné are thanked for comments and reviews that improved this manuscript.

8. ONLINE SUPPORTING MATERIALS AT WWW.MINSOCAM.ORG

Table A3.1. FAS compositions.

Table A3.2. Magnesian-suite compositions.

Table A3.3. Alkali-suite compositions: alkali anorthosite/norite.

Table A3.4. Alkali-suite compositions: granite/felsite & QMD/monzogabbro.

Table A3.5. KREEP basalt compositions.

Table A3.6. Impact-melt rocks & breccia compositions.

Table A3.7. Granulitic breccia compositions.

Table A3.8. Feldspathic fragmental breccia compositions.

Table A3.9. Lunar meteorite compositions.

Table A3.10. Remote sensing identifications of arthorthosite.

Table A3.11. Mare basalt group compositions.

Table A3.12. Volcanic glass group compositions.

Crustal thickness archive.

9. REFERENCES

- Agee CB (1998) Crystal-liquid density inversions in terrestrial and lunar magmas. *Phys Earth Planet Inter* 107:63-74
 Agrell SO, Scoon JH, Muir ID, Long JVP, McConnell JDC, Peckett A (1970) Observations on the chemistry, mineralogy and petrology of some Apollo 11 lunar samples. *Proc Apollo 11 Lunar Sci Conf* 1:93-128
 Albert RA, Phillips RJ (2000) Paleoflexure. *Geophys Res Lett* 27:2385-2388
 Albert RA, Phillips RJ, Dombard AJ, Brown CD (2000) A test of the validity of yield strength envelopes with an elastoviscoplastic finite element model. *Geophys J Int* 140:399-409
 Allaby A, Allaby M (eds) (1991) *The Concise Oxford Dictionary of Earth Sciences*. Oxford Univ. Press
 Anand M, Taylor LA, Nazarov MA, Patchen A (2003) Petrologic comparisons of lunar mare basalt meteorites Dh-287A and NWA 032. *Lunar Planet Sci XXXIV*:1787
 Anand M, Taylor LA, Neal C, Patchen A, Kramer G (2004) Petrology and geochemistry of LAP 02 205: A new low-Ti mare-basalt meteorite. *Lunar Planet Sci XXXV*:1626

[†] Definition of the LRO and Chandrayan missions has occurred only recently and is on-going, thus we have not attempted to incorporate fully the contributions expected from these missions and their instrument payloads.

- Anders E (1978) Procrustean science: indigenous siderophiles in the lunar highlands according to Delano and Ringwood. *Proc Lunar Planet Sci Conf* 9:161-184
- Anders E, Ganapathy R, Keays RR, Lau JC, Morgan JW (1971) Volatile and siderophile elements in lunar rocks: Comparison with terrestrial and meteoritic basalts. *Proc Lunar Sci Conf* 2:1021-1036
- Anderson DL (1975) On the composition of the lunar interior. *J Geophys Res* 80:1555-1557
- Anderson JD, Lau EL, Sjogren WL, Schubert G, Moore WB (1996a) Gravitational constraints on the internal structure of Ganymede. *Nature* 384:541-543
- Anderson JD, Schubert G, Jacobson RA, Lau EL, Moore WB, Sjogren WL (1998) Europa's differentiated internal structure: Inferences from four Galileo encounters. *Science* 281:2019-2022
- Anderson JD, Sjogren WL, Schubert G (1996b) Galileo gravity results and the internal structure of Io. *Science* 272: 709-712
- Andre CG, Wolfe RW, Andler I (1978) Evidence for a high-magnesium subsurface basalt in Mare Crisium from orbital X-ray fluorescence data. *In: Mare Crisium: The View from Luna 24*. Merrill RB, Papike JJ (eds) Pergamon Press, p 1-12
- Aoshima C, Namiki N (2001) Structures beneath lunar basins: Estimates of Moho and elastic thickness from local analysis of gravity and topography. *Lunar Planet Sci XXXII*:1561
- Arai T, Warren PH (1999) Lunar meteorite Queen Alexandra Range 94281: Glass compositions and other evidence for launch pairing with Yamato 793274. *Meteorit Planet Sci* 34:209-234
- Arkani-Hamed J (1998) The lunar mascons revisited. *J Geophys Res* 103:3709-3739
- Bailey ME, Dunlop DJ (1977) On the use of anhysteretic remanent magnetization in paleointensity determination. *Phys Earth Planet Inter* 13:360-362
- Baker M, Herzberg CT (1980) Spinel cataclasites in 15445 and 72435: Petrology and criteria for equilibrium. *Proc Lunar Planet Sci Conf* 11:535-553
- Baldwin RB (1970) A new method of determining the depth of lava in the lunar mare. *Publ Astron Soc Pacific* 82: 857-864
- Banerjee SK, Swits G (1974) Natural remanent magnetization studies of a layered breccia boulder from the lunar highland region. *Moon* 14:473-481
- Basaltic Volcanism Study Project (1981) Basaltic Volcanism on the Terrestrial Planets. Pergamon Press
- Beard BL, Taylor LA, Scherer EE, Johnson CM, Snyder GA (1998) The source region and melting mineralogy of high-titanium and low-titanium lunar basalts deduced from Lu-Hf isotope data. *Geochim Cosmochim Acta* 62: 525-544
- Beaty DW, Albee AL (1978) Comparative petrology and possible petrogenetic relations among the Apollo 11 basalts. *Lunar Planet Sci Conf* 9:359-463
- Bence AE, Delano JW, Papike JJ, Cameron KL (1974) Petrology of the highlands massifs at Taurus Littrow: An analysis of the 2-4 mm soil fraction. *Proc Lunar Sci Conf* 5:785-827
- Bertka CM, Fei Y (1998) Implications of Mars Pathfinder data for the accretion history of the terrestrial planets. *Science* 281:1838-1840
- Bickel CE, Warner JL (1978) Survey of lunar plutonic and granulitic lithic fragments. *Proc Lunar Planet Sci Conf* 9: 629-652
- Bills BG, Ferrari AJ (1977a) A harmonic analysis of lunar topography. *Icarus* 31:244-259
- Bills BG, Ferrari AJ (1977b) A lunar density model consistent with topographic, gravitational, librational, and seismic data. *J Geophys Res* 82:1306-1314
- Blanchard DP, Budahn JR (1979) Remnants from the ancient crust: Clasts from Consortium breccia 73255. *Proc Lunar Planet Sci Conf* 10:803-816
- Blanchard DP, McKay GA (1981) Remnants from the ancient lunar crust III: Norite 78236. *Lunar Planet Sci* 12:83-85
- Blewett DT, Hawke BR (2001) Remote sensing and geological studies of the Hadley-Apennine region of the Moon. *Meteor Planet Sci* 36:701-730
- Borg L, Norman M, Nyquist L, Bogard D, Snyder G, Taylor L, Lindstrom M (1999) Isotopic studies of ferroan anorthosite 62236: A young lunar crustal rock from a light-rare-earth-element-depleted source. *Geochim Cosmochim Acta* 63:2679-2691
- Borg LE, Shearer CK, Asmerom Y, Papike JJ (2004) Prolonged KREEP magmatism on the Moon indicated by the youngest dated lunar igneous rock. *Nature* 432:209-211
- Bratt SR, Solomon SC, Head JW, Thurber CH (1985) The deep structure of lunar basins: implications for basin formation and modification. *J Geophys Res* 90:3049-3064
- Brett R (1973) A lunar core of Fe-Ni-S. *Geochim Cosmochim Acta* 37:165-170
- Brett R, Butler PJ, Meyer C, Jr., Reid AM, Takeda H, Williams R (1971) Apollo 12 igneous rocks 12004, 12008, 12009, and 10022: a mineralogical and petrological study. *Proc Lunar Sci Conf* 2:301-318
- Buck WR, Toksöz MN (1980) The bulk composition of the Moon based on geophysical constraints. *Proc Lunar Planet Sci Conf* 11:2043-2058
- Budney CJ, Lucey PG (1998) Basalt thickness in Mare Humorum: the crater excavation method. *J Geophys Res* 103: 16,855-16,870

- Burns JA (1986) The evolution of satellite orbits. *In: Satellites*. Burns JA, Mathews MS (eds) Univ. Arizona Press, p 117-158
- Burov EB, Diamant M (1995) The effective elastic thickness (T_e) of continental lithosphere: What does it really mean? *J Geophys Res* 100:3905-3927
- Bursa M (1992) Parameters of common relevance of astronomy, geodesy and geodynamics. *Bull Geod* 66:193-197
- Busse FH (2000) Homogeneous dynamos in planetary cores and in the laboratory. *Annu Rev Fluid Mech* 32:383-408
- Bussey DBJ, Spudis PD (1997) Compositional analysis of the Orientale basin using full resolution Clementine data: Some preliminary results. *Geophys Res Lett* 24:445-448
- Bussey DBJ, Spudis PD (2000) Compositional studies of the Orientale, Humorum, Nectaris, and Crisium lunar basins. *J Geophys Res* 105:4235-4243
- Cameron AGW (1997) The origin of the Moon and the single impact hypothesis, V. *Icarus* 126:126-137
- Cameron AGW (2000) Higher-resolution simulations of the giant impact. *In: Origin of the Earth and Moon*. Canup RM, Righter K (eds) Univ. Arizona Press, p 133-144
- Canup R (2004) Simulations of a late lunar-forming impact. *Icarus* 168:433-456
- Canup RM, Asphaug E (2001) Origin of the Moon in a giant impact near the end of the Earth's formation. *Nature* 412: 708-712
- Canup RM, Esposito LW (1996) Accretion of the Moon from an impact-generated disk. *Icarus* 119:427-446
- Cerroni P, Martelli G (1982) Magnification of pre-existing magnetic fields in impact-produced plasmas, with reference to impact craters. *Planet Space Sci* 30:395-398
- Chowdhary SK, Collinson DW, Stephenson A, Runcorn SK (1987) Further investigations into lunar paleointensity determinations. *Phys Earth Planet Inter* 49:133-141
- Cintala MJ, Grieve RAF (1998) Scaling impact melting and crater dimensions: Implications for the lunar cratering record. *Meteorit Planet Sci* 33:889-912
- Circone S, Agee CB (1996) Compressibility of molten high-Ti mare glass: Evidence for crystal-liquid density inversions in the lunar mantle. *Geochim Cosmochim Acta* 60:2709-2720
- Cisowski SM, Collinson DW, Runcorn SK, Stephenson A, Fulle M (1983) A review of lunar paleointensity data and implications for origin of lunar magnetism. *Proc 13th Lunar Planet Sci Conf, Part 2, J Geophys Res, suppl.* 88: A691-A704
- Cisowski SM, Fuller M (1978) The effect of shock on the magnetism of terrestrial rocks. *J Geophys Res* 83:3441-3458
- Cisowski SM, Fuller M (1986) Lunar paleointensities via the IRMs normalization method and the early magnetic history of the Moon. *In: Origin of the Moon*. Hartmann WK, Phillips RJ, Taylor GJ (eds) Lunar and Planetary Institute, p 411-424
- Coe RS, Grommé S, Mankinen EA (1978) Geomagnetic paleointensities from radiocarbon-dated lava flows on Hawaii and the question of the Pacific nondipole low. *J Geophys Res* 83:1740-1756
- Cohen BA, James OB, Taylor LA, Nazarov MA, Baruskova LD (2004) Lunar highland meteorite Dhofar 026 and Apollo sample 15418: Two strongly shocked, partially melted, granulitic breccias. *Meteor Planet Sci* 39:1419-1447
- Cohen BA, Swindle TD, Kring DA (2000) Support for the lunar cataclysm hypothesis from lunar impact melt ages. *Science* 290:1754-1756
- Collinson DW (1984) On the existence of magnetic fields on the Moon between 3.6 Ga ago and the present. *Phys Earth Planet Inter* 34:102-116
- Collinson DW (1985) Primary and secondary magnetizations in lunar rocks: Implications for the ancient magnetic-field of the Moon. *Earth Moon Planets* 33:31-58
- Collinson DW (1993) Magnetism of the Moon: A lunar core dynamo or impact magnetization? *Surv Geophys* 14: 89-118
- Collinson DW, Stephenson A (1977) Paleointensity experiments using alternating field demagnetization. *Phys Earth Planet Inter* 13:380-385
- Collinson DW, Stephenson A, Runcorn SK (1973) Magnetic studies of Apollo 15 and 16 rocks. *Proc Lunar Sci Conf* 4:2963-2976
- Colson RO (1992) Mineralization on the Moon? Theoretical consideration of Apollo 16 "rusty rocks," sulfide replacement in 67016, and surface-correlated volatiles on lunar volcanic glasses. *Proc Lunar Planet Sci Conf* 22: 427-436
- Comer RP, Solomon SC, Head JW (1979) Elastic lithospheric thickness on the Moon from mare tectonic features: a formal inversion. *Proc Lunar Planet Sci Conf* 10:2441-2463
- Cook AC, Watters TR, Robinson MS, Spudis PD, Bussey DBJ (2000) Lunar polar topography derived from Clementine stereophotos. *J Geophys Res* 105:12,023-12,033
- Coombs CR, Hawke BR, Lucey PG, Owensby PD, Zisk SH (1990) The Alphonsus region: A geologic and remote sensing perspective. *Proc Lunar Planet Sci Conf* 20:161-174
- Cooper BL, Carter JL, Sapp CA (1994) New evidence for graben origin of Oceanus Procellarum from lunar sounder optical imagery. *J Geophys Res* 99:3799-3812
- Crawford DA, Schultz PH (1988) Laboratory observations of impact-generated magnetic fields. *Nature* 336:50-52

- Crawford DA, Schultz PH (1991) Laboratory investigations of impact-generated plasma. *J Geophys Res* 96:18,807-18,817
- Crawford DA, Schultz PH (1999) Electromagnetic properties of impact-generated plasma, vapor and debris. *Int J Impact Engng* 23:169-180
- Crawford I (2004) The scientific case for renewed human activities on the Moon. *Space Policy* 20:91-97
- Croft SK (1980) Cratering flow fields: Implications for the excavation and transient expansion stages of crater formation. *Proc Lunar Planet Sci Conf* 11:2347-2378
- Crosby A, McKenzie D (2005) Measurements of the elastic thickness under ancient lunar terrain. *Icarus* 173:100-107
- Cushing JA, Taylor GJ, Norman MD, Keil K (1999) The granulitic impactite suite: Impact melts and metamorphic breccias of the early lunar crust. *Meteor Planet Sci* 34:185-195
- Daily WD, Dyal P (1979) Magnetometer data errors and lunar induction studies. *J Geophys Res* 84:3313-3326
- Dainty AM, Toksöz MN, Stein S (1976) Seismic investigation of the lunar interior. *Proc Lunar Sci Conf* 7:3057-3075
- Dalrymple GB, Ryder G (1993) $^{40}\text{Ar}/^{39}\text{Ar}$ age spectra of Apollo 15 impact melt rocks by laser step-heating and their bearing on the history of the lunar basin formation. *J Geophys Res* 98:13,085-13,095
- Dalrymple GB, Ryder G (1996) Argon-40/argon-39 age spectra of Apollo 17 highlands breccia samples by laser step heating and the age of the Serenitatis basin. *J Geophys Res* 101:26,069-26,084
- De Hon RA (1974) Thickness of mare material in the Tranquilitatis and Nectaris basins. *Proc Lunar Sci Conf* 5:53-59
- De Hon RA (1977) Mare Humorum and Mare Nubium: Basalt thickness and basin-forming history. *Proc Lunar Sci Conf* 8:633-641
- De Hon RA (1979) Thickness of the western mare basalts. *Proc Lunar Planet Sci Conf* 10:2935-2955
- De Hon RA, Waskom JD (1976) Geologic structure of the eastern mare basins. *Proc Lunar Sci Conf* 7:2729-2746
- Delano JW (1986a) Abundances of cobalt, nickel, and volatiles in the silicate portion of the Moon. *In: Origin of the Moon*. Hartmann WK, Phillips RJ, Taylor GJ (eds) Lunar and Planetary Institute, p 231-248
- Delano JW (1986b) Pristine lunar glasses: criteria, data, and implications. *Proc 16th Lunar Planet Sci Conf, Part 2, J Geophys Res, suppl.* 91:D201-D213
- Delano JW (1990) Buoyancy-driven melt segregation in the Earth's Moon, I, Numerical results. *Proc Lunar Planet Sci Conf* 20:3-12
- Delano JW, Hanson BZ, Watson EB (1994) Abundance and diffusivity of sulfur in lunar picritic magmas. *Lunar Planet Sci* 25:325-326
- Delano JW, Lindsley DH, M.-S. M, Schmitt RA (1982) The Apollo 15 yellow impact glasses: Chemistry, petrology, and exotic origin. *Proc 13th Lunar Planet Sci Conf, Part 1, J Geophys Res, suppl.* 87:A159-A170
- Delano JW, Ringwood AE (1978) Siderophile elements in the lunar highlands: Nature of the indigenous component and implications for the origin of the Moon. *Proc Lunar Planet Sci Conf* 9:111-159
- Dence MR (1968) Shock zoning at Canadian craters: Petrography and structural implications. *In: Shock Metamorphism of Natural Materials*. French BM, Short NM (eds) Mono Book Corp., p 169-184
- Dickey JO, Bender PL, Faller JE, Newhall XX, Ricklefs RL, Ries JG, Shelus PJ, Veillet C, Whipple AL, Wiant JR, Williams JG, Yoder CF (1994) Lunar laser ranging: a continuing legacy of the Apollo program. *Science* 265:482-490
- Dickey JS, Frey FA, Hart SR, Watson EB, Thompson G (1977) Geochemistry and petrology of dredged basalts from the Bouvet triple junction, South Atlantic. *Geochim Cosmochim Acta* 41:1105-1118
- Dickinson T, Taylor GJ, Keil K, Schmitt RA, Hughes SS, Smith MR (1985) Apollo 14 aluminous mare basalts and their possible relationship to KREEP. *Proc 15th Lunar Planet Sci Conf, in J Geophys Res* 90:C365-C374
- Dobson DP, Crichton WA, Vocadlo L, Jones AP, Wang Y, Uchida T, Rivers M, Sutton S, Brodholt JP (2000) In situ measurement of viscosity of liquids in the Fe-FeS system at high pressures and temperatures. *Am Mineral* 85:1838-1842
- Dorman J, Evans S, Nakamura Y, Latham G (1978) On the time varying properties of the lunar seismic meteoroid population. *Proc Lunar Planet Sci Conf* 9:3615-3626
- Dowty E, Keil K, Prinz M (1974) Igneous rocks from Apollo 16 rake samples. *Lunar Science* V:174-176
- Drake DM (1986) Is lunar bulk material similar to Earth's mantle? *In: Origin of the Moon*. Hartmann WK, Phillips RJ, Taylor GJ (eds) Lunar and Planetary Institute, p 105-124
- Drake MJ, Newsom HE, Reed SJ, Enright MC (1984) Experimental determination of the partitioning of gallium between solid iron metal and synthetic basaltic melt: electron and ion microprobe study. *Geochim Cosmochim Acta* 48:1609-1615
- Duennebier F, Dorman J, Lammlein D, G. L, Nakamura Y (1975) Meteoroid flux from passive seismic experiment data. *Proc Lunar Planet Sci Conf* 6:2417-2426
- Duennebier F, Sutton GH (1974) Thermal moonquakes. *J Geophys Res* 79:4351-4363
- Duke M, Agee C, Bogard D, Carrier W, Coombs C, Gaddis L, Head JI, Jolliff B, Lofgren G, Papanastassiou D, Papike J, Pieters C, Ryder G (2000) South Pole-Aitken basin sample return mission. *In: Proceedings of the Fourth International Conference on Exploration and Utilization of the Moon SP-462*. European Space Agency, ESTEC, Noordwijk
- Dunlop DJ, Ozdemir O (1997) Rock Magnetism: Fundamentals and Frontiers. Cambridge Univ. Press

- Dyal P, Parkin CW, Daily WD (1976) Structure of the lunar interior from magnetic field measurements. *Proc Lunar Sci Conf* 7:3077-3095
- Dymek RF, Albee AL, Chodos AA (1976) Petrology and origin of Boulders #2 and #3, Apollo 17 Station 2. *Proc Lunar Sci Conf* 7:2335-2378
- Ebihara M, Wolf R, Warren PH, Anders E (1992) Trace elements in 59 mostly highland Moon rocks. *Proc Lunar Planet Sci* 22:417-426
- Eggleton RE, Schaber GG, Pike RJ (1974) Photogeologic detection of surfaces buried by mare basalts. *Lunar Science V*:200-2002
- El Goresy A, Prinz M, Ramdohr P (1976) Zoning in spinels as an indicator of the crystallization histories of mare basalts. *Proc Lunar Sci Conf* 7:1261-1279
- El Goresy A, Taylor LA, Ramdohr P (1972) *Fra Mauro* crystalline rocks: mineralogy, geochemistry, and subsolidus reduction of opaque minerals. *Proc Lunar Sci Conf* 3:333-349
- Elkins LT, Fernandes VA, Delano JW, Grove TL (2000) Origin of lunar ultramafic green glasses: Constraints from phase equilibrium studies. *Geochim Cosmochim Acta* 64:2339-2350
- Elkins-Tanton LT, Chatterjee N, Grove TL (2003) Experimental and petrologic constraints on lunar differentiation from the Apollo 15 green picritic glasses. *Meteorit Planet Sci* 38:515-527
- Elphic RC, Lawrence DJ, Feldman WC, Barraclough BL, Maurice S, Binder AB, Lucey PG (2000) Lunar rare earth element distribution and ramifications for FeO and TiO₂: Lunar Prospector neutron spectrometer observations. *J Geophys Res* 105:20,333-20,345
- Evensen NM, Murthy VR, Coscio Jr. MR (1974) Provenance of KREEP and the exotic component: Elemental and isotopic studies of grain size fractions in lunar soils. *Proc Lunar Sci Conf* 5:1401-1417
- Fabrichnaya OB, Kuskov OL (1994) Constitution of the Moon: 1. Assessment of thermodynamic properties and reliability of phase relation calculations in the FeO-MgO-Al₂O₃-SiO₂ system. *Phys Earth Planet Inter* 83:175-196
- Fagan TJ, Taylor GJ, Keil K, Bunch TE, Wittke JH, Korotev RL, Jolliff BL, Gillis JJ, Haskin LA, Jarosewich E, Clayton RN, Mayeda TK, Fernandes VA, Burgess R, Turner G, Eugster O, Lorenzetti S (2002) Northwest Africa 032: Product of lunar volcanism. *Meteorit Planet Sci* 37:371-394
- Fagan TJ, Taylor GJ, Keil K, Hicks TL, Killgore M, Bunch TE, Wittke JH, Mittlefehldt DW, Clayton RN, Mayeda TK, Eugster O, Lorenzetti S, Norman MD (2003) Northwest Africa 773: Lunar origin and iron-enrichment trend. *Meteor Planet Sci* 38:529-554
- Fei Y, Bertka CM, Finger LW (1997) High-pressure iron-sulfer compound, Fe₃S₂, and melting relations in the Fe-FeS system. *Science* 275:1621-1623
- Fernandes VA, Burgess R, Turner G (2003) ⁴⁰Ar-³⁹Ar chronology of lunar meteorites Northwest Africa 032 and 773. *Meteor Planet Sci* 38:555-564
- Floss C, James OB, McGee JJ, Crozaz G (1998) Lunar ferroan anorthosite petrogenesis: Clues from trace element distributions in FAN subgroups. *Geochim Cosmochim Acta* 62:1255-1283
- Fogel RA, Rutherford MJ (1995) Magmatic volatiles in primitive lunar glasses: FTIR and EMPA analyses of Apollo 15 green and yellow glasses and revision of the volatile assisted fire-fountaining theory. *Geochim Cosmochim Acta* 59:201-215
- Forsyth DW (1985) Subsurface loading and estimates of the flexural rigidity of continental lithospheres. *J Geophys Res* 90:12,623-12,632
- Freed AM, Melosh HJ, Solomon SC (2001) Tectonics of mascon loading: Resolution of the strike-slip faulting paradox. *J Geophys Res* 106:20,603-20,620
- Frey FA, Suen CJ, Stockman HW (1985) The Ronda high temperature peridotite: Geochemistry and petrogenesis. *Geochim Cosmochim Acta* 49:2469-2491
- Frost DJ, Liebske C, Langenhorst CA, McCammon RG, Trønnes RG, Rubie DC (2004) Experimental evidence for the existence of iron-rich metal in the Earth's lower mantle. *Nature* 428:409-412
- Fuller M, Cisowski SM (1987) Lunar paleomagnetism. In: *Geomagnetism*. Jacobs JA (ed) Academic Press, p 307-455
- Gagnepain-Beyneix J, Lognonné P, Chenet H, Lombardi D, Spohn T (2006) Seismic model of the Moon mantle and their constraints on the mantle temperature and mineralogy. *Phys Earth Planet Inter* (in press)
- Ganapathy R, Morgan JW, Krähenbühl U, Anders E (1973) Ancient meteoritic components in lunar highland rocks: clues from trace elements in Apollo 15 and 16 samples. *Proc Lunar Sci Conf* 4:1239-1261
- Gattacceca J, Rochette P (2004) Toward a robust normalized magnetic paleointensity method applied to meteorites. *Earth Planet Sci Lett* 227:377-393
- Gibson EKJ (1977) Volatile elements, carbon, nitrogen, sulfur, sodium, potassium, and rubidium in the lunar regolith. *Phys Chem Earth* 10:57-62
- Gibson EKJ, Brett R, Andrawes F (1977) Sulfur in lunar mare basalts as a function of bulk composition. *Proc Lunar Sci Conf* 8th 1417-1428
- Gibson EKJ, Chang S, Lennon K, Moore GW, Pearce GW (1975) Sulfur abundances and distributions in mare basalts and their source magmas. *Proc Lunar Sci Conf* 6:1287-1301
- Gibson EKJ, Moore GW (1974) Sulfur abundances and distributions in the valley of Taurus-Littrow. *Proc Lunar Sci Conf* 5:1823-1837

- Giguere TA, Taylor GJ, Hawke BR, Lucey PG (2000) The titanium contents of lunar mare basalts. *Meteor Planet Sci* 35:193-200
- Gillis JJ (1998) The composition and geologic setting of mare deposits on the far side of the Moon. Ph.D. thesis, Rice University, Houston
- Gillis JJ, Jolliff BL (1999) Lateral and vertical heterogeneity of thorium in the procellarum KREEP terrane; as reflected in the ejecta deposits of post-imbrrium craters. *In: Workshop on New views of the Moon II*. Flagstaff, AZ, p 18-19
- Gillis JJ, Jolliff BL, Elphic RC (2003) A revised algorithm for calculating TiO_2 from Clementine UVVIS data: A synthesis of rock, soil, and remotely sensed TiO_2 concentrations. *J Geophys Res* 108:10.1029/2001JE001515
- Gillis JJ, Jolliff BL, Lawrence DJ, Lawson SL, Prettyman TH (2002) The Compton-Belkovich region of the Moon: Remotely sensed observations and lunar sample association. *Lunar Planet Sci XXXIII*:1967
- Gillis JJ, Spudis PD (2000) Geology of the Smythii and Marginis region of the Moon: using integrated remotely sensed data. *J Geophys Res* 105:4217-4233
- Gnos E, Hofmann BA, A. A-K, Lorenzetti S, Eugster O, Whitehouse MJ, Villa IM, Jull AJT, Eikenberg J, Spettel B, Krähenbühl U, Franchi IA, Greenwood RC (2004) Pinpointing the source of a lunar meteorite: Implications for the evolution of the Moon. *Science* 305:657-659
- Goguitchaichvili AT, Prevot M, Camps P (1999) No evidence for strong fields during the R3-N3 Icelandic geomagnetic reversal. *Earth Planet Sci Lett* 167:15-34
- Goins NR, Dainty AM, Toksöz MN (1981a) Lunar seismology: The internal structure of the Moon. *J Geophys Res* 86: 5061-5074
- Goins NR, Dainty AM, Toksöz MN (1981b) Seismic energy release of the Moon. *J Geophys Res* 86:378-388
- Goins NR, Dainty AM, Toksöz MN (1981c) Structure of the lunar crust at highland site Apollo station 16. *Geophys Res Lett* 8:29-32
- Goldstein BE, Phillips RJ, Russell CT (1976) Magnetic evidence concerning a lunar core. *Proc Lunar Sci Conf* 7: 3321-3341
- Golombek MP (1985) Fault type predictions from stress distributions on planetary surfaces: Importance of fault initiation depth. *J Geophys Res* 90:3065-3074
- Goodrich CA, Taylor GJ, Keil K, Kallemyer GW, Warren PH (1986) Alkali norite, troctolites, and VHK mare basalts from Apollo 14 breccia 14304. *Proc 16th Lunar Planet Sci Conf, J Geophys Res* 91:D305-D318
- Gooley R, FBrett R, Warner J, Smyth JR (1974) A lunar rock of deep crustal origin: 76535. *Geochim Cosmochim Acta* 38:1329-1339
- Grande M, Browning R, Waltham N, Parker D, Dunkin SK, Kent B, Kellett B, Perry CH, Swinyard B, Perry A, Feraday J, Howe C, McBride G, Phillips K, Huovelin J, Muhli P, Hakala PJ, Vilhu O, Laukkanen J, Thomas N, Hughes D, Alleyne H, Grady M, Lundin R, Barabash S, Baker D, Clark PE, Murray CD, Guest JE, Casanova I, d'Uston LC, Maurice S, Foing B, Heather DJ, Fernandes VA, Muinonen K, Russell SS, Christou A, Owen C, Charles P, Koskinen H, Mato M, Sipila K, Nenonen S, Holmstrom M, Bhandari N, Elphic R, Lawrence D (2003) The D-CIXS X-ray mapping spectrometer on SMART-1. *Planet Space Sci* 51:427-433
- Green DH, Ringwood AE (1967) The stability field of aluminous pyroxene peridotite and garnet peridotite and their relevance in upper mantle structure. *Earth Planet Sci Lett* 3:151-160
- Gudkova TV, Zharkov VN (2002) The exploration of the lunar interior using torsional oscillations. *Planet Space Sci* 50: 1037-1048
- Haggerty SE, Boyd FR, Bell PM, Finger LW, Bryan WB (1970) Opaque minerals and olivine in lavas and breccias from Mare Tranquillitatis. *Proc Apollo 11 Lunar Sci Conf* 1:513-538
- Halekas JS, Lin RP, Mitchell DL (2003) Magnetic fields of lunar multi-ring impact basins. *Meteorit Planet Sci* 38: 565-578
- Halekas JS, Mitchell DL, Lin RP, Frey S, Hood LL, Acuña MH, Binder AB (2001) Mapping of crustal magnetic anomalies on the lunar near side by the Lunar Prospector electron reflectometer. *J Geophys Res* 106:27,841-27,852
- Halliday AN (2000) Terrestrial accretion rates and the origin of the Moon. *Earth Planet Sci Lett* 176:17-30
- Halliday AN, Lee D-C (1999) Tungsten isotopes and the early development of the Earth and Moon. *Geochim Cosmochim Acta* 63:4157-4179
- Halliday AN, Rehkämper M, Lee D-C, Yi W (1996) Early evolution of the Earth and Moon: New constraints from Hf-W isotope geochemistry. *Earth Planet Sci Lett* 142:75-90
- Haloda J, Irving AJ, Tycova P (2005) Lunar meteorite Northeast Africa 001: An anorthositic regolith breccia with mixed highland/mare components. *Lunar Planet Sci XXXVI*:1487
- Hartmann WK, Ryder G, Dones L, Grinspoon D (2000) The time-dependent intense bombardment of the primordial Earth/Moon system. *In: The Origin of the Earth and Moon*. Canup RM, Righter K (eds) Univ. Arizona Press, p 493-512
- Haskin LA (1998) The Imbrium impact event and the thorium distribution at the lunar highlands surface. *J Geophys Res* 103:1679-1689
- Haskin LA, Gillis JJ, Jolliff BL, Korotev RL (1999) On the distribution of Th in lunar surface materials. *Lunar Planet Sci XXX*:1858

- Haskin LA, Gillis JJ, Korotev RL, Jolliff BL (2000) The materials of the lunar Procellarum KREEP Terrane: A synthesis of data from geomorphological mapping, remote sensing, and sample analyses. *J Geophys Res* 105: 20,403-20,415
- Haskin LA, Helmke PA, Blanchard DP, Jacobs JW, Telander K (1973) Major and trace element abundances in samples from the lunar highlands. *Proc Lunar Sci Conf* 3:1275-1296
- Haskin LA, Korotev RL, Gillis JJ, Jolliff BL (2002) Stratigraphies of Apollo and Luna highland landing sites and provenances of materials from the perspective of basin impact ejecta modeling. *Lunar Planet Sci XXXIII*:1364
- Haskin LA, Korotev RL, Rockow KM, Jolliff BL (1998) The case for an Imbrium origin of the Apollo thorium-rich impact-melt breccias. *Meteorit Planet Sci* 33:959-975
- Haskin LA, Moss BE, McKinnon WB (2003) On estimating contributions of basin ejecta to regolith deposits at lunar sites. *Meteorit Planet Sci* 38:13-33
- Haskin LA, Shih C-Y, Bansal BM, Rhodes JM, Weismann H, Nyquist LE (1974) Chemical evidence for the origin of 76535 as a cumulate. *Proc Lunar Sci Conf* 5:1213-1225
- Hawke BR, Head JW (1978) Lunar KREEP volcanism: Geologic evidence for history and mode of emplacement. *Proc Lunar Planet Sci Conf* 9:3285-3309
- Hawke BR, Lawrence DJ, Blewett DT, Lucey PG, Smith GA, Spudis PD, Taylor GJ (2003a) Hansteen Alpha: A volcanic construct in the lunar highlands. *J Geophys Res* 108:doi:10.1029/2002JE002013
- Hawke BR, Lucey PG, Taylor GJ, Bell JF, Peterson CA, Blewett DT, Horton K, Smith GA, Spudis PD (1991) Remote sensing studies of the Orientale region of the Moon: A pre-Galileo view. *Geophys Res Lett* 18:2141-2144
- Hawke BR, Peterson CA, Blewett DT, Bussey DBJ, Lucey PG, Taylor GJ, Spudis PD (2003b) Distribution and modes of occurrence of lunar anorthosite. *J Geophys Res* 108:5050, doi:10.1029/2002JE001890
- Hawke BR, Peterson CA, Lucey PG, Taylor GJ, Blewett DT, Cambell BA, Coombs CR, Spudis PD (1993) Remote sensing studies of the terrain northwest of the Humorum basin. *Geophys Res Lett* 20:419-422
- Haxby WF, Turcotte DL (1978) On isostatic geoid anomalies. *J Geophys Res* 83:5473-5478
- Head JW, III, Adams JB, McCord TB, Pieters CM, Zisk SH (1978) Regional stratigraphy and geologic history of Mare Crisium. *In: Mare Crisium: The view from Luna 24*. Merrill RB, Papike JJ (eds) Pergamon Press, p 43-74
- Head JW, Wilson L (1992) Lunar mare volcanism: Stratigraphy, eruption conditions, and the evolution of secondary crusts. *Geochim Cosmochim Acta* 56:2155-2175
- Heather DJ, Dunkin SK (2002) A stratigraphic study of southern Oceanus Procellarum using Clementine multispectral data. *Planet Space Sci* 50:1299-1309
- Heiken GH, Vaniman DT, French BM (eds) (1991) *The Lunar Sourcebook: a user's guide to the Moon*. Cambridge Univ. Press
- Herbert F (1980) Time-dependent lunar density models. *Proc Lunar Planet Sci Conf* 11:2015-2030
- Herbert F, Drake MJ, Sonett CP (1978) Geophysical and geochemical evolution of the lunar magma ocean. *Proc Lunar Planet Sci Conf* 9:249-262
- Herrero-Bervera E, Valet J-P (2000) Paleointensity experiments using alternating field demagnetization. *Earth Planet Sci Lett* 177:43-58
- Herzberg CT (1978) The bearing of spinel-cataclasites on the crust-mantle structure of the Moon. *Lunar Planet Sci Conf* 9:319-336
- Herzberg CT, Baker MB (1980) The cordierite- to spinel-cataclasite transition: Structure of the lunar crust. *In: Proc Conf. Lunar Highlands Crust*. Merrill RB (ed) Pergamon, p 113-132
- Hess PC (1991) Diapirism and the origin of high TiO₂ mare glasses. *Geophys Res Lett* 18:2069-2072
- Hess PC (1993) Ilmenite liquidus and depths of segregation of high-Ti picritic glasses. *Lunar Planet Sci XXIV*:649-650
- Hess PC (1998) Source regions to lunar troctolite parent magmas. *Lunar Planet Sci XXVIII*:1225
- Hess PC (2000) On the source regions for mare picrite glasses. *J Geophys Res* 105:4347-4360
- Hess PC, Finnla A (1997) Depths of segregation of high-TiO₂ picrite mare glasses. *Lunar Planet Sci* 28:559-560
- Hess PC, Parmentier EM (1995) A model for the thermal and chemical evolution of the Moon's interior: Implications for the onset of mare volcanism. *Earth Planet Sci Lett* 134:501-514
- Hess PC, Parmentier EM (2001) Thermal evolution of a thicker KREEP liquid layer. *J Geophys Res* 106:28,023-28,032
- Hide R, Roberts PH (1979) How strong is the magnetic field in the Earth's liquid core? *Phys Earth Planet Inter* 20: 124-126
- Hiesinger H, Head JW, III (2003) Ages and stratigraphy of mare basalts in Oceanus Procellarum, Mare Nubium, Mare Cognitum, and Mare Insularum. *J Geophys Res* 108:5065, doi:10.1029/2002JE001985
- Hiesinger H, Head JW, III, Wolf U, Jaumann R, Neukum G (2002) Lunar mare basalt flow units: Thicknesses determined from crater size-frequency distributions. *Geophys Res Lett* 29:10.1029/2002GL014847
- Hiesinger H, Jaumann R, Neukum G, Head JW, III (2000) Ages of mare basalts on the lunar nearside. *J Geophys Res* 105:29,239-29,275
- Hill DH, Boynton WV (2003) Chemistry of the Calcalong Creek lunar meteorite and its relationship to lunar terranes. *Meteorit Planet Sci* 38:595-626

- Hillgren VJ (1991) Partitioning behavior of Ni, Co, Mo, and W between basaltic liquid and Ni-rich metal: Implications for the origin of the Moon and lunar core formation. *Geophys Res Lett* 18:2077-2080
- Hillgren VJ, Drake MJ, Rubie DC (1994) High-pressure and high-temperature experiments on core-mantle segregation in the accreting Earth. *Science* 264:1442-1445
- Hillgren VJ, Drake MJ, Rubie DC (1996) High-pressure and high-temperature metal-silicate partitioning of siderophile elements: The importance of silicate liquid composition. *Geochim Cosmochim Acta* 60:2257-2263
- Hirayama Y, Fujii T (1993) The melting relation of the system iron and carbon at high pressure and its bearing on the early stage of the Earth. *Geophys Res Lett* 20:2095-2098
- Hobbs BA, Hood LL, Herbert F, Sonnett CP (1983) An upper bound on the radius of a highly electrically conducting lunar core. *Proc 14th Lunar Planet Sci Conf, Part 1, J Geophys Res, suppl.* 88:B97-B102
- Hood LL (1986) Geophysical constraints on the lunar interior. *In: Origin of the Moon.* Hartmann WK, Phillips RJ, Taylor GJ (eds) *Lunar and Planet. Inst.*, p 361-410
- Hood LL (1995) Frozen fields. *Earth Moon Planets* 67:131-142
- Hood LL (2000) Reply to comment on "Initial measurements of the lunar induced magnetic dipole moment using Lunar Prospector magnetometer data" by Hood et al. *Geophys Res Lett* 27:1079
- Hood LL, Herbert F, Sonnett CP (1982) The deep lunar electrical conductivity profile: Structural and thermal inferences. *J Geophys Res* 87:5311-5326
- Hood LL, Huang Z (1991) Formation of magnetic anomalies antipodal to lunar impact basins: Two-dimensional model calculations. *J Geophys Res* 96:9837-9846
- Hood LL, Jones JH (1987) Geophysical constraints on the lunar bulk composition and structure: A reassessment. *Proc 17th Lunar Planet Sci Conf, Part 2, J Geophys Res, suppl.* 92:E396-E410
- Hood LL, Mitchell DL, Lin RP, Acuna MH, Binder AB (1999) Initial measurements of the lunar induced magnetic dipole moment using Lunar Prospector magnetometer data. *Geophys Res Lett* 26:2327-2330
- Hood LL, Vickery A (1984) Magnetic field amplification and generation in hypervelocity meteoroid impacts with application to lunar paleomagnetism. *Proc 15th Lunar Planet Sci Conf, Part 1, J Geophys Res, suppl.* 89:C211-C223
- Hood LL, Zakharian A, Halekas J, Mitchell DL, Lin RP, Acuña MH, Binder AB (2001) Initial mapping and interpretation of lunar crustal magnetic anomalies using Lunar Prospector magnetometer data. *J Geophys Res* 106:27,825-27,840
- Hood LL, Zuber MT (2000) Recent refinements in geophysical constraints on lunar origin and evolution. *In: Origin of the Earth and Moon.* Canup RM, Righter K (eds) Univ. of Arizona Press, p 397-412
- Hubbard NJ, Gast PW (1971) Chemical composition and origin of nonmare lunar basalts. *Proc Lunar Sci Conf* 2: 999-1020
- Hubbard NJ, Meyer Jr. C, Gast PW, Wiesmann H (1971) The composition and derivation of Apollo 12 soils. *Earth Planet Sci Lett* 10:341-350
- Hughes HG, App FN, McGetchin TR (1977) Global seismic effects of basin-forming impacts. *Phys Earth Planet Inter* 15:251-263
- Hughes SS, Delano JW, Schmitt RA (1988) Apollo 15 yellow-brown volcanic glass: Chemistry and petrogenetic relations to green volcanic glass and olivine-normative mare basalts. *Geochim Cosmochim Acta* 52:2379-2391
- Hughes SS, Delano JW, Schmitt RA (1989) Petrogenetic modelling of 74220 high-Ti orange volcanic glasses and the Apollo 11 and 17 high-Ti mare basalts. *Proc Lunar Planet Sci Conf* 19:175-188
- Hunter RH, Taylor LA (1983) The magma ocean from the Fra Mauro shoreline: An overview of the Apollo 14 crust. *Proc. 13th Lunar Planet Sci Conf, J Geophys Res* 88:A591-A602
- Hörz F (1978) How thick are the lunar mare basalts? *Proc Lunar Planet Sci Conf* 9:3311-3331
- Ito E, Katsura T, Suzuki T (1998) Metal/silicate partitioning of Mn, Co, and Ni at high pressures and high temperatures and implications for core formation in a deep magma ocean. *In: Properties of Earth and Planetary Materials at High Pressure and Temperature.* Manghnani MH (ed) American Geophysical Union, p 215-225
- Jacobsen SB, Harper CL (1996) Accretion and early differentiation history of the Earth based on extinct radionuclides. *In: Earth Processes: Reading the Isotope Code.* Basu A, Hart S (eds), American Geophysical Union, p 47-74
- Jagoutz E, Baddehausen H, Blum K, Cendales M, Dreibus G, Spettel B, Lorenz V, Wänke H (1979) The abundance of major, minor, and trace elements in the Earth's mantle as derived from primitive ultramafic nodules. *Proc Lunar Planet Sci Conf* 10:2031-2050
- James OB (1980) Rocks of the early lunar crust. *Proc Lunar Planet Sci Conf* 11:365-393
- James OB (1981) Petrologic and age relations of Apollo 16 rocks: Implications for subsurface geology and the age of the Nectaris basin. *Proc Lunar Planet Sci Conf* 12B:209-233
- James OB, Flohr MK (1983) Subdivision of the Mg-suite noritic rocks into Mg-gabbronorites and Mg-norites. *Proc 13th Lunar Planet Sci Conf, Part 2, J Geophys Res, suppl.* 88:A603-A614
- James OB, Flohr MK, Lindstrom MM (1984) Petrology and geochemistry of lunar dimict breccia 61015. *Proc 15th Lunar Planet Sci Conf, J Geophys Res* 89:C63-C86
- James OB, Hammarstrom JG (1977) Petrology of four clasts from consortium breccia 73215. *Proc Lunar Sci Conf* 8: 2459-2494

- James OB, Lindstrom MM, Flohr MK (1987) Petrology and geochemistry of alkali gabbronorites from lunar breccia 67975. *Proc 17th Lunar Planet Sci Conf, J Geophys Res* 89:E314-E330
- James OB, Lindstrom MM, Flohr MK (1989) Ferroan anorthosite from lunar breccia 64435: Implications for the origin and history of lunar ferroan anorthosites. *Proc Lunar Planet Sci Conf* 19:219-243
- James OB, McGee JJ (1979) Consortium breccia 73255: Genesis and history of two coarse-grained "norite" clasts. *Proc Lunar Planet Sci Conf* 10:713-743
- Jeffreys H (1970) *The Earth*. Cambridge Univ. Press
- Jolliff BJ, Gillis JJ, Lawrence DJ, Maurice S (2001) Thorium content of mare basalts of the western Procellarum region. *Lunar and Planetary Science XXXII*:2144
- Jolliff BL (1991) Fragments of quartz monzodiorite and felsite in Apollo 14 soil particles. *Lunar and Planetary Science* 21:101-118
- Jolliff BL (1998) Large-scale separation of K-frac and REEP-frac in the source regions of Apollo impact-melt breccias, and a revised estimate of the KREEP composition. *Int Geol Rev* 40:916-935
- Jolliff BL, Floss C, McCallum IS, Schwartz JM (1999) Geochemistry, petrology, and cooling history of 14161,7373: A plutonic lunar sample with textural evidence of granitic-fraction separation by silicate-liquid immiscibility. *Am Mineral* 84:821-837
- Jolliff BL, Gillis JJ (2002) Lunar Crustal and Bulk Composition. *In: Workshop on The Moon Beyond 2002: Next Steps in Lunar Science and Exploration*. Abstract 3056
- Jolliff BL, Gillis JJ, Haskin L, Korotev RL, Wieczorek MA (2000a) Major lunar crustal terranes: Surface expressions and crust-mantle origins. *J Geophys Res* 105:4197-4216
- Jolliff BL, Gillis JJ, Haskin LA (2002) Eastern Basin Terrane and South Pole-Aitken Basin ejecta: Mid-level Crust? *Lunar Planet Sci XXXIII*:1157
- Jolliff BL, Gillis JJ, Korotev RL, Haskin LA (2000b) On the origin of nonmare materials at the Apollo 12 landing site. *Lunar and Planetary Science XXXI*:1671
- Jolliff BL, Haskin LA (1995) Cogenetic rock fragments from a lunar soil: Evidence of a ferroan noritic-anorthositic plution on the Moon. *Geochim Cosmochim Acta* 59:2345-2374
- Jolliff BL, Haskin LA, Colson RO, Wadhwa M (1993) Partitioning in REE-saturating minerals: Theory, experiment, and modelling of whitlockite, apatite, and evolution of lunar residual magmas. *Geochim Cosmochim Acta* 57: 4069-4094
- Jolliff BL, Korotev RL, Haskin LA (1991a) A ferroan region of the lunar highlands crust as recorded in meteorites MAC88104 and MAC88105. *Geochim Cosmochim Acta* 55:3051-3071
- Jolliff BL, Korotev RL, Haskin LA (1991b) Geochemistry of 2-4 mm particles from Apollo 14 soil (14161) and implications regarding igneous components and soil-forming processes. *Proc Lunar Planet Sci Conf* 21:193-219
- Jolliff BL, Korotev RL, Rockow KM (1998) Geochemistry and petrology of lunar meteorite Queen Alexandra Range 94281, a mixed mare and highland regolith breccia, with special emphasis on very-low-Ti mafic components. *Meteorit Planet Sci* 33:581-601
- Jolliff BL, Korotev RL, Zeigler RA, Floss C (2003) Northwest Africa 773: Lunar mare breccia with a shallow-formed olivine-cumulate component, inferred very-low-Ti (VLT) heritage, and a KREEP connection. *Geochim Cosmochim Acta* 24:4857-4879
- Jolliff BL, Rockow KM, Korotev RL, Haskin LA (1996) Lithologic distribution and geologic history of the Apollo 17 site: The record in soils and small rock particles from the highland massifs. *Meteor Planet Sci* 31:116-145
- Jolliff BL, Zeigler RA, Korotev RL (2004) Petrography of lunar meteorite LAP 02205, a new low-Ti basalt possibly launch paired with NWA 032. *Lunar Planet Sci XXXV*:1438
- Jones JH, Palme H (2000) Geochemical constraints on the origin of the Earth and Moon. *In: Origin of the Earth and Moon*. Canup RM, Righter K (eds) Univ. Arizona Press, p 197-216
- Kaiden H, Kojima H (2002) Yamato 983885: A second lunar meteorite from the Yamato 98 collection. *Antarctic Meteorites XXVII*, Tokyo, Nat Inst Polar Res:49-51
- Karner J, Papike JJ, Shearer CK (2003) Olivine from planetary basalts: Chemical signatures that indicate planetary parentage and those that record igneous setting and process. *Am Mineral* 88:806-816
- Kaula WM (1967) Theory of statistical analysis of data distributed over a sphere. *Rev Geophys* 5:83-107
- Kaula WM (2000) *Theory of Satellite Geodesy: Applications of Satellites to Geodesy*. Dover
- Kaula WM, Schubert G, Lingenfelter RE, Sjogren WL, Wollenhaupt WR (1972) Analysis and interpretation of lunar laser altimetry. *Proc Lunar Sci Conf* 3:2189-2204
- Kaula WM, Schubert G, Lingenfelter RE, Sjogren WL, Wollenhaupt WR (1974) Apollo laser altimetry and inferences as to lunar structure. *Proc Lunar Sci Conf* 5:3049-3058
- Keller HU, Mall U, Nathues A (2001) Mapping the Moon with SIR and infrared spectrometer for SMART-1. *Earth Moon Planets* 85:545
- Kesson SE, Lindsley DH (1976) Mare basalt petrogenesis-A review of experimental studies. *Rev Geophys Space Phys* 14:361-373
- Kettrup B, Deutsch A, Masaitis VL (2003) Homogeneous impact melts produced by a heterogeneous target? Sr-Nd isotopic evidence from the Popigai crater, Russia. *Geochim Cosmochim Acta* 67:733-750

- Khan A, Connolly JAD, MacLennan J, Mosegaard K (2006) Joint inversion of seismic and gravity data for lunar composition and thermal state. *Geophys J Int* (in press)
- Khan A, Mosegaard K (2001) New information on the deep lunar interior from an inversion of lunar free oscillation periods. *Geophys Res Lett* 28:1791-1794
- Khan A, Mosegaard K (2002) An enquiry into the lunar interior--A non-linear inversion of the Apollo lunar seismic data. *J Geophys Res* 107:10.1029/2001JE001658
- Khan A, Mosegaard K, Rasmussen KL (2000) A new seismic velocity model for the Moon from a monte carlo inversion of the Apollo lunar seismic data. *Geophys Res Lett* 27:1591-1594
- Khan A, Mosegaard K, Williams JG, Lognonné P (2004) Does the Moon possess a molten core? Probing the deep lunar interior using results from LLR and Lunar Prospector. *J Geophys Res* 109:doi:10.1029/2004JE002294
- Klein N, Rutherford MJ (1998) Volcanic gas formed during eruption of Apollo 17 orange glass magma: evidence from glassy melt inclusions and experiments. *Lunar Planet Sci XXVIII*:1448
- Kleine T, Münker C, Mezger K, Palme H (2002) Rapid accretion and early core formation on asteroids and the terrestrial planets from Hf-W chronometry. *Nature* 418:952-955
- Kletetschka G, Acuña MH, Kohout T, Wasilewski PJ, Connerney JEP (2004) An empirical scaling law for acquisition of thermoremanent magnetization. *Earth Planet Sci Lett* 226:521-528
- Kletetschka G, Kohout T, Wasilewski PJ (2003) Magnetic remanence in the Murchison meteorite. *Meteor Planet Sci* 38:399-405
- Kohlstedt DL, Evans B, Mackwell SJ (1995) Strength of the lithosphere: Constraints imposed by laboratory experiments. *J Geophys Res* 100:17,587-17,602
- Kono M (1987) Changes in TRM and ARM in a basalt due to laboratory heating. *Phys Earth Planet Inter* 46:1-8
- Konopliv AS, Asmar SW, Yuan DN (2001) Recent gravity models as a result of the Lunar Prospector mission. *Icarus* 150:1-18
- Konopliv AS, Binder AB, Hood LL, Kucinskas AB, Sjogren WL, Williams JG (1998) Improved gravity field of the Moon from Lunar Prospector. *Science* 281:1476-1480
- Korotev R (1998) Concentrations of radioactive elements in lunar materials. *J Geophys Res* 103:1691-1701
- Korotev RL (1994) Compositional variation in Apollo 16 impact-melt breccias and inferences for the geology and bombardment history of the Central Highlands of the Moon. *Geochim Cosmochim Acta* 58:3931-3969
- Korotev RL (1996) On the relationship between the Apollo 16 ancient regolith breccias and feldspathic fragmental breccias, and the composition of the prebasin crust in the central highlands of the moon. *Meteor Planet Sci* 31:403-412
- Korotev RL (1997) Some things we can infer about the moon from the composition of the Apollo 16 regolith. *Meteor Planet Sci* 32:447-478
- Korotev RL (1999) A new estimate of the composition of the feldspathic upper crust of the Moon. *Lunar Planet Sci XXX*:1303
- Korotev RL (2000) The great lunar hot spot and the composition and origin of the Apollo mafic ("LKFM") impact-melt breccias. *J Geophys Res* 105:4317-4345
- Korotev RL, Gillis JJ (2001) A new look at the Apollo 11 regolith and KREEP. *J Geophys Res* 106:12,339-12,354
- Korotev RL, Haskin LA (1988) Europium mass balance in polymict samples and implications for plutonic rocks of the lunar crust. *Geochim Cosmochim Acta* 52:1795-1813
- Korotev RL, Irving AJ (2005) Compositions of three lunar meteorites: Meteorite Hills 01210, Northeast Africa 001, and Northwest Africa 3136. *Lunar Planet Sci XXXVI*:1220
- Korotev RL, Jolliff BL (2001) The curious case of the lunar magnesian granulitic breccias. *Lunar Planet Sci XXXII*:1013
- Korotev RL, Jolliff BL, Zeigler RA, Gillis JJ, Haskin LA (2003a) Feldspathic lunar meteorites and their implications for compositional remote sensing of the lunar surface and the composition of the lunar crust. *Geochim Cosmochim Acta* 67:4895-4923
- Korotev RL, Jolliff BL, Zeigler RA, Haskin LA (2003b) Compositional constraints on the launch pairing of three brecciated lunar meteorites of basaltic composition. *Antarctic Meteor Res* 16:152-175
- Korotev RL, Jolliff BL, Zeigler RA, Haskin LA (2003c) Compositional evidence for launch pairing of the YQ and Elephant Moraine lunar meteorites. *Lunar Planet Sci XXXIV*:1357
- Korotev RL, Lindstrom MM, Lindstrom DJ, Haskin LA (1983) Antarctic meteorite ALHA81005—Not just another lunar anorthositic norite. *Geophys Res Lett* 10:829-832
- Korotev RL, Zeigler RA, Jolliff BL (2004) Compositional constraints on the launch pairing of LAP 02205 and PCA 02007 with other lunar meteorites. *Lunar Planet Sci XXXV*:1416
- Kreutzberger ME, Drake MJ, Jones JH (1986) Origin of Earth's Moon: Constraints from alkali volatile trace elements. *Geochim Cosmochim Acta* 50:91-98
- Kuckes AF (1977) Strength and rigidity of the elastic lunar lithosphere and implications for present-day mantle convection in the Moon. *Phys Earth Planet Inter* 14:1-12
- Kuehner SM, Irving AJ, Rumble D III, Hupé AC, Hupé GM (2005) Mineralogy and petrology of lunar meteorite NWA 3136: A glass-welded mare regolith breccia of mixed heritage. *Lunar Planet Sci XXXVI*:1228

- Kuskov OL (1995) Constitution of the Moon: 3. Composition of middle mantle from seismic data. *Phys Earth Planet Inter* 90:55-74
- Kuskov OL (1997) Constitution of the Moon: 4. Composition of the mantle from seismic data. *Phys Earth Planet Inter* 102:239-257
- Kuskov OL, Fabrichnaya OB (1994) Constitution of the Moon: 2. Composition and seismic properties of the lower mantle. *Phys Earth Planet Inter* 83:197-216
- Kuskov OL, Kronrod VA (1998) Constitution of the Moon: 5. Constraints on composition, density, temperature, and radius of a core. *Phys Earth Planet Inter* 107:285-306
- Kuskov OL, Kronrod VA (2001) Core sizes and internal structure of Earth's and Jupiter's satellites. *Icarus* 152:204-227
- Kuskov OL, Kronrod VA, Hood LL (2002) Geochemical constraints on the seismic properties of the lunar mantle. *Phys Earth Planet Inter* 134:175-189
- Lambeck K (1988) Geophysical geodesy: The slow deformations of the Earth. Clarendon Press
- Lambeck K, Pullan S (1980) The lunar fossil bulge hypothesis revisited. *Phys Earth Planet Inter* 22:29-35
- Lammlein DR, Latham GV, Dorman J, Nakamura Y, Ewing M (1974) Lunar seismicity, structure and tectonics. *Rev Geophys Space Phys* 12:1-21
- Langseth MG, Keihm SJ, Peters K (1976) Revised lunar heat-flow values. *Proc Lunar Sci Conf* 7:3143-3171
- Latham G, Ewing M, Dorman J, Press F, Toksöz MN, Sutton G, Meissner F, Duennbier F, Nakamura Y, Kovach R, Yates M (1970a) Seismic data from man-made impacts on the Moon. *Science* 170:620-626
- Latham G, Ewing M, Press F, Sutton G, Dorman J, Nakamura Y, Toksöz MN, Wiggins R, Derr J, Duennbier F (1970b) Passive seismic experiment. *Science* 167:455-457
- Laul JC (1986) Chemistry of the Apollo 12 highland component. *Proc 16th Lunar Planet Sci Conf, J Geophys Res* 91: D251-D261
- Lawrence DJ, Feldman WC, Barraclough BL, Binder AB, Elphic RC, Maurice S, Miller MC, Prettyman TH (2000) Thorium abundances on the lunar surface. *J Geophys Res* 105:20,307-20,331
- Lawrence DJ, Feldman WC, Barraclough BL, Binder AB, Elphic RC, Maurice S, Thomsen DR (1998) Global elemental maps of the Moon: The Lunar Prospector gamma-ray spectrometer. *Science* 281:1484-1489
- Lawrence DJ, Feldman WC, Elphic RC, Little RC, Prettyman TH, Maurice S, Lucey PG, Binder AB (2002) Iron abundances on the lunar surface as measured by the Lunar Prospector gamma-ray and neutron spectrometer. *J Geophys Res* 107:5130, doi:10.1029/2001JE001530
- Le Maître RW, editor (1989) A Classification of Igneous Rocks and Glossary of Terms. Blackwell Scientific Publications
- Lee D-C, Halliday AN (1995) Hafnium-tungsten chronometry and the timing of terrestrial core formation. *Nature* 378: 771-774
- Lee D-C, Halliday AN (1997) Core formation on Mars and differentiated asteroids. *Nature* 388:854-857
- Lee D-C, Halliday AN, Leya I, Wieler R, Wiechert U (2002) Cosmogenic tungsten and the origin and earliest differentiation of the Moon. *Earth Planet Sci Lett* 198:267-274
- Lee D-C, Halliday AN, Snyder GA, Taylor LA (1997) Age and origin of the Moon. *Science* 278:1098-1103
- Lemoine FG, Smith DE, Zuber MT, Neumann GA, Rowlands DD (1997) A 70th degree lunar gravity model (GLGM-2) from Clementine and other tracking data. *J Geophys Res* 102:16,339-16,359
- Levi S, Banerjee SK (1976) On the possibility of obtaining relative paleointensities from lake sediments. *Earth Planet Sci Lett* 29:219-226
- Liebermann RC, Ringwood AE (1976) Elastic properties of anorthite and the nature of the lunar crust. *Earth Planet Sci Lett* 31:69-74
- Lin RP, Anderson KA, Hood LL (1988) Lunar surface magnetic field concentrations antipodal to young large impact basins. *Icarus* 74:529-541
- Lin RP, Mitchell DL, Curtis DW, Anderson KA, Carlson CW, McFadden J, Acuña MH, Hood LL, Binder AB (1998) Lunar surface magnetic fields and their interaction with the solar wind: results from lunar prospector. *Science* 281:1480-1484
- Lindgren BW (1993) Statistical theory. Chapman and Hall
- Lindstrom MM, Knapp SA, Shervais JW, Taylor LA (1984) Magnesian anorthosites and associated troctolites and dunite in Apollo 14 breccias. *Proc 15th Lunar Planet Sci Conf, J Geophys Res* 89:C41-C49
- Lindstrom MM, Lindstrom DJ (1986) Lunar granulites and their precursor anorthositic norites of the early lunar crust. *Proc 16th Lunar Planet Sci Conf, J Geophys Res* 91:D263-D276
- Lindstrom MM, Marvin UB, Vetter SK, Shervais JW (1988) Apennine front revisited: Diversity of Apollo 15 highland rock types. *Proc Lunar Planet Sci Conf* 18:169-185
- Lindstrom MM, Mittlefehldt DW, Martinez RR, Lipschutz MJ, Wang M-S (1991) Geochemistry of Yamato-82192, -86032 and -793274 lunar meteorites. *Proc NIPR Symp, Antarct Meteorit Res* 4:12-32
- Lindstrom MM, Nava DF, Lindstrom DJ, Winzer SR, Lum RKL, Schuhmann PJ, Schuhmann S, Philpotts JA (1977) Geochemical studies of the white breccia boulders at North Ray Crater, Descartes region of the lunar highlands. *Proc Lunar Sci Conf* 8:2137-2151

- Lindstrom MM, Salpas PA (1981) Geochemical studies of rocks from North Ray Crater, Apollo 16. *Proc Lunar Planet Sci Conf* 12B:305-322
- Lognonné P (2005) Planetary seismology. *Annu Rev Earth Planet Sci* 33:571-604
- Lognonné P, Gagnepain-Beyneix J, Chenet H (2003) A new seismic model for the Moon: Implications for structure, thermal evolution and formation of the Moon. *Earth Planet Sci Lett* 211:27-44
- Lognonné P, Mossner B (1993) Planetary seismology. *Surv Geophys* 14:239-302
- Longhi J (1977) Magma oceanography 2: Chemical evolution and crustal formation. *Proc Lunar Sci Conf* 8:601-621
- Longhi J (1980) A model of early lunar differentiation. *Proc Lunar Planet Sci Conf* 11:289-315
- Longhi J (1981) Preliminary modeling of high pressure partial melting. Implications for early lunar differentiation. *Proc Lunar Sci Conf* 12B:1001-1018
- Longhi J (1992) Experimental petrology and petrogenesis of mare volcanics. *Geochim Cosmochim Acta* 56:2235-2251
- Longhi J (1995) Liquidus equilibria of some primary lunar and terrestrial melts in the garnet stability field. *Geochim Cosmochim Acta* 59:2375-2386
- Longhi J (2000) Anorthosite petrogenesis revisited. *Lunar and Planetary Science XXXI*:1592
- Longhi J, Ashwal LD (1985) Two-stage models for lunar and terrestrial anorthosites: Petrogenesis without a magma ocean. *Proc Lunar Planet Sci Conf* 15:C571-C584
- Longhi J, Boudreau AE (1979) Complex igneous processes and the formation of the primitive lunar crustal rocks. *Proc Lunar Planet Sci Conf* 10:2085-2105
- Lucey PG (2004) Mineral maps of the Moon. *Geophys Res Lett* 31:L08701, doi:10.1029/2003GL019406
- Lucey PG, Blewett DT, Hawke BR (1998a) Mapping the FeO and TiO₂ content of the lunar surface with multispectral imagery. *J Geophys Res* 103:3679-3699
- Lucey PG, Blewett DT, Jolliff BL (2000) Lunar iron and titanium abundance algorithms based on final processing Clementine UVMR images. *J Geophys Res* 105:20,297-20,305
- Lucey PG, Hawke BR (1989) A remote mineralogical perspective on gabbroic units in the lunar highlands. *Proc Lunar Planet Sci Conf* 19:355-363
- Lucey PG, Hawke BR, Pieters CM, Head JW, III, McCord TB (1986) A compositional study of the Aristarchus region of the Moon using near-infrared reflectance spectroscopy. *J Geophys Res* 91:D344-D354
- Lucey PG, Spudis PD, Zuber M, Smith D, Malaret E (1994) Topographic-compositional units on the Moon and the early evolution of the lunar crust. *Science* 266:1855-1858
- Lucey PG, Taylor GJ, Hawke BR, Spudis PD (1998b) FeO and TiO₂ concentrations in the South Pole-Aitken basin: Implications for mantle composition and basin formation. *J Geophys Res* 103:3701-3708
- Lucey PG, Taylor GJ, Malaret E (1995) Abundance and distribution of iron on the Moon. *Science* 268:1150-1153
- Ma M-S, Schmitt RA, Taylor GJ, Warner RD, Keil K (1981) Chemical and petrographic study of spinel troctolite in 67435: Implication for the origin of Mg-rich plutonic rocks. *Lunar Planet Sci* 12:640-642
- Margot J-L, Campbell DB, Jurgens RF, Slade MA (1999a) Topography of the lunar poles from radar interferometry: A survey of cold trap locations. *Science* 284:1658-1660
- Margot J-L, Campbell DB, Jurgens RF, Slade MA (1999b) Topography of Tycho crater. *J Geophys Res* 104:11,875-11,882
- Martelli G, Newton G (1977) Hypervelocity cratering and impact magnetisation of basalt. *Nature* 269:478-480
- Marti K, Aeschlimann U, Eberhardt P, Geiss J, Grogler N, Jost DT, Laul JC, Ma M-S, Schmitt RA, Taylor GJ (1983) Pieces of the ancient lunar crust: Ages and composition of clasts in consortium breccia 67915. *Proc 14th Lunar Planet Sci Conf*, *J Geophys Res* 88:B165-B175
- Marvin UB, Carey JW, Lindstrom MM (1989) Cordierite-spinel troctolite, a new magnesium-rich lithology from the lunar highlands. *Science* 243:925-928
- Marvin UB, Lindstrom MM, Bernatowicz TJ, Podosek FA, Sugiura N (1987) The composition and history of breccia 67015 from North Ray Crater. *Proc 17th Lunar Planet Sci Conf*, *J Geophys Res* 92:E472-E490
- Marvin UB, Lindstrom MM, Holmberg BB, Martinez RR (1991) New observations on the quartz monzonodiorite-granite suite. *Proc Lunar Planet Sci Conf* 21:119-135
- Marvin UB, Warren PH (1980) A pristine eucrite-like gabbro from Descartes and its exotic kindred. *Proc Lunar Planet Sci Conf* 11:507-521
- Maxwell TA, Phillips RJ (1978) Stratigraphic correlation of the radar-detected subsurface interface in Mare Crisium. *Geophys Res Lett* 5:811-814
- McCallum IS (1998) The stratigraphy and evolution of the lunar crust. *In: Workshop on New Views of the Moon: Integrated Remotely Sensed, Geophysical, and Sample Datasets*. Lunar and Planetary Institute, p 54-55
- McCallum IS (2001) A new view of the Moon in light of data from Clementine and Prospector missions. *Earth Moon Planets* 85-85:253-269
- McCallum IS, O'Brien HE (1996) Stratigraphy of the lunar highlands crust: Depth of burial of lunar samples from cooling rate studies. *Am Mineral* 81:1166-1175
- McCallum IS, Schwartz JM (2001) Lunar Mg suite: Thermobarometry and petrogenesis of parental magmas. *J Geophys Res* 106:27,969-27,983

- McCord TB, Clark RN, Hawke BR, McFadden LA, Owensby PD, Pieters CM, Adams JB (1981) Moon: Near-infrared spectral reflectance, a good first look. *J Geophys Res* 86:10,883-10,892
- McEwen AS, Robinson MS, Eliason EM, Lucey PG, Duxbury TC, Spudis PD (1994) Clementine observations of the Aristarchus region of the Moon. *Science* 266:1858-1861
- McGovern PJ, Solomon SC (1993) State of stress, faulting, and eruption characteristics of large volcanoes on Mars. *J Geophys Res* 98:23,533-23,579
- McGovern PJ, Solomon SC (1998) Growth of large volcanoes on Venus: Mechanical models and implications for structural evolution. *J Geophys Res* 103:11,071-11,101
- McKay DS, Morrison DA, Clanton US, Ladle GH, Lindsay JF (1971) Apollo 12 soil and breccia. *Proc Lunar Sci Conf* 2:755-773
- McKay GA, Wagstaff J, Le L (1990) REE distribution coefficients for pigeonite: Constraints on the origin of the mare basalt europicum anomaly. *LPI Tech Rep* 90-02:48-49
- McNutt MK (1984) Lithospheric flexure and thermal anomalies. *J Geophys Res* 89:11,180-11,194
- Melosh HJ (1978) The tectonics of mascon loading. *Proc Lunar Planet Sci Conf* 9:3513-3525
- Melosh HJ (1979) Acoustic fluidization: A new geologic process? *J Geophys Res* 84:7513-7520
- Melosh HJ (1989) Impact Cratering: A Geologic Process. Oxford Univ. Press
- Metzger AE, Trombka JI, Peterson LE, Reedy RC, Arnold JR (1973) Lunar surface radioactivity: Preliminary results of the Apollo 15 and Apollo 16 gamma-ray spectrometer experiments. *Science* 179:800-803
- Meyer C, Jr., Brett R, Hubbard NJ, Morrison DA, McKay DS, Aitken FK, Takeda H, Schonfeld E (1971) Mineralogy, chemistry, and origin of the KREEP component in soil samples from the Ocean of Storms. *Proc Lunar Sci Conf* 2:393-411
- Meyer C, Jr., Williams IS, Compston W (1989) Uranium-lead ages for lunar zircons: Evidence for prolonged period of granophyre formation from 4.32 to 3.88 Ga. *Meteor Planet Sci* 31:379-387
- Morgan JW (1986) Ultramafic xenoliths: Clues to Earth's late accretionary history. *J Geophys Res* 91:12,375-12,387
- Morgan JW, Ganapathy R, Higuchi H, Krähenbühl U, Anders E (1974) Lunar basins: tentative characterization of projectiles from meteoritic elements in Apollo 17 boulders. *Proc Lunar Sci Conf* 5:1703-1736
- Morgan JW, Krähenbühl U, Ganapathy R, Anders E (1972a) Trace elements in Apollo 15 samples: implications for meteorite influx and volatile depletion on the Moon. *Proc Lunar Sci Conf* 3:1361-1376
- Morgan JW, Laul JC, Krähenbühl U, Ganapathy R, Anders E (1972b) Major impacts on the Moon: characterization from trace elements in Apollo 12 and 14 samples. *Proc Lunar Sci Conf* 3:1377-1395
- Morgan JW, Walker RJ, Brandon AD, Horan MF (2001) Siderophile elements in Earth's upper mantle and lunar breccias: Data synthesis suggests manifestations of the same late influx. *Meteorit Planet Sci* 36:1257-1275
- Morris RW, Taylor GJ, Newsom HE, Keil K, Garcia SR (1990) Highly evolved and ultramafic lithologies from Apollo 14 soils. *Proc Lunar Planet Sci Conf* 20:61-75
- Morrison DA (1998) Did a thick South Pole-Aitken basin melt sheet differentiate to form cumulates? *Lunar Planet Sci XXIX*:1657
- Morse SA (1982) Adcumulus growth of anorthosite at the base of the lunar crust. *Proc 13th Lunar Planet Sci Conf, J Geophys Res* 87:A10-A18
- Mueller S, Taylor GJ, Phillips RJ (1988) Lunar composition: A geophysical and petrological synthesis. *J Geophys Res* 93:6338-6352
- Muller PM, Sjogren WL (1968) Masons: lunar mass concentrations. *Science* 161:680-684
- Nakamura Y (1977) HFT events: Shallow moonquakes? *Phys Earth Planet Inter* 14:217-223
- Nakamura Y (1978) A₁ moonquakes: Source distribution and mechanism. *Proc Lunar Planet Sci Conf* 9:3589-3607
- Nakamura Y (1983) Seismic velocity structure of the lunar mantle. *J Geophys Res* 88:677-686
- Nakamura Y (2003) New identification of deep moonquakes in the Apollo lunar seismic data. *Phys Earth Planet Inter* 139:197-205
- Nakamura Y (2005) Farside deep moonquakes and deep interior of the Moon. *J Geophys Res* 110:E01001, doi:10.1029/2004JE002332
- Nakamura Y, Duennebier F, Latham GV, Dorman HJ (1976) Structure of the lunar mantle. *J Geophys Res* 81:4818-4824
- Nakamura Y, Koyama J (1982) Seismic Q of the lunar upper mantle. *J Geophys Res* 87:4855-4861
- Nakamura Y, Lammlein D, Latham G, Ewing M, Dorman J, Press F, Toksöz MN (1973) New seismic data on the state of the deep lunar interior. *Science* 181:49-51
- Nakamura Y, Latham G, Lammlein D, Ewing M, Duennebier F, Dorman J (1974) Deep lunar interior inferred from recent seismic data. *Geophys Res Lett* 1:137-140
- Nakamura Y, Latham GV, Dorman HJ (1982) Apollo lunar seismic experiment Final summary. *Proc 13th Lunar Planet Sci Conf, Part 1, J Geophys Res* 87:A117-A123
- Nakamura Y, Latham GV, Dorman HJ, Ibrahim AK, Koyama J, Horvath P (1979) Shallow moonquakes: Depth, distribution and implications as to the present state of the lunar interior. *Proc Lunar Planet Sci Conf* 10:2299-2309
- National Research Council SSES, Space Studies Board (2003) New Frontiers in the Solar System: An Integrated Exploration Strategy. National Academies Press

- Nazarov MA, Demidova SI, Patchen A, Taylor LA (2002) Dhofar 301, 302 and 303: Three new lunar highland meteorites from Oman. *Lunar Planet Sci XXXII*:1293
- Nazarov MA, Demidova SI, Patchen A, Taylor LA (2004) Dhofar 311, 730 and 731: New lunar meteorites from Oman. *Lunar Planet Sci XXXV*:1233
- Neal CR (2001) Interior of the Moon: The presence of garnet in the primitive deep lunar mantle. *J Geophys Res* 106: 27,865-27,885
- Neal CR, Ely JC (2002) Sulfide immiscibility in the lunar magma ocean: evidence for a primitive lunar lower mantle and the origin of high- μ mare basalts. *Lunar Planet Sci XXXIII*:1821
- Neal CR, Taylor LA, Lindstrom MM (1988) Apollo 14 mare basalt petrogenesis: Assimilation of KREEP-like components by a fractionating magma. *Proc Lunar Planet Sci Conf* 18:139-153
- Neal CR, Taylor LA, Schmitt RA, Hughes SS, Lindstrom MM (1989) High-alumina (HA) and very high potassium (VHK) basalt clasts from Apollo 14 breccia, part 2, whole rock geochemistry: Further evidence for combined assimilation and fractional crystallization within the lunar crust. *Proc Lunar Planet Sci Conf* 19:147-161
- Neumann GA, Zuber MT, Smith DE, Lemoine FG (1996) The lunar crust: Global structure and signature of major basins. *J Geophys Res* 101:16,841-16,843
- Newhall XX, Williams JC (1997) Estimates of the lunar physical librations. *Celest Mech Dyn Astron* 66:21-30
- Newsom H (1984) The lunar core and the origin of the Moon. *EOS* 65:369-370
- Newsom H (1986) Constraints on the origin of the Moon from the abundance of molybdenum and other siderophile elements. *In: Origin of the Moon*. Hartmann WK, Phillips RJ, Taylor GJ (eds) Lunar and Planetary Institute, p 203-229
- Newsom H, Drake MJ (1983) Experimental investigations of the partitioning of phosphorus between metal and silicate phases: Implications for the Earth, Moon, and eucrite parent body. *Geochim Cosmochim Acta* 47:93-100
- Newsom HE (1995) Composition of the solar system, planets, meteorites, and major terrestrial reservoirs. *In: Global Earth Physics: A Handbook of Physical Constants*. Ahrens TJ (ed) American Geophysical Union p 159-189
- Newsom HE, Palme H (1984) The depletion of siderophile elements in the Earth's mantle: New evidence from molybdenum and tungsten. *Earth Planet Sci Lett* 69:354-364
- Newsom HE, Sims KWW, Noll PD, Jaeger WL, Maehr SA, Beserra TB (1996) The depletion of tungsten in the bulk silicate Earth: Constraints on core formation. *Geochim Cosmochim Acta* 60:115-1169
- Newsom HE, White WM, Jochum KP, Hofmann AW (1986) Siderophile and chalcophile element abundances in oceanic basalts, Pb isotope evolution and growth of the Earth's core. *Earth Planet Sci Lett* 80:299-313
- Nord GL, Wandless M-V (1983) Petrology and comparative thermal and mechanical histories of clasts in breccia 62236. *Proc 13th Lunar Planet Sci Conf, J Geophys Res* 88:A645-A657
- Norman M, Borg L, Nyquist LE, Bogard D, Snyder G, Taylor L, Lindstrom M (1998) Composition and age of the lunar highlands: Petrogenesis of ferroan noritic anorthosites 62236. *Lunar Planet Sci XXVIII*:1551
- Norman MD (1981) Petrology of suevitic lunar breccia 67016. *Proc Lunar Planet Sci Conf* 12B:235-252
- Norman MD, Borg LE, Nyquist LE, Bogard DD (2003) Chronology, geochemistry, and petrology of a ferroan noritic anorthosite clast from Descartes breccia 67215: Clues to the age, origin, structure, and impact history of the lunar crust. *Meteor Planet Sci* 38:645-661
- Norman MD, Garcia MO (1999) Primitive magmas and source characteristics of the Hawaiian plume: Petrology and geochemistry of shield picroites. *Earth Planet Sci Lett* 168:27-44
- Norman MD, Keil K, Griffin WL, Ryan CG (1995) Fragments of ancient lunar crust: Petrology and geochemistry of ferroan noritic anorthosites from the Descartes region of the Moon. *Geochim Cosmochim Acta* 59:831-847
- Norman MD, Ryder G (1980) Geochemical constraints on the igneous evolution of the lunar crust. *Proc Lunar Planet Sci Conf* 11:317-331
- Norman MD, Taylor SR (1992) Geochemistry of lunar crustal rocks from breccia 67016 and the composition of the Moon. *Geochim Cosmochim Acta* 56:1013-1024
- Nyquist LE, Shih C-Y (1992) The isotopic record of lunar volcanism. *Geochim Cosmochim Acta* 56:2213-2234
- O'Keefe JD, Ahrens TJ (1993) Planetary cratering mechanics. *J Geophys Res* 98:17,011-17,028
- O'Neill HSC (1991) The origin of the Moon and the early history of the Earth—chemical model. Part 1: The Moon. *Geochim Cosmochim Acta* 55:1143-1158
- Oberst J (1987) Unusually high stress drops associated with shallow moonquakes. *J Geophys Res* 92:1397-1405
- Oberst J (1989) Meteoroids near the Earth-Moon system as inferred from temporal and spatial distribution of impacts detected by the lunar seismic network. Ph.D. thesis, University of Texas, Austin
- Oberst J, Nakamura Y (1991) A search for clustering among the meteoroid impacts detected by the Apollo lunar seismic network. *Icarus* 91:315-325
- Ockendon JR, Turcotte DL (1977) On the gravitational potential and field anomalies due to thin mass layers. *Geophys J R Astron Soc* 48:479-492
- Palme H, Baddenhausen H, Blum K, Cendales M, Dreibus G, Hofmeister H, Kruse H, Palme C, Spettel B, Vilczek E, Wänke H, Kurat G (1978) New data on lunar samples and achondrites and a comparison of the least fractionated samples from the Earth, Moon, and the eucrite parent body. *Proc Lunar Planet Sci Conf* 9:25-57
- Palme H, Nickel KG (1986) Ca/Al ratio and composition of the Earth's primitive upper mantle. *Geochim Cosmochim Acta* 49:2123-2132

- Papike JJ, Fowler GW, Shearer CK (1994) Orthopyroxene as a recorder of lunar crust evolution: An ion microprobe investigation of Mg-suite norites. *Am Mineral* 79:796-800
- Papike JJ, Fowler GW, Shearer CK, Layne GD (1996) Ion microprobe investigation of plagioclase from lunar Mg-suite norites: Implications for calculating parental melt REE concentrations and for assessing post-crystallization REE distribution. *Geochim Cosmochim Acta* 60:3967-3978
- Papike JJ, Ryder G, Shearer CK (1998) Lunar samples. *Rev Mineral* 36:5.1-5.234
- Parker RL (1972) The rapid calculation of potential anomalies. *Geophys J R Astron Soc* 31:447-455
- Parmentier EM, Zhong S, Zuber MT (2002) Gravitational differentiation due to initial chemical stratification: origin of lunar asymmetry by the creep of dense KREEP? *Earth Planet Sci Lett* 201:473-480
- Peale SJ, Cassen P (1978) Contribution of tidal dissipation to lunar thermal history. *Icarus* 36:245-269
- Peeples WJ, Sill WR, May TW, Ward SH, Phillips RJ, Jordan RL, Abbott EA, Killpack TJ (1978) Orbital radar evidence for lunar subsurface layering in Maria Serenitatis and Crisium. *J Geophys Res* 83:3459-3468
- Phillips RJ, Adams GF, Brown WE, Jr., Eggleton RE, Jackson P, Jordan R, Peeples WJ, Porcello LJ, Ryu J, Schaber GG, Sill WR, Thompson TW, Ward SH, Zelenka JS (1973) The Apollo 17 lunar sounder. *Proc Lunar Sci Conf* 4: 2821-2831
- Phillips RJ, Dvorak J (1981) The origin of lunar mascons: analysis of the Bouguer gravity associated with Grimaldi. *In: Multi-ring Basins.* Schultz PH, Merrill RB (eds) Pergamon Press, p 91-104
- Phillips RJ, Lambeck K (1980) Gravity fields of the terrestrial planets: long-wavelength anomalies and tectonics. *Rev Geophys Space Phys* 18:27-76
- Phinney WC (1994) FeO and MgO in plagioclase of lunar anorthosites: Igneous or metamorphic? *Lunar Planet Sci XXXV*:1081-1082
- Phipps Morgan J, Blackman DK (1993) Inversion of combined gravity and bathymetry data for crustal structure: A prescription for downward continuation. *Earth Planet Sci Lett* 119:167-179
- Pieters CM (1978) Mare basalt types on the front side of the Moon: A summary of spectral reflectance data. *Proc Lunar Planet Sci Conf* 9:2825-2849
- Pieters CM (1986) Composition of the lunar highland crust from near-infrared spectroscopy. *Rev Geophys* 24:557-578
- Pieters CM (1991) Bullialdus: Strengthening the case for lunar plutons. *Geophys Res Lett* 18:2129-2132
- Pieters CM, Duke M, Head JW, Jolliff B (2003) Science options for sampling South Pole-Aitken Basin. *Lunar Planet Sci XXXIV*:1366
- Pieters CM, et al. (1993) Crustal diversity of the Moon: Compositional analyses of Galileo solid state imaging data. *J Geophys Res* 98:17,127-17,148
- Pieters CM, Head JW, III, Gaddis L, Jolliff BL, Duke M (2001) Rock types of the South Pole-Aitken basin and extent of basaltic volcanism. *J Geophys Res* 106:28,001-28,022
- Pieters CM, Tompkins S, Head JW, Hess PC (1997) Mineralogy of the mafic anomaly in the South Pole-Aitken Basin: Implications for excavation of the lunar mantle. *Geophys Res Lett* 24:1903-1906
- Presnall DC (1995) Phase diagrams of Earth-forming minerals. *In: Mineral Physics and Crystallography: A Handbook of Physical Constants* (AGU reference shelf 2). Ahrens TJ (ed) American Geophysical Union, p 248-268
- Press WH, Teukolsky SA, Vetterling WT, Flannery BP (1992) *Numerical Recipes in Fortran 77: The Art of Scientific Computing*. Cambridge Univ. Press
- Pritchard ME, Stevenson DJ (2000) Thermal aspects of a lunar origin by giant impact. *In: Origin of the Earth and Moon.* Canup R, Righter K (eds) Univ. Arizona Press, p 179-196
- Pullan S, Lambeck K (1981) Mascons and loading of the lunar lithosphere. *Proc Lunar Planet Sci Conf* 12:853-865
- Pérez-Gussinyé M, Lowry AR, Watts AB, Velicogna I (2004) On the recovery of effective elastic thickness using spectral methods: Examples from synthetic data and from the Fennoscandian Shield. *J Geophys Res* 109:B10409, doi:10.1029/2003JB002788
- Quick JE, Albee AL, Ma M-S, Murali AV, Schmitt RA (1977) Chemical composition and possible immiscibility of two silicate melts in 12013. *Proc Lunar Sci Conf* 8:2153-2189
- Raedeke LD, McCallum IS (1980) A comparison of fractionation trends in the lunar crust and the Stillwater Complex. *In: Proc. Conf. Lunar Highlands Crust.* Papike JJ, Merrill RB (eds) Pergamon Press, p 133-153
- Rees CE, Thode HG (1972) Sulfur concentrations and isotope ratios in lunar samples. *Proc Lunar Sci Conf* 3:1479-1485
- Rees CE, Thode HG (1974) Sulfur concentrations and isotope ratios in Apollo 16 and 17 samples. *Proc Lunar Sci Conf* 5:1963-1973
- Reid AM, Duncan AR, Richardson SH (1977) In search of LKFM. *Proc Lunar Sci Conf* 8:2321-2338
- Richmond NC, Hood LL, Halekas JS, Mitchell DL, Lin RP, Acuña MH, Binder AB (2003) Correlation of strong lunar magnetic anomaly with a high-albedo region of the Descartes mountains. *Geophys Res Lett* 30:1395, doi: 10.1029/2003GL016938
- Ridley WI, Hubbard NJ, Rhodes JM, Wiesmann H, Bansal BM (1973) The petrology of lunar breccia 15445 and petrogenetic implications. *J Geol* 81:621-631
- Righter K (2002) Does the Moon have a metallic core? Constraints from giant-impact modeling and siderophile elements. *Icarus* 158:1-13

- Righter K, Drake M (1996) Core formation in Earth's Moon, Mars, and Vesta. *Icarus* 124:513-529
- Righter K, Drake MJ (1997) Metal-silicate equilibrium in a homogeneously accreting Ear: New results for Re. *Earth Planet Sci Lett* 146:541-553
- Righter K, Drake MJ (1999) Effect of water on metal-silicate partitioning of siderophile elements: A high pressure and temperature terrestrial magma ocean and core formation. *Earth Planet Sci Lett* 171:383-399
- Righter K, Drake MJ (2000) Metal-silicate equilibrium in the early Ear: New constraints from volatile moderately siderophile elements Ga, Sn, Cu, P. *Geochim Cosmochim Acta* 64:3581-3597
- Righter K, Hervig RL, Kring D (1998) Accretion and core formation in Mars: Molybdenum contents of melt inclusion glasses from three SNC meteorites. *Geochim Cosmochim Acta* 62:2167-2177
- Righter K, Shearer CK (2003) Magmatic fractionation of Hf and W: constraints on the timing of core formation and differentiation in the Moon and Mars. *Geochim Cosmochim Acta* 67:2497-2507
- Righter K, Walker RJ, Warren PH (2000) The origin and significance of highly siderophile elements in the lunar and terrestrial mantles. *In: Origin of the Earth and Moon*. Canup R, Righter K (eds) Univ. Arizona Press, p 291-322
- Ringwood AE (1979) *Origin of the Earth and Moon*. Springer-Verlag
- Ringwood AE, Kesson SE, Hibberson W (1981) Rhenium depletion in mare basalts and redox state of the lunar interior. *Lunar Planet Sci XII*:891-893
- Ringwood AE, Seiferl S (1986) Nickel-cobalt abundance systematics and their bearing on lunar origin. *In: Origin of the Moon*. Hartmann WK, Phillips RJ, Taylor GJ (eds) Lunar and Planetary Institute, p 249-277
- Roberts PH, Glatzmaier GA (2000) Geodynamo theory and simulations. *Rev Mod Phys* 72:1081-1123
- Rochette P (2000) Comment on "Initial measurements of the lunar induced magnetic dipole moment using Lunar Prospector magnetometer data" by Hood et al. *Geophys Res Lett* 27:1077-1078
- Roddy DJ (1977) Large-scale impact and explosion craters: Comparisons of morphological and structural analogs. *In: Impacts and Explosion Cratering*. Roddy DJ, Pepin RO, Merrill RB (eds) Pergamon Press, p 815-841
- Rose HJ Jr, Baedecker PA, Berman S, Christian RP, Dwornik EJ, Finkelman RB, Schnepp MM (1975) Chemical composition of rocks and soils returned by the Apollo 15, 16, and 17 missions. *Proc Lunar Sci Conf* 6:1363-1373
- Rubie DC, Melosh HJ, Reid JE, Liebske C, Righter K (2003) Mechanisms of metal-silicate equilibration in the terrestrial magma ocean. *Earth Planet Sci Lett* 205:
- Runcorn SK (1994) The early magnetic-field and primeval satellite of the Moon: Clues to planetary formation. *Philos Trans R Soc London Ser A* 349:181-196
- Runcorn SK (1996) The formation of the lunar core. *Geochim Cosmochim Acta* 60:1205-1208
- Russell CT, Coleman PJ, Goldstein BE (1981) Measurements of the lunar induced magnetic moment in the geomagnetic tail: Evidence for a lunar core. *Proc Lunar Planet Sci Conf* 12:831-836
- Russell SS, Folco L, Grady MM, Zolensky ME, Jones R, Righter K, Zipfel J, Grossman JN (2004) The Meteoritical Bulletin No. 88, 2004, July. *Meteorit Planet Sci* 39:A215-A272
- Russell SS, Zipfel J, Folco L, Jones R, Grady MM, McCoy T, Grossman JN (2003) The Meteoritical Bulletin, No. 87, 2003, July. *Meteorit Planet Sci* 38:A194
- Russell SS, Zipfel J, Grossman JN, Grady MM (2002) The Meteoritical Bulletin, No. 86, 2002, July. *Meteor Planet Sci* 37:A157-A184
- Ryder G (1976) Lunar sample 15405: Remnant of a KREEP basalt-granite differentiated pluton. *Earth Planet Sci Lett* 29:255-268
- Ryder G (1979) The chemical components of highlands breccias. *Proc Lunar Planet Sci Conf* 10:561-581
- Ryder G (1985) Catalog of Apollo 15 Rocks. Curatorial Publication 20787. NASA Johnson Space Center, Houston
- Ryder G (1991) Lunar ferroan anorthosites and mare basalt sources: The mixed connection. *Geophys Res Lett* 18: 2065-2068
- Ryder G (1994) Coincidence in time of the Imbrium basin impact and Apollo 15 KREEP volcanic flows: The case for impact-induced melting. *Spec Paper Geol Soc Am* 293:11-18
- Ryder G, Koeberl C, Mojzsis SJ (2000) Heavy bombardment of the Earth at ~3.85 Ga: The search for petrologic and geochemical evidence. *In: Origin of the Earth and Moon*. Canup R, Righter K (eds) Univ. Arizona Press, p 475-492
- Ryder G, Martinez RR (1991) Evolved hypabyssal rocks from Station 7, Apennine Front, Apollo 15. *Proc Lunar Planet Sci* 21:137-150
- Ryder G, Norman MD (1978) Catalog of Pristine Nonmare Materials Part 2. Anorthosites. NASA Johnson Space Center
- Ryder G, Norman MD (1979) Catalog of Pristine Non-mare Materials Part 1, Non-Anorthosites (Revised). NASA Johnson Space Center Curatorial Facility
- Ryder G, Norman MD (1980) Catalog of Apollo 16 Rocks. NASA Johnson Space Center Curatorial Facility
- Ryder G, Norman MD, Taylor GJ (1997) The complex stratigraphy of the highland crust in the Serenitatis region of the Moon inferred from mineral fragment chemistry. *Geochim Cosmochim Acta* 61:1083-1105
- Ryder G, Sherman SB (1989) The Apollo 15 coarse fines (4-10 mm). National Aeronautics and Space Administration Lyndon B. Johnson Space Center, TM-101934

- Ryder G, Spudis PD (1987) Chemical composition and origin of Apollo 15 impact melts. Proc 17th Lunar Planet Sci Conf, J Geophys Res 92:E432-E446
- Ryder G, Stoesser DB, Wood JA (1977) Apollo 17 KREEPy basalt: A rock type intermediate between KREEP and mare basalts. Earth Planet Sci Lett 35:1-13
- Ryder G, Wood JA (1977) Serenitatis and Imbrium impact melts: Implications for large-scale layering in the lunar crust. Proc Lunar Sci Conf 8:655-668
- Sack RO, Ghiorso MS (1991) Chromian spinel as petrogenetic indicators: Thermodynamic and petrologic applications. Am Mineral 76:827-847
- Salpas PA, Taylor LA, Lindstrom MM (1987) Apollo 17 KREEPy basalts: Evidence for the non-uniformity of KREEP. Proc 17th Lunar Planet Sci Conf, J Geophys Res 92:E340-E348
- Sato M (1978) Oxygen fugacity of basaltic magmas and the role of gas forming elements. Geophys Res Lett 5:447-449
- Sato M (1979) The driving mechanism of lunar pyroclastic eruptions inferred from the oxygen fugacity behavior of the Apollo 17 orange glass. Proc Lunar Planet Sci Conf 10:311-325
- Sato M, Helz RT (1971) Oxygen fugacity values of Apollo 12 basaltic rocks. Lunar Sci II:144-145
- Sato M, Hickling NL, McLane JE (1973) Oxygen fugacity values of Apollo 12, 14 and 15 lunar samples and reduced state of lunar magmas. Proc Lunar Sci Conf 4:1061-1079
- Schaber GG (1973) Lava flows in Mare Imbrium: geologic evaluation from Apollo orbital photography. Proc Lunar Sci Conf 4:73-92
- Schaber GG, Boyce JM, Moore HJ (1976) The scarcity of mappable flow lobes on the lunar maria: Unique morphology of the Imbrium flows. Proc Lunar Sci Conf 7:2783-2800
- Schaeffer GA, Schaeffer OA (1977) ^{39}Ar - ^{40}Ar ages of lunar rocks. Proc Lunar Sci Conf 8:2253-2300
- Schoenberg R, Kamber BS, Collerson KD, Eugster O (2002) New W-isotope evidence for rapid terrestrial accretion and very early core formation. Geochim Cosmochim Acta 66:3151-3160
- Schultz PH (1997) Forming the South-Pole Aitken basin: the extreme games. Lunar Planet Sci XXVIII:1787
- Schultz PH, Spudis PD (1983) Beginning and end of lunar mare volcanism. Nature 302:233-236
- Schultz RA, Zuber MT (1994) Observations, models, and mechanisms of failure of surface rocks surrounding planetary surface loads. J Geophys Res 99:14,691-14,702
- Segatz M, Spohn T, Ross N, Schuber G (1988) Tidal dissipation, surface heat flow, and figures of viscoelastic models of Io. Icarus 75:187-206
- Selkin PA, Tauxe L (2000) Long-term variations in palaeointensity. Philos Trans R Soc London Ser A 358:1065-1088
- Sellers PC (1992) Seismic evidence for a low-velocity lunar core. J Geophys Res 97:11,663-11,672
- Sharpton VL, Head JW III (1982) Stratigraphy and structural evolution of southern Mare Serenitatis: A reinterpretation based on Apollo lunar sounder experiment data. J Geophys Res 87:10,983-10,998
- Shearer CK, Floss C (2000) Evolution of the Moon's mantle and crust as reflected in trace-element microbeam studies of lunar magmatism. In: Origin of the Earth and Moon. Canup R, Righter K (eds) Univ. Arizona Press, p 339-359
- Shearer CK, Papike JJ (1993) Exploring volcanism on the Moon: A perspective from volcanic picritic glass beads. Geochim Cosmochim Acta 57:4785-4812
- Shearer CK, Papike JJ (1999) Magmatic evolution of the Moon. Am Mineral 84:1469-1494
- Shearer CK, Papike JJ, Layne GD (1996) The role of ilmenite in the source region for mare basalts: Evidence from niobium, zirconium, and cerium in picritic glasses. Geochim Cosmochim Acta 60:3521-3530
- Shearer CK, Papike JJ, Simon SB, Galbreath KC, Shimizu N (1990) Ion microprobe studies of REE and other trace elements in Apollo 14 'volcanic' glass beads and comparison to Apollo 14 mare basalts. Geochim Cosmochim Acta 54:851-867
- Shearer CK, Righter K (2003) Behavior of tungsten and hafnium in silicates: a crystal chemical basis for understanding the early evolution of the terrestrial planets. Geophys Res Lett 30:doi:10.1029/2002GL015523
- Shearer CK, Weidenbeck MG, Fowler GW, Papike JJ (1997) Volatiles in planetary mantles. The behavior of sulfur in lunar picritic magmas and the Moon's mantle. Geol Soc Amer Abstr with Prog 29:A-192
- Shearer CK, Weidenbeck MG, Fowler GW, Papike JJ (1998) S and other volatiles in lunar picritic magmas and the lunar mantle. An approach using secondary ion mass spectrometry. Lunar Planet Sci XXVIII:1284
- Shervais JW, McGee JJ (1998) Ion and electron microprobe study of troctolites, norite, and anorthosites from Apollo 14: Evidence for urKREEP assimilation during petrogenesis of Apollo 14 Mg-suite rocks. Geochim Cosmochim Acta 62:3009-3023
- Shervais JW, McGee JJ (1999) KREEP in the western lunar highlands: Ion and electron microprobe study of alkali anorthosites and norites from Apollo 14. Am Mineral 84:806-820
- Shervais JW, Taylor LA (1986) Petrologic constraints on the origin of the Moon. In: Origin of the Moon. Hartmann WK, Phillips RJ, Taylor GJ (eds) Lunar and Planetary Institute, p 173-201
- Shervais JW, Taylor LA, Laul JC (1983) Ancient crustal components in Fra Mauro breccias. Proc 14th Lunar Sci Conf, J Geophys Res 88:B177-B192
- Shervais JW, Taylor LA, Laul JC, Smith MR (1984) Pristine highlands clasts in consortium breccia 14305: Petrology and geochemistry. Proc 15th Lunar Planet Sci Conf, J Geophys Res 89:C25-C40

- Shih C-Y, Nyquist LE, Bansal BM, Wiesmann H (1992) Rb-Sr and Sm-Nd chronology of an Apollo 17 KREEP basalt. *Earth Planet Sci Lett* 108:203-215
- Shih C-Y, Nyquist LE, Bogard DD, Bansal BM, Wiesmann H (1993) Ages of pristine noritic clasts from lunar breccia 15445 and 15455. *Geochim Cosmochim Acta* 57:915-931
- Simmons G, Siegfried R, Richter D (1975) Characteristics of microcracks in lunar samples. *Proc Lunar Sci Conf* 6: 3227-3254
- Simmons G, Todd T, Wang H (1973) The 25-km discontinuity: Implications for lunar history. *Science* 182:158-161
- Simon SB, Papike JJ (1985) Petrology of the Apollo 12 highland component. *Proc 16th Lunar Planet Sci Conf*, J Geophys Res 90:D47-D60
- Simons FJ, Dahlen FA, Wieczorek MA (2006) Spatirospectral concentration on a sphere. *SIAM Rev* (in press)
- Simons FJ, Zuber MT, Korenaga J (2000) Isostatic response of the Australian lithosphere: Estimations of effective elastic thickness and anisotropy using multitaper spectral analysis. *J Geophys Res* 105:19,163-19,184
- Simons M, Solomon SC, Hager BH (1997) Localization of gravity and topography: constraints on the tectonics and mantle dynamics of Venus. *Geophys J Int* 131:24-44
- Sjogren WL, Smith JC (1976) Quantitative mass distribution models for Mare Orientale. *Proc Lunar Planet Sci Conf* 7:2639-2648
- Smith DE, Zuber MT, Neumann GA, Lemoine FG (1997) Topography of the Moon from Clementine lidar. *J Geophys Res* 102:1591-1611
- Smith JV, Anderson AT, Newton RC, Olsen EJ, Wyllie PJ, Crewe AV, Isaacson MS, Johnson D (1970) Petrologic history of the Moon inferred from petrography, mineralogy, and petrogenesis of Apollo 11 rocks. *In: Proceedings of the Apollo 11 Lunar Science Conference*. Pergamon Press, p 897-925
- Snyder GA, Borg LE, Nyquist LE, Taylor LA (2000) Chronology and isotopic constraints on lunar evolution. *In: Origin of the Earth and Moon*. Canup R, Righter K (eds) Univ. Arizona Press, p 361-395
- Snyder GA, Neal CR, Taylor LA (1995a) Processes involved in the formation of magnesian-suite plutonic rocks from the highlands of the Earth's Moon. *J Geophys Res* 100:9365-9388
- Snyder GA, Taylor LA, Halliday A (1995b) Chronology and petrogenesis of the lunar highlands alkali suite: Cumulates from KREEP basalt crystallization. *Geochim Cosmochim Acta* 59:1185-1203
- Snyder GA, Taylor LA, Liu Y-G, Schmitt RA (1992a) Petrogenesis of the western highlands of the Moon: Evidence from a diverse group of whitlockite-rich rocks from the Fra Mauro Formation. *Proc Lunar Planet Sci* 22:399-416
- Snyder GA, Taylor LA, Neal CR (1992b) A chemical model for generating the sources of mare basalts: Combined equilibrium and fractional crystallization of the lunar magmasphere. *Geochim Cosmochim Acta* 56:3809-3823
- Sohl F, Spohn T (1997) The interior structure of Mars: Implications from SNC meteorites. *J Geophys Res* 102:1613-1635
- Solomon SC (1978) The nature of isostasy on the Moon: How big of a Pratt-fall for Airy methods. *Proc Lunar Planet Sci Conf* 9:3499-3511
- Solomon SC, Chaiken J (1976) Thermal expansion and thermal stress in the Moon and terrestrial planets: Clues to early thermal history. *Proc Lunar Sci Conf* 7:3229-3243
- Solomon SC, Head JW (1979) Vertical movement in mare basins: Relation to mare emplacement, basin tectonics, and lunar thermal history. *J Geophys Res* 84:1667-1682
- Solomon SC, Head JW (1980) Lunar mascon basins: lava filling, tectonics, and evolution of the lithosphere. *Rev Geophys Space Phys* 18:107-141
- Solomon SC, Longhi J (1977) Magma oceanography, I, Thermal evolution. *Proc Lunar Sci Conf* 8:583-599
- Sonnett CP (1982) Electromagnetic induction in the Moon. *Rev Geophys Space Phys* 20:411-455
- Sonnett CP, Smith BF, Colburn DS, Schubert G, Schwartz K (1972) The induced magnetic field of the moon: Conductivity profiles and inferred temperature. *Proc Lunar Sci Conf* 3:2309-2336
- Spera FJ (1992) Lunar magma transport phenomena. *Geochim Cosmochim Acta* 56:2253-2265
- Spudis P, Pieters C (1991) Global and regional data about the Moon (Chapter 10). *In: Lunar Sourcebook: A Users Guide to the Moon*. Heiken GH, Vaniman DT, French BM (eds) Cambridge University Press, p 595-632
- Spudis PD (1978) Composition and origin of the Apennine Bench Formation. *Proc Lunar Planet Sci Conf* 9:3379-3394
- Spudis PD (1993) The Geology of Multi-Ring Impact Basins. Cambridge Univ. Press
- Spudis PD, Davis PA (1986) A chemical and petrological model of the lunar crust and implications for lunar crustal origin. *Proc 17th Lunar Planet Sci Conf*, Part 1, *J Geophys Res suppl.* 91:E84-E90
- Spudis PD, Hawke BR, Lucey P (1984) Composition of Orientale basin deposits and implications for the lunar basin-forming process. *Proc 15th, Lunar Planet Sci Conf*, Part 1, *J Geophys Res, suppl.* 89:C197-C210
- Spudis PD, Hawke BR, Lucey PG, Taylor GJ, Stockstill K (1996) Composition of the ejecta deposits of selected lunar basins from Clementine elemental maps. *Lunar Planet Sci XXVII*:1255-1256
- Spudis PD, Reisse RA, Gillis JJ (1994) Ancient multiring basins on the Moon revealed by Clementine laser altimetry. *Science* 266:1848-1851
- Spudis PD, Ryder G (1981) Apollo 17 impact melts and their relation to the Serenitatis basin. *Multi-Ring Basins*, *Proc Lunar Planet Sci Conf* 12A:133-148

- Spudis PD, Ryder G, Taylor GJ, McCormick KA, Keil K, Grieve RAF (1991) Source of mineral fragments in impact melts 15445 and 15455: Toward the origin of Low-K Fra Mauro basalt. *Proc Lunar Planet Sci Conf* 21:151-165
- Srnka LJ (1977) Spontaneous magnetic field generation in hypervelocity impacts. *Proc Lunar Sci Conf* 8:785-792
- Srnka LJ, Martelli G, Newton G, Cisowski SM, Fuller MD, Schaal RB (1979) Magnetic field and shock effects and remanent magnetization in a hypervelocity impact experiment. *Earth Planet Sci Lett* 42:127-137
- Staid MI, Pieters CM (2000) Integrated spectral analysis of mare soils and craters: Application to eastern nearside basalts. *Icarus* 145:122-139
- Staid MI, Pieters CM (2001) Mineralogy of the last lunar basalts: Results from Clementine. *J Geophys Res* 106:27887-27900
- Stegman DR, Jellinek AM, Zatman SA, Baumgardner JR, Richards MA (2003) An early lunar core dynamo driven by thermochemical mantle convection. *Nature* 421:143-146
- Steinhart J (1967) Mohorovicic discontinuity. *In: International Dictionary of Geophysics*. Runcorn S (ed) Pergamon Press, p 991-994
- Stephenson A, Collinson DW, Runcorn SK (1974) Lunar magnetic field paleointensity determinations on Apollo 11, 16, and 17 rocks. *Proc Lunar Planet Sci Conf* 10:2859-2871
- Stevenson DJ (2003) Planetary magnetic fields. *Earth Planet Sci Lett* 208:1-11
- Streckeisen A (1976) To each plutonic rock, its proper name. *Earth Sci Rev* 12:1-33
- Stöffler D, Bischoff A, Borchardt R, Burghel A, Deutsch A, Jessberger EK, Ostertag R, Palme H, Spettel B, Reimold WU, Wacker K, Wänke H (1985) Composition and evolution of the lunar crust in the Descartes Highlands, Apollo 16. *Proc 15th Lunar Planet Sci Conf, Part 2*, *J Geophys Res* 90:C449-C506
- Stöffler D, Knoll H-D, Marvin UB, Simonds CH, Warren PH (1980) Recommended classification and nomenclature of lunar highland rock—committee report. *In: Proc. Conf Lunar Highland Crust*. Papike JJ, Merrill RB (eds) Pergamon Press, p 51-70
- Sugano T, Heki K (2004) Isostasy of the Moon from high-resolution gravity and topography data: Implication for its thermal history. *Geophys Res Lett* 31:L24703, doi:10.1029/2004GL022059
- Sugiura N (1979) ARM, TRM, and magnetic interactions: concentration dependence. *Earth Planet Sci Lett* 42:451-455
- Sugiura N, Strangway DW (1980) Comparisons of magnetic paleointensity methods using a lunar sample. *Proc Lunar Planet Sci Conf* 9:1801-1813
- Sugiura N, Strangway DW (1983) Magnetic paleointensity determination on lunar sample 62235. *Proc 13th Lunar Planet Sci Conf, Part 2*, *J Geophys Res, suppl.* 88:A684-690
- Tauxe L (1993) Sedimentary records of relative paleointensity of the geomagnetic field: Theory and practice. *Rev Geophys* 31:319-354
- Taylor GJ, Hawke BR, Spudis PD (2002) Bulk composition of the Moon: Importance, uncertainties, and what we need to know. *In: Workshop on Moon Beyond 2002: Next Steps in Lunar Exploration abstract 3049*. Lunar and Planetary Institute, Houston, Taos, New Mexico
- Taylor GJ, Warren P, Ryder G, Delano J, Pieters C, G. L (1991) Lunar Rocks. *In: Lunar Sourcebook, A User's Guide to the Moon*. Heiken GH, Vaniman DT, French BM (eds) Cambridge University Press, p 183-284
- Taylor LA, Mosie AB (1979) Breccia Guidebook #3, 67915. NASA Johnson Space Center
- Taylor LA, Nazarov MA, Cohen BA, Warren PH, Barsukova LD, Clayton RN, Mayeda TK (2001) Bulk chemistry and oxygen isotopic compositions of lunar meteorites Dhofar 025 and Dhofar 026: A second-generation impact melt. *Lunar Planet Sci XXXII:1985*
- Taylor LA, Shervais JW, Hunter RH, Shih CY, Bansal BM, Wooden J, Nyquist LE, Laul LC (1983) Pre-4.2 AE mare-basalt volcanism in the lunar highlands. *Earth Planet Sci Lett* 66:33-47
- Taylor SR (1975) *Lunar Science: a Post-Apollo View; Scientific Results and Insights from the Lunar Samples*. Pergamon Press
- Taylor SR (1982) *Planetary Science: A Lunar Perspective*. Lunar and Planetary Institute
- Taylor SR (1992) *Solar System Evolution: A New Perspective*. Cambridge Univ. Press
- Taylor SR, Rudowski R, Muir P, Graham A, Kaye M (1971) Trace element chemistry of lunar samples from the Ocean of Storms. *Proc Lunar Sci Conf* 2:1083-1099
- Tera F, Papanastassiou DA, Wasserburg GJ (1974) Isotopic evidence for a terminal lunar cataclysm. *Earth Planet Sci Lett* 22:1-21
- Thurber CH, Solomon SC (1978) An assessment of crustal thickness variations on the lunar near side: models, uncertainties, and implications for crustal differentiation. *Proc Lunar Planet Sci Conf* 9:3481-3497
- Thurber CH, Toksöz MN (1978) Martian lithospheric thickness from elastic flexure theory. *Geophys Res Lett* 5:977-980
- Todd T, Richter DA, Simmons G, Wang H (1973) Unique characterization of lunar samples by physical properties. *Proc Lunar Sci Conf* 4:2639-2662
- Toksöz MN, Dainty AM, Solomon SC, Anderson KR (1974) Structure of the Moon. *Rev Geophys* 12:539-567
- Toksöz MN, Press F, Dainty A, Anderson K, Latham G, Ewing M, Dorman J, Lammlein D, Sutton G, Duennebier F (1972) Structure, composition, and properties of lunar crust. *Proc Lunar Sci Conf* 3:2527-2544
- Tompkins S, Pieters CM (1999) Mineralogy of the lunar crust: Results from Clementine. *Meteorit Planet Sci* 34:25-41

- Ulrych TJ, Sacchi MD, Woodbury A (2001) A Bayes tour of inversion: A tutorial. *Geophysics* 66:55-69
- Vinnik L, Chenet H, Gagnepain-Beyneix J, Lognonné P (2001) First seismic receiver functions on the Moon. *Geophys Res Lett* 28:3031-3034
- Vocadlo L, Alfè D, Price GD, Gillan MJ (2000) First principles calculations on the diffusivity and viscosity of liquid Fe-S at experimentally accessible conditions. *Phys Earth Planet Int* 120:145-152
- von Fress RRB, Tan L, Potts LV, Kim JW, Merry CJ, Bossler JD (1997) Lunar crustal analysis of Mare Orientale from topographic and gravity correlations. *J Geophys Res* 102:25,657-25,676
- Wagner TP, Grove TL (1997) Experimental constraints on the origin of lunar high-Ti ultramafic glasses. *Geochim Cosmochim Acta* 61:1315-1327
- Walker D, Norby L, Jones JH (1993) Superheating effects on metal/silicate partitioning of siderophile elements. *Science* 262:1858-1861
- Walter MJ, Newsom H, Ertel W, Holzheid A (2000) Siderophile elements in the Earth and Moon: Metal/silicate partitioning and implications for core formation. *In: Origin of the Earth and Moon.* Canup R, Righter K (eds) Univ. Arizona Press, p 265-290
- Wang H, Todd T, Richter D, Simmons G (1973) Elastic properties of plagioclase aggregates and seismic velocities in the Moon. *Proc Lunar Sci Conf* 4:2663-2671
- Wänke H, Baddenhausen H, Balaceanu A, Teschke F, Spettel B, Dreibus G, Palme H, Quijano-Rico M, Kruse H, Wlotzka F, Begemann F (1972) Multi-element analyses of lunar samples and some implications of the results. *Proc Lunar Sci Conf* 3:1251-1268
- Wänke H, Baddenhausen H, Blum K, Cendales M, Dreibus G, Hofmeister H, Kruse H, Jagoutz E, Palme C, Spettel B, Thacker R, Vilczek E (1977) On the chemistry of lunar samples and achondrites. *Proc Lunar Planet Sci Conf* 8: 2191-2213
- Wänke H, Dreibus G (1986) Geochemical evidence for the formation of the Moon by impact-induced fission of the proto-Earth. *In: Origin of the Moon.* Hartmann WK, Phillips RJ, Taylor GJ (eds) Lunar and Planetary Institute, p 649-672
- Wänke H, Palme H, Baddenhausen H, Dreibus G, Jagoutz E, Kruse H, Palme C, Spettel B, Teshke F, Thacker R (1975) New data on the chemistry of lunar samples: Primary matter in the lunar highlands and the bulk composition of the Moon. *Proc Lunar Sci Conf* 6:1313-1340
- Wänke H, Palme H, Baddenhausen H, Dreibus G, Jagoutz E, Kruse H, Spettel B, Teschke F, Thacker R (1974) Chemistry of Apollo 16 and 17 samples: Bulk composition, late stage accumulation and early differentiation of the Moon. *Proc Lunar Sci Conf* 5:1307-1335
- Ward WR (1975) Past Orientation of the lunar spin axis. *Science* 189:377-379
- Warner JL, Phinney WC, Bickel CE, Simonds CH (1977) Feldspathic granulitic impactites and pre-final bombardment lunar evolution. *Proc Lunar Sci Conf* 8:2051-2066
- Warner RD, Taylor GJ, Keil K (1980) Petrology of 60035: Evolution of a polymict ANT breccia. *In: Proc. Conf. Lunar Highlands Crust.* Papike JJ, Merrill RB (eds) Pergamon, p 377-394
- Warner RD, Taylor GJ, Mansker WL, K. K (1978) Clast assemblage of possible deep-seated (77517) and immiscible-melt (77538) origins in Apollo 17 breccias. *Proc Lunar Planet Sci Conf* 9:941-958
- Warren P (1994) Lunar and martian meteorite delivery services. *Icarus* 111:338-363
- Warren PH (1985) The magma ocean concept and lunar evolution. *Annu Rev Earth Planet Sci* 13:201-240
- Warren PH (1988) The origin of pristine KREEP: Effects of mixing between urKREEP and the magmas parental to the Mg-rich cumulates. *Proc Lunar Planet Sci Conf* 18:233-241
- Warren PH (1989) KREEP: Major-element diversity, trace-element uniformity (almost). *In: Workshop on Moon in Transition: Apollo 14, KREEP, and Evolved Lunar Rocks* LPI Tech. Report. 89-03:149-153. Lunar and Planetary Institute
- Warren PH (1990) Lunar anorthosites and the magma-ocean plagioclase-flotation hypothesis: importance of FeO enrichment in the parent magma. *Am Mineral* 75:46-58
- Warren PH (1993) A concise compilation of petrologic information on possibly pristine nonmare Moon rocks. *Am Mineral* 78:360-376
- Warren PH (2000) Bulk composition of the Moon as constrained by Lunar Prospector Th data. I. Application of ground truth for calibration. *Lunar Planet Sci XXXI:1756*
- Warren PH (2001) Early lunar crustal genesis: the ferroan anorthosite epsilon-neodymium paradox as a possible result of crustal overturn. *Meteorit Planet Sci* 36(supplement):A219
- Warren PH, Bridges JC (2004) Lunar meteorite Yamato-983885: A relatively KREEPy regolith breccia not paired with Y-791197. *In: 67th Annual Meteoritical Society Meeting #5095.* Meteorit Planet Sci, August 2-6, 2004, Rio de Janeiro, Brazil
- Warren PH, Humphrys TL (2003) Bulk composition of the moon as constrained by thorium data: Comparison of Lunar Prospector versus Apollo GRS results. *Lunar Planet Sci XXXIV:2034*
- Warren PH, Jerde EA, Kallemeij GW (1987) Pristine Moon rocks: A “large” felsite and a metal-rich ferroan anorthosite. *Proc 17th Lunar Planet Sci Conf, J Geophys Res* 92:E303-E313
- Warren PH, Jerde EA, Kallemeij GW (1990) Pristine moon rocks: An alkali anorthosite with coarse augite exsolution from plagioclase, a magnesian harzburgite, and other oddities. *Proc Lunar Planet Sci Conf* 20:31-59

- Warren PH, Jerde EA, Kallemyen GW (1991) Pristine Moon rocks: Apollo 17 anorthosites. *Proc Lunar Planet Sci* 21: 51-61
- Warren PH, Rasmussen KL (1987) Megaregolith insulation, internal temperatures, and bulk uranium content of the Moon. *J Geophys Res* 92:3453-3465
- Warren PH, Shirley DN, Kallemyen GW (1986) A potpourri of pristine lunar rocks, including a VHK mare basalt and a unique, augite-rich Apollo 17 anorthosite. *Proc 16th Lunar Planet Sci Conf, Part 2, J Geophys Res, suppl.* 91: D319-D330
- Warren PH, Taylor GJ, Kallemyen GW, Cohen BA, Nazarov MA (2001) Bulk-compositional study of three lunar meteorites: Enigmatic siderophile element results for Dhofar 026. *Lunar Planet Sci XXXII:2197*
- Warren PH, Taylor GJ, Keil K, Kallemyen GW, Rosener PS, Wasson JT (1983a) Sixth foray for pristine nonmare rocks and an assessment of the diversity of lunar anorthosites. *Proc 13th Lunar Planet Sci Conf, in J Geophys Res* 88: A615-A630
- Warren PH, Taylor GJ, Keil K, Kallemyen GW, Shirley DN, Wasson JT (1983b) Seventh foray: Whitlockite-rich lithologies, a diopside-bearing troctolitic anorthosite, ferroan anorthosites, and KREEP. *Proc 14th Lunar Planet Sci Conf, J Geophys Res* 88:B151-B164
- Warren PH, Taylor GJ, Keil K, Marshall C, Wasson JT (1981) Foraging westward for pristine non-mare rocks: Complications for petrogenetic models. *Proc Lunar Planet Sci* 12B:21-40
- Warren PH, Taylor GJ, Keil K, Shirley DN, Wasson JT (1983c) Petrology and chemistry of two "large" granite clasts from the Moon. *Earth Planet Sci Lett* 64:175-185
- Warren PH, Wasson JT (1977) Pristine nonmare rocks and the nature of the lunar crust. *Proc Lunar Sci Conf* 8:2215-2235
- Warren PH, Wasson JT (1978) Compositional-petrographic investigation of pristine nonmare rocks. *Proc Lunar Planet Sci Conf* 9:185-217
- Warren PH, Wasson JT (1979a) The compositional-petrographic search for pristine nonmare rocks: Third foray. *Proc Lunar Sci Conf* 10:583-610
- Warren PH, Wasson JT (1979b) The origin of KREEP. *Rev Geophys* 17:73-88
- Warren PH, Wasson JT (1980) Further foraging for pristine nonmare rocks: Correlations between geochemistry and longitude. *Proc Lunar Planet Sci Conf* 11:431-470
- Wasson JT, Baedecker PA (1972) Provenance of Apollo 12 KREEP. *Proc Lunar Sci Conf* 3rd:1315-1326
- Wasson JT, Warren PH (1980) Contribution of the mantle to the lunar asymmetry. *Icarus* 44:752-771
- Watts AW, Greeley R, Melosh HJ (1991) The formation of terrains antipodal to major impact basins. *Icarus* 93:159-168
- Webb DJ (1982) Tides and the evolution of the Earth-Moon system. *Geophys J R Astron Soc* 70:261-271
- Weitz CM, Rutherford MJ, Head JW (1997) Oxidation states during ascent and eruption of the volcanic glasses as inferred from metal-melt equilibria in the 74001/2 core. *Geochim Cosmochim Acta* 61:2765-2775
- Wellman TR (1970) Gaseous species in equilibrium with Apollo 11 holocrystalline rocks during their crystallization. *Nature* 225:716-717
- Wentworth SJ, McKay DS, Lindstrom DJ, Basu A, Martinez RR, Bogard DD, Garrison DH (1994) Apollo 12 rocky glasses revisited. *Meteorit Planet Sci* 29:323-333
- Whitford-Stark JL, Head JW (1977) The Procellarum volcanic complexes: Contrasting styles of volcanism. *Proc Lunar Sci Conf* 8:2705-2724
- Whitford-Stark JL, Head JW III (1980) Stratigraphy of Oceanus Procellarum basalts: Sources and styles of emplacement. *J Geophys Res* 85:6579-6609
- Wieczorek MA, Phillips RJ (1997) The structure and compensation of the lunar highland crust. *J Geophys Res* 102: 10,933-10,943
- Wieczorek MA, Phillips RJ (1998) Potential anomalies on a sphere: Applications to the thickness of the lunar crust. *J Geophys Res* 103:1715-1724
- Wieczorek MA, Phillips RJ (1999) Lunar multiring basins and the cratering process. *Icarus* 139:246-259
- Wieczorek MA, Phillips RJ (2000) The Procellarum KREEP Terrane: Implications for mare volcanism and lunar evolution. *J Geophys Res* 105:20,417-20,430
- Wieczorek MA, Simons FJ (2005) Localized spectral analysis on the sphere. *Geophys J Int* in press
- Wieczorek MA, Zuber MT (2001a) The composition and origin of the lunar crust: Constraints from central peaks and crustal thickness modeling. *Geophys Res Lett* 28:4023-4026
- Wieczorek MA, Zuber MT (2001b) A Serenitatis origin for the Imbrium grooves and South Pole-Aitken thorium anomaly. *J Geophys Res* 106:27,825-27,840
- Wieczorek MA, Zuber MT (2002) The "core" of the Moon: Iron or titanium rich? *Lunar Planet Sci XXXIII:1384*
- Wieczorek MA, Zuber MT (2004) Thickness of the Martian Crust: Improved Constraints from geoid-to-topography Ratios. *J Geophys Res* 109:E01009, doi:10.1029/2003JE002153
- Wieczorek MA, Zuber MT, Phillips RJ (2001) The role of magma buoyancy on the eruption of lunar basalts. *Earth Planet Sci Lett* 185:71-83
- Wilhelms DE (1984) Moon. In: *The Geology of the Terrestrial Planets*. Carr MH (ed) NASA SP-469, 106-205
- Wilhelms DE (1987) The Geologic History of the Moon. US Geol Surv Spec Pap 1348

- Williams JG, Boggs DH, Ratcliff JT (2005) Lunar fluid core and solid-body tides. *Lunar Planet Sci XXXVI*:1503
- Williams JG, Boggs DH, Ratcliff JT, Yoder CF, Dickey JO (2001a) Influence of a fluid lunar core on the Moon's orientation. *Lunar Planet Sci XXXII*:2028
- Williams JG, Boggs DH, Yoder CF, Ratcliff JT, Dickey JO (2001b) Lunar rotational dissipation in solid body and molten core. *J Geophys Res* 106:27,933-27,968
- Williams KK, Zuber MT (1998) Measurement and analysis of lunar basin deposits from Clementine altimetry. *Icarus* 131:107-122
- Wilson L, Head JW, III (1981) Ascent and eruption of basaltic magma on the Earth and Moon. *J Geophys Res* 86: 2971-3001
- Winzer SR, Nava DF, Schuhmann S, Kouna CW, Lum RKL, Philpotts JA (1974) Major, minor, and trace element abundances in samples from the Apollo 17 Station 7 boulder: Implications for the origin of early crustal rocks. *Earth Planet Sci Lett* 23:439-444
- Wise DU, Yates MT (1970) Mascons as structural relief on a lunar 'Moho'. *J Geophys Res* 75:261-268
- Wolf R, Woodrow A, Anders E (1979) Lunar basalts and pristine highland rocks: Comparison of siderophile and volatile elements. *Proc Lunar Planet Sci Conf* 10:2107-2130
- Wood JA, Dickey JS, Marvin UB, Powell BN (1970) Lunar anorthosites and a geophysical model of the Moon. *In: Proceedings of the Apollo 11 Lunar Science Conference*. Pergamon Press, p 965-988
- Yanai K, Ueda M (2000) Achondrite polymict breccia 1153: A new lunar meteorite classified to anorthositic regolith breccia. *Lunar Planet Sci XXXI*:1101
- Yin Q, Jacobsen SB, Yamashita K, Blichert-Toft J, Télouk P, Albarède F (2002) A short timescale for terrestrial planet formation from Hf-W chronometry of meteorites. *Nature* 418:949-952
- Yingst RA, Head JW (1999) Geology of mare deposits in South Pole-Aitken basin as seen by Clementine UV/VIS data. *J Geophys Res* 104:18,957-18,979
- Yingst RA, Head JW III (1997) Volumes of lunar lava ponds in South Pole-Aitken and Orientale basins: Implications for eruption conditions, transport mechanisms, and magma source regions. *J Geophys Res* 102:10,909-10,931
- Yingst RA, Head JW III (1998) Characteristics of lunar mare deposits in Smythii and Marginis basins: implications for magma transport mechanisms. *J Geophys Res* 103:11,135-11,158
- Yoder CF (1981) The free librations of a dissipative Moon. *Philos Trans R Soc London Ser A* 303:327-338
- Yoder CF (1995a) Astrometric and geodetic properties of Earth and the solar system. *In: Global Earth Physics: A Handbook of Physical Constants* (AGU reference shelf 1). Ahrens TJ (ed) American Geophysical Union, p 1-31
- Yoder CF (1995b) Venus' free obliquity. *Icarus* 117:250-286
- Yuan D-N, Sjogren WL, Konopliv AS, Kucinskas AB (2001) Gravity field of Mars: A 75th degree and order model. *J Geophys Res* 106:23,377-23,401
- Zhang K, Jones CA (1994) Convective motions in the Earth's fluid core. *Geophys Res Lett* 21:1939-1942
- Zhong S, Parmentier EM, Zuber MT (2000) A dynamic origin for the global asymmetry of lunar mare basalts. *Earth Planet Sci Lett* 177:131-140
- Zhong S, Zuber MT (2000) Long-wavelength topographic relaxation for self-gravitating planets and implications for the time-dependent compensation of surface topography. *J Geophys Res* 105:4153-4164
- Zuber MT, Smith DE, Lemoine FG, Neumann GA (1994) The shape and internal structure of the Moon from the Clementine mission. *Science* 266:1839-1843

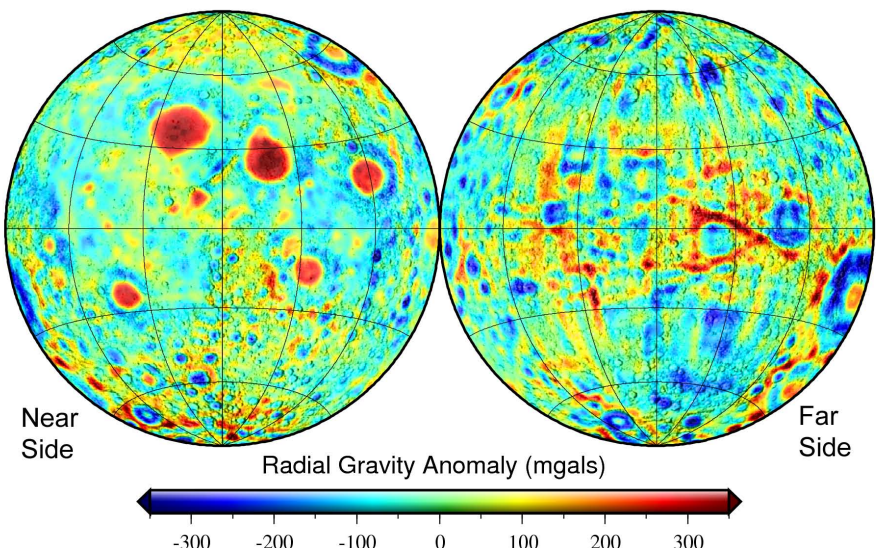


Plate 3.1. Radial gravity anomalies of the Moon as determined from the model LP150Q, expanded to degree 90 with the degree-zero and J_2 terms removed. The gravity anomalies (determined at 1738 km radius) range from a minimum of -545 mgal to a maximum of 604 mgal. Images are in Lambert azimuthal equal area projection.

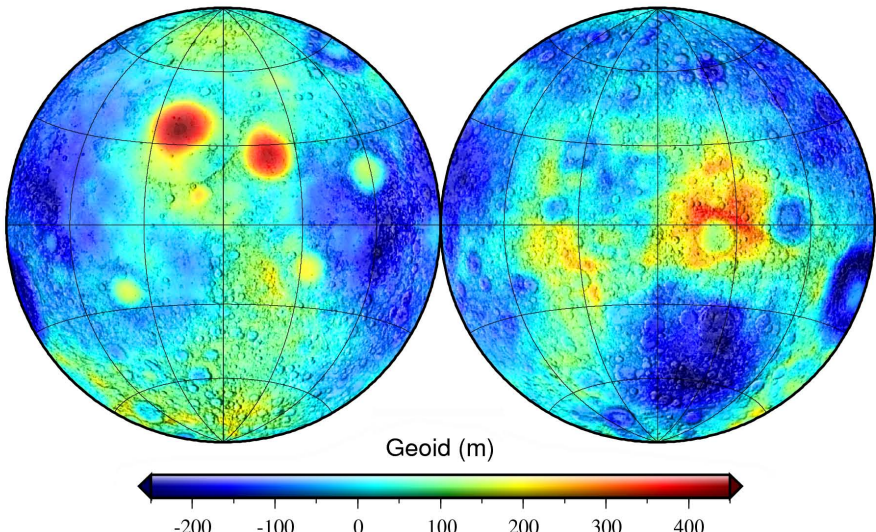


Plate 3.2. The geoid of the Moon as determined from the model LP150Q, expanded to degree 150 with the J_2 term removed. The maximum and minimum geoid elevations in this figure are 461 and -296 meters, respectively. Images are in Lambert azimuthal equal area projection.

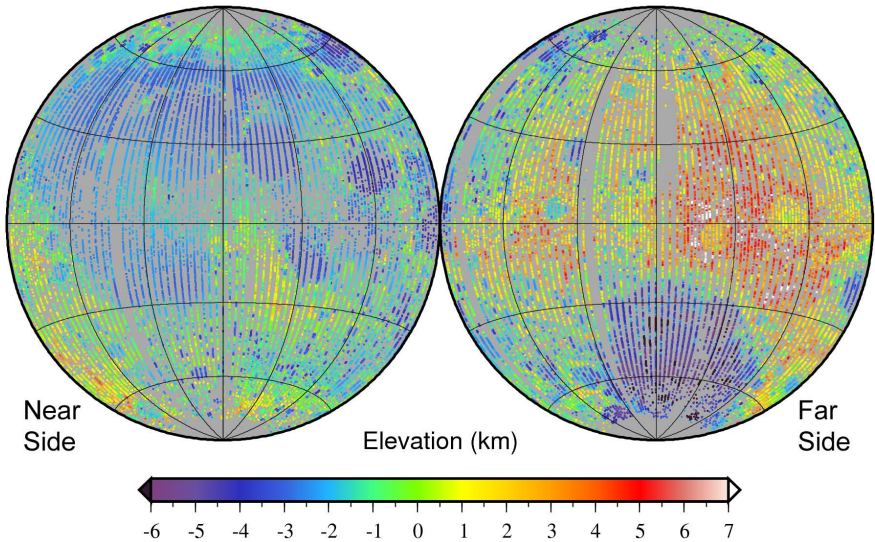


Plate 3.3. Topography of the Moon as determined by the individual range measurements of the Clementine Lidar. The elevation is measured with respect to a spheroid of radius 1738 km at the equator and with a flattening of 1/3234.93 (which corresponds to the J_2 portion of the lunar geoid). Images are in Lambert azimuthal equal area projection.

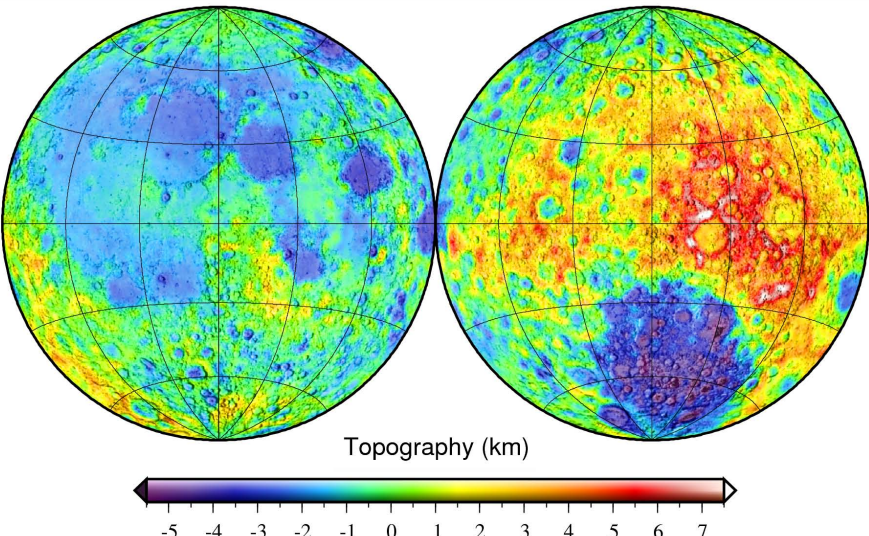


Plate 3.4. Topography of the Moon (GLTM2c) referenced to the full lunar geoid (LP150Q) expanded to degree 90. Maximum and minimum elevations are -6.3 and 8.4 km respectively. Images are in Lambert azimuthal equal area projection.

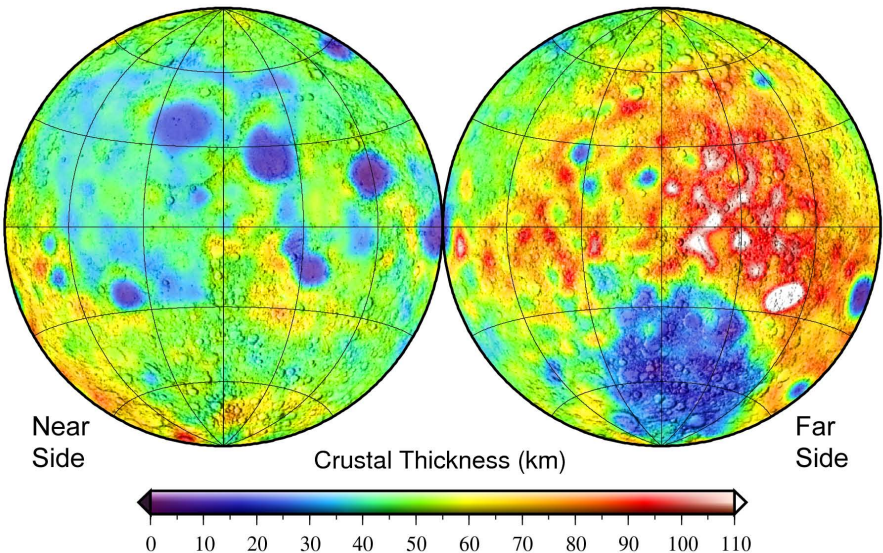


Plate 3.5. Total crustal thickness of the Moon (Model 1). Crustal thicknesses range from ~3 km beneath the Crisium basin to 154 km northeast of the South Pole-Aitken basin. Images are in Lambert azimuthal equal area projection.

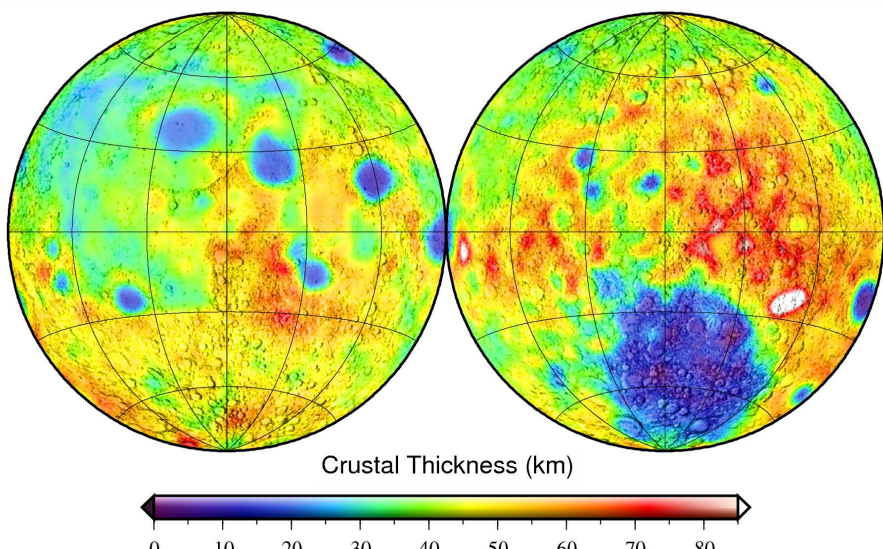


Plate 3.6. Total crustal thickness of the Moon (Model 2). Crustal thicknesses range from ~0 km beneath the Apollo basin to 104 km northeast of the South Pole-Aitken basin. This model assumes that the degree-1 Bouguer anomaly is a result of lateral density variations. Images are in Lambert azimuthal equal area projection.

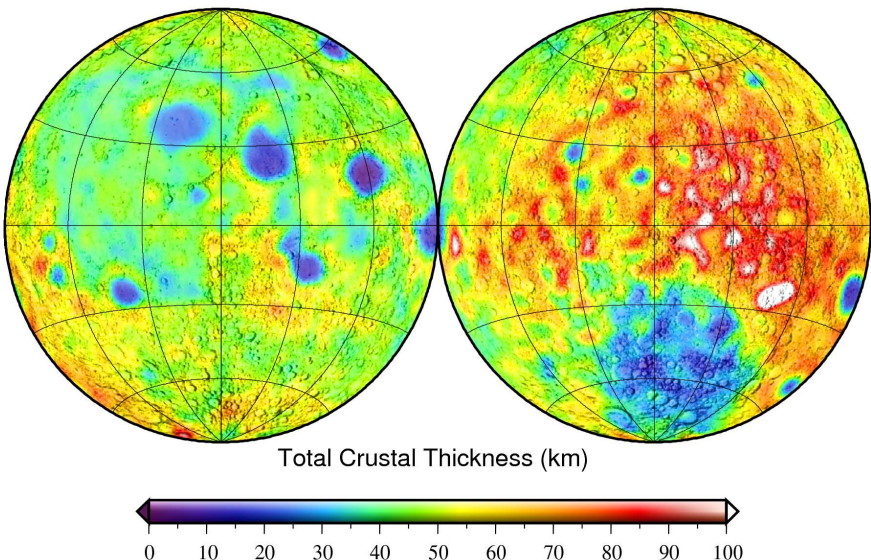
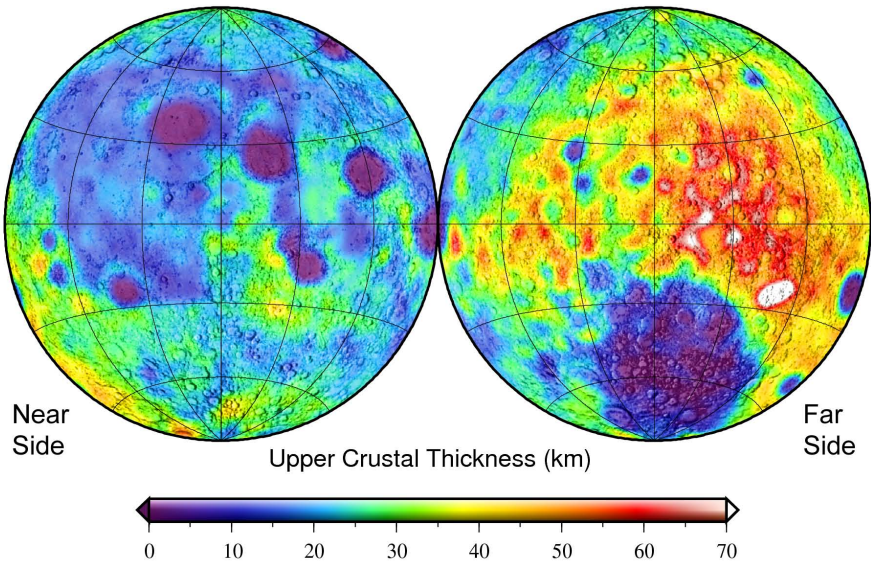


Plate 3.7. Crustal thickness of the Moon (Model 3). Upper image is the thickness of the upper crust (excluding mare fill), whereas the lower image is the total thickness of the crust. The total thickness of the crust for this model ranges from ~3 km beneath the Crisium basin to 134 km northeast of the South Pole-Aitken basin. Images in Lambert azimuthal equal area projections.

Plate 3.8

Map showing locations of craters in the Tompkins and Pieters (1999) study, and the inferred lithologies present in their central peaks.

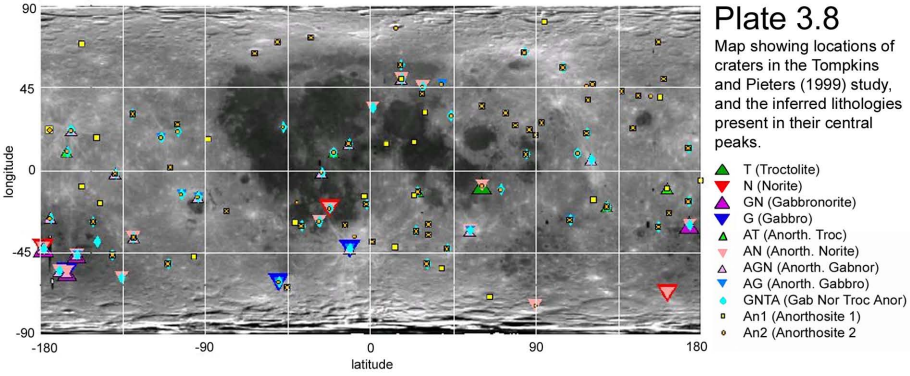


Plate 3.9

Anorthositic distribution shown on the Clementine 750 nm global basemap. Circles show locations where anorthositic is observed with telescopic near-infrared spectra (Hawke et al. 2003b); cyan triangles represent locations on central peaks of craters where Tompkins and Pieters (1999) identified anorthositic (An1); and crosses are locations on central peaks of craters where anorthositic plus one or more additional rock types were identified. Base map is in simple cylindrical projection.

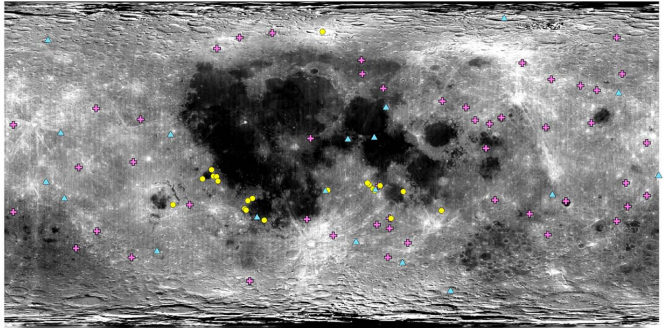


Plate 3.10

Surface expression of major lunar terranes as inferred from the distribution of FeO and Th on the lunar surface. After Jolliff et al. 2000.

